Novel determinants of cardiovascular disease: a population approach

Submitted in partial fulfilment of the requirements of the Degree of Doctor of Philosophy

Queen Mary University of London

Candidate: Zahra Raisi Estabragh

Supervisors:

Prof. Steffen E. Petersen (primary)

Prof. Patricia B. Munroe (secondary)

Prof. Nicholas C. Harvey (external)

Statement of originality

I, Zahra Raisi Estabragh, confirm that the research included within this thesis is my own work or that where it has been carried out in collaboration with, or supported by others, that this is duly acknowledged below and my contribution indicated. Previously published material is also acknowledged below.

I attest that I have exercised reasonable care to ensure that the work is original, and does not to the best of my knowledge break any UK law, infringe any third party's copyright or other Intellectual Property Right, or contain any confidential material.

I accept that the College has the right to use plagiarism detection software to check the electronic version of the thesis

I confirm that this thesis has not been previously submitted for the award of a degree by this or any other university.

The copyright of this thesis rests with the author and no quotation from it or information derived from it may be published without the prior written consent of the author.

Signature:

Date: 10th May 2021

Details of collaboration and publications

Publications with direct relevance to the thesis

Methods and Resources (Chapter 2)

1. Raisi-Estabragh Z, Harvey NC, Neubauer S, Petersen SE. Cardiovascular magnetic resonance imaging in the UK Biobank: a major international health research resource. Eur Hear J - Cardiovasc Imaging 2021;22:251-258. doi:10.1093/ehjci/jeaa297. (**Section 2.1**).
2. Raisi-Estabragh Z, Petersen SE. Cardiovascular research highlights from the UK Biobank: opportunities and challenges. Cardiovasc Res 2020;116:e12–e15. doi:10.1093/cvr/cvz294. (**Section 2.1**).
3. Raisi-Estabragh Z, Izquierdo C, Campello VM, Martin-isla C, Jaggi A, Harvey NC, Lekadir K, Petersen SE. Cardiac magnetic resonance radiomics: basic principles and clinical perspectives. Eur Hear J - Cardiovasc Imaging 2020;**21**:349–356. doi:10.1093/ehjci/jeaa028. (**Section 2.3**).

Results (Chapters 3-7):

4. Raisi-Estabragh Z, Cooper J, Judge R, Khanji MY, Munroe PB, Cooper C, Harvey NC, Petersen SE. Age, sex and disease-specific associations between resting heart rate and cardiovascular mortality in the UK BIOBANK. PLoS One 2020;**15**:e0233898. doi:10.1371/journal.pone.0233898 (**Chapter 3**)
5. Raisi-Estabragh Z*, M'Charrak A*, McCracken C, Biasiolli L, Ardissino M, Curtis EM, Aung N, Suemoto CK, Mackay C, Suri S, Nichols TE, Harvey NC, Petersen SE, Stefan Neubauer. Associations of cognitive performance with cardiovascular magnetic resonance phenotypes in the UK Biobank. Eur Hear J - Cardiovasc Imaging 2021. doi: 10.1093/ehjci/jeab075. Accepted, in press. (**Chapter 4**)
6. Raisi-Estabragh Z, Biasiolli L, Cooper J, Aung N, Fung K, Paiva JM, Sanghvi MM, Thomson RJ, Curtis E, Paccou J, et al. Poor Bone Quality is Associated With Greater Arterial Stiffness: Insights From the UK Biobank. J Bone Miner Res 2021;36:90-99. doi:10.1002/jbmr.4164. (**Chapter 5**).
7. Raisi-Estabragh Z, McCracken C, Gkontra P, Jaggi A, Ardissino M, Cooper J, Biasiolli L, Aung N, Piechnik SK, Neubauer S, Munroe PB, Lekadir K, Harvey NC, Petersen SE. Associations of meat and fish consumption with conventional and radiomics cardiovascular phenotypes in the UK Biobank. Front Cardiovasc Med. 2021. doi: 10.3389/fcvm.2021.667849. (**Chapter 6**)

8. Raisi-Estabragh Z, McCracken C, Cooper J, Fung K, Paiva JM, Khanji MY, Rauseo E, Biasiolli L, Raman B, Piechnik SK, Neubauer S, Munroe PB, Harvey NC, Petersen SE. Adverse cardiovascular magnetic resonance phenotypes are associated with greater likelihood of incident coronavirus disease 2019: findings from the UK Biobank. Aging Clin Exp Res 2021;33:1133-1144. doi:10.1007/s40520-021-01808-z. (**Chapter 7**)

Other publications during the doctoral period

1. Carvalho C, Williams C, Raisi-Estabragh Z, Patel, R, Timmis A, Rison SCG, Robson J. Application of a Risk stratification tool for Familial Hypercholesterolaemia in Primary Care. Heart 2021. Accepted, in press
2. Raisi-Estabragh Z, Gkontra P, Jaggi A, Cooper J, Augusto JB, Bhuva A, Davies RH, Manisty CH, Moon JC, Munroe PB, Harvey NC, Lekadir K, Petersen SE. Repeatability of cardiac magnetic resonance radiomics: a multicentre multi-vendor multi-centre test-retest study. Front Cardiovasc Med. 2020. doi:10.3389/fcvm.2020.586236
3. Raisi-Estabragh Z, Izquierdo C, Campello VM, Martin-isla C, Jaggi A, Harvey NC, Lekadir K, Petersen SE. Cardiac magnetic resonance radiomics: basic principles and clinical perspectives. Eur Hear J - Cardiovasc Imaging 2020;1–8. doi:10.1093/ehjci/jeaa028
4. Martin-Isla C, Campello VM, Izquierdo C, Raisi-Estabragh Z, Baeßler B, Petersen SE, Lekadir K. Image-Based Cardiac Diagnosis With Machine Learning: A Review Front Cardiovasc Med 2020;7. doi:10.3389/fcvm.2020.00001
5. Cetin I, Raisi-Estabragh Z, Petersen SE, Napel S, Piechnik SK, Neubauer S, Ballester MAG, Camara O, Lekadir K. Radiomics signatures of cardiovascular risk factors in cardiac MRI: Results from the UK Biobank. Front Cardiovasc Med. 2020. doi:10.3389/fcvm.2020.591368
6. Zemrak F*, Raisi-Estabragh Z*, Khanji MY, Mohiddin SA, Bruder O, Wagner A, Lombardi M, Schwitter J, Van Rossum AC, Pilz G, Nothnage D, Steen H, Nagel E, Prasad S, Deluigi CC, Dill T, Frank H, Schneider S, Mahrholdt H, Petersen SE. Left ventricular hyper-trabeculation is not associated with cardiovascular morbidity or mortality: Insights from the EuroCMR registry. Front Cardiovasc Med. 2020;7:158. doi:10.3389/fcvm.2020.00158
7. Raisi-Estabragh Z, McCracken C, Ardissino M, Bethell MS, Cooper J, Cooper C, Harvey NC, Petersen SE. Renin-Angiotensin-Aldosterone System Blockers Are Not Associated With Coronavirus Disease 2019 (COVID-19) Hospitalization : Study of 1,439 UK Biobank Cases. Front Cardiovasc Med 2020;7(July):1–8. doi:10.3389/fcvm.2020.00138
8. Raisi-Estabragh Z, McCracken C, Bethell MS, Cooper J, Cooper C, Caulfield MJ, Munroe PB, Harvey NC, Petersen SE. Greater risk of severe COVID-19 in Black, Asian and Minority

Ethnic populations is not explained by cardiometabolic, socioeconomic or behavioural factors, or by 25(OH)-vitamin D status: study of 1326 cases from the UK Biobank. J Public Health. 2020;25:1–10. doi:10.1093/pubmed/fdaa095

9. Khanji MY, Jensen MT, Kenawy AA, Raisi-Estabragh Z, Paiva JM, Aung N, Fung K, Lukaschuk E, Zemrak F, Lee AM, et al. Association Between Recreational Cannabis Use and Cardiac Structure and Function. JACC Cardiovasc Imaging 2020;13:886–888. doi:10.1016/j.jcmg.2019.10.012
10. Raisi-Estabragh Z, Khanji MY. A rare case of persistent left superior vena cava with absent right superior vena cava. Eur Heart J. 2019: ehz466. doi: 10.1093/eurheartj/ehz466
11. Harvey NC, D'Angelo S, Paccou J, Curtis EM, Edwards M, Raisi-Estabragh Z, Walker-Bone K, Petersen SE, Cooper C. Calcium and Vitamin D Supplementation Are Not Associated With Risk of Incident Ischemic Cardiac Events or Death: Findings From the UK Biobank Cohort. J Bone Miner Res. 2018. doi:10.1002/jbmr.3375.
12. Raisi-Estabragh Z, Kenawy AAM, Aung N, Cooper J, Munroe PB, Harvey NC, Petersen SE, Khanji MY. Variation in left ventricular cardiac magnetic resonance normal reference ranges: systematic review and meta-analysis. Eur Hear J - Cardiovasc Imaging 2020;1–11. doi:10.1093/ehjci/jeaa089

Collaborations

Professor Steffen Petersen, Professor Nick Harvey, and Professor Patricia Munroe provided supervision and support for all aspects of the work presented. The work was conceived and developed by Dr Zahra Raisi Estabragh with support of the supervisory team. The statistical analysis plans were developed by Dr Zahra Raisi Estabragh with guidance from Ms Jackie Cooper. Data analysis was performed with support of Ms Jackie Cooper and Ms Celeste McCracken. Professor Karim Lekadir and Dr Polyxeni Gkontra provided advice on all content relating to radiomics analysis. Dr Polyxeni Gkontra led on extraction of radiomics features and performed related analyses. Dr Zahra Raisi Estabragh led on interpretation of the findings and write up of the work, including writing of all peer-review publications generated from the work.

Acknowledgements

I am extremely grateful to the British Heart Foundation for funding this period of dedicated research. I would also like to extend my gratitude to the UK Biobank scientific team for creating an exceptional research resource and the UK Biobank participants who have generously contributed their time and data, on which the work in this thesis is based.

I would like to express my deepest appreciation to my supervisors, Professor Steffen Petersen, Professor Nick Harvey, and Professor Patricia Munroe, whose support and guidance has been instrumental in the completion of this work.

I would like to thank my collaborators, Professor Karim Lekadir and Dr Polyxeni Gkontra, for sharing their expertise and invaluable insight. I am also grateful to my colleagues, Ms Jackie Cooper and Ms Celeste McCracken for their excellent advice and contributions.

Finally, I would like to express my gratitude to my family for their unconditional support throughout all of my studies and my friends for their encouragement and support.

Abstract

Background: Cardiovascular disease remains the biggest cause of mortality and morbidity worldwide. New aetiological models for chronic non-communicable conditions, such as cardiovascular disease, propose a more extensive and complex network of interconnected disease determinants than is suggested by traditional risk factor models. Understanding novel disease determinants and their interactions across different organ systems may be key in alleviating the global burden of cardiovascular disease. The UK Biobank comprises comprehensive characterisation of demographics, lifestyle, and clinical status for over half a million participants along with prospective tracking of health outcomes and, for a large subset of participants, detailed cardiovascular magnetic (CMR) imaging. Thus, the UK Biobank provides an ideal platform for investigation of novel cardiovascular disease determinants.

Methods: We present a series of observational studies investigating the association of several novel exposures with cardiovascular health in the UK Biobank, with consideration given to exposures acting across key organ systems (heart, brain, gut, bone) and integrated use of CMR data. Additionally, we describe and illustrate the utility of CMR radiomics, a novel image analysis technique for deeper cardiovascular phenotyping. Finally, in light of the coronavirus disease 2019 (COVID-19) pandemic, we investigate the association of pre-existing CMR phenotypes with incident COVID-19.

Summary of results: Our findings demonstrate associations between cardiovascular health and novel disease exposures acting across different organ systems. We demonstrate the value of a multi-system approach to understanding cardiovascular health and the importance of cross-system interactions in disease occurrence and progression. We further illustrate the utility of large scale CMR data for epidemiologic research in gaining added insights into such relationships and demonstrate the use of deeper cardiovascular phenotyping with novel CMR radiomics.

Conclusions: Our findings suggest that the search for such novel disease determinants is worthwhile and important for improving population burden of cardiovascular diseases.

Table of Contents

List of Tables

List of Figures

List of abbreviations

AD: aortic distensibility

ALP: Alkaline Phosphatase

AMI: acute myocardial infarction

ASI: arterial stiffness index

BMI: body mass index

bpm: beats per minute

BSA: body surface area

BUA: broadband ultrasound attenuation

CI: confidence interval

CMR: cardiovascular magnetic resonance

COVID-19: coronavirus disease 2019

CRP: C Reactive Protein

DAG: directed acyclic graph

DXA: dual-energy x-ray absorptiometry

FI: fluid intelligence

GDP: gross domestic product

GLCM: grey level co-occurrence matrix

GLDM: grey level difference matrix

GLRLM: grey level run length matrix

GLS: global longitudinal strain

GLSZM: grey level size zone matrix

HES: hospital episode statistics

HR: hazard ratio

HCM: hypertrophic cardiomyopathy

IGF1: Insulin-like Growth Factor 1

IHD: ischaemic heart disease

IPAQ: international physical activity questionnaire

IQR: interquartile range

LGE: late gadolinium enhancement

LV: left ventricle

MESA: multi-ethnic study of atherosclerosis

MET: metabolic equivalents

NGTDM: neighbouring grey tone difference matrix

NHS: national health service

PWV: pulse wave velocity

ROI: region of interest

RT: reaction time

RV: right ventricle

SARS-CoV-2: severe acute respiratory syndrome coronavirus 2

SD: standard deviation

SHBG: Sex Hormone Binding Globulin

SHR: subdistribution hazard ratio

SOS: speed of sound

TMAO: Trimethylamine N-oxide

UK: United Kingdom

1 Background

1.1 Brief overview of cardiovascular epidemiology

1.1.1 Historical public health perspectives

In the 20th century, successful public health strategies led to dramatic improvements in population health and life expectancy[1]. The most striking achievements were in the prevention and control of infectious diseases, which placed a heavy burden on public health at the start of the century[1]. Improved sanitation greatly reduced infections transmitted through contaminated water, such as, typhoid and cholera. In addition, development of effective vaccines and coordinated global vaccination programmes resulted in the eradication of smallpox[2] and control of conditions, such as polio, measles, rubella, tetanus, and diphtheria[1]. Furthermore, the development and availability of antimicrobial agents enabled control of conditions such as tuberculosis and sexually transmitted illnesses[1]. In the United Kingdom (UK), establishment of the National Health Service (NHS) permitted cohesive population level provision of public health programmes[3]. Life expectancy, in developed nations, increased more during the 20th century than in any previous century[4].

As population demographics shifted towards greater longevity and burden from infectious diseases declined, non-communicable conditions, in particular ischaemic heart disease (IHD), emerged as dominant public health problems[5]. The Framingham Heart Study, the first large scale study of cardiovascular disease epidemiology, was initiated in 1948 and led to identification of key cardiovascular risk factors, such as, cigarette smoking, high cholesterol, high blood pressure, and lack of exercise[6]. In 1964, the United States Surgeon General released a landmark report warning of the health hazards of cigarette smoking with relation to cancer and heart disease[7]. Risk factor modification, better treatments, and earlier disease detection resulted in significant improvements in cardiovascular outcomes in the latter years of the 20th century[1].

1.1.2 Contemporary state of cardiovascular epidemiology

The 2018 Global Burden of Disease study documents a global epidemiological transition of reduced burden from infectious, maternal, and neonatal illnesses whilst, at the same time, reporting increasing burden from cardiovascular diseases and neoplasms[8]. Cardiovascular diseases caused an estimated 17.8 million (17.5–18.0) deaths worldwide, the highest number of all non-communicable conditions[8]. In Europe, cardiovascular diseases account for 45% of all deaths and are estimated to cause over 4 million deaths each year[9]. Of these, the most common underlying conditions are IHD and cerebrovascular disease, accounting for 1.8 million and 1.0 million deaths per year, respectively[9]. In

the UK, there are approximately 7.6 million people living with cardiovascular diseases and 168,000 related deaths per year[10].

There are increasing reports of major heterogeneities in cardiovascular disease outcomes, with poorer outcomes observed in women and younger adults (<55 years-old)[11]. In Europe, the number of deaths from cardiovascular disease is higher in women (2.2 million) than men (1.8 million), with cardiovascular disease accounting for 49% of all deaths in women and 40% of all deaths in men[9]. Indeed, recent data indicate stagnation of improvements in cardiovascular outcomes for young adults, particularly for younger women[9,11,12]. The drivers of these sex and age differences are incompletely understood.

1.1.3 New aetiological models for cardiovascular disease

Early epidemiologic studies identified important modifiable risk factors for cardiovascular disease, such as, smoking, high blood pressure, high cholesterol, and lack of exercise[13]. Modification of these factors has led to substantial improvements in cardiovascular outcomes. However, recent data demonstrate that trends in improvement of cardiovascular outcomes are starting to plateau, indicating that the level of outcome improvement achievable from targeting these factors alone may be nearing saturation. Additionally, whilst control of classical cardiovascular risk factors remains a public health priority, it is evidently not feasible, with current available therapies, to fully optimise these risk factors in large populations[14]. Furthermore, it is increasingly apparent that chronic non-communicable diseases, such as cardiovascular diseases, are not adequately accounted for by traditional risk factor models, which rely on simplistic linear exposure-outcome relationships with large effect sizes. Newer aetiological models suggest that these conditions may be better explained through consideration of complex interactions between a wider network of causal agents, often acting across multiple organ systems[15]. Thus, there is, in general, strong support for seeking novel cardiovascular disease determinants, and understanding their interconnected relationships, to advance knowledge, improve disease prevention, and achieve further improvements in clinical outcomes[16–18].

1.1.4 The evolution of contemporary epidemiology approaches

Epidemiology is concerned with the distribution and determinants of disease and other factors which influence health[19]. Investigating factors which may be causing disease is important, because it may be possible to prevent disease by intervening on causal agents[17]. However, disentangling cause and effect is difficult.

Suppose we wish to study the effect of smoking on cardiovascular disease. Using observational data, it may not be possible to isolate, with confidence, the causal effect of smoking. This is because smokers are, on average, different from non-smokers in other important ways. They are more likely, for example, to drink more heavily and have unhealthy diets. We cannot know for sure whether health differences between smokers and non-smokers are explained by these confounding factors or by smoking itself. The most common approach when seeking to establish an independent association is to fit a multivariable regression model and adjust for possible confounders[20]. However, even if we were to measure and adjust for these confounders, we may not measure them perfectly or there may be other confounders (e.g., socioeconomic status) that we have not measured. This means that there is always a possibility of residual confounding. On the other hand, erroneous adjustment for a mediating variable, which lies on the causal pathway, may attenuate the true exposure-outcome association. There is also the possibility that risk factors themselves may be modified by disease. For instance, as people become ill, they may cut down or give up smoking, which could reverse the true relationship by suggesting that reduced smoking increases the risk of disease. To reduce the likelihood of reverse causation or spurious associations resulting from confounding, we could randomly assign a group of people to smoke and another group to not smoke and follow them up to monitor their health. However, this would, of course, be neither ethical nor practical.

Well conducted randomised controlled trials provide the most convincing causal evidence, however, due to practical and ethical constraints, they may only be applied to a narrow range of exposures[21]. Observational studies do not provide direct evidence of causal association but, in practice, most causal effects must be estimated from non-experimental data[22]. Unfortunately, many of the associations identified in epidemiological studies are likely explained by confounding, often by factors which are difficult to quantify[20]. In the last two decades, there has been greater recognition of the limitations and biases of non-experimental data, which has led to more cautious interpretation of findings and changes in approach to study design[4]. Whilst many of the core methods have remained unchanged, the approach to problem solving has shifted.

Codification of epidemiology and attempts to develop more diligent and methodical ways of thinking about research questions have contributed to greater rigour and transparency in the field[17]. The counterfactual model for causal inference, which focuses primarily on counterfactual and potential outcome reasoning and utilises directed acyclic graphs (DAG) as a tool for visual representation, has gained particular popularity[23,24]. This model advocates explicit consideration of the role of each variable in the exposure-outcome relationship and provides a simple and transparent method for researchers to illustrate their knowledge, hypotheses, and assumptions[25]. Within this framework, all the key variables (such as, exposure, outcome, confounders, and mediators) are accounted for and any assumptions are declared (**Figure 1.1**)[25].

This rule-based approach to reasoning ensures deliberate consideration of the research question and provides a logical structure to study designs. However, some have argued that limiting epidemiological approaches to the counterfactual model may have a stifling effect[26]. Complex and nuanced, but highly important concepts, such as, social inequality, do not neatly fit into the counterfactual model. Restricting research to questions that may be addressed by DAG based reasoning, may limit the types of questions that are asked, overlooking important aspects of public health, such as, the societal determinants of disease[26].

Figure 1.1. A directed acyclic graph approach to the smoking-cardiovascular disease problem

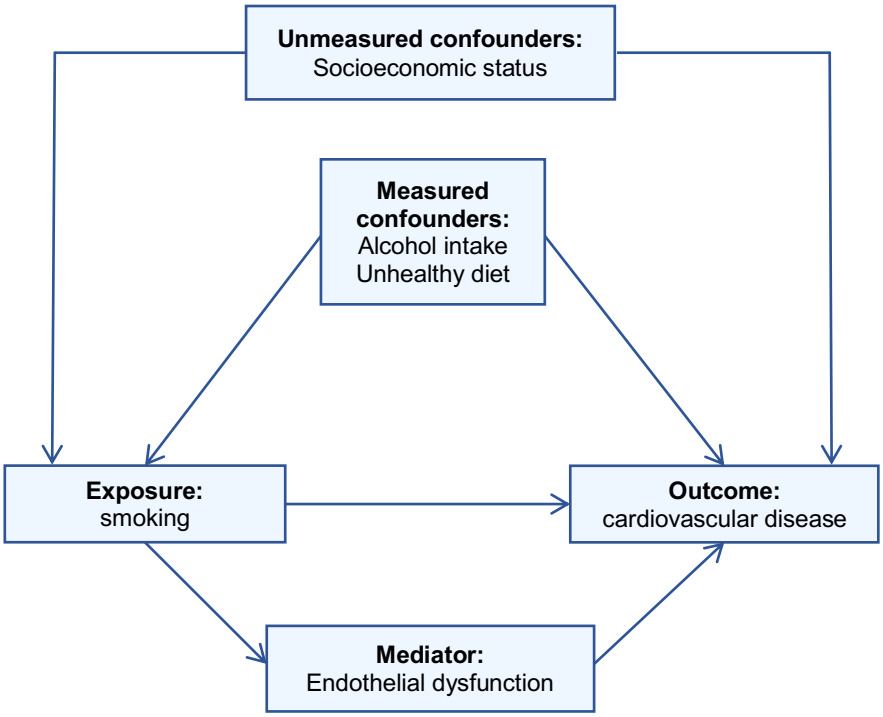

It has been proposed, through a framework termed "triangulation of evidence", that the best way to reach definitive conclusions about the accuracy of a research finding is by integrating evidence from a range of study designs, which have different and unrelated biases[27]. The premise is, that a finding is more likely to be true if different studies using different approaches with independent sources of bias (preferably by different researchers and in different settings) show the same result, than if the same result was reported by several studies using the same approach. Of course, the key question about new methodologies and approaches, which as yet remains unanswered, is whether they result in real advances in our understanding of disease determinants and ultimately contribute meaningfully to the alleviation of disease[28].

1.1.5 Summary

In summary, there is evidence of dramatic epidemiological shifts in global disease patterns with greatly increased health burden from cardiovascular diseases. There have been substantial improvements in cardiovascular outcomes over the last four decades. However, cardiovascular disease remains the most common cause of morbidity and mortality worldwide with evidence of differential disease outcomes across age and sex[8,9]. To further improve cardiovascular disease outcomes, there is increased interest in understanding the relationships of novel disease determinants and their interconnectedness both within and across organ systems. Observational studies are helpful in understanding these relationships; however, such studies need to be planned carefully to minimise bias and reporting of spurious associations.

1.2 Cardiovascular magnetic resonance (CMR)

1.2.1 The role of CMR in clinical practice and research

Cardiovascular imaging is the cornerstone of clinical decision making in cardiology. Cardiovascular magnetic resonance (CMR) imaging technology has advanced exponentially in the last 20 years[29]. Accurate volumetric quantification due to superior endocardial border definition, versatile imaging planes, and detailed tissue characterisation have established CMR as the reference modality for assessment of cardiac structure and function[29]. Global consensus standards for image acquisition ensure comparable images within and between centres[30]. Furthermore, CMR image acquisitions are less operator dependent than alternative modalities, such as, echocardiography, contributing further to its greater reproducibility[29]. Accordingly, CMR has gained an important role in clinical practice and a notable presence in international clinical guidelines[31,32]. Furthermore, the capability to produce uniform high quality images using a radiation-free approach has made CMR an attractive modality for population imaging studies[33]. Indeed, CMR has been used in several large cohort studies, including the Multi-ethnic Study of Atherosclerosis (MESA)[34], the Framingham Heart Study[35], and the UK Biobank[36].

1.2.2 The CMR assessment

Magnetic resonance imaging (MRI) utilises the proton spin properties of hydrogen atoms within tissues, with signals generated through manipulation of their excitation and relaxation properties with magnetic fields and radiowaves. There are different types of CMR acquisition sequences. Most ‘cine’ imaging uses balanced steady state free precession (bSSFP) techniques. The protocol for CMR scans typically consists of a minimum basic dataset for cardiac chamber quantification and qualitative

assessment of valvular structure and function. The remainder of the scan is adapted to include acquisition of images tailored to the specific clinical question (e.g., detailed quantification of a valve lesion or assessment of myocardial perfusion defects).

1.2.2.1 Left and right ventricular assessment

CMR provides highly reproducible volumetric quantification of the left and right ventricles (LV, RV). Intrinsic contrast created by differences in inherent magnetic properties of the blood pool and myocardium results in high endocardial border definition. Unlike echocardiography, CMR is not reliant on acoustic windows for high quality imaging. Additionally, deliberate placement of the long axis image planes though the LV apex avoids foreshortening of the LV, a recognised source of inaccuracies for echocardiography. Accurate quantification of the LV and RV in end-systole and end-diastole is performed using a series of short axis cine image slices covering the ventricles from base to apex. Contouring the endocardial and epicardial borders in the short axis stack images allows estimation of chamber volumes and LV mass (LVM) at different time points in the cardiac cycle. Image analysis software often include 'threshold' tools that allow semi-automatic identification of the myocardium and blood pool. Automated image analysis tools are now also increasingly available in clinical settings. The derived anatomic and functional CMR metrics are key to many important clinical decisions (e.g., referral for surgery or placement of an intracardiac defibrillator).

1.2.2.2 Myocardial tissue characterisation

CMR uniquely permits the non-invasive assessment of myocardial tissue character. These assessments are made using dedicated sequences including parametric mapping techniques such as myocardial native T1 mapping (a contrast-free technique), T2 mapping, and extracellular volume (ECV) fraction assessment. Evaluation of myocardial character can also be undertaken using late gadolinium enhancement (LGE) images, which requires administration exogenous contrast.

1.2.2.3 Assessment of ischaemic heart disease

There are three key features of IHD that may be assessed with CMR: resting LV function, functional significance of coronary artery disease (CAD), and myocardial infarction/viability. Resting LV function is assessed from volumetric quantification of the LV as described in **section 1.2.2.1**. The functional significance of CAD is typically assessed using pharmacological (typically adenosine) stress CMR with gadolinium contrast administered at peak stress. Evaluation of first-pass perfusion images can allow detection of inducible myocardial perfusion defects, which, particularly if within a coronary territory, are taken to indicate the presence of flow limiting CAD. Finally, identification of myocardial infarction can be undertaken using LGE images, with delayed wash-out of contrast from

the myocardium indicating areas of infarction. The transmurality of an infarcted area is used as an indicator of viability, with 50% transmurality typically taken as a threshold for viable vs non-viable tissue. These assessments of viability are used to guide revascularisation decisions (i.e., coronary artery bypass grafting or percutaneous coronary intervention).

1.2.2.4 Valvular heart disease

CMR can provide a useful adjunct for assessment of valve disease, particularly for difficult to quantify lesions or when assessment of the consequences of valve disease on the ventricles and other structures (e.g. aorta) is needed. Indeed, CMR has received increased mention in the latest European and American Valve guidelines[37,38]. Assessment of valve disease with CMR requires careful planning of cut planes to properly align with appropriate valve planes and flow jets.

1.2.3 Limitations of conventional CMR image analysis

Current clinical CMR image analysis is largely reliant on basic geometric measures and qualitative descriptors. Existing quantifiers of tissue character, such as parametric mapping techniques are limited by ongoing technical challenges and poor discrimination of health and disease. There are shortcomings with the current approach to CMR image analysis. For example, it is not always possible to distinguish between conditions with similar morphology, such as, hypertensive heart disease and hypertrophic cardiomyopathy (HCM) or athletic cardiac remodelling and dilated cardiomyopathy. Such distinctions are important because treatment of these conditions is very different. Furthermore, predictions of important clinical outcomes are suboptimal. For example, almost half of the patients who receive a prophylactic intracardiac defibrillator based on low ejection fraction never need any therapies from their device[39], whilst less than a third of sudden cardiac death cases would have been eligible for a primary prevention device based on existing guidelines[40]. Thus, whilst CMR has a central role in research and clinical decision making, there is need for novel imaging biomarkers that may improve its diagnostic accuracy and predictive capabilities.

1.2.4 Background to CMR radiomics

The application of radiomics analysis to CMR images is a novel method permitting extraction of quantitative ventricular shape and myocardial texture metrics. Image segmentations used for conventional volumetric quantification may be used to define regions of interest for radiomics analysis, which typically include the 1) RV cavity, 2) LV cavity, and 2) LV myocardium. These segmentations are used to build 3D masks of the defined regions of interest, from which radiomics

features are extracted. There are three categories of radiomics features: shape, first-order, and texture. The shape features provide advanced quantification of the geometry of the defined region of interest. These include metrics such as volume, axial dimensions, and quantitative descriptions of the overall shape (e.g., elongation, sphericity, flatness). The first-order and texture features are derived from analysis of the pattern and distribution of voxel signal intensities in the defined region of interest. The signal intensity levels in magnetic resonance images reflect the magnetic properties of the underlying tissue, which are in turn influenced by tissue composition[29]. Therefore, the radiomics signal intensity features applied to the LV myocardium may provide insight into myocardial tissue characteristics. First-order radiomics features describe the global distribution of signal intensities in the region of interest using histogram-based statistics such as mean, variation, and skewness. Texture features rely on more advanced statistical methods to describe local signal intensity patterns. Further details on CMR radiomics are provided in section **2.3 CMR radiomics.**

1.3 Objectives of this doctoral project

This doctoral thesis makes use of the UK Biobank, a highly detailed research resource incorporating demographic, lifestyle, and clinical data for over half a million participants. A subset of participants has also completed CMR scanning as part of the UK Biobank Imaging study.

We hypothesise that non-classical risk factors are influential in determining cardiovascular health and of importance in population health. Thus, we investigate the relationships between a selection of non-classical exposures with indicators of cardiovascular health in the UK Biobank and aim to elucidate effects independent of classical vascular risk factors.

The presented work comprises a series of observational studies exploring novel cardiovascular disease determinants with a focus on interconnected relationships across different organ systems (specifically: heart, brain, bone, gut) and integrated use of conventional CMR phenotypes. In addition, we describe a novel CMR image analysis technique, CMR radiomics, demonstrating the feasibility of this methodology and its utility as a research tool. Finally, in light of the coronavirus disease 2019 (COVID-19) pandemic, we examine the relationship between CMR phenotypes and the subsequent risk of severe acute respiratory syndrome coronavirus 2 (SARS-CoV-2) infection in the UK Biobank.

2 Methods and Resources

2.1 The UK Biobank as a research resource

2.1.1 Overview of UK Biobank

The UK Biobank is a very large cohort study comprising over half a million men and women recruited from across the UK between 2006-2010 (**Figure 2.1**). Recruitment was by postal invitation of individuals aged 40-69 years identified from NHS registers. All participants completed a detailed baseline assessment including characterisation of demographics, lifestyle, medical history, as well as a series of physical measures and blood sampling[41]. The UK Biobank protocol is publicly available[42] and summary data may be viewed on the UK Biobank online data showcase[43]. In 2015, the UK Biobank imaging study was launched with the aim of scanning 100,000 of the original participants[44]. The imaging protocol comprises multisystem multimodality imaging, including magnetic resonance imaging of the brain, heart, and abdomen, carotid ultrasound, and dual-energy x-ray absorptiometry (DXA). Repeat imaging of 10,000 participants commenced in 2019. There is longitudinal tracking of health outcomes for all UK Biobank participants through linkages with Hospital Episode Statistics (HES), primary care records, death registers, and cancer registers. In addition, the UK Biobank has released adjudicated algorithmically defined incident health outcomes for key illnesses, such as acute myocardial infarction (AMI) and stroke, through integration of data from multiple sources[45].

Figure 2.1. Summary of participant phenotyping in the UK Biobank

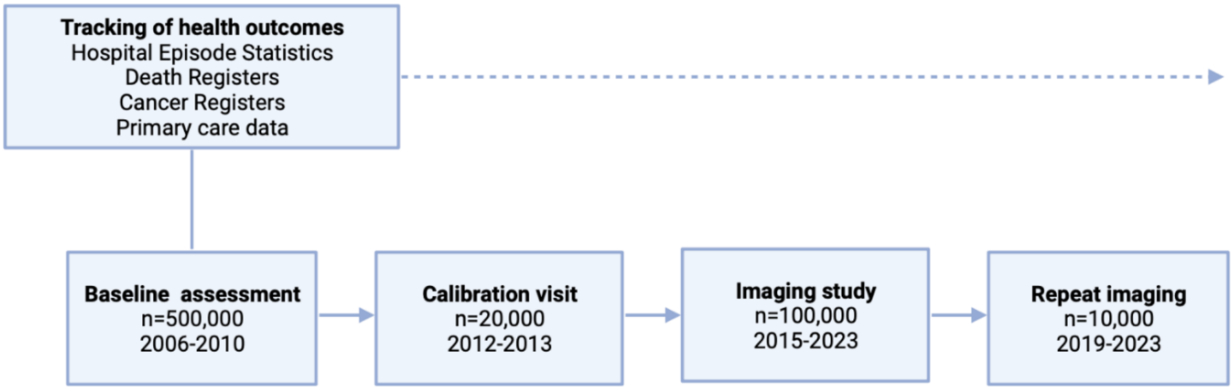

2.1.2 Tracking of incident health outcomes

Prospective follow up of health outcomes is important, as it means that exposure-outcome associations may be interpreted with the knowledge that the two are temporally separate. This is relevant, as risk factors themselves may be modified by disease status, for example, the tendency to give up smoking after a heart attack. However, prospective cohorts need large samples, because although every participant is informative to the wider picture, only a subset will develop any

particular disease. The large number of participants recruited into the UK Biobank and their indefinite follow up means that adequate number of a wide range of incident illnesses are expected to be observed, permitting adequately powered statistical analyses (**Table 2.1**)[42]. Linkages with routinely collected national level data allow reliable recording of incident health events for the whole cohort.

Table 2.1. Estimated number of years from baseline to accrue cases of selected conditions in UK Biobank

	Time to achieve				
	1,000 cases	2,500 cases	5,000 cases	10,000 cases	20,000 cases
MI and coronary death	2 years	4 years	5 years	8 years	13 years
Stroke	5 years	8 years	12 years	18 years	28 years
Diabetes mellitus	2 years	3 years	4 years	6 years	10 years
COPD	4 years	6 years	8 years	13 years	23 years
Colorectal cancer	5 years	9 years	14 years	22 years	42 years
Hip fracture	7 years	11 years	15 years	21 years	31 years
Alzheimer's disease	7 years	10 years	13 years	18 years	23 years
Parkinson's disease	6 years	10 years	15 years	23 years	37 years

Table 2.1. *COPD: chronic obstructive pulmonary disease; MI: myocardial infarction.* [*]*Estimated years from start of recruitment in 2006 with allowance for healthy cohort effect, overseas migration, and comprehensive withdrawal of 1 in 500 participants. Adapted from: UK Biobank: Protocol for a large-scale prospective epidemiological resource (2007)*[42].

2.1.3 Repeat measurements

Selected components of the baseline UK Biobank assessment were repeated for a random subset of 20,000 participants between 2012-2013 and at both imaging visits. Repetition of measurements is important, because in order to understand how risk factors relate to incident disease, we need to distinguish between individuals on different disease trajectories before disease occurrence. Detailed baseline phenotyping is helpful in distinguishing the different trajectory groups, but it is not perfect, because overlap of measurements between groups may lead to misclassification of participants or inability to discriminate the different trajectories. However, assessment at more than one time point allows for more accurate stratification of both exposures and potential confounders[20]. Thus, repeat assessment of the same individual at multiple time points allows evaluation of longitudinal change, more accurate distinction between disease trajectories, and more confident assertions about exposure-outcome associations.

2.1.4 The importance of scale and depth of participant characterisation

Many studies of cardiovascular epidemiology are powered to detect large exposure-outcome effects. As such, these studies may overlook potentially important exposures with moderate effect sizes on which intervention is worthwhile. The scale and comprehensive participant characterisation in the UK Biobank allow consideration of many exposures with moderate effects and their possible interactions on a wide range of illnesses. The extensive phenotypic information also presents unique opportunities to investigate risk factors for disease across organ systems.

2.1.5 Heterogeneity and generalisability

In common with other similar cohorts, there is a healthy participant effect within the UK Biobank. That is, the UK Biobank participants, are on average healthier and more affluent than UK national averages[46,47]. Some have argued that this limits the generalisability of findings from the UK Biobank. However, to consider the practical importance of this observation, we should think about what representativeness actually means for a resource that is expected to be used internationally and have longevity across many decades. Even if the UK Biobank was representative of the current UK population, it is unlikely to be representative of the population in other countries or indeed of the UK population in 10 or 20 years' time. Therefore, striving for representativeness of the current UK population would not provide a broad and long-term solution, because the characteristics of "general populations" are dynamic and location specific. For findings in the UK Biobank to be reliable and widely generalisable there is need for scale and heterogeneity in exposure levels.

Consider that we are interested in the association of smoking with heart attacks. Although the overall proportion of smokers in the UK Biobank is lower than the current national UK average, there are still a large number of smokers (and non-smokers) and adequate number of heart attacks within the sample to allow reliable appreciation of associations. Whether the overall rate of smoking within the sample is similar to that of the general population is less relevant in this context. There is wide variation in risk factor levels and disease rates within the UK Biobank, including substantial number of participants at the extreme levels of exposure. This means that, in general, exposure-outcome associations from the UK Biobank are reliable and widely generalisable[46–48].

2.1.6 CMR in the UK Biobank

Imaging in the UK Biobank is performed across four sites (Reading, Stockport, Newcastle, Bristol) using uniform staff training and equipment[44]. A dedicated 20 minute CMR acquisition protocol was

designed with the aim of obtaining comprehensive anatomic and functional information in a safe and time efficient manner[36]. CMR scans are performed using 1.5 Tesla scanners (MAGNETOM Aera, Syngo Platform VD13A, Siemens Healthcare, Erlangen, Germany). The acquisition protocol includes bright blood anatomic images (sagittal, coronal, axial), long and short axis cine images of the left and right ventricles (LV, RV), native T1 mapping, and imaging of the thoracic aorta[49]. The protocol does not include administration of contrast or stress agents, due to ethical and safety constraints[33,36].

Conventional LV and RV metrics (volumes, ejection fraction, stroke volume, LV mass) can be derived from the short axis cine stack, which covers both ventricles from base to apex. Chamber volumes (e.g., LV end-diastolic volume) are an indicator of cardiac remodelling and provide key information about cardiac health when interpreted in conjunction with functional measures[50]. LV mass[51] and ejection fraction[52] are established markers of cardiac risk. Measures of myocardial strain tend to be more sensitive to early and subclinical changes in myocardial function than measures such as ejection fraction[53,54]. They may, therefore, provide more detailed functional imaging phenotypes which are more sensitive to disease/risk factors. In the UK Biobank, myocardial strain may be estimated from long and short axis cine images using feature/tissue tracking techniques. Tissue tracking makes use of block-matching algorithms which mark regions of interest along the myocardial borders and use these to estimate myocardial motion[55]. Uniquely CMR imaging may be used to assess myocardial tissue character without the use of exogenous contrast agents. Non-contrast parametric mapping techniques (T1/T2 mapping) are increasingly used in clinical and research settings for identification of areas of myocardial fibrosis, infarction, and oedema[56]. The UK Biobank protocol includes native T1 mapping at the mid-ventricular level on short axis images. Aortic distensibility (AD) is a measure of local aortic compliance. It can be calculated from transverse cine image of the thoracic aorta, by considering the relative cross-sectional area change per unit pressure[57]. Lower distensibility indicates a less compliant (stiffer) aorta, poorer aortic bio-elastic function, and worse arterial health[58]. There is an inverse association between AD and cardiovascular risk, specifically, ischaemic heart disease and stroke[59]. Thus, AD provides a continuous measure of ischaemic cardiovascular risk.

The large volume of images in the UK Biobank necessitates the development of automated standardised image analysis pipelines. The first 5,000 UK Biobank CMR scans have been manually segmented (all four cardiac chambers) by trained readers across two core laboratories (London, Oxford) according to pre-defined analysis protocols and standardised quality control procedures[60]. This 5,000 ground truth dataset has been used to develop and evaluate machine learning methods for cardiac chamber segmentation[61]. Notably, Attar et al.[62] have used the 5,000 manual segmentation cohort to develop a fully automated image analysis pipeline for LV and RV segmentation from cine

images in the UK Biobank. Similarly, a fully automated image analysis tool for measurement of AD has also been developed and validated on a large subset of UK Biobank studies[63].

In summary, the UK Biobank CMR protocol provides a comprehensive assessment of cardiovascular health, providing measures of cardiac structure, function, and tissue characterisation alongside prognostic indices and imaging biomarkers of subclinical disease. The CMR imaging phenotypes allow objective assessment and quantification of exposure effects on cardiovascular health and permit finer delineation of disease trajectories with potential for disease-specific assertions. Automated image analysis tools enable derivation of CMR imaging phenotypes from large imaging samples.

2.2 Use of UK Biobank in this project

2.2.1 Ethics and data access

The presented work is covered by the ethical approval for UK Biobank studies from the NHS National Research Ethics Service on 17th June 2011 (Ref 11/NW/0382) and extended on 10th May 2016 (Ref 16/NW/0274). All participants provided written informed consent. Data access was granted through UK Biobank access application 2964.

2.2.2 Characterisation of study participants

Characterisation of study participants was based on information recorded at the baseline and/or imaging visits, unless stated otherwise. Assessments at these visits included a touchscreen questionnaire, a verbal face-to-face interview with a trained researcher, a series of physical measures, and blood sampling.

We ascertained demographic details, such as sex and ethnicity based on self-report at baseline. Age was taken as recorded by UK Biobank at recruitment and, if needed, calculated for the time point of interest. The UK Biobank records the Townsend score as a measure of deprivation relative to national averages taking into account four components of home ownership, household size, car ownership and employment status[64]. A Townsend score of zero indicates deprivation levels similar to national averages, whilst negative scores indicate less and positive score more deprivation than average. Educational level, smoking status, and alcohol intake frequency were taken from self-report. The level of physical activity was self-reported by participants on a series of touchscreen questions. Using this information, we derived a continuous value for the amount of physical activity measured in metabolic equivalent (MET) minutes/week calculated by weighting different types of activity by its energy requirements using values derived from the International Physical Activity Questionnaire (IPAQ)

study[65]. Participants completed a food frequency questionnaire reporting their average weekly consumption of a range of food products over the preceding 12 months. The touchscreen questions also included a battery of cognitive function tests covering a range of skills including processing speed, memory, and reasoning.

With regards physical measures, height and weight were recorded at baseline and imaging visits, we have used these to calculate body mass index (BMI) and body surface area (BSA). Blood pressure and resting heart rate were recorded using standardised equipment and measurement protocols. In addition, finger plethysmography was used to derive a non-invasive measure of large artery stiffness reported as the arterial stiffness index (ASI). Participants also had a quantitative heel ultrasound, which provided quantitative measures of bone quality.

Cardiometabolic morbidities, including diabetes, hypertension, and high cholesterol were ascertained using a combination of self-report questions, blood biochemistry, and linked international classification of disease (ICD) codes from HES data (**Table 2.2**).

Table 2.2. Approach to definition of cardiometabolic morbidities in UK Biobank

Condition	ICD code or data field	Code description
Diabetes	20002	diabetes
Diabetes	2443	"Diabetes diagnosed by doctor" – Answer "Yes"
Diabetes	6177	"Do you regularly take any of the following medications?"– Answer: "Insulin"
Diabetes	6153	"Do you regularly take any of the following medications?"– Answer: "Insulin"
Diabetes	30750	Glycated haemoglobin (HbA1c) ≥48mmol/mol indicates diabetes
Diabetes	E100	Type 1 diabetes mellitus: With coma
Diabetes	E101	Type 1 diabetes mellitus: With ketoacidosis
Diabetes	E102	Type 1 diabetes mellitus: With renal complications
Diabetes	E103	Type 1 diabetes mellitus: With ophthalmic complications
Diabetes	E104	Type 1 diabetes mellitus: With neurological complications
Diabetes	E105	Type 1 diabetes mellitus: With peripheral circulatory complications
Diabetes	E106	Type 1 diabetes mellitus: With other specified complications
Diabetes	E107	Type 1 diabetes mellitus: With multiple complications
Diabetes	E108	Type 1 diabetes mellitus: With unspecified complications
Diabetes	E109	Type 1 diabetes mellitus: Without complications
Diabetes	E110	Type 2 diabetes mellitus: With coma
Diabetes	E111	Type 2 diabetes mellitus: With ketoacidosis
Diabetes	E112	Type 2 diabetes mellitus: With renal complications
Diabetes	E113	Type 2 diabetes mellitus: With ophthalmic complications
Diabetes	E114	Type 2 diabetes mellitus: With neurological complications
Diabetes	E115	Type 2 diabetes mellitus: With peripheral circulatory complications
Diabetes	E116	Type 2 diabetes mellitus: With other specified complications
Diabetes	E117	Type 2 diabetes mellitus: With multiple complications

Condition	ICD code or data field	Code description
Diabetes	E118	Type 2 diabetes mellitus: With unspecified complications
Diabetes	E119	Type 2 diabetes mellitus: Without complications
Diabetes	E130	Other specified diabetes mellitus: With coma
Diabetes	E131	Other specified diabetes mellitus: With ketoacidosis
Diabetes	E132	Other specified diabetes mellitus: With renal complications
Diabetes	E133	Other specified diabetes mellitus: With ophthalmic complications
Diabetes	E134	Other specified diabetes mellitus: With neurological complications
Diabetes	E135	Other specified diabetes mellitus: With peripheral circulatory complications
Diabetes	E136	Other specified diabetes mellitus: With other specified complications
Diabetes	E137	Other specified diabetes mellitus: With multiple complications
Diabetes	E138	Other specified diabetes mellitus: With unspecified complications
Diabetes	E139	Other specified diabetes mellitus: Without complications
Diabetes	E140	Unspecified diabetes mellitus: With coma
Diabetes	E141	Unspecified diabetes mellitus: With ketoacidosis
Diabetes	E142	Unspecified diabetes mellitus: With renal complications
Diabetes	E143	Unspecified diabetes mellitus: With ophthalmic complications
Diabetes	E144	Unspecified diabetes mellitus: With neurological complications
Diabetes	E145	Unspecified diabetes mellitus: With peripheral circulatory complications
Diabetes	E146	Unspecified diabetes mellitus: With other specified complications
Diabetes	E147	Unspecified diabetes mellitus: With multiple complications
Diabetes	E148	Unspecified diabetes mellitus: With unspecified complications
Diabetes	E149	Unspecified diabetes mellitus: Without complications
Diabetes	G590	Diabetic mononeuropathy
Diabetes	G632	Diabetic polyneuropathy
Diabetes	H280	Diabetic cataract
Diabetes	H360	Diabetic retinopathy
Diabetes	M142	Diabetic arthropathy
Diabetes	N083	Glomerular disorders in diabetes mellitus
Diabetes	O240	Diabetes mellitus in pregnancy: Pre-existing type 1 diabetes mellitus
Diabetes	O241	Diabetes mellitus in pregnancy: Pre-existing type 2 diabetes mellitus
Diabetes	O243	Diabetes mellitus in pregnancy: Pre-existing diabetes mellitus, unspecified
Diabetes	O244	Diabetes mellitus arising in pregnancy
Diabetes	O249	Diabetes mellitus in pregnancy, unspecified
Diabetes	Y423	Insulin and oral hypoglycaemic [antidiabetic] drugs
Hypertension	6177	“Do you regularly take any of the following medications?”- Answer: “Blood pressure medication”
Hypertension	6153	“Do you regularly take any of the following medications?”- Answer: “Blood pressure medication”
Hypertension	20002	“hypertension”
Hypertension	I10X	Essential (primary) hypertension
Hypertension	I110	Hypertensive heart disease with (congestive) heart failure
Hypertension	I119	Hypertensive heart disease without (congestive) heart failure
Hypertension	I120	Hypertensive renal disease with renal failure
Hypertension	I129	Hypertensive renal disease without renal failure
Hypertension	I130	Hypertensive heart and renal disease with (congestive) heart failure
Hypertension	I131	Hypertensive heart and renal disease with renal failure
Hypertension	I132	Hypertensive heart and renal disease with both (congestive) heart failure and renal failure
Hypertension	I139	Hypertensive heart and renal disease, unspecified

Condition	ICD code or data field	Code description
High cholesterol	20002	“high cholesterol”
High cholesterol	6153	“Do you regularly take any of the following medications?”- Answer: “Cholesterol lowering medication”
High cholesterol	6177	“Do you regularly take any of the following medications?”- Answer: “Cholesterol lowering medication”
High cholesterol	E780	Pure hypercholesterolaemia
High cholesterol	E782	Mixed hyperlipidaemia
High cholesterol	E783	Hyperchylomicronaemia
High cholesterol	E784	Other hyperlipidaemia
High cholesterol	E785	Hyperlipidaemia, unspecified

Table 2.2. *ICD: international classification of disease.*

2.2.3 Ascertainment of prevalent and incident cardiovascular disease

Cardiovascular disease was ascertained from combining self-report at verbal interview, relevant ICD codes from HES, and UK Biobank Algorithmically defined outcomes. The latter combines data from multiple data sources and is produced by UK through a formal adjudication process[66]. Using this approach, we were able to define all cardiovascular diseases, which we subcategorised into broad disease subtypes (e.g., IHD), but with the ability to examine specific conditions in each category (**Table 2.3**). For incident outcomes, we selected events occurring after baseline as recorded by algorithmically defined outcomes, HES, or death register data.

Table 2.3. Approach to definition of cardiovascular disorders in the UK Biobank

Source	Definitions and disease categories
	Ischaemic heart disease
Self-report	Angina (data field 20002)
Self-report	heart attack/myocardial infarction (data field 20002)
Algorithm	AMI on algorithmically defined outcomes (data field 42000)
ICD10	I20 Angina pectoris
ICD10	I21 Acute myocardial infarction
ICD10	I22 Subsequent myocardial infarction
ICD10	I23 Certain current complications following acute myocardial infarction
ICD10	I24 Other acute ischaemic heart diseases
ICD10	I25 Chronic ischaemic heart disease
	Valvular heart disease
Self-report	mitral stenosis (data field 20002)
Self-report	mitral regurgitation / incompetence (data field 20002)
Self-report	aortic valve disease (data field 20002)
Self-report	aortic stenosis (data field 20002)
Self-report	aortic regurgitation / incompetence (data field 20002)
ICD10	I34.0 Mitral (valve) insufficiency
ICD10	I34.2 Nonrheumatic mitral (valve) stenosis
ICD10	I34.8 Other nonrheumatic mitral valve disorders

Source	Definitions and disease categories
ICD10	I34.9 Nonrheumatic mitral valve disorder, unspecified
ICD10	I35.0 Aortic (valve) stenosis
ICD10	I35.1 Aortic (valve) insufficiency
ICD10	I35.2 Aortic (valve) stenosis with insufficiency
ICD10	I35.8 Other aortic valve disorders
ICD10	I35.9 Aortic valve disorder, unspecified
ICD10	I36.0 Nonrheumatic tricuspid (valve) stenosis
ICD10	I36.1 Nonrheumatic tricuspid (valve) insufficiency
ICD10	I36.8 Other nonrheumatic tricuspid valve disorders
ICD10	I36.9 Nonrheumatic tricuspid valve disorder, unspecified
ICD10	I37.0 Pulmonary valve stenosis
ICD10	I37.1 Pulmonary valve insufficiency
ICD10	I37.2 Pulmonary valve stenosis with insufficiency
ICD10	I37.8 Other pulmonary valve disorders
ICD10	I37.9 Pulmonary valve disorder, unspecified
ICD10	I38 Endocarditis, valve unspecified
ICD10	I39.0 Mitral valve disorders in diseases classified elsewhere
ICD10	I39.1 Aortic valve disorders in diseases classified elsewhere
ICD10	I39.3 Pulmonary valve disorders in diseases classified elsewhere
ICD10	I39.4 Multiple valve disorders in diseases classified elsewhere
ICD10	I39.8 Endocarditis, valve unspecified, in diseases classified elsewhere
ICD10	I05 Rheumatic mitral valve diseases
ICD10	I06 Rheumatic aortic valve diseases
ICD10	I07 Rheumatic tricuspid valve diseases
ICD10	I08 Multiple valve diseases
	Non-ischaemic cardiomyopathies
Self-report	Cardiomyopathy (data field 20002)
Self-report	hypertrophic cardiomyopathy (hcm/hocm) (data field 20002)
ICD10	I42.0 Dilated cardiomyopathy
ICD10	I42.1 Obstructive hypertrophic cardiomyopathy
ICD10	I42.2 Other hypertrophic cardiomyopathy
ICD10	I42.5 Other restrictive cardiomyopathy
ICD10	I42.6 Alcoholic cardiomyopathy
ICD10	I42.7 Cardiomyopathy due to drugs and other external agents
ICD10	I42.8 Other cardiomyopathies
ICD10	I42.9 Cardiomyopathy, unspecified
ICD10	I43.0 Cardiomyopathy in infectious and parasitic diseases classified elsewhere
ICD10	I43.1 Cardiomyopathy in metabolic diseases
ICD10	I43.2 Cardiomyopathy in nutritional diseases
ICD10	I43.8 Cardiomyopathy in other diseases classified elsewhere
ICD10	I11.0 Hypertensive heart disease with (congestive) heart failure
ICD10	I11.9 Hypertensive heart disease without (congestive) heart failure
ICD10	I13.0 Hypertensive heart and renal disease with (congestive) heart failure
ICD10	I13.1 Hypertensive heart and renal disease with renal failure
ICD10	I13.2 Hypertensive heart and renal disease with both (congestive) heart failure and renal failure
ICD10	I13.9 Hypertensive heart and renal disease, unspecified
	Heart failure (unspecified aetiology)
Self-report	heart failure/pulmonary odema (data field 20002)
ICD10	I50.0 Congestive heart failure
ICD10	I50.1 Left ventricular failure

Source	Definitions and disease categories
ICD10	I50.9 Heart failure, unspecified
	Cardiac arrhythmia
Self-report	sick sinus syndrome (data field 20002)
Self-report	svt / supraventricular tachycardia (data field 20002)
Self-report	atrial fibrillation (data field 20002)
Self-report	atrial flutter (data field 20002)
ICD10	I44.1 Atrioventricular block, second degree
ICD10	I44.2 Atrioventricular block, complete
ICD10	I45.6 Preexcitation syndrome
ICD10	I46.0 Cardiac arrest with successful resuscitation
ICD10	I46.1 Sudden cardiac death, so described
ICD10	I46.9 Cardiac arrest, unspecified
ICD10	I47.0 Re-entry ventricular arrhythmia
ICD10	I47.1 Supraventricular tachycardia
ICD10	I47.2 Ventricular tachycardia
ICD10	I47.9 Paroxysmal tachycardia, unspecified
ICD10	I48.0 Paroxysmal atrial fibrillation
ICD10	I48.1 Persistent atrial fibrillation
ICD10	I48.2 Chronic atrial fibrillation
ICD10	I48.3 Typical atrial flutter
ICD10	I48.4 Atypical atrial flutter
ICD10	I48.9 Atrial fibrillation and atrial flutter, unspecified
ICD10	I49.0 Ventricular fibrillation and flutter
ICD10	I49.5 Sick sinus syndrome

Table 2.3. *ICD: international classification of disease.*

2.2.4 General approach to statistical methods

2.2.4.1 Descriptive summary statistics

Categorical variables are summarised as frequencies and percentages. For continuous numerical variables, we present mean and standard deviation (SD) or, for variables with significantly skewed distributions, median and interquartile range (IQR).

2.2.4.2 Approach to modelling

The general principles outlined in **Section 1.1.4** were considered when planning studies. At the outset, the study question and objectives were explicitly outlined. The analysis sample for each study was then defined based on selecting an appropriate sample for the study question whilst maximising sample size. We then defined the exposures and outcomes of interest with deliberate consideration given to potential confounders and biological mediators. True confounders were considered variables that associated with both the exposure and outcome. Mediators were considered as covariates potentially on the causal pathway. Covariates were defined a priori based on existing evidence and biological plausibility. In cases where there was uncertainty about the confounding effect of a

variable, we performed preliminary analysis to test its associations with the exposure and outcome. In general, the main models include adjustment for true confounders allowing quantification of the magnitude of the exposure-outcome association. In selected cases, we gave consideration to the impact of mediating variables, either through formal mediation analysis or additional adjustment for these variables. Multivariable linear regression models were used as the default approach to modelling. We tested for multicollinearity between covariates using variance inflation factor (VIF) setting a conservative limit (VIF <2). Where there was indication of possible non-linearity of relationships, this was explored either with polynomial terms or using cubic spline models. When the outcome of interest was an incident event, we used competing risk multivariable regression models, as per Fine and Gray methods[67]. When appropriate, p-values were corrected for multiple testing.

2.2.5 Conventional CMR metrics

2.2.5.1 LV and RV indices

The UK Biobank acquisition protocol is discussed in **Section 2.1.6** and detailed in a separate publication[36]. Assessment of the left and right ventricles (LV, RV) included a complete short axis stack acquired using balanced steady-state free precession sequences. The first 5,000 CMR scans were manually analysed according to a pre-defined segmentation protocol[60] using CVI[42]® post-processing software (Version 5.1.1, Circle Cardiovascular Imaging Inc., Calgary, Canada). LV endocardial and epicardial borders were manually contoured in end-diastole and end-systole in the short axis view. The first phase of acquisition was selected as end-diastole. End-systole was defined as the phase with the smallest mid-ventricular LV intra-cavity blood pool as determined by visual inspection. The most basal slice for the LV was selected when at least half of the LV blood pool was surrounded by myocardium. LV papillary muscles were excluded from LV mass. RV endocardial borders were traced in end-diastole and end-systole with volumes below the pulmonary valve plane considered as part of the RV. This ground truth manual analysis dataset was used to develop a fully automated image analysis pipeline with inbuilt quality control, which has been applied to the first 20,000 UK Biobank CMR studies[62]. Details of reproducibility performance of the automated algorithm are available in a dedicated publication[60,62]. This work has generated the following metrics: LV and RV volumes in end-diastole and end-systole, LV and RV ejection fraction, LV and RV stroke volume, and LVM.

2.2.6 Measures of arterial compliance

2.2.6.1 Aortic distensibility

As discussed in **Section 2.1.6**, AD is a direct measure of local aortic compliance. Higher distensibility indicates a more compliant aorta and better arterial health. AD is calculated by considering the relative in aortic cross-sectional area from systole to diastole (aortic strain) per unit pressure (**Equation 1**)[68].

Equation 1. Formula for calculation of aortic distensibility

$$AD = \frac{A_{MAX} - A_{MIN}}{A_{MIN} \times CPP}$$

Equation 1. where A_{max} is the maximal and A_{min} the minimal aortic lumen area (mm^2). AD: aortic distensibility; CPP: central pulse pressure.

In the UK Biobank, aortic strain was measured from segmentation of the ascending and descending aorta on transverse cine CMR images at the level of the pulmonary artery bifurcation (**Figure 2.2**). Central pulse pressure was derived from Vicorder® readings taken at the time of imaging. A fully automated image analysis workflow has been developed for generation of AD measures in the UK Biobank[63]. This pipeline has been validated on a large subset of UK Biobank studies (n=5,065) and applied to the first 20,000 scans[63]. Thus, AD measured at the ascending aorta and the proximal descending aorta is available for 20,000 UK Biobank participants.

Figure 2.2. Measurement of aortic distensibility from cardiovascular magnetic resonance images in the UK Biobank

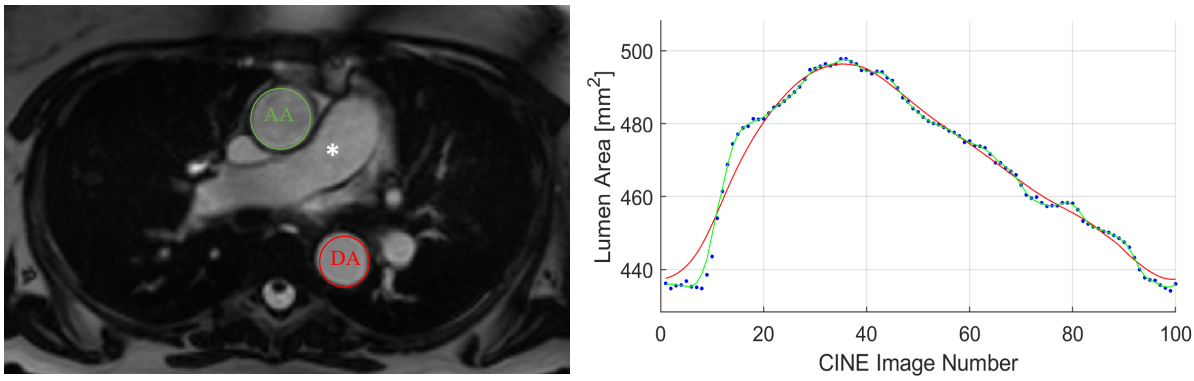

Figure 2.2. *Aortic distensibility determined by considering systolic-diastolic variation in cross-sectional lumen area of the ascending (AA) and descending aorta (DA) measured at the level of the pulmonary artery bifurcation (*) on transverse cine cardiac magnetic resonance images. Image used with permission of UK Biobank and reproduced from Raisi-Estabragh et al. 2020*[69]

2.2.6.2 Arterial stiffness index

ASI is an indirect measure of large artery stiffness. It is an independent measure of cardiovascular risk and can be measured non-invasively through analysis of the contour of a pulse waveform obtained at the fingertip using an infra-red sensor[58,59]. This digital volume pulse represents the time it takes for the pulse waveform to travel through the arterial tree and be reflected back to the finger[58]. Lower ASI values indicate greater arterial compliance and better vascular health.

In the UK Biobank, ASI was measured at the baselined visit using the PulseTrace PCA2 (CareFusion, USA). Measurement was in lined with a pre-defined standard operating procedure, which is detailed in a dedicated document[70]. The participant was asked to remove or loosen restrictive clothing from the upper arm and seated with both feet flat on the floor and their arm fully supported on the desktop in the supine position. Prior to measurement recording the participant was asked to take five slow breaths in and out. The infra-red sensor was then clipped onto a finger. Measurement was preferentially taken from the index finger of the non-dominant hand, but any finger/thumb could be used. If the signal at the fingertip was poor due to dark nail varnish, the sensor could be placed transversely across the finger. Measurement was taken over 10-15s. The device generated a pulse trace with a systolic and diastolic peak and the time interval between the two peaks (**Figure 2.3**).

Figure 2.3. Illustration of a digital volume pressure waveform from PulseTrace sensor

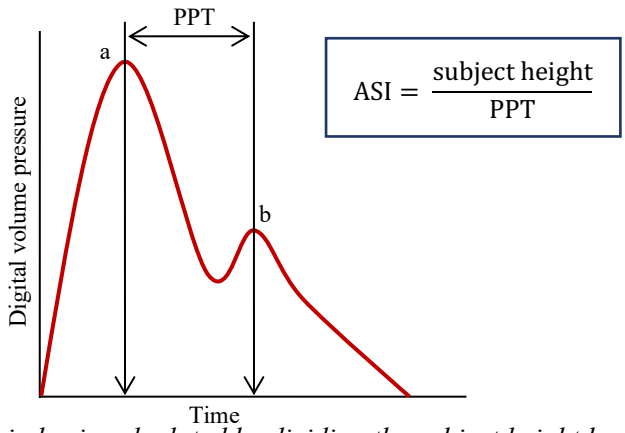

Figure 2.3. *Arterial stiffness index is calculated by dividing the subject height by the time between the systolic (a) and diastolic (b) peaks [peak-to-peak time (PPT)]. Reproduced from Raisi-Estabragh et al. 2020*[69].

The peak-to-peak time (PPT) is an estimate of the time taken to the pulse to propagate to the root of the subclavian artery and return to the fingertip. Faster reflections indicate stiffer arteries. As the path length for the pulse is dependent on the individuals' height, ASI is obtained by dividing height by PPT. ASI is reported in the UK Biobank in m/s. It was a later addition to the UK Biobank protocol

and is available for 169,791 participants at baseline and for all participants completing the imaging study.

2.3 CMR radiomics

Radiomics is a novel image analysis technique, which allows derivation of a multitude of shape and texture quantifiers from voxel-level data[71]. Radiomics analysis does not require any dedicated acquisitions and may be retrospectively applied to region(s) of interest (ROI) on existing standard of care images from any modality. Indeed, existing work describes application of radiomics to computed tomography, ultrasound, positron emission tomography, and magnetic resonance images. Radiomics quantifiers (or features) provide deeper quantitative imaging phenotypes than conventional analysis methods. As such, they may provide novel insights into end-organ effect of various exposures. Furthermore, radiomics features may also be considered as predictor variables in statistical (or machine learning) models for disease discrimination or outcome prediction.

The most extensive work on radiomics has been within oncology, where radiomics models have demonstrable utility for tumour classification[72], prediction of treatment response[73,74], and prognostication[75]. There is growing interest in application of radiomics analysis to cardiac imaging. Early attempts to apply radiomics analysis to echocardiography produced promising results for discrimination of conditions such as cardiac amyloid[76] and haemochromatosis[77]. However, poor reproducibility of radiomics features from echocardiography severely limited the generalisability of these models. Radiomics analysis has also been applied to cardiac computed tomography images, producing promising results from detailed quantitative characterisation of coronary plaques and perivascular fat[78,79]. CMR is a highly attractive modality for radiomics analysis, due to highly reproducible standardised views and availability of large imaging datasets. Limited studies have demonstrated the feasibility and potential clinical value of CMR radiomics for disease discrimination and outcome prediction[80–89]. Thus, CMR radiomics has potential as a novel imaging biomarker.

In the remainder of this section, we provide a general description of CMR radiomics pipeline, existing literature on the application of this methodology, and apply the technique in the study presented in **Chapter 6.**

2.3.1 The CMR radiomics pipeline

2.3.1.1 Image acquisition

Radiomics analysis can be applied to standard of care images with no requirement for dedicated protocols or acquisitions. Any image from the study may be selected for radiomics analysis. The short axis stack is the most convenient choice, as it allows use of existing segmentations for standard volumetric assessment avoiding extra image analysis steps.

2.3.1.2 Volume segmentation

Any ROI can be selected for analysis. For example, we could select a localised area in the LV myocardium which is suspicious for disease. Alternatively, we could select the entire LV myocardium for analysis. Using existing epicardial and endocardial contours in short axis stack images we can define three ROIs for analysis: LV cavity, LV myocardium, and RV cavity. Radiomics features may then be extracted from these defined regions within the image. Variation in contouring can have substantial impact on radiomics features and it is important that a standardised approach, preferably with minimal manual adjustment, is taken.

2.3.1.3 Radiomics feature extraction

Radiomics features may be extracted from defined ROIs using pipelines developed in-house or open access platforms, such as, pyradiomics[90]. Radiomics features have pre-defined mathematical definitions and are calculated in a standardised manner. Prior to feature extraction, normalisation techniques may be applied to images to ensure that variation in signal intensities reflected in radiomics features represent underlying biology rather than variation in image acquisition parameters. There are three categories of radiomics features: shape, first-order, and texture. Radiomics shape features provide advanced geometric quantifiers of the defined ROI. The first-order and texture are derived from pixel signal intensity levels (brightness) and describe the global distribution of signal intensity levels and the pattern of signal intensities. Intensity-based features are typically extracted from the whole or selected areas within the myocardium.

2.3.1.4 Radiomics shape features

Data derived from the ROI contours is used to build a 3D image mask, from which shape features are calculated. Radiomics shape features include basic measures such as volume and axis dimensions, as well as more complex geometric measures such as sphericity (how much the overall shape of the ROI resembles a sphere) or elongation (**Figure 2.4)**. For example, standard epicardial and endocardial

contours from a short axis cine stack may be used to select radiomics features from three ROIs: LV myocardium, LV cavity, and RV cavity.

Figure 2.4. Image mask derived from segmented cardiovascular magnetic resonance image and selected radiomics shape features

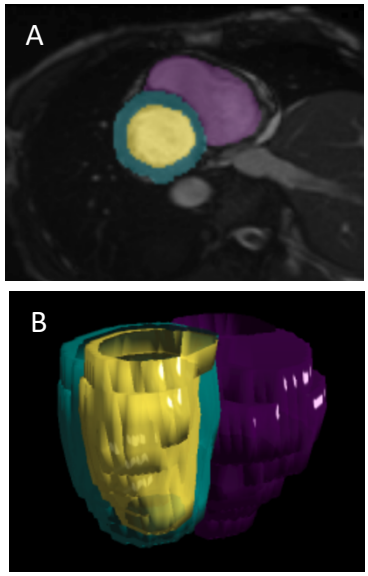

Volume
Surface area
Surface area to volume ratio
Sphericity
Spherical Disproportion
Compactness
Max 3D diameter
Max 2D diameter
Major Axis
Minor Axis
Least Axis
Elongation
Flatness

Figure *2.4. Panel A:* *Conventional epicardial and endocardial contours from short axis cine images have been used to define three regions of interest for radiomics analysis: LV myocardium (turquoise), LV cavity (yellow), and RV cavity (purple).* ***Panel B:*** *The contours are used to build a 3D image mask of the three ROIs. Radiomics shape features are derived from these masks and include conventional and more advanced geometric quantifiers (exemplar list on right). CMR: cardiac magnetic resonance; LV: left ventricle; RV: right ventricle; ROI: region of interest). Reproduced from Raisi-Estabragh et al. 2020*[71].

2.3.1.5 Radiomics first-order features

Radiomics first-order features quantify the global distribution of pixel signal intensities within the defined ROI. Each pixel within the ROI is assigned an intensity (brightness) level. The intensity levels and the frequency with which they appear within the defined ROI are then simply plotted as a histogram. First-order features are histogram-based statistics derived from this signal intensity histogram (**Figure 2.5**). They include familiar metrics such as mean, median, and standard deviation, as well as less familiar measures such as, kurtosis (pointiness), entropy (disorder), and skewness.

Figure 2.5. Selected first-order histogram-based statistics to describe global signal intensity distribution within the selected region of interest

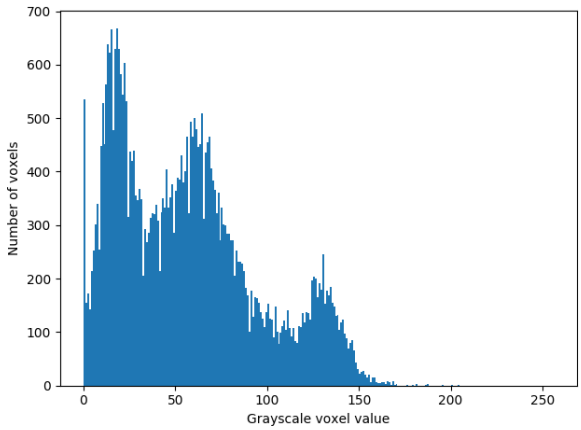

Minimum	Robust mean absolute deviation
Maximum	Root mean squared
10th Percentile	Standard deviation
90th Percentile	Skewness
Mean	Kurtosis
Median	Variance
Interquartile Range	Uniformity
Range	Energy
Mean absolute deviation	Entropy

Figure 2.5. *The figure depicts a histogram of signal intensity values observed in the region of interest selected for radiomics analysis. The x axis represents the signal intensity value of the voxels within the region of interest and the y axis the frequency with which these signal intensities values are observed. Below the figure we present a selection of the summary statistics derived from the histogram (histogram-based statistics). Reproduced from Raisi-Estabragh et al. 2020*[71].

2.3.1.6 Radiomics texture features

First-order features quantify the intensity levels within the ROI as a whole, however, they do not provide information on the relationship of signal intensities between neighbouring ROIs. In order to quantify inter-pixel relationships, more complex mathematical approaches are required. The first step involves building a 'signal intensity matrix' (**Figure 2.6A**). To do this, a signal intensity level (brightness level) is allocated to each pixel within the ROI. This data is then displayed in a matrix with positioning of pixels in the matrix corresponding to their positions within the ROI (this means that each pixel would have the same neighbouring pixels in the matrix as they do in the ROI). Texture features derived from this matrix are intended to quantify heterogeneity, repeatability, and complexity of the signal intensity matrix[91,92]. They are calculated by application of various mathematical

processes to new matrices which are constructed based on specified rules from the signal intensity matrix. The grey level co-occurrence matrix (GLCM) is commonly used to consider the relationship between pixels pairs. This secondary matrix is constructed by tabulating the frequency of different signal intensity pairings occurring within the signal intensity matrix (**Figure 2.6B)**. Different mathematical processes are applied to the GLCM to calculate, as per standardised definitions, measures, such as angular second moment (homogeneity), contrast (local variation), and entropy (disorder)[93]. Another commonly used matrix is the grey level run length matrix (GLRLM)[94–97]. This matrix allows consideration of the spatial relationship of any number of voxels (not just pairs). The GLRLM is tabulated by recording the number of times a certain intensity level is recorded in an uninterrupted run within the signal intensity matrix in a specified direction (**Figure 2.6C**). In a simplified manner, we can think of this as the number of pixels with the same intensity level occurring in an uninterrupted run. The GLRLM is used to compute features such as short-run emphasis, run length non-uniformity, and run entropy.

Several other matrices, constructed according to different rules, are available for calculation of additional texture features [grey level size zone matrix (GLSZM), grey level difference matrix (GLDM), neighbouring grey tone difference matrix (NGTDM)].

2.3.2 Making sense of radiomics features

CMR radiomics analysis will yield a large number (hundreds) of features per study. The deep phenotyping provided can be used to gain novel insights into associations between cardiac phenotypes and exposures/outcomes. The features may also be used as predictor variables in models for disease discrimination or outcome prediction. As the number of features is large (often larger than number of study subjects), it is common to undertake a feature reduction/selection process prior to model building. This is to avoid overfitting the model (where the model is too closely modelled to the training set such that it picks up noise from the training set and thus performs poorly when applied to external datasets), to remove non-robust features, and features that represent inter-related metrics. The goal is to reduce the number of features based on robustness and non-redundancy. Recent work has provided guidance on repeatability and reproducibility performance of CMR radiomics features, this work may be used as a reference to guide selection of the most robust features in modelling[98,99]. From the remaining robust features, it is advisable to exclude inter-related features. A number of different strategies may be undertaken, including clustering analyses or forward feature selection. The reduced feature set may then be taken forward for modelling. Although simple methods, such as logistic regression, may be attempted, optimal model performance is often achieved using machine learning techniques such as support vector machine.

Figure 2.6. Simplified worked example of grey level co-occurrence and run-length matrices

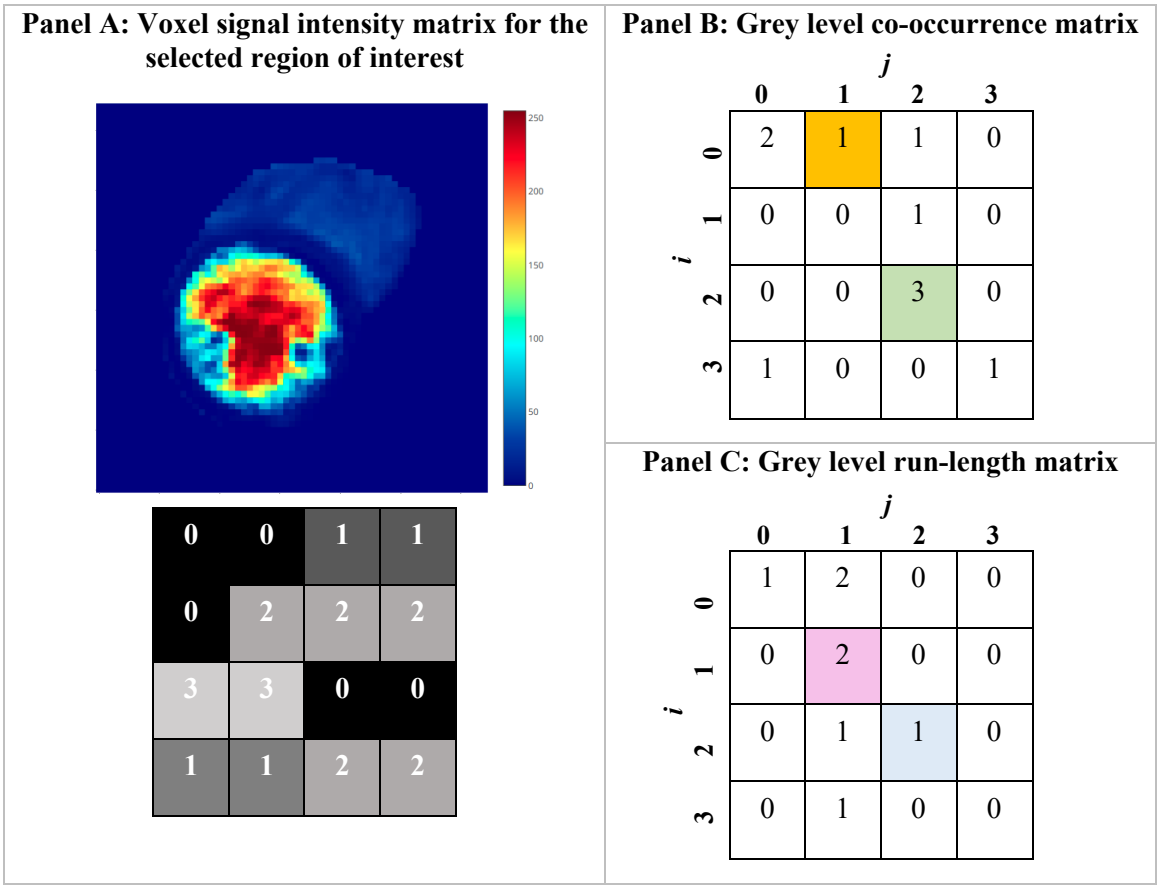

Figure 2.6. Panel A: *A signal intensity (SI) level is assigned to each voxel within the selected region of interest and tabulated in a matrix. In this example we suppose a 4×4 matrix with 16 voxels at four signal intensity levels.* ***Panel B:*** *Grey-level co-occurrence matrix corresponding to Panel A. In this example, we will consider any voxel with SI j, that appears to the right of a reference voxel with SI of i. e.g. to fill the orange cell (j=1, i=0), we count one instance in the Panel A matrix, where a voxel with signal intensity level of 1 (j=1) appears to the right of a voxel with signal intensity of 0 (i=0). Hence, we fill the cell in the GLCM matrix with the number one. Similarly, for the green cell (j=2, i=2), we observe that in the whole of the matrix in Panel A, there are three instances where a voxel with SI value of 2 (j=2) appears to the right of a voxel with the SI of 2 (i=2), hence cell (2, 2) is filled with the number 3. In the same way, the rest of the matrix is completed.* ***Panel C:*** *Grey-level run-length matrix corresponding to Panel A. To complete this matrix, we consider the number of time Panel A contains an uninterrupted train of length j (measured in number of voxels) with SI of i. For example, consider the pink cell (j=2, i=1); in the matrix of Panel A, we count two instances of voxel with SI of 1 (i=1) occurring in an uninterrupted run of length 2 (j=2), hence the cell is filled with the number 2. Similarly, consider the blue cell (j=3, i=2), in our SI matrix, we count one instance where SI of 2 (i=2) appears in an uninterrupted run of three voxels (j=3), hence this cell is filled with the number 1. Reproduced from Raisi-Estabragh et al. 2020*[71]

2.3.3 Review of existing work in CMR radiomics

Several studies have demonstrated the feasibility and potential clinical utility of CMR radiomics to distinguish healthy and disease states. Baessler et al.[80] demonstrate significant differences between texture features of individuals with HCM (n=32) and healthy comparators (n=30). They identify GLevNonU (Grey-level non-uniformity), a feature derived from the GLRLM indicative of high heterogeneity of signal intensities, as the best discriminator of the two cohorts. This is interesting, because myocardial disarray and hypertrophy are key hallmarks of HCM and so the observations by Baessler et al.[80] suggest, that radiomics texture features may reflect tissue level myocardial alterations in a pathologically meaningful manner. In a similar vein, Cetin et al.[100] demonstrate the ability of radiomics models to distinguish, with good accuracy, the hearts of individuals with hypertension from those of healthy controls. The model comprised eleven LV texture features, suggesting that individuals with hypertension have myocardial level alterations detectable with radiomics analysis. Indeed, in a larger study, Cetin et al.[82] demonstrate superior discrimination of several key cardiovascular risk factors (smoking, diabetes, hypertension, high cholesterol – vs healthy controls) with CMR radiomics models compared to conventional CMR indices.

Radiomics models also have potential capability for distinguishing different disease states. For example, Neisius et al.[83] demonstrate that radiomics analysis applied to native T1 maps provides incremental diagnostic accuracy over global T1 measures in distinction of hypertensive heart disease from HCM. In another study, Baessler et al.[84] demonstrate the superior diagnostic accuracy of radiomics texture analysis applied to T1 and T2 maps in discriminating biopsy proven infarct-like acute myocarditis in comparison to mean T1, mean T2, or Lake Louise diagnostic criteria.

Reliable assessment for myocardial infarction is a major strength of CMR and accounts for many clinical CMR requests. Existing approaches for detection of myocardial infarction are based on visual inspection of late gadolinium enhancement (LGE) images. These images necessitate administration of exogenous gadolinium-based contrast agents followed by a pause of approximately 10-20 minutes prior to image acquisition. Although modern cyclical gadolinium-based contrast agents have an excellent safety profile, there is risk of severe allergic reactions, nephrogenic sclerosing fibrosis (particularly where renal function is impaired), and possible adverse effects related to intracranial gadolinium deposition[29,101]. Furthermore, the wait time prior to image acquisition is a significant limiting factor. Several radiomics studies have demonstrated the possibility of making clinical distinctions that would ordinarily require contrast images, through analysis of gadolinium-free images. Such analysis is clearly highly desirable both from a safety and time efficiency perspective. For example, Baessler et al.[85] demonstrate accurate discrimination of studies with myocardial infarction from healthy controls through texture analysis of contrast free cine images. Similarly,

Larroza et al.[86] were able to discriminate non-viable myocardium (as per LGE) using texture analysis of non-contrast cine images. In another study, Larroza et al.[87] demonstrate the ability of texture analysis to accurately identify myocardial infarction from non-contrast cine images. Furthermore, they demonstrate the ability to distinguish acute myocardial infarction (within a week of imaging) from chronic myocardial infarction (>6 months before imaging) from radiomics analysis of LGE images.

Limited studies report on the potential of radiomics models for prediction of key health outcomes. In a study of 34 individuals with chronic myocardial infarction, Kotu et al.[88] report incremental value of texture features extracted from LGE scar, over scar size and location in predicting life-threatening arrhythmias. Amano et al.[102] demonstrate differences in textural features of LGE images in HCM patients with a history of ventricular tachycardia compared to those with no history of arrhythmia. Furthermore, Cheng et al.[89] demonstrate strong association of LGE texture features with a composite of several adverse endpoints (including all-cause mortality and life-threatening arrhythmia) in individuals with HCM and impaired LV systolic function.

Overall, work to date demonstrates the potential of CMR radiomics to enhance existing image analysis approaches and thus improve disease discrimination and outcome prediction. Radiomics may be applied to existing standard of care images without the need for dedicated acquisitions or image processing. As such radiomics analysis may be readily implemented into existing clinical pathways. The possibility of deriving from radiomics analysis of non-contrast images equivalent information to contrast enhanced images is highly desirable. Further, the limited CMR radiomics literature and the more extensive work from radiomics in cancer imaging suggest that image phenotype deciphered through radiomics texture analysis may represent cellular pathology, with the potential to provide, non-invasively, unique insights into disease pathophysiology[103].

3 Resting heart rate and incident cardiovascular outcomes

3.1 Abstract

Objective: We sought to define the sex, age, and disease-specific associations of resting heart rate with cardiovascular and mortality outcomes in 502,534 individuals from the UK Biobank over 7–12 years of prospective follow-up.

Methods and Results: The primary outcomes were all-cause, cardiovascular, and IHD mortality. Additional outcomes included incident AMI, fatal AMI, and cancer mortality. We considered a wide range of confounders and the effects of competing hazards. Results are reported as hazard ratios (HR) for all-cause mortality and sub-distribution hazard ratios (SHR) for other outcomes with corresponding 95% confidence intervals (CI) per 10bpm increase in heart rate. In men, for every 10bpm increment of heart rate there was 22% (HR: 1.22; 95% CI: 1.20, 1.24; $p=3\times10^{-123}$) greater hazard of all-cause mortality and 17% (SHR: 1.17; 95% CI: 1.13, 1.21; $p=5.6\times10^{-18}$) greater hazard of cardiovascular mortality; for women, corresponding figures were 19% (HR: 1.19; 95% CI: 1.16, 1.22; $p=8.9\times10^{-45}$) and 14% (SHR: 1.14; 95% CI: 1.07, 1.22; $p=8.0\times10^{-5}$). Associations between heart rate and ischaemic outcomes were of greater magnitude amongst men than women, but with similar magnitude of association for non-cardiovascular cancer mortality [men (SHR: 1.18; 95% CI: 1.15, 1.21; $p=5.2\times10^{-46}$); women (SHR: 1.15; 95% CI: 1.11, 1.18; $p=3.1\times10^{-18}$)]. The magnitude of associations with all-cause, incident AMI, and cancer mortality was greater at younger than older ages.

Conclusions: Resting heart rate is an independent predictor of mortality, with sex-, age-, and disease-specific associations. Ischaemic cardiovascular diseases appeared an important driver of this relationship in men, but not in women. For both men and women, associations were more marked at younger ages.

3.2 Background

Previous work suggests that resting heart rate may have potential as a low tech, inexpensive, and reliable risk predictor. Higher resting heart rate has been linked to greater risk of all-cause mortality in diverse healthy and disease cohorts[104–108]. There is consensus that for men, cardiovascular mortality is the main driver of excess mortality in this relationship. However, in women, the association of heart rate with cardiovascular mortality is inconsistently reported, ranging from a more pronounced relationship than men[109] to a weakened or absent association[110–113].

Whilst sex differential patterns of cardiovascular disease are widely recognised[9], potential sex specific associations of heart rate with cardiovascular mortality have not been adequately addressed. Women are under-represented in existing studies with several reports limited to men only cohorts[114–116]. Similarly, existing literature suggests a modifying effect of age, however findings from these reports are inconclusive[117–119]. Existing studies of the possible interaction effect of sex and age are limited by small sample sizes, lack of consideration of specific causes of death, and inadequate adjustment for confounders and competing outcomes.

In this study, we report the sex, age, and cause-specific associations of resting heart rate with incident cardiovascular and mortality outcomes in the UK Biobank cohort.

3.3 Methods

3.3.1 Study population

This analysis includes all UK Biobank participants who completed baseline assessment (n=502,534), further details on the cohort are presented in **Section 2.1.**

3.3.2 Measurement of resting heart rate

There was measurement and recording of resting heart rate at the baseline UK Biobank visit in accordance with a pre-defined standard operating procedure. The full protocol is published online[120]. Pulse rate was taken at the time of blood pressure measurement using the Omron 705 IT electronic blood pressure monitor (OMRON Healthcare Europe B.V. Kruisweg 577 2132 NA Hoofddorp). Participants were asked to sit with the soles of their feet resting on the floor, feet parallel to each other, and toes pointing forward. Researchers were instructed to avoid engaging in conversation with participants. Measurement was taken, preferably, from the left arm. In cases where using the left arm

was not possible (amputation, vascular shunt, axillary clearance), measurement was taken from the right arm. Tight or restrictive clothing on the upper arm was loosened or removed. The participant rested their arm on the desktop and was asked to take several slow relaxed breaths in and out. The circumference of the upper arm was measured at the midpoint to select the correct cuff size. The researcher started the measurement by selecting 'start' on the monitor; blood pressure and heart rate measures were generated by the machine and auto populated into the participants' computer records. After obtaining one measurement, the inflation tube was disconnected from the monitor, the cuff remained in place but was allowed to fully deflate. The participant was asked to gently shake and open and close their hand. The blood pressure and pulse rate measurements were repeated after waiting for a minimum of one minute. There was an inbuilt timer in the measurement device, which ensured that it was not possible to take a second measurement before one minute has lapsed. In our analysis, we used the mean of the two heart rate readings.

3.3.3 Ascertainment of outcomes

We considered three main outcomes: all-cause mortality, cardiovascular disease mortality, and IHD mortality. The secondary outcomes included: incident AMI, fatal AMI, and cancer mortality. We considered outcomes occurring after baseline (2006–2010) to the latest available UK Biobank censor dates (mortality outcomes: 31/01/2018, incident AMI: 31/03/2017) giving follow-up duration of 7-12 years.

The mortality outcomes were ascertained from death register records of 'primary cause of death'. For cardiovascular mortality, we included participants with record of primary cause of death due to any cardiovascular diseases defined from ICD codes as outlined in **Section 2.2.3** and in **Table 2.3**. IHD mortality included deaths due to any manifestation of IHD as per ICD codes in **Table 2.3**. Incident and fatal AMI were derived from UK Biobank algorithmically defined outcomes, the outcome adjudication process for which is detailed in a dedicated document[66]. We considered cancer mortality as a secondary outcome representing a major cause of non-cardiovascular mortality, defined as primary cause of death due to any cancer.

3.3.4 Statistical analysis

Statistical analysis was with R studio version 3.6.0 [https://www.R-project.org/] and Stata version 14 [StataCorp. 2015. Stata Statistical Software: Release 14. College Station, TX: StataCorp LP]. We modelled associations with all-cause mortality using Cox proportional hazard models. For all other outcomes, we used competing risk regression models, as per Fine and Gray[67]. Heart rate was

considered as a continuous exposure variable. Result of associations are reported as hazard ratios (HRs) for all-cause mortality and sub-distribution hazard ratios (SHRs) for all other outcomes per 10 bpm (beats per minute) increase of heart rate, with corresponding 95% confidence intervals (CIs) and p-values. We tested for non-linearity of associations for all outcomes by comparing linear and non-linear model fits. In cases where there was evidence of non-linearity, we further characterised the relationship using cubic spline models.

3.3.5 Approach to covariate adjustment

Confounders were identified a priori based on biological plausibility and existing literature and confirmed through preliminary analyses. We considered the following confounders as defined at baseline visit: age, sex, BMI, exercise level, smoking status, diabetes, hypertension, high cholesterol, deprivation, and heart rate modifying medications (**Figure 3.1**) The approach to ascertainment of covariates is as described in **Section 2.2.2.** Medications were self-reported by participants at baseline and coded by UK Biobank researchers. We considered 'heart rate modifying medications' as any formulation of beta-blockers, oral nitrates, non-dihydropyridine calcium channel blockers, amiodarone, digoxin, or flecainide. The full list of medications is presented in **Table 3.1**. We present models with sequential addition of covariates. There was no evidence of collinearity. Interactions with sex and age were investigated by adding interaction terms to the main models. Age and sex stratified analyses are presented for all outcomes. The threshold for statistical significance, for non-interaction regressions, was set at p=0.0008 after application of Bonferroni correction for multiple testing.

Figure 3.1. Confounders considered in modelling association of resting heart rate and cardiovascular outcomes

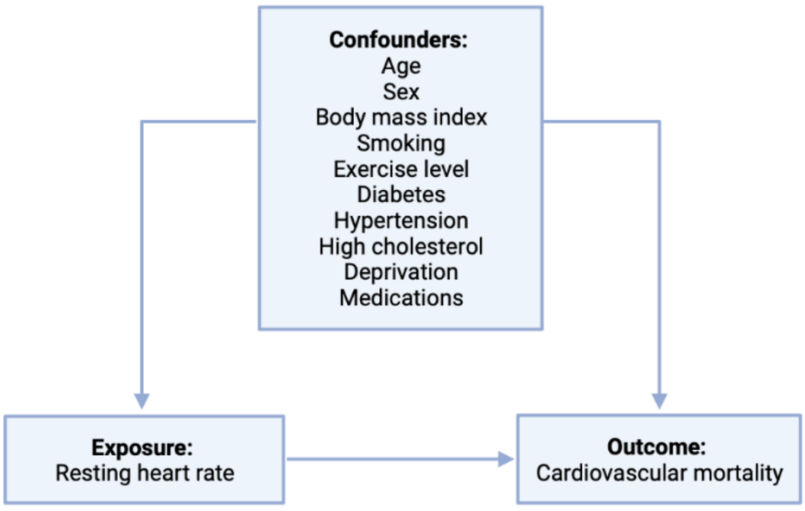

Table 3.1. List of rate-modifying medications identified from self-report

Oral betablocker preparations
Atenolol
bisoprolol
metoprolol
carvedilol
propranolol
inderal 10mg tablet
apsolol 10mg tablet
propanix 10mg tablet
sotalol
nebivolol
dorzolamide+timolol
atenolol+bendroflumethiazide
latanoprost+timolol
betaxolol
atenolol+bendrofluazide
nadolol
prindolol
Timolol
ethambutolol
pindolol
atenolol+chlortalidone
atenolol+nifedipine 50mg/20mg m/r capsule
atenolol+chlorthalidone
atenolol+co to amilozide
nadolol+bendroflumethiazide 40mg/5mg tablet
timolol maleate+bendroflumethiazide 10mg/2.5mg tablet
bisoprolol fumarate+hydrochlorothiazide 10mg/6.25mg tablet
celiprolol
labetalol
oxprenolol
acebutolol
propranolol hydrochloride+bendrofluazide 80mg/2.5mg capsule
sotalol hydrochloride+hydrochlorothiazide 80mg/12.5mg tablet
metoprolol tartrate+hydrochlorothiazide 100mg/12.5mg tablet
beta to blocker
tenormin 25 tablet
bedranol 10mg tablet
levobunolol
sotalol hydrochloride+hydrochlorothiazide 80mg/12.5mg tablet
propranolol hydrochloride+bendrofluazide 80mg/2.5mg capsule
carteolol
metoprolol tartrate+chlorthalidone 100mg/12.5mg tablet
half beta to prograne 80mg m/r capsule
beta to prograne 160mg m/r capsule
timolol maleate+co to amilozide 10mg/2.5mg/25mg tablet
cardinol 10mg tablet
Non-dihydropyridine calcium channel blocker preparations
cordilox 40mg tablet

adizem to xl plus m/r capsule
diltiazem
tildiem 60mg m/r tablet
verapamil
dilzem sr 60mg long acting m/r capsule
diltiazem hcl+hydrochlorothiazide 150mg/12.5mg m/r capsule
adizem to 60 m/r tablet
slozem 120mg m/r capsule
viazem xl 120mg m/r capsule
zemtard 120 xl m/r capsule
metazem 60mg m/r tablet
bi to carzem sr 60mg m/r capsule
adizem to xl plus m/r capsule
Angitil sr 90 m/r capsule
Oral nitrate preparations (excluding GTN spray/sl)
mycardol 30mg tablet
elantan 10 tablet
isosorbide mononitrate
ismn to isosorbide mononitrate
imdur 60mg durule
half to inderal la 80mg m/r capsule
isosorbide dinitrate
ismo to isosorbide mononitrate
isosorbide mononitrate product
xismox xl 60 m/r tablet
monomil xl 60mg m/r tablet
monomax sr 40 m/r capsule
isib 20mg tablet
ismo 10 tablet
isdn to isosorbide dinitrate
Other rate modifying drugs
amiodarone
digoxin
flecainide
digoxin product
medigoxin

3.4 Results

3.4.1 Baseline population characteristics

From the 502,534 participants who completed baseline assessment, resting heart rate was recorded for 501,331 individuals (missing for 0.002%, n=1,203) all of whom were included in the analysis. Thus, the analysis sample comprised 228,594 men and 272,737 women. Men and women had comparable median ages of 58 [50-64] years and 57 [50-63] years respectively. The mean heart rate for women was 70.3 (10.6) bpm, slightly higher than the average for men at 68.4 (11.9) bpm. There were higher rates of all vascular risk factors in men compared to women: smoking 13% vs 9%, diabetes 7% vs

4%, hypertension 33% vs 24%, high cholesterol 24% vs 14%. Detailed baseline characteristics are presented in **Table 3.2**.

Table 3.2. Baseline participant characteristics

	Whole cohort n= 501,331	Men n=228,594	Women n=272,737
Age (years)	56.5(8.1)	56.7 (8.2)	56.3 (8.0)
Townsend score	-1.29 (3.10)	-1.25 (3.16)	-1.33 (3.04)
Current smoker	52979 (10.6%)	28612 (12.5%)	24367 (8.9%)
Body mass index (kg/m^2)	27.4 (4.8)	27.8 (4.3)	27.1 (5.2)
Systolic blood pressure (mmHg)	137.9 (18.7)	140.9 (17.5)	135.3 (19.2)
Diastolic blood pressure (mmHg)	82.3 (10.1)	84.1 (10.0)	80.7 (10.0)
Diabetes	26,833 (5.3%)	16,271 (7.1%)	10,562 (3.9%)
Hypertension	141,019 (28.1%)	74,803 (32.6%)	66,216 (24.2%)
Hypercholesterolaemia	93,822 (18.7%)	55,722 (24.3%)	38,100 (13.9%)
Resting heart rate (bpm)	69.4 (11.3)	68.4 (11.9)	70.3 (10.6)
Physical Activity (MET/week)	2043.5 (2239.5) 1370 [648 to 2586]	2191.6 (2490.4) 1413 [658 to 2772]	1907.0 (1970.5) 1308 [636 to 2445]

Table 3.2. *Results are mean (standard deviation), number (percentage), or median [interquartile range]. AMI: acute myocardial infarction; bpm: beats per minute; MET: metabolic equivalent minutes.*

3.4.2 Follow up and number of events

Median duration of follow-up from baseline was 9.0 [8.2-9.7] years for mortality outcomes and 8.1 [7.5-8.8] years for incident AMI. In this period, 20,126 deaths and 8,605 cases of incident AMI were recorded. Full details of observed events are presented in **Table 3.3**.

Table 3.3. Observed events during the study period for the whole cohort, and separately for men and women

	Whole cohort (n= 501,331)	Men (n=228,594)	Women (n=272,737)
All-cause mortality	20,126 (4.0%)	12,137 (5.3%)	7,989 (2.9%)
CVD mortality	4,197 (0.8%)	3,069 (1.3%)	1,128 (0.4%)
IHD mortality	2,285 (0.5%)	1,877 (0.8%)	408 (0.1%)
Fatal AMI	920 (0.2%)	741 (0.3%)	179 (0.1%)
Incident AMI	8,605 (1.7%)	6,069 (2.7%)	2,536 (0.9%)
Cancer mortality	11,167 (2.2%)	6,041 (2.6%)	5,126 (1.9%)
Follow-up (days) median [IQR] Death AMI	 9.0 [8.2-9.7] 8.1 [7.5-8.8]	 8.9 [8.2-9.7] 8.1 [7.4-8.8]	 9.0 [8.3-9.7] 8.2 [7.5-8.8]

Table 3.3. *Results are presented as number of outcomes (percentage). AMI: acute myocardial infarction; CVD: cardiovascular disease; IHD: ischaemic heart disease; IQR: interquartile range.*

3.4.3 Association between resting heart rate and all-cause mortality

Higher resting heart rate was associated with greater hazard of all-cause mortality in both men and women (**Table 3.4**). In fully adjusted models, a 10-bpm increase of heart rate was associated with 22% (HR 1.22, CI 1.20-1.24, $p=3 \times 10^{-123}$) greater hazard of all-cause mortality in men and 19% (HR 1.19, CI 1.16-1.22, $p=8.9 \times 10^{-45}$) greater hazard in women.

3.4.4 Association between resting heart rate and cardiovascular outcomes

Higher resting heart rate was associated with increased hazard of cardiovascular disease mortality in both men and women (**Table 3.4**). In men, every 10-bpm increase in heart rate was associated with 17% (SHR 1.17, CI 1.13-1.21, p-value 5.6×10^{-18}) greater hazard of cardiovascular disease mortality in men and 14% (SHR 1.14, CI 1.07-1.22, p-value 0.00008) greater hazard in women. For men, ischaemic aetiology was a significant driver of this relationship: 14% (SHR 1.14, CI 1.09-1.19, p-value 1.2×10^{-8}) greater hazard of IHD mortality, 5% (SHR 1.05, CI 1.02-1.07, p-value 0.0003) greater hazard of incident AMI, and 12% (SHR 1.12, CI 1.05-1.21, p-value 0.002) greater hazard of fatal AMI per 10 bpm increment of resting heart rate (**Table 3.4**). For women, there were no statistically significant associations between resting heart rate and IHD mortality or fatal AMI.

Table 3.4. Cox proportional hazard models and sub-distribution hazard models for resting heart rate-outcome relationships

Outcomes	Model 1: Univariate	Model 2: Age	Model 3: Age, smoking, exercise, BMI	Model 4: Model 3 + CVD risk factors*	Model 5: Model 4 + rate modifying medications**
All-cause mortality					
Men	1.25 (1.24 to 1.27)	1.26 (1.24 to 1.28)	1.21 (1.19 to 1.23)	1.19 (1.17 to 1.21)	1.22 (1.20 to 1.24)
p-value	2.5×10^{-228}	6.7×10^{-246}	5.2×10^{-122}	7.9×10^{-95}	3.0×10^{-123}
Women	1.25 (1.23 to 1.28)	1.22 (1.20 to 1.25)	1.16 (1.14 to 1.19)	1.15 (1.13 to 1.18)	1.19 (1.16 to 1.22)
p-value	7.2×10^{-119}	1.2×10^{-98}	2.6×10^{-35}	4.4×10^{-32}	8.9×10^{-45}
CVD mortality					
Men	1.21 (1.18 to 1.25)	1.22 (1.18 to 1.25)	1.14 (1.10 to 1.18)	1.10 (1.06 to 1.14)	1.17 (1.13 to 1.21)
p-value	4.6×10^{-37}	4.0×10^{-41}	1.9×10^{-12}	6.0×10^{-8}	5.6×10^{-18}
Women	1.22 (1.16 to 1.29)	1.19 (1.13 to 1.26)	1.08 (1.01 to 1.17)	1.07 (1.00 to 1.15)	1.14 (1.07 to 1.22)
p-value	5.6×10^{-13}	9.2×10^{-11}	0.028	0.042	0.00008
IHD mortality					
Men	1.18 (1.14 to 1.23)	1.19 (1.14 to 1.23)	1.10 (1.05 to 1.15)	1.06 (1.01 to 1.11)	1.14 (1.09 to 1.19)
p-value	4.0×10^{-17}	5.1×10^{-19}	0.0001	0.015	1.2×10^{-8}
Women	1.19 (1.08 to 1.30)	1.16 (1.06 to 1.27)	1.02 (0.87 to 1.12)	0.98 (0.87 to 1.10)	1.06 (0.94 to 1.18)
p-value	0.0004	0.002	0.82	0.67	0.36
Fatal AMI					
Men	1.16 (1.09 to 1.23)	1.17 (1.10 to 1.24)	1.08(1.00 to 1.16)	1.05 (0.98 to 1.12)	1.12 (1.05 to 1.21)
p-value	1.4×10^{-6}	2.7×10^{-7}	0.044	0.21	0.002
Women	1.05 (0.90 to 1.22)	1.03 (0.97 to 1.33)	0.85 (0.70 to 1.04)	0.85 (0.70 to 1.03)	0.92 (0.77 to 1.10)
p-value	0.52	0.70	0.11	0.09	0.36
Incident AMI					
Men	1.09 (1.07 to 1.11)	1.09 (1.07 to 1.11)	1.04 (1.01 to 1.06)	1.01 (0.99 to 1.04)	1.05 (1.02 to 1.07)
p-value	1.1×10^{-15}	6.7×10^{-16}	0.007	0.36	0.0003
Women	1.08 (1.04 to 1.13)	1.06 (1.02. to 1.11)	1.00 (0.95 to 1.05)	0.99 (0.94 to 1.04)	1.03 (0.98 to 1.08)
p-value	0.0001	0.002	0.89	0.72	0.28
Cancer mortality					
Men	1.20 (1.18 to 1.23)	1.21 (1.18 to 1.23)	1.18 (1.16 to 1.21)	1.17 (1.14 to 1.20)	1.18 (1.15 to 1.21)
p-value	9.9×10^{-75}	7.9×10^{-83}	1.6×10^{-48}	1.8×10^{-42}	5.2×10^{-46}
Women	1.20 (1.17 to 1.23)	1.17 (1.15 to 1.20)	1.14 (1.11 to 1.18)	1.14 (1.10 to 1.17)	1.15 (1.11 to 1.18)
p-value	6.8×10^{-48}	6.4×10^{-39}	2.9×10^{-17}	1.7×10^{-16}	3.1×10^{-18}

Table 3.4. *Results are hazard ratio (95% confidence interval) for all-cause mortality and sub-distribution hazard ratio (95% confidence interval) for all other outcomes per 10 beat per minute increase in resting heart rate. Significance level is p-value <0.0008. Those with prevalent MI have been excluded from analysis of incident AMI and fatal AMI. *CVD risk factors: diabetes, hypertension, hypercholesterolaemia, deprivation. **rate modifying medications include: betablockers, non-dihydropyridine calcium channel blockers, oral nitrates, digoxin, flecainide, amiodarone. AMI: acute myocardial infarction; BMI: body mass index; CVD: cardiovascular disease; IHD: ischaemic heart disease.*

3.4.5 Non-linearity of association with AMI

There was evidence of non-linearity for the association between resting heart rate and incident AMI in women (non-linear vs linear model: p-value=0.002, **Table 3.5**). Restricted spline models demonstrated a U-shaped relationship for this association. We further illustrated this relationship using stratified analysis by quintiles of heart rate (**Table 3.6**). For women, there was significantly increased hazard of incident AMI in the highest and lowest quintiles when compared to the middle quintile (**Table 3.6**).

There was no evidence of significant non-linearity in the association of resting heart rate with any of the other outcomes, or with incident AMI in men (**Table 3.5**, **Table 3.6**).

Table 3.5. Testing for non-linearity of the resting heart rate-outcome relationships

	p-value non-linear vs. linear model
All-cause mortality	0.39
Men	0.94
Women	0.13
CVD mortality	0.11
Men	0.21
Women	0.38
IHD mortality	0.06
Men	0.14
Women	0.21
AMI mortality	0.78
Men	0.69
Women	0.66
Incident AMI	**0.03**
Men	0.53
Women	**0.002**
Cancer mortality	0.59
Men	0.32
Women	0.41

Table 3.5. *Results are from the fully adjusted model, including following covariates: age, diabetes, hypertension, hypercholesterolaemia, smoking, BMI, Townsend deprivation index, and rate modifying medications. AMI: acute myocardial infarction; CVD: cardiovascular disease; IHD: ischaemic heart disease.*

Table 3.6. The association of resting heart rate with incident acute myocardial infarction in quintiles for men and women

	Hazard ratio (95% confidence interval)				
heart rate (bpm)	<59	59-64	65-70	71-77	≥78
Men	0.96 (0.87-1.06)	0.97 (0.88-1.06)	1.00	1.06 (0.96-1.16)	1.15 (1.05-1.27)
heart rate (bpm)	<62	62-67	68-72	73-78	≥79
Women	1.21 (1.02-1.42)	1.08 (0.91-1.28)	1.00	1.16 (0.98-1.36)	1.22 (1.04-1.43)

Table 3.6. *Results are hazard ratio as compared to the middle quintile, fully adjusted model (age, smoking, body mass index, exercise, diabetes, hypertension, hypercholesterolaemia, smoking, deprivation, rate modifying medications). AMI: acute myocardial infarction; bpm: beats per minute.*

3.4.5.1 Association between resting heart rate and cancer mortality

Higher resting heart rate was associated with significantly greater hazard of cancer mortality in both men and women (**Table 3.4**). Every 10 bpm increase of resting heart rate was associated with 18% (SHR 1.18, CI 1.15-1.21, p-value 5.2×10^{-46}) greater hazard of cancer mortality in men and 15% (SHR 1.15, CI 1.11-1.18, p-value 3.1×10^{-18}) greater hazard in women.

3.4.6 Modifying effect of age

We tested the potential interaction of effect of age in fully adjusted models. There was evidence of significant interaction effect of age in associations with all-cause mortality, cancer mortality, and incident AMI (**Table 3.7**). For ease of interpretation, we present hazard ratios by age group in even deciles: <50years, 50-59years, >60years. In age-stratified analyses (**Table 3.7**), there was a significant trend for greater effect size in younger participants for all-cause mortality [HR 1.30 (1.24-1.36) <50 years-old vs 1.15 (1.13-1.16) ≥60 years-old] and cancer mortality [HR 1.21 (1.13-1.30) <50 years-old vs 1.15 (1.13-1.18) ≥60 years-old]. Similarly, for incident AMI, the association was attenuated in the oldest age category [HR: 1.14 (1.06-1.22) <50 years-old vs 1.02 (0.99-1.05) ≥60 years-old].

Table 3.7. Age interactions and age stratified analyses for all outcomes

Outcome	Age group (years)	n	HR (95% CI)*	interaction term p-value (age-heart rate)
All-cause mortality	<50	117,535	1.30 (1.24 to 1.36)	9.5×10^{-15}
	50-59	166,778	1.26 (1.22 to 1.29)	
	≥60	217,018	1.15 (1.13 to 1.16)	
CVD mortality	<50	117,535	1.11 (0.99 to 1.24)	0.15
	50 to 59	166,778	1.28 (1.21 to 1.36)	
	≥60	217,018	1.15 (1.11 to 1.20)	
IHD mortality	<50	117,535	1.06 (0.91 to 1.24)	0.51
	50 to 59	166,778	1.24 (1.15 to 1.34)	
	≥60	217,018	1.11 (1.06 to 1.17)	
Incident AMI	<50	116,875	1.14 (1.06 to 1.22)	0.0004
	50 to 59	164,030	1.06 (1.02 to 1.10)	
	≥60	208,372	1.02 (0.99 to 1.05)	
Fatal AMI	<50	117,535	1.09 (0.84 to 1.40)	0.09
	50 to 59	166,778	1.26 (1.11 to 1.43)	
	≥60	217,018	1.05 (0.97 to 1.14)	
Cancer mortality	<50	117,535	1.21 (1.13 to 1.30)	0.0007
	50-59	166,778	1.22 (1.18 to 1.26)	
	≥60	217,018	1.15 (1.13 to 1.18)	

Table 3.7. *Results are Hazard ratio (95% Confidence interval) per 10 bpm increase in heart rate. AMI: acute myocardial infarction; CI: confidence interval; CVD: cardiovascular disease; HR: hazard ratio; IHD: ischaemic heart disease.*

3.5 Summary of findings

In this analysis of 228,594 men and 272,737 women with 7–12 years of prospective follow-up, we demonstrate the association of higher baseline resting heart rate with all-cause mortality and cardiovascular disease mortality in both men and women, independent of a wide range of confounders. For men, ischaemic cardiac events were a significant and consistent driver of this association. However, for women, there was no significant association between resting heart rate and IHD mortality or fatal AMI and there was a non-linear (U-shaped) relationship with incident AMI. Notably, for both men and women, the mortality association is not entirely explained by cardiovascular events. We demonstrate significant associations between higher resting heart rate and cancer mortality. With regards the modifying effect of age, the effect of resting heart rate appeared greater in younger individuals for all-cause mortality, cancer mortality, and incident AMI.

3.6 Discussion

3.6.1 Comparison with existing literature

Multiple studies have demonstrated the association of higher resting heart rate with greater mortality risk [104–107]. Our findings confirm these reports and provide added insight into sex and disease specific associations. In existing work, there is general agreement that greater cardiovascular mortality is a

major driver of the heart rate-mortality association in men[114–116], reports in women are inconsistent[109–113]. Furthermore, whilst in men these associations have been attributed to ischaemic cardiovascular outcomes, there are conflicting reports in women[109–111].

In a large population study, Tverdal et al.[113] report no significant association between resting heart rate and cardiovascular mortality or IHD mortality in women. In contrast, in a prospective cohort of 129,135 women, Hsia et al.[121] report association of higher resting heart rate with greater risk of incident ischaemic cardiovascular events (composite of AMI and IHD mortality). The findings of Hsai et al.[121] are consistent with several smaller studies[111,119,122]. A pooled analysis of 12 cohort studies, documents, in women, a positive association of resting heart rate with cardiovascular mortality but no significant association with ischaemic cardiovascular outcomes[118]. Our analysis, in the largest cohort studied internationally, demonstrates association of higher resting heart rate with greater all-cause mortality and cardiovascular mortality for both men and women. With regards specific link to IHD events, we demonstrate significant positive association between resting heart rate and IHD outcomes (incident AMI, fatal AMI, IHD mortality) in men, but not in women. This may indicate a disease-specific association for men. However, it may also reflect differences in the number of ischaemic events observed in men and women (**Table 3.3**). As there were notably fewer ischaemic events in women compared to men, we may have been underpowered to detect specific associations for these outcomes in women. Similar limitations may explain some of the inconsistencies observed in existing literature. The disease-specific associations likely reflect sex-differential pattern of cardiovascular diseases in middle age, rather than biological differences, although the latter cannot be ruled out. Overall, our results indicate that resting heart rate could be a useful indicator of cardiovascular risk for both men and women.

Several studies suggest a possible differential effect of resting heart rate on mortality outcomes by age, however there are inconsistencies in reports of the nature of this relationship[112,114,117]. For example, whilst several studies demonstrate larger effect at younger ages [118,119], others have suggested that effects are larger for older ages[117], and some report no differential relationship with age[112]. Overall, our findings from a much larger cohort indicate larger effects at younger ages. However, this relationship was less clear for cardiovascular disease mortality, IHD mortality, or fatal AMI outcomes. For these, the greatest magnitude of effect was seen in the middle age band, rather than a linear attenuation of effects with age. The interaction effect of age on incident AMI was convincing, and showed greater relative magnitude compared to all-cause mortality. It is possible, that age may influence the association between heart rate and incident AMI, but once an AMI has occurred, the subsequent mortality risk is less dependent on or differently influenced by prior resting heart rate. It is

also possible that the relationships with cardiovascular mortality are modified by medications which strongly influence heart rate (e.g. beta blockers). Although, we attempt to account for the influence of rate-modifying medications in our analysis, ascertaining this information based on self-report at a single time point likely does not fully capture the participants medication use and is subject to inaccuracies.

3.6.2 Possible biological mechanisms

Limited studies have proposed mechanisms by which the association between heart rate and cardiovascular outcomes may be explained (**Figure 3.2**). It has been suggested that faster resting heart rates have adverse haemodynamic consequences[123,124], which promote pathological arterial and myocardial remodelling, thereby increasing the likelihood of atherogenesis and heart failure syndromes. Higher resting heart rate may be driven by variations in autonomic system balance and greater background sympathetic tone[125]. These observations are in line with the growing body of evidence in support of the interconnectedness of heart and brain health. It is also possible that higher resting heart rate is downstream of other systemic biological processes, such as, inflammatory cascades. These processes may themselves be the causal agents in promoting cardiovascular disease (heart rate is a proxy indicator of these processes) or they may act through the adverse haemodynamic related to higher heart rate (heart rate is the mediator). It is of course also possible, that higher resting heart rate is a consequence of subclinical cardiovascular disease.

Figure 3.2. Possible mechanisms for the association of higher resting heart rate with increased cardiovascular mortality

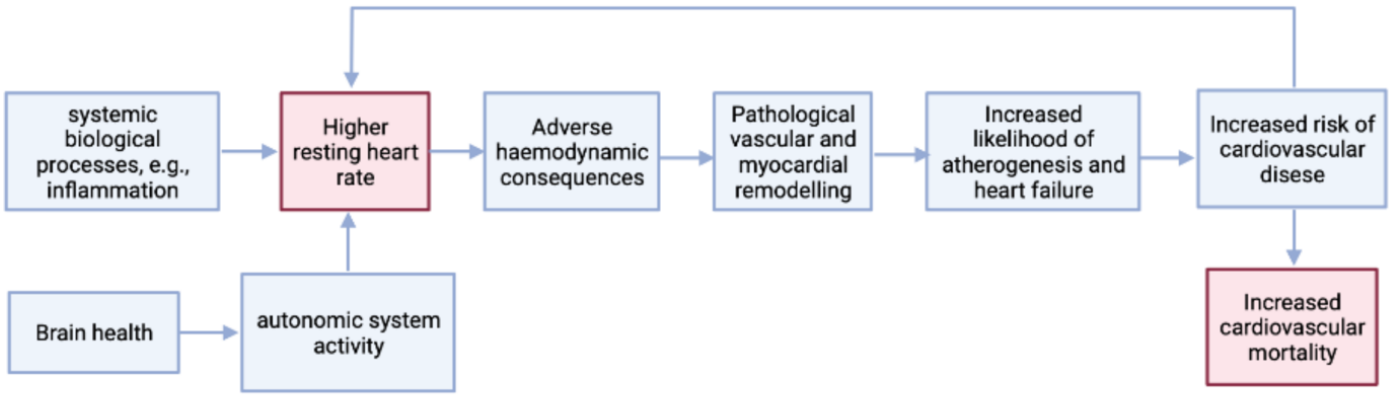

3.7 Critical appraisal of the results

In this study, we observed association of higher baseline resting heart rate with incident mortality and first occurrence of cardiovascular outcomes over 7-12 years follow-up, whilst adjusting for a range of confounders. Our findings are broadly consistent with previous studies, whilst providing more granularity regarding the sex and disease specific nature of these relationships. Measurement of the exposure (heart rate) was with standardised uniform equipment and according to a pre-defined protocol. The outcomes considered are unambiguous and their ascertainment through data linkage with death register data is highly reliable. Considering biological plausibility (as outlined in **section 3.6.2**), a multitude of systemic physiological stressors linked to poorer health status may manifest as an elevation of resting heart rate. Thus, resting heart rate may plausibly be an early indicator of adverse health outcomes. In our study, the long temporal separation of the heart rate measurement from the incident events and the nature of events considered (mortality), means that reverse causation is highly unlikely for the events of interest. There are, inevitably, imperfections in measurement of potential confounders, which mean that we cannot exclude the possibility of residual confounding. These are in part limited by the nature of recording of variables in the UK Biobank (e.g., smoking status reported as a categorical rather than continuous variable). Overall, the relationships between resting heart rate and the incident events considered are likely an indirect causal relationship, with higher heart rate possibly a downstream effect of other biological factors.

3.8 Conclusions

We demonstrate in this large, well characterised cohort, the sex-, age-, and disease-specific aspects of the relationship between higher resting heart rate and greater risk of cardiovascular mortality outcomes. Our findings confirm resting heart rate as an independent predictor of all-cause and cardiovascular disease mortality for both men and women. In men, ischaemic outcomes were important and consistent drivers of the relationship. The association with ischaemic cardiac events was less convincing for women, perhaps due to fewer ischaemic events; suggesting that for this age group of women, non-ischaemic outcomes were more significant drivers of the relationship between resting heart rate and cardiovascular mortality. In conclusion, our findings in the largest cohort studied internationally to date, support consideration of resting heart rate as a risk indicator for cardiovascular outcomes in men and women.

4 Cardiovascular phenotypes and cognitive performance

4.1 Abstract

Objectives: Previous work indicates links between heart and brain health. We evaluated relationships between CMR phenotypes and cognition in 29763 UK Biobank participants.

Methods and results: We included individuals with CMR and cognitive function testing. We included the fluid intelligence score (FI, 13 verbal-numeric reasoning questions), and reaction time (RT, a timed pairs matching exercise). Both were treated as continuous variables in models. We considered the following CMR measures: LV and RV volumes in end-diastole and end-systole, LV and RV ejection fractions, LV and RV stroke volumes, LV mass, and aortic distensibility. We used multivariable linear regression models to estimate the association of each CMR metric with FI and RT, adjusting for age, sex, smoking, education, deprivation, diabetes, hypertension, high cholesterol, previous MI, alcohol consumption, and physical activity. We report standardised beta-coefficients, 95% CIs, and p-values with multiple testing adjustment. In this predominantly healthy cohort of middle-aged adults (average age 63.0±7.5 years), better cognition (higher FI, lower RT) was linked to larger LV/RV volumes, higher LV/RV stroke volumes, greater LV mass, and greater aortic distensibility, in fully adjusted models. There was suggestion of non-linearity in the association between FI and LV end-systolic volume, with reversal of the direction of association at very high volumes. These relationships were consistent for men and women and across different ages.

Conclusions: Better cognition is associated with CMR measures likely representing a healthier cardiovascular phenotype. These relationships appeared significant after adjustment for a range of metabolic morbidities, lifestyle habits, and demographic variables, suggesting mediation of the relationship through novel biological pathways.

4.2 Background

Increased life expectancy and global trends of population aging present significant public health challenges[126]. Age-related cognitive decline and related illnesses have been highlighted as a public health priority by the World Health Organisation[127]. The worldwide cost of dementia is estimated at 1% of the aggregated world gross domestic product (GDP)[128]. Trends in dementia are expected to increase to epidemic levels with projected quadrupling of the prevalence by 2050[129,130]. However, our understanding of cerebral aging is limited. As a result, current disease prediction, treatment, and prevention strategies are inadequate.

Existing work suggests interactions across heart-brain organ systems with potential inter-related disease mechanisms. There is evidence to suggest that the brain may be a target for end-organ damage from cardiovascular disease and risk factors[131]. Indeed, cardiometabolic illnesses have been linked to more rapid decline in cognitive ability[132,133] and their optimised management with decelerated progression of dementia[134]. Cardiovascular risk factors have been associated with both vascular[135] and Alzheimer's dementia[133]. In people without dementia, vascular risk factors are linked to worse cognitive performance, with an incremental effect from increasing number of risk factors[136]. Furthermore, cardiovascular risk factors are associated with poorer brain health across grey and white matter macrostructure and microstructure assessed on brain magnetic resonance imaging[137].

There is support for common heart-brain disease pathways mediated by atherosclerosis[131]. However, the precise mechanisms by which cardiovascular diseases and risk factors may cause cognitive impairment are incompletely understood, and it is not known if alternative mechanisms may play a role in the observed associations. Exploring the relationship between cognitive performance and indices of cardiovascular structure and function may provide novel insights into these relationships and their underlying mechanisms; however, to date, this has not been studied in large cohorts.

We investigate the association of CMR measures of cardiovascular structure and function with measures of cognitive performance in the UK Biobank. We hypothesised that poorer cognitive function would be associated with adverse CMR phenotypes.

4.3 Methods

4.3.1 Study population

This analysis includes UK Biobank participants with CMR and cognitive performance testing data available. Further information about the study population is detailed in **Section 2.1.** Participants with dementia were excluded.

4.3.2 Measures of cognitive function

We selected two components from the UK Biobank cognitive function assessment, fluid intelligence (FI) and reaction time (RT), based on biological relevance and repeatability. The FI test is designed to assess problem solving capabilities using logic and reasoning independent of acquired knowledge. RT is a measure of attention, reaction speed, and raw processing speed. Together these measures provide a broad assessment of cognitive performance across a range of different processes. In addition, for both measures, internal consistency and longitudinal stability has been demonstrated in previous publications[138,139]. Furthermore, the availability of these data points for a large subset of the UK Biobank imaging cohort, ensures adequately powered analyses of associations with CMR phenotypes.

4.3.3 Fluid intelligence

Assessment of FI in the UK Biobank comprised a series of 13 verbal numeric questions to be completed within a 2-minute time limit (**Table 4.1**). A point is awarded for each correct answer. There is no negative marking; unanswered or incorrect answers score zero. The final score is the sum of correct answers, the maximum possible score is 13 with higher scores indicating higher FI and better cognition. The full protocol for FI assessment in UK Biobank is available in a dedicated document[140]. The Cronbach alpha reliability (internal consistency) score for this test is 0.62[138]. As the FI variable in our sample was normally distributed, we treated it as a continuous numerical variable for the purpose of modelling, as per established methods[141].

Table 4.1. Fluid intelligence assessment questions

Question	Multiple choice options
Add the following numbers together: 1 2 3 4 5, is the answer?	13, 14, 15, 16, 17, Do not know, Prefer not to answer
Which number is the largest?	642, 308, 987, 714, 253, Do not know, Prefer not to answer
Bud is to flower as child is to?	Grow, Develop, Improve, Adult, Old, Do not know, Prefer not to answer
11 12 13 14 15 16 17 18; Divide the sixth number to the right of twelve by three. Is the answer?	5, 6, 7, 8, Do not know, Prefer not to answer
If Truda's mother's brother is Tim's sister's father, what relation is Truda to Tim?	Aunt, Sister, Niece, Cousin, No relation, Do not know, Prefer not to answer
If sixty is more than half of seventy-five, multiply twenty- three by three. If not subtract 15 from eighty-five. Is the answer?	68, 69, 70, 71, 72, Do not know, Prefer not to answer
Stop means the same as?	Pause, Close, Cease, Break, Rest, Do not know, Prefer not to answer
If David is twenty-one and Owen is nineteen and Daniel is nine years younger than David, what is half their combined age?	25, 26, 27, 28, 29, Do not know, Prefer not to answer
Age is to years as height is to?	Long, Deep, Top, Metres, Tall, Do not know, Prefer not to answer
150...137...125...114...104... What comes next?	96, 95, 94, 93, 92, Do not know, Prefer not to answer

Question	Multiple choice options
Relaxed means the opposite of?	Calm, Anxious, Cool, Worried, Tense, Do not know, Prefer not to answer
100...99...95...86...70... What comes next?	50, 49, 48, 47, 46, 45, Do not know, Prefer not to answer
If some flinks are plinks and some plinks are stinks then some flinks are definitely stinks?	False, True, Neither true nor false, Not sure, Do not know, Prefer not to answer

4.3.4 Reaction time

The RT assessment comprised a pairs matching exercise. Participants were asked to press a button as soon as two identical cards (a match) appeared on the screen (**Figure 4.1**). The button was positioned under the dominant hand of the participant. Two cards were displayed on the screen at the same time. The exercise included a total of 12 card pairs (rounds). There was no time limit and no option to skip rounds. The RT variable is a derived variable representing the mean time in milliseconds (ms) to identify correct matches (i.e., mean time to press the button in cases where the card symbols matched). The first 4 rounds were considered as "training" and are not included in the calculation of the derived mean RT.

Figure 4.1. In the UK Biobank reaction time was tested by measuring time to identifying matching cards as they appeared on a screen

Figure 4.1. *Reproduced with permission from UK Biobank cognitive function, resources, available at: http://biobank.ctsu.ox.ac.uk/crystal/crystal/images/ukb_snap.jpg*

4.3.5 CMR image acquisition and analysis

The UK Biobank imaging study imaging protocol includes dedicated CMR scanning. The acquisition protocol is detailed in **Section 2.1.6.** We considered LV and RV quantification metrics and AD, with image analysis as described in **Section 2.2.5.1** and **Section 2.2.6.1**, respectively. Thus, the following CMR measures were available for inclusion in the analysis: LV and RV volumes in end-diastole and

end-systole, LV and RV ejection fraction, LV and RV stroke volume, LV mass, AD (measured at the proximal descending aorta).

4.3.6 Statistical analysis

Statistical analysis was with R version 3.6.2[142] and RStudio Version 1.3.1093[143]. Participants with history of dementia, as ascertained from UK Biobank algorithmically defined health outcomes, were excluded. We estimated the association of CMR measures with measures of cognitive function (FI and RT). Based on existing evidence and biological plausibility, we selected a priori the following covariates: age, sex, smoking, alcohol intake, exercise level, education, deprivation, diabetes, hypertension, hypercholesterolaemia, and prior myocardial infarction (**Figure 4.2**). There was no evidence of multicollinearity (VIF <2). We report standardised beta-coefficients with corresponding 95% CIs and p-values. Therefore, results presented are standard deviation change in FI or RT per one SD increase in CMR measure. To account for multiple testing, p-values were corrected using the Benjamin Hochberg method, setting a conservative false discovery rate of below 5%[144]. Results are presented for the whole sample and separately for men and women. We test for evidence of interaction by age or sex. We used squared and cubic polynomial terms to screen all models for evidence of non-linearity.

Figure 4.2. Covariates considered in the association between cognitive performance and cardiovascular phenotypes

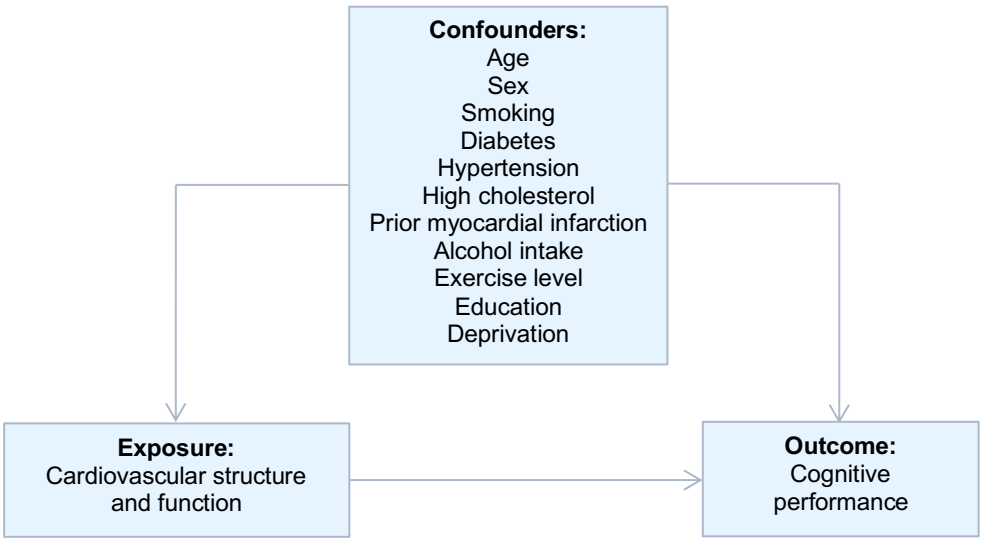

4.3.7 Ascertainment of covariates

We used age and sex as recorded at the imaging visit. Smoking status, alcohol intake, exercise level, education, deprivation, hypertension, high cholesterol, and diabetes were ascertained as detailed in

Section 2.2.2 and **Section 2.2.3.** Prior myocardial infarction was ascertained from UK Biobank algorithmically defined outcome data[45].

4.4 Results

4.4.1 Baseline population characteristics

There were 32,107 participants with CMR data and without dementia. Of these, FI and RT were available for 29,243 and 29,683 participants respectively. There were in total 29,763 participants with CMR data and at least one cognitive function measure, comprising 14,379 men and 15,384 women (**Table 4.2**). Mean age was 63.0 (± 7.5) years. Average FI and RT were 6.7 (± 2.1) items and 573 [518, 644] ms respectively.

Table 4.2. Baseline population characteristics

	Whole cohort (n= 29,763)	**Men (n= 14,379; 48.3%)**	**Women (n= 15,384; 51.7%)**
Age at imaging	63.0 (±7.5)	63.7 (±7.6)	62.4 (±7.3)
Current smoker	1,851 (6.2%)	1,066 (7.4%)	785 (5.1%)
Education:			
Left school age ≤14 years without qualifications	75 (0.3%)	42 (0.3%)	33 (0.2%)
Left school at age ≥15 without qualifications	1,981 (6.7%)	954 (6.6%)	1,027 (6.7%)
High school diploma or equivalent	3,900 (13.1%)	1,500 (10.4%)	2,400 (15.6%)
Sixth form qualification or equivalent	1,691 (5.7%)	751 (5.2%)	940 (6.1%)
Professional qualification	8,283 (27.8%)	4,198 (29.2%)	4,085 (26.6%)
Higher education university degree	13,526 (45.4%)	6,782 (47.2%)	6,744 (43.8%)
Townsend score	-2.7 [-3.9, -0.7]	-2.7 [-4.0, -0.7]	-2.6 [-3.9, -0.6]
Exercise level (MET minutes/week)	1,530 [671, 3,016]	1,590 [693, 3,111]	1,464 [642, 2,933]
Alcohol intake			
Daily or almost daily	6,554 (22.0%)	3,832 (26.6%)	2,722 (17.7%)
Three or four times a week	8,426 (28.3%)	4,388 (30.5%)	4,038 (26.2%)
Once or twice a week	7,731 (26.0%)	3,632 (25.3%)	4,099 (26.6%)
One to three times a month	3,223 (10.8%)	1,227 (8.5%)	1,996 (13.0%)
Special occasions only	2,423 (8.1%)	717 (5.0%)	1,706 (11.1%)
Never	1,390 (4.7%)	574 (4.0%)	816 (5.3%)
Diabetes	893 (3.0%)	581 (4.0%)	312 (2.0%)
Hypertension	4,016 (13.5%)	2,417 (16.8%)	1,599 (10.4%)
High cholesterol	6,640 (22.3%)	3,616 (25.1%)	3,024 (19.7%)
Prior MI	590 (2.0%)	494 (3.4%)	96 (0.6%)
Fluid intelligence (items)	6.7 (±2.1)	6.8 (±2.1)	6.5 (±2.0)
Reaction time (ms)	573 [518, 644]	565 [510, 636]	581 [526, 655]
LVEDVi (ml/m^2)	78.8 (±13.9)	83.8 (±14.7)	74.1 (±11.1)
LVESVi (ml/m^2)	31.1 [26.3, 36.7]	34.5 [29.5, 40.3]	28.3 [24.5, 32.7]
LVEF (%)	59.5 (±6.1)	57.8 (±6.2)	61.0 (±5.6)

	Whole cohort (n= 29,763)	Men (n= 14,379; 48.3%)	Women (n= 15,384; 51.7%)
LVSVi (ml/m^2)	46.6 (±8.3)	48.2 (±9.0)	45.1 (±7.4)
LVMi (g/m^2)	45.7 (±8.7)	51.1 (±7.9)	40.6 (±5.9)
RVEDVi (ml/m^2)	83.2 (±15.2)	90.0 (±15.3)	76.9 (±12.1)
RVESVi (ml/m^2)	35.9 (±9.4)	40.5 (±9.3)	31.5 (±7.1)
RVEF (%)	57.2 (±6.1)	55.1 (±5.9)	59.1 (±5.6)
RVSVi (ml/m^2)	47.4 (±8.7)	49.5 (±9.3)	45.4 (±7.7)
Aortic distensibility (10^{-3} mmHg^{-1})	2.3 [1.6, 3.1]	2.3 [1.7, 3.1]	2.2 [1.5, 3.0]

Table 4.2. Continuous data is presented as mean (standard deviation) or median [interquartile range], *categorical data as frequency (percentage; LVEDVi: left ventricular end-diastolic volume; LVEF: left ventricular ejection fraction; LVM: left ventricular mass; LVESVi: left ventricular end-systolic volume; LVSVi: left ventricular stroke volume; MET: metabolic equivalents; MI: myocardial infarction; RVEDVi: right ventricular end-diastolic volume; RVEF: right ventricular ejection fraction; RVESVi: right ventricular end-systolic volume; RVSVi: right ventricular stroke volume. i denotes indexation to body surface area.*

4.4.2 Association of CMR measures with fluid intelligence

Higher FI (better cognition) was associated with larger LV volumes in end-diastole and end-systole, higher LV stroke volume, and greater LV mass in fully adjusted models (**Table 4.3**). There was no significant association between FI and LV ejection fraction. Higher FI was associated with greater AD (**Table 4.3**)**.** For illustration, univariate relationships are presented in **Figure 4.3.**

A similar pattern of associations was seen between FI and RV metrics with higher FI associated with larger RV volumes in end-diastole and end-systole, and with larger RV stroke volumes (**Table 4.4**). In stratified analyses, we observed comparable associations for men and women **(Table 4.3, Table 4.4)**.

There was no evidence of interaction effect with sex or age in relationships with the LV or RV measures (**Table 4.5**). For the association between FI and AD, we observed a significant interaction effect with age. On further examination of this relationship, we found that individuals with higher AD had less rapid age-related decline in FI (**Figure 4.4**).

Figure 4.3. Univariate linear regression models of the association between fluid intelligence and cardiovascular magnetic resonance measures

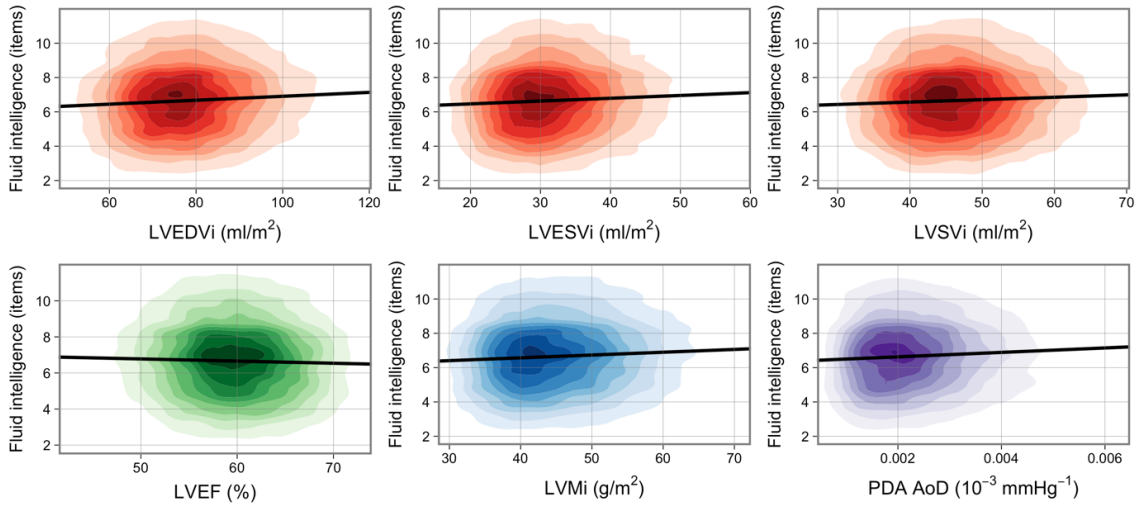

Figure 4.3. *Each graph displays a kernel density plot of one CMR variable against one cognition variable. The nine coloured rings each represent a decile of the data, while the remaining 10% lies in the uncoloured area. Univariate linear regression is shown by black line. All plot areas are trimmed at the 1st and 99th percentile in both x and y directions. Fluid intelligence has had uniform random jitter/noise (-0.5, 0.5) added for visual smoothing. CMR: cardiovascular magnetic resonance; LVEDVi: left ventricular end-diastolic volume; LVEF: left ventricular ejection fraction; LVESVi: left ventricular end-systolic volume; LVSVi: left ventricular stroke volume; PDA AoD: Aortic distensibility at the proximal descending aorta. i denotes indexation to body surface area. Reproduced from Raisi-Estabragh et al (doi: 10.1093/ehjci/jeab075, in press)*

Figure 4.4. Interaction effect between aortic distensibility and age in the relationship with fluid intelligence

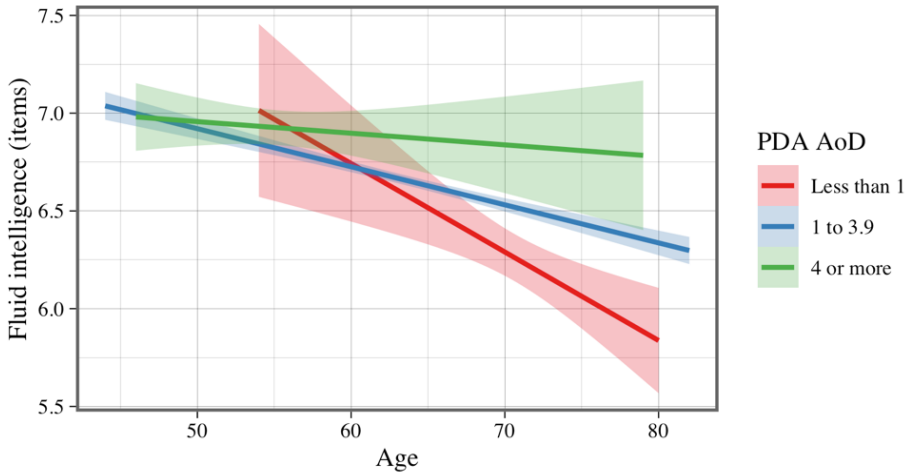

Figure 4.4. *participants with higher distensibility show less rapid age-related decline in fluid intelligence. PDA AoD: aortic distensibility at the ascending aorta, units are x10^{-3} mmHg^{-1}. Reproduced from Raisi-Estabragh et al (doi: 10.1093/ehjci/jeab075, in press)*

Table 4.3. Multivariable linear regression models representing standard deviation change in fluid intelligence and reaction time per one standard deviation increase in cardiovascular magnetic resonance measures

		Whole cohort	Men	Women
LVEDVi (ml/m2)	FI	0.043* [0.031, 0.056]	0.046* [0.030, 0.062]	0.040* [0.020, 0.060]
		1.45 x 10-11	3.06 x 10-8	9.31 x 10-5
	RT	-0.028* [-0.040, -0.015]	-0.031* [-0.047, -0.015]	-0.024* [-0.044, -0.004]
		1.24 x 10-5	1.64 x 10-4	0.018
LVESVi (ml/m2)	FI	0.040* [0.028, 0.053]	0.044* [0.028, 0.059]	0.035* [0.014, 0.055]
		2.76 x 10-10	6.28 x 10-8	0.001
	RT	-0.019* [-0.031, -0.006]	-0.020* [-0.036, -0.005]	-0.017 [-0.038, 0.004]
		0.003	0.011	0.104
LVEF (%)	FI	-0.018* [-0.030, -0.006]	-0.026* [-0.043, -0.010]	-0.009 [-0.026, 0.008]
		0.003	0.002	0.303
	RT	0.002 [-0.010, 0.014]	0.002 [-0.014, 0.018]	0.002 [-0.015, 0.019]
		0.725	0.831	0.792
LVSVi (ml/m2)	FI	0.026* [0.015, 0.038]	0.027* [0.011, 0.043]	0.026* [0.008, 0.044]
		1.17 x 10-5	7.70 x 10-4	0.004
	RT	-0.024* [-0.035, -0.012]	-0.028* [-0.043, -0.012]	-0.019 [-0.037, -0.001]
		7.81 x 10-5	5.03 x 10-4	0.039
LVMi (g/m2)	FI	0.048* [0.034, 0.063]	0.042* [0.023, 0.060]	0.058* [0.035, 0.081]
		3.50 x 10-11	1.09 x 10-5	6.87 x 10-7
	RT	-0.039* [-0.053, -0.025]	-0.045* [-0.063, -0.027]	-0.032* [-0.055, -0.010]
		8.25 x 10-8	1.26 x 10-6	0.005
PDA AoD (x10-3 mmHg-1)	FI	0.030* [0.014, 0.045]	0.033* [0.010, 0.057]	0.032* [0.010, 0.053]
		2.02 x 10-4	0.006	0.003
	RT	-0.017 [-0.032, -0.001]	-0.016 [-0.039, 0.006]	-0.015 [-0.036, 0.006]
		0.036	0.159	0.171

Table 4.3. *Results are standardised beta coefficients with 95% confidence interval and p-value. An asterisk indicates where the p-value is significant using a false discovery rate of 5%. Each cell represents results from an individual linear regression model. Models are adjusted for: age, sex (whole cohort only), education, deprivation, diabetes, hypertension, hypercholesterolaemia, prior myocardial infarction, smoking, alcohol, exercise. CMR: cardiovascular magnetic resonance; FI: fluid intelligence; LVEDVi: left ventricular end-diastolic volume; LVEF: left ventricular ejection fraction; LVESVi: left ventricular end-systolic volume; LVSVi: left ventricular stroke volume; PDA*

AoD: Aortic distensibility at the proximal descending aorta. RT: reaction time. i denotes indexation to body surface area.

Table 4.4. Multivariable linear regression models representing standard deviation change in fluid intelligence and reaction time per one standard deviation increase in cardiovascular magnetic resonance measures

		Whole cohort	Men	Women
RVEDVi (ml/m2)	FI	0.072* [0.059, 0.085] $4.24x10^{-27}$	0.070* [0.052, 0.087] $2.98x10^{-15}$	0.075* [0.055, 0.096] $3.31x10^{-13}$
	RT	-0.036* [-0.049, -0.023] $5.26x10^{-8}$	-0.038* [-0.055, -0.021] $1.25x10^{-5}$	-0.035* [-0.056, -0.015] $6.94x10^{-4}$
RVESVi (ml/m2)	FI	0.079* [0.066, 0.093] $1.01x10^{-31}$	0.072* [0.055, 0.089] $4.92x10^{-16}$	0.091* [0.070, 0.112] $1.52x10^{-17}$
	RT	-0.035* [-0.049, -0.022] $1.50x10^{-7}$	-0.035* [-0.053, -0.018] $5.13x10^{-5}$	-0.038* [-0.058, -0.017] $4.59x10^{-4}$
RVEF (%)	FI	-0.039* [-0.050, -0.027] $2.76x10^{-10}$	-0.033* [-0.050, -0.016] $1.60x10^{-4}$	-0.045* [-0.062, -0.028] $1.76x10^{-7}$
	RT	0.012 [-0.000, 0.024] 0.052	0.011 [-0.006, 0.028] 0.195	0.013 [-0.004, 0.030] 0.136
RVSVi (ml/m2)	FI	0.035* [0.024, 0.047] $5.83x10^{-9}$	0.038* [0.022, 0.054] $2.70x10^{-6}$	0.031* [0.013, 0.049] $6.80x10^{-4}$
	RT	-0.022* [-0.033, -0.010] $3.49x10^{-4}$	-0.025* [-0.040, -0.009] 0.002	-0.019 [-0.037, -0.000] 0.044

Table 4.4. *Results are standardised beta coefficients with 95% confidence interval and p-value. An asterisk indicates where the p-value is significant using a false discovery rate of 5%. Each cell represents results from an individual linear regression model. Covariates included: age, sex (whole cohort only), education, deprivation, diabetes, hypertension, hypercholesterolaemia, prior myocardial infarction, smoking, alcohol, exercise. RVEDVi: right ventricular end-diastolic volume; RVEF: right ventricular ejection fraction; RVESVi: right ventricular end-systolic volume; RVSVi: right ventricular stroke volume. i denotes indexation to body surface area.*

Table 4.5. Interaction effects between cardiovascular magnetic resonance measures and age, and between cardiovascular magnetic resonance and sex for fluid intelligence in fully adjusted models

Interaction term	CMR measure	Fluid intelligence (p-value)	Reaction time (p-value)
CMR with age	LVEDVi (ml/m^2)	0.8721	0.6148
	LVESVi (ml/m^2)	0.6195	0.7075
	LVEF (%)	0.8935	0.5582
	LVSVi (ml/m^2)	0.7148	0.7223
	LVMi (g/m^2)	0.9119	0.0828
	RVEDVi (ml/m^2)	0.7007	0.1755
	RVESVi (ml/m^2)	0.6907	0.0378
	RVEF (%)	0.0410	0.1080
	RVSVi (ml/m^2)	0.4968	0.891
	PDA AoD (10^{-3} mmHg^{-1})	$7.09x10^{-4}$ *	0.0109 *
CMR with sex	LVEDVi (ml/m^2)	0.2904	0.9246
	LVESVi (ml/m^2)	0.2668	0.8309
	LVEF (%)	0.1278	0.8687
	LVSVi (ml/m^2)	0.5094	0.8088
	LVMi (g/m^2)	0.4451	0.6434
	RVEDVi (ml/m^2)	0.8876	0.7219
	RVESVi (ml/m^2)	0.3882	0.5442
	RVEF (%)	0.4180	0.8233
	RVSVi (ml/m^2)	0.2858	0.9470
	PDA AoD (10^{-3} mmHg^{-1})	0.0548	0.3882

Table 4.5. *Models adjusted for: age, sex, education, deprivation, diabetes, hypertension, hypercholesterolaemia, prior myocardial infarction, smoking, alcohol, exercise. AoD PDA: aortic distensibility at the proximal descending aorta; LVEDVi: left ventricular end-diastolic volume; LVEF: left ventricular ejection fraction; LVESVi: left ventricular end-systolic volume; RVEDVi: right ventricular end-diastolic volume; RVEF: right ventricular ejection fraction; RVESVi: right ventricular end-systolic volume; LVSVi: left ventricular stroke volume; RVSVi: right ventricular stroke volume. i denotes indexation to body surface area. An asterisk indicates where the p-value is significant using a false discovery rate of 5%.*

4.4.3 Association of CMR metrics with reaction time

Shorter RT (better cognition) was associated with larger LV volumes in end-diastole, higher LV stroke volume, and greater LV mass in fully adjusted models (**Table 4.3**). This pattern of associations was consistent across RV measures (**Table 4.4**). Lower RT was also associated with higher AD, but this relationship was not statistically significant (**Table 4.3**). Overall, associations were consistent for both men and women (**Table 4.3**). For illustration, univariate relationships are presented in **Figure**

4.5. There was no evidence of interaction effect with sex or age in relationships with the LV or RV measures (**Table 4.5**).

Figure 4.5. Univariate linear regression models of the association between reaction time and cardiovascular magnetic resonance measures

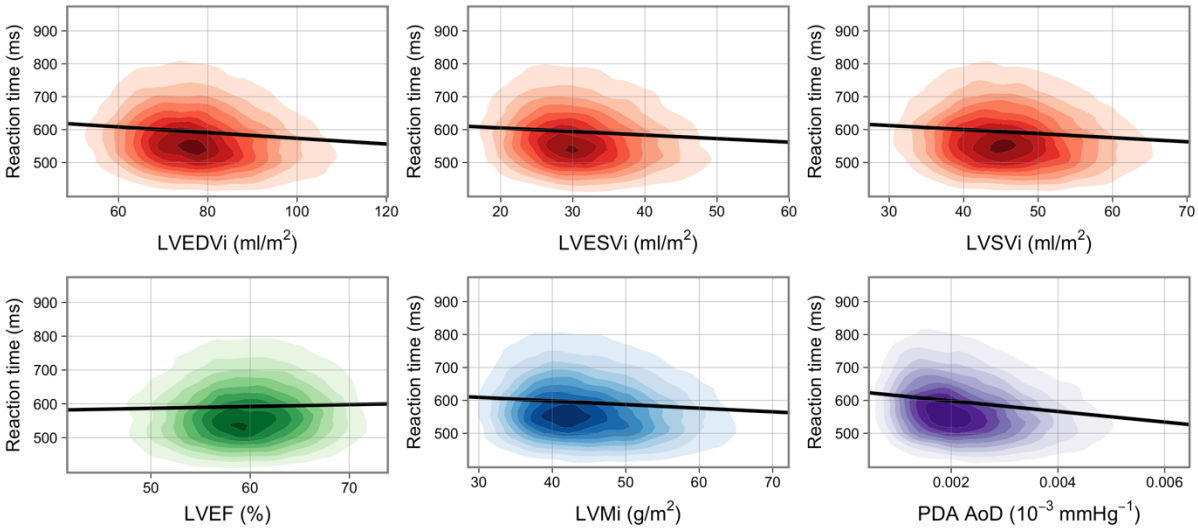

Figure 4.5. *Each graph displays a kernel density plot of one CMR variable against one cognition variable. The nine coloured rings each represent a decile of the data, while the remaining 10% lies in the uncoloured area. Univariate linear regression is shown by black line. All plot areas are trimmed at the 1st and 99th percentile in both x and y directions. CMR: cardiovascular magnetic resonance; LVEDVi: left ventricular end-diastolic volume; LVEF: left ventricular ejection fraction; LVESVi: left ventricular end-systolic volume; LVSVi: left ventricular stroke volume; PDA AoD: Aortic distensibility at the proximal descending aorta. i denotes indexation to body surface area. Reproduced from Raisi-Estabragh et al (doi: 10.1093/ehjci/jeab075, in press).*

4.4.4 Non-linearity of relationships

All models were screened for non-linearity with cubic and squared polynomials. For both FI and RT, in fully adjusted models, there was a trend towards attenuation of associations at the high extremes of the distribution for LV volumes and mass (very high volumes and mass). This appeared most convincing for the relationship between FI and LV end-systolic volume, where there was suggestion of attenuation and possible reversal of the direction of association at the very high extremes of the distribution (**Figure 4.6**). However, nested model testing indicated that none of the non-linear models showed a statistically significant improvement upon linear model fits (**Table 4.6**).

Figure 4.6. Fully adjusted linear (blue) and polynomial (red) models of associations between fluid intelligence (A) and reaction time (B) with cardiovascular magnetic resonance measures

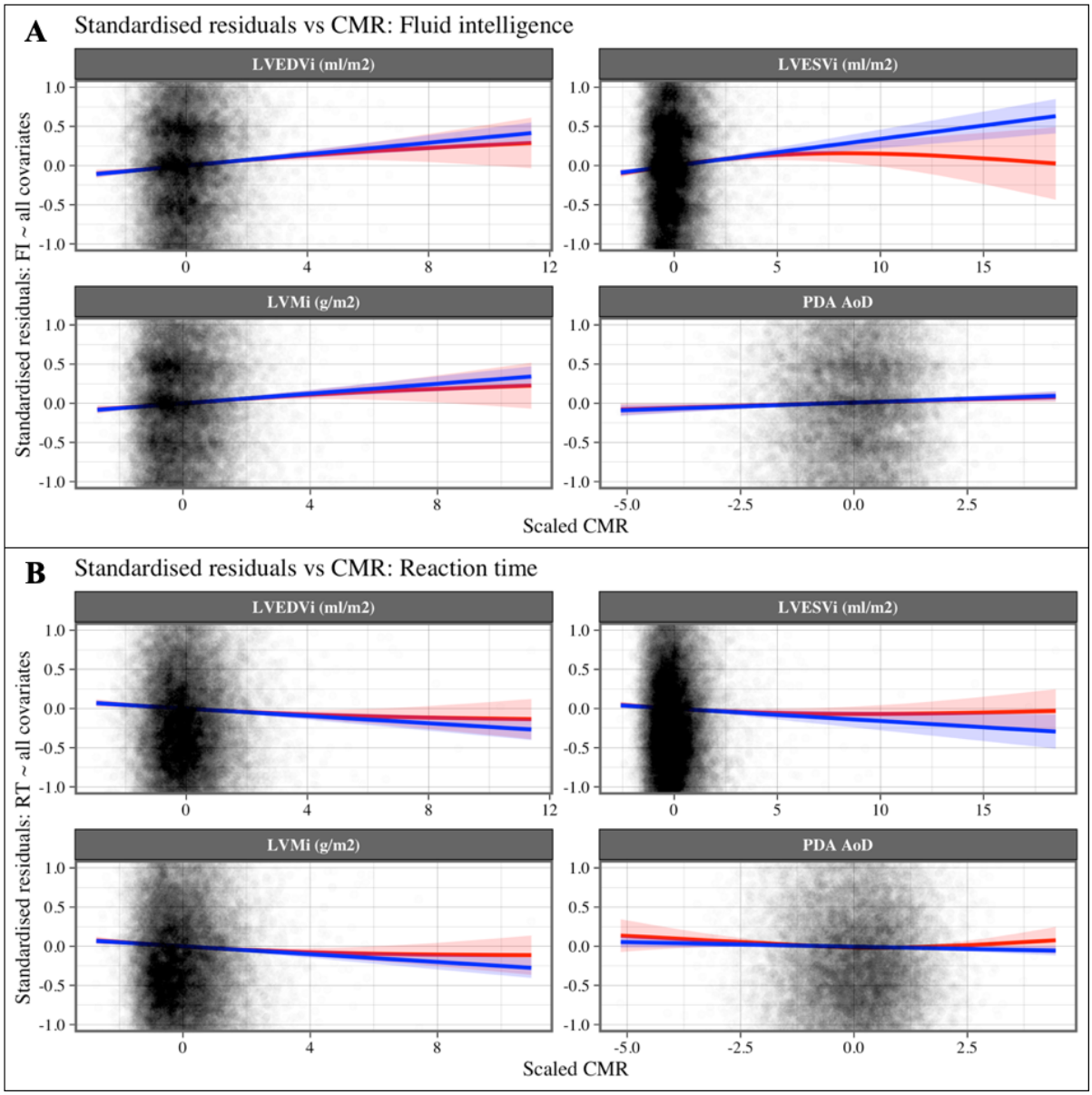

Figure 4.6. *CMR: cardiovascular magnetic resonance; LVEDVi: left ventricular end-diastolic volume; LVEF: left ventricular ejection fraction; LVESVi: left ventricular end-systolic volume; LVSVi: left ventricular stroke volume; PDA AoD: Aortic distensibility at the proximal descending aorta. i denotes indexation to body surface area. Reproduced from Raisi-Estabragh et al (doi: 10.1093/ehjci/jeab075, in press).*

Table 4.6. Comparison tests between linear and non-linear models

	Fluid intelligence		Reaction time	
CMR	Linear vs 2d polynomial	Linear vs 3d polynomial	Linear vs 2d polynomial	Linear vs 3d polynomial
LVEDVi (ml/m^2)	0.4956	0.2325	0.0991	0.1555
LVESVi (ml/m^2)	0.0076	0.0233	0.0495	0.1251
LVEF (%)	0.2230	0.4714	0.4174	0.6345
LVSVi (ml/m^2)	0.5845	0.2343	0.6092	0.4265
LVMi (g/m^2)	0.7945	0.8490	0.0351	0.1069
RVEDVi (ml/m^2)	0.4312	0.5715	0.7481	0.8136
RVESVi (ml/m^2)	0.3604	0.4604	0.8565	0.8858
RVEF (%)	0.0526	0.1496	0.5481	0.8097
RVSVi (ml/m^2)	0.2767	0.2204	0.9821	0.8759
PDA AoD (x10^{-3} mmHg^{-1})	0.8463	0.8409	0.0078	0.0020

Table 4.6. *Numbers are p-values, (pr(F)) from analysis of variance tests for nested models. None of the p-values above were significant using a false discovery rate of 5%. Significance threshold is p<0.0013. PDA AoD: aortic distensibility at the proximal descending aorta; LVEDVi: left ventricular end-diastolic volume; LVEF: left ventricular ejection fraction; LVESVi: left ventricular end-systolic volume; RVEDVi: right ventricular end-diastolic volume; RVEF: right ventricular ejection fraction; RVESVi: right ventricular end-systolic volume; LVSVi: left ventricular stroke volume; RVSVi: right ventricular stroke volume. i denotes indexation to body surface area.*

4.4.5 Interpretation of associations with cardiovascular phenotypes

There is a significant healthy participant effect in the UK Biobank, as such, our analysis sample comprises a predominantly healthy cohort. As such, observed associations are trends within the spectrum of normality rather than transitions from health to “disease”.

Our findings demonstrate association of better cognitive performance with larger ventricular cavity volumes, larger LV and RV stroke volumes, and higher LV mass. This pattern of associations, interpreted within the spectrum of normality, reflects a pattern of decelerated heart aging (the pattern of associations is the reverse of the pattern of alterations seen in healthy aging). At the high extremes of the distribution for LV end-systolic volume, there was suggestion of reversal of the direction of associations with FI, indicating that LV volumes larger than the normal range are linked with poorer cognition. However, model fit was not significantly improved with the non-linear models. This may be because there were very few participants with extreme CMR measures in our sample. Better cognitive performance was also linked to greater AD, further supporting argument that the observed associations indicate a healthy cardiovascular phenotype.

4.5 Summary of findings

In this study of a predominantly healthy cohort of 29,763 UK Biobank participants, we demonstrate association of better cognitive performance with CMR measures likely representing a healthier cardiovascular phenotype, independent of a range of lifestyle, demographic, and vascular risk factors. In particular, better cognitive function (higher FI, lower RT) was associated with larger LV and RV volumes, greater LV and RV stroke volumes, higher LV mass, and greater AD. There was some evidence of non-linearity for the relationship between FI and LV end-systolic volume, with a trend towards reversal of the direction of association at the high extremes of the distribution (very high volumes). Associations appeared consistent for men and women and with age.

4.6 Discussion

4.6.1 Comparison with existing literature

Existing studies of the association between cognitive performance and cardiovascular imaging phenotypes are highly heterogeneous and limited to small cohorts of highly select patient populations. In a study of 57 patients with systolic heart failure, Zuccala' et al.[145] report an independent association between poorer LV ejection fraction on echocardiography and worse cognitive performance as assessed by the mini mental examination and Raven score. In another study of a small heart failure cohort (n=58), Vogels et al.[146] report greater pathological brain magnetic resonance imaging (MRI) alterations (periventricular and white matter hyperintensities, lacunar and cortical infarcts, global and medial temporal lobe atrophy) in patients with heart failure compared to a comparator group. In a study of 93 dementia patients, Oh et al.[147] demonstrate association pathological white matter alterations on brain MRI with atrial dilatation, an early indicator of LV diastolic dysfunction. Other studies have also demonstrated greater rates of diastolic impairment in patients with Alzheimer's dementia compared to controls[148,149]. Manolio et al.[150] document an association between greater carotid intima medial thickness (marker of poorer vascular health) and greater cerebral atrophy on brain MRI in a study of 303 individuals.

Our study is the first to evaluate association of cardiovascular phenotypes in a large cohort of predominantly healthy adults. We demonstrate association of poorer cognitive performance with smaller ventricular volumes and smaller stroke volumes, together with the association with greater aortic stiffness. These observations are in keeping with studies linking poorer brain health with diastolic dysfunction and poorer arterial health. Overall, our findings are supportive of links between brain and cardiovascular health and demonstrate that these links extend beyond disease cohorts to apparently healthy populations.

4.6.2 Potential biological mechanisms

Multiple studies have linked classical vascular risk factors to worse cognition[151–155] and with both vascular and Alzheimer's dementia[135,156,157]. It has thus been suggested that the links between cardiovascular disease and brain health may be mediated by these common risk factors and the systemic atherosclerotic disease that occurs as a result (**Figure 4.7**). However, in our study, the associations between CMR phenotypes and cognitive performance were broadly robust to adjustment for cardiometabolic morbidities indicating the importance of alternative mechanisms. For example, limited studies in small cohorts of Alzheimer's patients have suggested that the Aβ protein, which is characteristically deposited in the brain may also accumulate in the myocardium of these patients and manifest as a cardiac amyloid phenotype[149]. It is also possible, that poorer brain and heart health may be a reflection of accelerated multisystem aging, which may occur as a result of indolent elevation of inflammatory cytokines (inflammaging) and has been linked to both cardiovascular disease and dementia[158,159]. Whatever the underlying case, it seems that initiation of disease in one organ system initiates a positive feedback cycle of adverse heart-brain interactions which perpetuates poorer health in both systems (**Figure 4.7**).

Figure 4.7. Possible mechanisms for the associations between heart and brain health

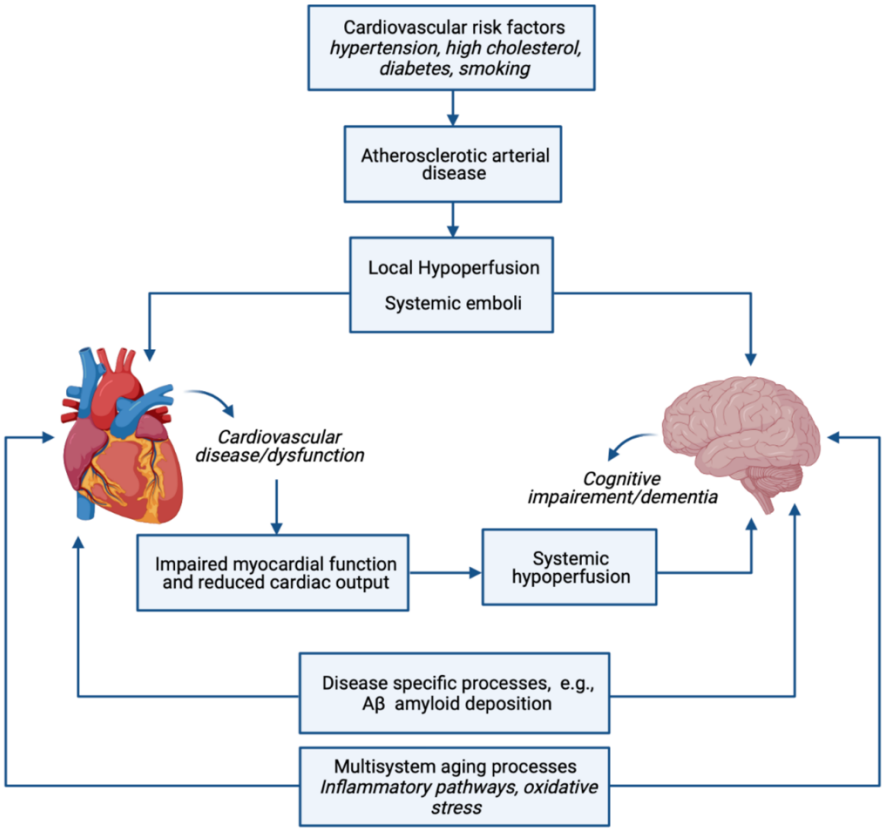

Figure 4.7. *Reproduced from Raisi-Estabragh et al. (doi: 10.1093/ehjci/jeab075)*

4.7 Critical appraisal of the results

Our findings indicate cross-sectional associations between cardiac structure and function derived from detailed CMR and cognition measured using validated cognitive performance tests. Our findings are consistent with existing work and extend previous reports of heart-brain relationships in disease cohorts to a large population-based cohort. Previous studies using clinical diagnoses of heart disease may be limited by subjectivity and misclassification of these diagnoses. Furthermore, due to their binary nature, such classifications of heart health status are limited in the detail that they provide. The use of CMR measures is advantageous in providing objective, quantitative, and continuous indicators of heart health. Furthermore, CMR in the UK Biobank is performed in a highly standardised manner in dedicated imaging centres and using uniform acquisition and analysis protocols. Thus, active steps are taken to minimise potential systemic measurement bias of these variables. The cognitive function tests in the UK Biobank were conducted according to pre-defined protocols and their repeatability performance has been evaluated in dedicated publications. Inherent to all such measures of cognitive performance, it is challenging to separate cognition from prior knowledge and life experiences. Furthermore, we cannot exclude residual confounding due to imperfections of covariate measurement. The precise mechanisms through which the heart and brain may be independently linked are yet to be outlined. We demonstrate cross-sectional associations between heart and brain health independent of common classical vascular risk factors. Thus, our findings indicate independent relationships between the two organ systems. The direction of the association (which may also be bidirectional) and precise mechanisms require further evaluation.

4.8 Conclusions

In this study, better cognitive performance was associated with CMR and AD measures likely representing a healthy cardiovascular phenotype. The associations were consistent between men and women and remained robust after accounting for lifestyle, demographic, and vascular risk factors, implying a potential importance of alternative underlying mechanism. Our findings indicate relationships between cardiovascular and brain health, provide insight into possible mechanisms, and support a rationale for a cross-system approach to risk stratification for related clinical endpoints.

5 Bone and cardiovascular health

5.1 Abstract

Objectives: Osteoporosis and ischaemic heart disease (IHD) are important public health problems. Previous work suggests an association between the two conditions beyond shared risk factors, with a potentially causal relationship. We evaluated the relationship between bone and vascular health in the UK Biobank.

Methods and Results: We tested the association of calcaneal SOS from quantitative heel ultrasound with (1) CMR measures of arterial compliance (AD); (2) finger photoplethysmography (ASI); and (3) incident AMI and IHD mortality. We considered the potential mediating role of selected blood biomarkers and cardiometabolic morbidities and evaluated differential relationships by sex, menopause status, smoking, diabetes, and obesity. Furthermore, we considered whether associations with arterial compliance explained association of SOS with ischemic cardiovascular outcomes. Higher SOS was linked to lower arterial compliance by both ASI and AD for both men and women. The relationship was most consistent with ASI, likely due to larger sample size available for this measure (n= 159,542 vs n= 18,229). There was no convincing evidence of differential relationships by menopause, smoking, diabetes, or BMI. Blood biomarkers appeared influential in mediating the observed relationships for both men and women, but with differing directions of effect and did not fully explain the observed effects. In fully adjusted models, higher SOS was associated with significantly lower IHD mortality in men, but less robustly in women. The association of SOS with ASI did not explain this observation.

Conclusions: Our findings support positive association of bone and vascular health independent of shared risk factors. These relationships were consistent for men and women, and with menopause status. The underlying mechanisms are likely complex and vary by sex.

5.2 Background

Osteoporosis and IHD are major public health problems, particularly in aging populations. IHD is a global public health priority and the most common cause of morbidity and mortality worldwide[8]. Fragility fractures, that occur as a consequence of osteoporosis, place a significant burden on individuals, society, and health and social care services. In the UK, approximately one in three women and one in five men will sustain at least one fragility fracture in their lifetime[160]. Fragility fractures cost the UK economy approximately £4.4 billion each year[161].

Osteoporosis and atherosclerosis have several shared risk factors, such as older age, cigarette smoking, and sedentary lifestyle. Existing work suggests links between the two conditions beyond these shared risk factors[162–165]. Furthermore, limited studies indicate possible common biological and genetic mechanisms underlying bone mineralisation and atherogenesis[166–168]. Thus, existing evidence suggests possible common causal mechanisms linking the two disease processes. Understanding such novel disease pathways may provide new targets for disease prevention or treatment. However, existing studies are limited by small sample size, lack of robust objective measures of bone and vascular health, and inadequate consideration of mediating and confounding variables. In addition, although sex differential disease patterns and the modifying effect of menopause status are widely reported for both conditions, such distinctions have not been adequately addressed in existing work.

We hypothesised that poorer bone health would be associated with poorer vascular health. We thus studied the association of quantitative heel ultrasound measures of bone health with measures of arterial compliance (AD, ASI). We considered a wide range of covariates and potential differential relationships by sex, menopause, smoking status, diabetes, and obesity. We assessed the mediating effect of a range of metabolic morbidities and blood biomarkers in driving the association between bone health and arterial stiffness. Finally, we evaluated the association of heel ultrasound measures with incident ischaemic cardiovascular outcomes (incident AMI, IHD mortality) and tested the importance of arterial stiffness in driving these relationships.

5.3 Methods

5.3.1 Study population

This analysis includes all UK Biobank participants who completed heel ultrasound at baseline, finger photoplethysmography measurement at baseline visit, and/or CMR at the imaging visit. Further information about the study population is detailed in **Section 2.1**.

5.3.2 Quantitative heel ultrasound

Quantitative heel ultrasound is a non-invasive and radiation-free method for objective assessment of bone quality. Quantitative ultrasound metrics associate reliably with reference standard bone mineral density measured by DXA and with incident fragility fractures[169,170]. In the UK Biobank, bone quality was assessed at the baseline visit based on heel ultrasound measures obtained from the Sahara Clinical Bone Sonometer (Hologic, USA) (**Figure 5.1**). Measurement was taken according to a pre-defined standard operating procedure, which is detailed in a dedicated document[171]. There were standardised quality control checks of the sonometer using a phantom at the start of each day. Measurement was not taken for participants with open wounds, breaks, sores, or metal implants (e.g. plates, wires, pins) around the heel area.

Figure 5.1. The Sahara bone sonometer

Figure 5.1. *Adapted from "UK Biobank, Ultrasound Bone Densitometry, 2011"[171]; Figure used with permission from UK Biobank.*

The participant was asked to remove shoes and socks. The lateral and medial sides of the heel (where the measurement was to be taken from) were cleaned and dried with disposable wipes. Gel was applied to the sonometer transducer pads. The participant was asked to sit with their back straight and the heel was guided to fit snugly into the device footwell and secured in position using straps. The 'measure now' option was then selected, which generated two readings: the speed of sound (SOS) and broadband ultrasound attenuation (BUA). SOS is the speed at which the ultrasound pulse traverses the body part under study and is calculated by dividing the ultrasound transit time by the distance travelled. BUA is the slope between the attenuation of the signal amplitude and its frequency as it propagates through the soft tissue and bone. Higher SOS and BUA values indicate better bone health. Within the UK Biobank, in cases where BUA was missing, it was estimated from the SOS measure. For this reason, in our analysis, we consider SOS as the measure of bone health, as it is always directly measured. In the early stages of UK Biobank, measurement was taken from a single foot. In

the latter stages, bilateral measurements were made. In cases where two measurements were available, we took the mean value.

5.3.3 Measures of arterial compliance

We consider AD and ASI as measures of arterial compliance, derived from CMR and finger plethysmography respectively, as described in **Section 2.2.6.**

5.3.4 Ascertainment of cardiovascular outcomes

Approach to outcome ascertainment was as discussed in **Section 2.2.3.** The clinical endpoints of interest were incident AMI and IHD mortality. We considered outcomes occurring after baseline assessment (2006-2010) to the latest available UK Biobank censor dates (mortality: 31/01/2018, incident AMI: 31/03/2017). Thus, follow up duration was between 7-12 years. We defined IHD mortality was as primary cause of death attributed to any IHD manifestation on death registration (as per ICD codes in **Table 2.3**). Incident AMI was derived from algorithmically defined outcomes generated by UK Biobank[66].

5.3.5 Ascertainment of covariates

Covariates were taken as defined at baseline UK Biobank assessment. Age, sex, ethnicity, smoking, alcohol intake, deprivation, exercise level, hypertension, diabetes, high cholesterol, and BMI were ascertained as detailed in **Section 2.2.2**. Menopause status was recorded as a binary variable based on self-report at baseline. The following serum biochemistry measures (from bloods collected at the baseline visit) were considered as potential mediators: C Reactive Protein (CRP), Creatinine, Vitamin D, Calcium, Alkaline Phosphatase (ALP), Insulin-like Growth Factor 1 (IGF1), Sex Hormone Binding Globulin (SHBG), Testosterone, Testosterone/SHBG, Oestradiol, Phosphate, Cystatin C.

5.3.6 Statistical analysis

Statistical analysis was performed using R studio version 3.6.0 [https://www.R-project.org/] and Stata version 14 [StataCorp. 2015. Stata Statistical Software: Release 14. College Station, TX: StataCorp LP]. The analysis considers the relationships as summarised in **Figure 5.2**.

We used the Tukey method for outlier elimination (1.5× IQR method)[172] to remove outliers from the SOS, ASI, and AD variables. We used multivariable linear regression models to estimate the association of SOS with measures of arterial compliance (ASI, AD). Analysis was performed

separately for men and women. Models were adjusted for age, exercise level, smoking, material deprivation, alcohol intake, hypercholesterolaemia, diabetes, and hypertension. Results are reported as SD change in vascular measure per 1 SD increase of SOS, alongside corresponding 95% CIs and p-values. We tested for potential non-linearity using restricted cubic spline models. We tested for differential relationship by menopause status, diabetes, smoking, and obesity.

Figure 5.2. Potential confounding and mediating pathways considered in the relationship between bone and cardiovascular health

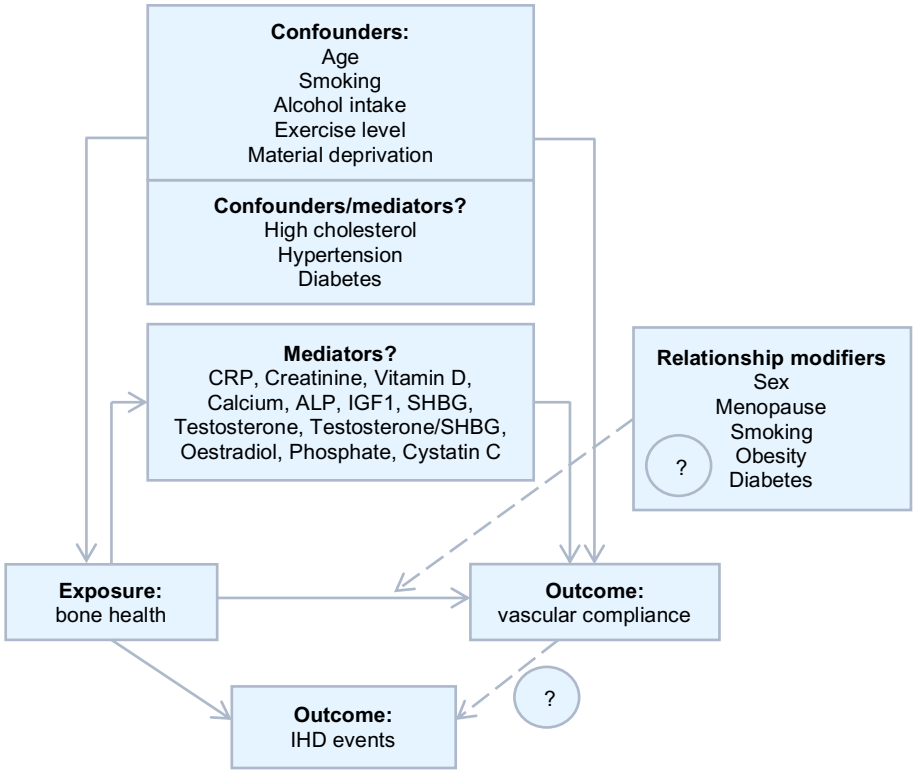

Figure 5.2. *ALP: Alkaline Phosphatase; CRP: C Reactive Protein (CRP), Insulin-like Growth Factor 1 (IGF1); IHD: ischaemic heart disease; SHBG: Sex Hormone Binding Globulin.*

Based on review of the literature, we identified and evaluated the potential mediating effect of a range of blood biomarkers (CRP, Creatinine, Vitamin D, Calcium, ALP, IGF1, SHBG, Testosterone, Testosterone/SHBG, Oestradiol, Phosphate, Cystatin C) and cardiometabolic conditions (hypertension, diabetes, hypercholesterolaemia). The mediating effect of each mediator was first tested individually, variables with a significant effect ($p<0.003$, corrected for 15 mediators), were taken forward for multiple mediation analysis. As such, we were able to report the proportion of effect mediated by each variable independent of other potential mediators. Independent indirect effects were calculated as described by Van Der Weele and Vansteelandt[173] and CIs were derived using bootstrap re-sampling. We thus calculate the direct and indirect effect of each mediator and present the proportion of effect mediated as a percentage of the total effect. A variable associated with a positive

effect from this analysis indicates mediation effect from the variable, whilst a negative effect indicates a suppression (rather than mediation) effect on the exposure-outcome association.

Finally, we tested, separately for men and women, associations between SOS and incident AMI and IHD mortality using multivariable competing risk regression models, as per Fine and Gray[67]. We report SHR per one standard deviation increase in SOS, with 95% CIs and p-values. We tested the importance of the associations of SOS with arterial compliance in mediating the relationships with ischaemic cardiac outcomes.

5.4 Results

5.4.1 Baseline population characteristics

There were 159,542 participants with both SOS and ASI recorded at baseline (**Table 5.1A**) with average age of 58 [50-63] years and comprising 71,949 men and 87,593 women. There was a greater burden of cardiovascular risk factors in men. Most women were post-menopause (73.0%). There were 18,229 participants with both SOS and AD data available (**Table 5.1B**).

Table 5.1. Baseline participant characteristics

A: Baseline participant characteristics (SOS and ASI)			
	Whole cohort (n=159,542)	**Men (n=71,949)**	**Women (n=87,593)**
Age	58 [50-63]	59 [51-64]	58 [50-63]
Ethnicity (White Caucasian)	145,627 (91.9%)	65,804 (92.2%)	79,823 (91.6%)
Townsend deprivation score	-1.8 [-3.4 to 0.8]	-1.8 [-3.4 to 0.8]	-1.8 [-3.4 to 0.7]
Body mass index (kg/m^2)	26.7 [24.1 to 29.8]	27.2 [24.9 to 29.9]	26.1 [23.4 to 29.8]
Current smoking	16,085 (10.1%)	8,637 (12.0%)	7,448 (8.5%)
Regular alcohol use	67,664 (42.5%)	36,478 (50.9%)	31,186 (35.7%)
Physical activity (METS/week)	1,891 [874 to 3,786]	1,908 [864 to 3,930]	1,866 [878 to 3,666]
Hypertension	44,626 (28.0%)	23,676 (32.9%)	20,950 (23.9%)
Diabetes	8,981 (5.6%)	5,351 (7.4%)	3,630 (4.1%)
Hypercholesterolaemia	31,465 (19.7%)	18,571 (25.8%)	12,894 (14.7%)
Post-menopausal	–	–	53,940 (73.0%)
ASI (m/s)	9.0 [6.9 to 11.2]	9.8 [7.8 to 11.8]	8.3 [15.3 to15.7]
SOS (10^2m/s)	15.5 (0.3)	15.6 (0.3)	15.5 (0.3)
B: Baseline participant characteristics (SOS and AD)			
	Whole cohort (n=18,229)	**Men (n=8,767)**	**Women (n=9,462)**
Age	56 [49-61]	57 [50-62]	55 [48-60]
Ethnicity (White)	17,701 (97.4%)	8,485 (97.2%)	9,216 (97.6%)
Townsend deprivation score	-2.7 [-3.9 to -0.7]	-2.7 [-4.0 to -0.7]	-2.6 [-3.9 to -0.7]
Body mass index kg/m^2	26.0 [23.6 to 28.7]	26.7 [24.5 to 29.0]	25.2 [22.9 to 28.3]
Current smoking	1,147 (6.3%)	671 (7.7%)	476 (5.0%)
Regular alcohol use	5,069 (57.9%)	4, 167 (44.0%)	9,236 (50.7%)

	Whole cohort (n=18,229)	Men (n=8,767)	Women (n=9,462)
Physical activity (METS/week)	1,733 [810 to 3,339]	1,740 [809 to 3,394]	1,714 [810 to 3,306]
Hypertension	3,597 (18.7%)	2,121 (24.2%)	1,476 (15.6%)
Diabetes	472 (2.6%)	308 (3.5%)	164 (1.7%)
Hypercholesterolaemia	2,435 (13.4%)	1.632 (18.6%)	803 (8.5%)
Post-menopausal	–	–	5,129 (64.4%)
AD at the ascending aorta (10^{-3} $mmHg^{-1}$)	1.2 [0.8-1.9]	1.3 [0.8-1.9]	1.2 [0.7-2.0]
AD at the descending aorta (10^{-3} $mmHg^{-1}$)	2.3 [1.8-2.9]	2.2 [1.7-2.8]	2.3 [1.8-2.9]
Speed of sound (10^2 m/s)	15.6 (0.3)	15.6 (0.3)	15.5 (0.3)

Table 5.1. *Continuous variables are median [interquartile range] or mean (standard deviation). Discrete data are frequencies (percentages). ASI: arterial stiffness index; SOS: speed of sound; METS: metabolic equivalent minutes.*

5.4.2 Association of SOS with measures of arterial compliance

In fully adjusted multivariable linear regression models, higher SOS was associated with lower ASI (**Table 5.2**), that is, better bone health was associated with better vascular health. This association was significant for both men and women with similar magnitude of effect. Higher SOS was associated with greater AD at the ascending aorta for women, but not for men (**Table 5.2**). Higher SOS was associated with greater AD at the descending aorta for men, but not for women (**Table 5.2**). There was no convincing evidence of a sex differential relationship as per stratified analysis and the interaction effect of sex was not statistically significant. There was no evidence of non-linearity of these associations (**Table 5.3**). In stratified analysis by menopause status, higher SOS was associated with lower ASI in pre- and post-menopausal women (**Table 5.4**). The associations with AD were not significant, perhaps due to loss of power with the smaller sample size. Overall, we did not find evidence for a modifying effect of menopause.

Table 5.2. Association of speed of sound with measures of arterial stiffness in men and women

		Model 1: Age	Model 2: Age, exercise, smoking, deprivation, alcohol	Model 3: Model 2+ hypercholesterolaemia, diabetes, hypertension
	ASI			
Men	B (95% CI)	-0.030 (-0.037, -0.023)	-0.021 (-0.028, -0.013)	-0.020 (-0.028, -0.012)
n=71,949	p-value	4.8×10^{-17}*	1.5×10^{-7}*	2.6×10^{-7}*
Women	B (95% CI)	-0.027 (-0.034, -0.021)	-0.024 (-0.031, -0.016)	-0.026 (-0.033, -0.018)
n=87,593	p-value	5.6×10^{-16}*	6.0×10^{-10}*	2.8×10^{-11}*
p-value for interaction		0.605	0.541	0.307
	AD (ascending aorta)			
Men	B (95% CI)	0.018 (0.000, 0.036)	0.017 (-0.002, 0.036)	0.017 (-0.002, 0.036)
n=8,767	p-value	0.046	0.085	0.085
Women	B (95% CI)	0.025 (0.008, 0.042)	0.020 (0.000, 0.039)	0.020 (0.000, 0.039)
n=9,462	p-value	0.004*	0.045*	0.043*
p-value for interaction		0.588	0.846	0.829
	AD (descending aorta)			
Men	B (95% CI)	0.040 (0.021,-0.059)	0.037 (0.018, 0.057)	0.037 (0.017, 0.056)
n=8,767	p-value	2.2×10^{-5}*	0.0002*	0.0002*
Women	B (95% CI)	0.017 (-0.000, 0.035)	0.019 (-0.001, 0.039)	0.019 (-0.000, 0.039)
n=9,462	p-value	0.057	0.063	0.054
p-value for interaction		0.081	0.194	0.217

Table 5.2. *ASI: arterial stiffness index; AD: aortic distensibility; B: beta coefficient; CI: confidence interval; SOS: speed of sound. B= increase (number of SDs) in outcome for a 1 SD increase in SOS. *indicates p-value <0.05.*

Table 5.3. Tests for non-linearity using cubic spline models with 5 knots showing p-values for non-linear vs linear models

		Model 1: Age adjusted	Model 2: Age, exercise, smoking, deprivation, alcohol	Model 3: Model 2+ hypercholesterolaemia, diabetes, hypertension
	ASI			
Men	p-value	0.354	0.117	0.099
Women	p-value	0.126	0.782	0.849
	AD (ascending aorta)			
Men	p-value	0.909	0.755	0.823
Women	p-value	0.764	0.724	0.699
	AD (descending aorta)			
Men	p-value	0.494	0.608	0.560
Women	p-value	0.393	0.640	0.654

Table 5.3. *AD: aortic distensibility; ASI: arterial stiffness index.*

Table 5.4. Multivariable linear regression models showing association of speed of sound with measures of arterial stiffness in women stratified by menopause status

		Model 1: Age	Model 2: Age, exercise, smoking, deprivation, alcohol	Model 3: Model 2+ hypercholesterolaemia, diabetes, hypertension
	ASI			
Pre-menopause	Beta (95% CI)	-0.026 (-0.041, -0.011)	-0.025 (-0.041, -0.008)	-0.025 (-0.042, -0.009)
n=33,653	p-value	0.0008*	0.003*	0.003*
Post-menopause	Beta (95% CI)	-0.019 (-0.028, -0.010)	-0.015 (-0.025, -0.005)	-0.018 (-0.028, -0.007)
n=53,940	p-value	4.9×10^{-5}*	0.005*	0.0009*
p-value for interaction		0.433	0.327	0.449
	AD (ascending aorta)			
Pre-menopause	Beta (95% CI)	0.016 (-0.017, 0.049)	0.012 (-0.024, 0.048)	0.012 (-0.024, 0.048)
n=4,333	p-value	0.338	0.522	0.516
Post-menopause	Beta (95% CI)	0.013 (-0.011, 0.037)	0.011 (-0.016, 0.038)	0.012 (-0.015, 0.039)
n=5,129	p-value	0.288	0.483	0.370
p-value for interaction		0.884	0.964	0.984
	AD (descending aorta)			
Pre-menopause	Beta (95% CI)	0.003 (-0.029, 0.036)	0.001 (-0.035. 0.036)	0.001 (-0.035, 0.036)
n=4,333	p-value	0.837	0.973	0.957
Post-menopause	Beta (95% CI)	0.004 (-0.020, 0.028)	0.008 (-0.019, 0.035)	0.009 (-0.018, 0.035)
n=5,129	p-value	0.741	0.563	0.513
p-value for interaction		0.977	0.749	0.727

Table 5.4. *ASI: arterial stiffness index; AD: aortic distensibility; B: beta coefficient; CI: confidence interval; SOS: speed of sound. Beta= SD increase in outcome per 1 SD increase in SOS.*

5.4.3 Association of SOS and arterial compliance stratified by sex and smoking status

In multivariable models stratified by sex and smoking status, we observed no evidence of a significant differential relationship between SOS and AD or ASI in the different subgroups (**Table 5.5**).

Table 5.5. Multivariable linear regression models showing association of speed of sound with measures of arterial stiffness stratified by sex and smoking status

		Model 1: Age	Model 2: Age, exercise, deprivation, alcohol	Model 3: Model 2+ hypercholesterolaemia, diabetes, hypertension
Men	**ASI**			
Non-smokers	B (95% CI)	-0.023 (-0.030, -0.016)	-0.021 (-0.028, -0.013)	-0.020 (-0.028, -0.013)
n=63,312	p-value	8.8×10^{-11}*	1.2×10^{-7}*	2.1×10^{-7}*
Current smokers	B (95% CI)	-0.042 (-0.060, -0.024)	-0.037 (-0.058, -0.017)	-0.037 (-0.058, -0.016)
n=8,637	p-value	5.9×10^{-6}*	0.0004*	0.0004*
p-value for interaction		0.054	0.142	0.138
	AD (ascending aorta)			
Non-smokers	B (95% CI)	0.018 (0.001, 0.037)	0.015 (-0.004, 0.034)	0.015 (-0.004, 0.034)
n=8,096	p-value	0.040*	0.127	0.116
Current smokers	B (95% CI)	0.029 (-0.032, 0.090)	0.039 (-0.025, 0.104)	0.036 (-0.028, 0.101)
n=671	p-value	0.354	0.233	0.271
p-value for interaction		0.754	0.474	0.539
	AD (descending aorta)			
Non-smokers	B (95% CI)	0.043 (0.023, 0.062)	0.037 (0.016, 0.057)	0.036 (0.016, 0.057)
n=8,096	p-value	1.6×10^{-5}*	0.0005*	0.0006*
Current smokers	B (95% CI)	0.034 (-0.033, 0.100)	0.040 (-0.031, 0.111)	0.038 (-0.033, 0.108)
n=671	p-value	0.324	0.268	0.297
p-value for interaction		0.793	0.928	0.969
Women	**ASI**			
Non-smokers	B (95% CI)	-0.018 (-0.026, -0.011)	-0.020 (-0.029, -0.012)	-0.023 (-0.031, -0.014)
n=80,145	p-value	5.5×10^{-7}*	1.7×10^{-6}*	1.1×10^{-7}*
Current smokers	B (95% CI)	-0.026 (-0.050, -0.003)	-0.023 (-0.050, 0.004)	-0.026 (-0.053, 0.001)
n=7,448	p-value	0.025*	0.096	0.056
p-value for interaction		0.536	0.873	0.818
	AD (ascending aorta)			
Non-smokers	B (95% CI)	0.011 (-0.007, 0.030)	0.007 (-0.013, 0.028)	0.008 (-0.012, 0.028)
n=8,986	p-value	0.223	0.496	0.444
Current smokers	B (95% CI)	0.023 (-0.06, 0.107)	0.005 (-0.087, 0.097)	0.012 (-0.080, 0.103)
n=476	p-value	0.586	0.909	0.800
p-value for interaction		0.786	0.970	0.936
	AD (descending aorta)			
Non-smokers	B (95% CI)	0.007 (-0.011, 0.025)	0.009 (-0.011, 0.029)	0.009 (-0.011, 0.029)
n=8,986	p-value	0.464	0.396	0.380
Current smokers	B (95% CI)	-0.020 (-0.101, 0.062)	-0.028 (-0.118, 0.062)	-0.021 (-0.111, 0.069)
n=476	p-value	0.635	0.536	0.644
p-value for interaction		0.533	0.429	0.521

Table 5.5. *ASI: arterial stiffness index; AD: aortic distensibility; B: beta coefficient; CI: confidence interval; SOS: speed of sound. B= increase (number of SDs) in outcome for a 1 SD increase in SOS. *indicates p-value <0.05.*

5.4.4 Association of SOS and arterial compliance stratified by sex and diabetic status

Subgroup analysis by sex and diabetes, appeared to demonstrate a differential relationship with greater effect in non-diabetes (**Table 5.6**). The interaction term (diabetes × SOS) was significant (p=0.012) in fully adjusted models of the association between SOS and ASI in men (**Table 5.6**).

Table 5.6. Multivariable linear regression models showing association of speed of sound with measures of arterial stiffness stratified by sex and diabetic status

		Model 1: Age adjusted	Model 2: Age, exercise, smoking, deprivation, alcohol	Model 3: Model 2+ hypercholesterolaemia, hypertension
Men	**ASI**			
Non-diabetic	B (95% CI)	-0.033 (-0.040, -0.026)	-0.025 (-0.033, -0.018)	-0.025 (-0.032, -0.017)
n=66,598	p-value	6.4×10^{-22}*	3.5×10^{-11}*	6.8×10^{-11}*
Diabetic	B (95% CI)	-0.002 (-0.025, 0.021)	0.009 (-0.017, 0.036)	0.011 (-0.016, 0.037)
n=5,351	p-value	0.873	0.489	0.436
p-value for interaction		0.012	0.014	0.012
	AD (ascending aorta)			
Non-diabetic	B (95% CI)	0.019 (0.002, 0.037)	0.015 (-0.004, 0.033)	0.015 (-0.003, 0.034)
n=8,459	p-value	0.03*	0.120	0.109
Diabetic	B (95% CI)	0.053 (-0.045, 0.151)	0.071 (-0.031, 0.172)	0.068 (-0.033, 0.169)
n=308	p-value	0.289	0.171	0.187
p-value for interaction		0.504	0.286	0.312
	AD (descending aorta)			
Non-diabetic	B (95% CI)	0.042 (0.023, 0.061)	0.037 (0.017, 0.058)	0.037 (0.017, 0.057)
n=8,459	p-value	0.00001*	0.0003*	0.0003*
Diabetic	B (95% CI)	0.026 (-0.08, 0.134)	0.013 (-0.101, 0.127)	0.004 (-0.110, 0.118)
n=308	p-value	0.638	0.818	0.942
p-value for interaction		0.773	0.684	0.574
Women	**ASI**			
Non-diabetic	B (95% CI)	-0.026 (-0.033, -0.019)	-0.022 (-0.030, -0.013)	-0.023 (-0.031, -0.015)
n=83,963	p-value	2.1×10^{-12}*	2.6×10^{-7}*	3.5×10^{-8}*
Diabetic	B (95% CI)	-0.025 (-0.058, 0.007)	-0.020 (-0.060, 0.019)	-0.022 (-0.061, 0.018)
n=3,630	p-value	0.129	0.321	0.289
p-value for interaction		0.981	0.943	0.936
	AD (ascending aorta)			
Non-diabetic	B (95% CI)	0.012 (-0.006, 0.030)	0.007 (-0.013. 0.027)	0.008 (-0.012, 0.028)
n=9298	p-value	0.185	0.487	0.439
Diabetic	B (95% CI)	0.026 (-0.116, 0.169)	0.013 (-0.161, 0.188)	0.025 (-0.149, 0.199)
n=164	p-value	0.719	0.881	0.780
p-value for interaction		0.850	0.945	0.850
	AD (descending aorta)			
Non-diabetic	B (95% CI)	0.042 (0.021, 0.061)	0.037 (0.017, 0.058)	0.037 (0.017, 0.057)
n=9,298	p-value	0.00001*	0.0003*	0.0003*
Diabetic	B (95% CI)	0.061 (-0.081, 0.203)	0.048 (-0.125, 0.221)	0.057 (-0.115, 0.229)
n=164	p-value	0.398	0.585	0.519
p-value for interaction		0.773	0.684	0.574

Table 5.6. *ASI: arterial stiffness index; AD: aortic distensibility; B: beta coefficient; CI: confidence interval; SOS: speed of sound. B= increase (number of SDs) in outcome for a 1 SD increase in SOS. *indicates p-value <0.05.*

5.4.5 Association of SOS and arterial compliance stratified by sex and BMI

We stratified BMI into three categories of normal (BMI ≤25 kg/m^2), overweight (BMI >25 but ≤30), and obese (BMI >30). Stratified analysis by sex and these BMI categories suggested a possible differential effect of SOS on ASI in men, with significant negative associations in the normal/overweight categories and a non-significant relationship in the obese category (**Table 5.7**). The p-value for interaction effect in this model was significant (p=0.0008).

Table 5.7. Multivariable linear regression models showing association of speed of sound with measures of arterial compliance stratified by sex and body mass index

		Model 1: Age adjusted	Model 2: Age, exercise, smoking, social deprivation, alcohol	Model 3: Model 2+ hypercholesterolaemia, diabetes, hypertension
Men	**ASI**			
Normal	B (95% CI)	-0.054 (-0.066, -0.041)	-0.037 (-0.050, -0.023)	-0.036 (-0.050, -0.023)
	p-value	2.3×10^{-17}*	1.0×10^{-7}*	1.7×10^{-7}*
Overweight	B (95% CI)	-0.040 (-0.050, -0.031)	-0.036 (-0.046, -0.025)	-0.035 (-0.046, -0.025)
	p-value	1.1×10^{-17}*	8.1×10^{-12}*	9.1×10^{-12}*
Obese	B (95% CI)	-0.004 (-0.017, 0.009)	0.001 (-0.014, 0.015)	0.001 (-0.014, 0.015)
	p-value	0.545	0.946	0.944
p-value for interaction		2.1×10^{-7}	0.0006	0.0008
	AD (ascending aorta)			
Normal	B (95% CI)	0.030 (-0.001, 0.061)	0.028 (-0.005, 0.061)	0.028 (-0.005, 0.061)
	p-value	0.059	0.095	0.098
Overweight	B (95% CI)	0.021 (-0.003, 0.044)	0.013 (-0.012, 0.038)	0.014 (-0.011, 0.038)
	p-value	0.301	0.310	0.279
Obese	B (95% CI)	0.003 (-0.039, 0.044)	0.007 (-0.037, 0.052)	0.006 (-0.038, 0.051)
	p-value	0.901	0.742	0.788
p-value for interaction		0.352	0.474	0.461
	AD (descending aorta)			
Normal	B (95% CI)	0.068 (0.034, 0.101)	0.067 (0.031, 0.103)	0.067 (0.032, 0.103)
	p-value	8.6×10^{-5}*	0.0002*	0.0002*
Overweight	B (95% CI)	0.028 (0.002, 0.054)	0.022 (-0.006, 0.049)	0.020 (-0.007, 0.048)
	p-value	0.036*	0.125	0.147
Obese	B (95% CI)	0.049 (0.004, 0.094)	0.044 (-0.004, 0.092)	0.042 (-0.006, 0.089)
	p-value	0.031	0.070	0.085
p-value for interaction		0.322	0.269	0.233
Women	**ASI**			
Normal	B (95% CI)	-0.035 (-0.045, -0.024)	-0.030 (-0.042, -0.018)	-0.030 (-0.042. -0.018)
	p-value	2.5×10^{-10}*	1.2×10^{-6}*	7.1×10^{-7}*
Overweight	B (95% CI)	-0.032 (-0.044, -0.021)	-0.024 (-0.038, -0.011)	-0.025 (-0.039, -0.012)
	p-value	$4.9\text{x}10^{-8}$*	0.0003*	0.0002*
Obese	B (95% CI)	-0.024 (-0.039, -0.010)	-0.026 (-0.043, -0.009)	-0.027 (-0.044, -0.010)
	p-value	0.001*	0.003*	0.002*
p-value for interaction		0.262	0.657	0.687
	AD (ascending aorta)			
Normal	B (95% CI)	0.012 (-0.013, 0.037)	0.007 (-0.021, 0.034)	0.008 (-0.019, 0.035)
	p-value	0.351	0.634	0.570
Overweight	B (95% CI)	0.007 (-0.023, 0.037)	0.003 (-0.031, 0.036)	0.003 (-0.031, 0.036)
	p-value	0.641	0.883	0.873
Obese	B (95% CI)	0.020 (-0.028, 0.067)	0.013 (-0.042, 0.068)	0.014 (-0.040, 0.069)
	p-value	0.421	0.638	0.614
p-value for interaction		0.827	0.876	0.894
	AD (descending aorta)			
Normal	B (95% CI)	0.003 (-0.022, 0.027)	-0.000 (-0.027, 0.027)	0.001 (-0.026, 0.028)
	p-value	0.816	0.976	0.964
Overweight	B (95% CI)	0.008 (-0.022, 0.037)	0.011 (-0.022, 0.044)	0.011 (-0.022, 0.043)
	p-value	0.616	0.499	0.526
Obese	B (95% CI)	-0.009 (-0.056, 0.037)	0.012 (-0.041, 0.065)	0.012 (-0.040,0.065)
	p-value	0.680	0.658	0.644
p-value for interaction		0.797	0.556	0.585

Table 5.7. *ASI: arterial stiffness index; AD: aortic distensibility; B: beta coefficient; BMI: body mass index; CI: confidence interval; SOS: speed of sound. B= increase (number of SDs) in outcome for a 1 SD increase in SOS. Overweight (BMI >25 but <= 30 kg/m^2); Obese (BMI >30 kg/m^2). *indicates p-value <0.05.*

5.4.6 Mediation analysis

In testing the effect of various mediators, we elected to focus on the association between SOS and ASI, as this analysis allowed inclusion of the largest sample size and because the ASI relationships had demonstrated most consistency in the previous analyses. In separate analyses for men and women, we considered the potential mediating effect of the following variables: CRP, Creatinine, Vitamin D, Calcium, ALP, IGF1, SHBG, Testosterone, Testosterone/SHBG, Oestradiol, Phosphate, Cystatin C, hypertension, diabetes, and hypercholesterolaemia.

In the first instance, we evaluated the mediating effect of each variable individually for men (**Table 5.8**) and women (**Table 5.9**). Variables with a significant mediating effect in this analysis were taken forward for multiple mediation analysis. In the final models, we included variables that had statistically significant effects in the multiple mediator model (**Table 5.10**, **Table 5.11**). In the multiple mediation analysis, biomarkers relating to bone mineralisation appeared important for both men and women. For men, ALP, phosphate, and vitamin D accounted for 7.5%, 4.6%, and 3.2% of the observed effect. In women, ALP and phosphate accounted for 9.6% and 13.2% of the observed effect. CRP accounted for 6.1% of the mediated effect in men and -8.6% in women. SHBG had an important suppressing effect for both men and women as adjustment for this variable increased the effect by 17.1% and 19.6% respectively.

Table 5.8. Indirect effect (mediated effect) of speed of sound on arterial stiffness index through each mediator in men, tested individually

Mediator	Beta	95% CI	p-value	Percentage mediated
Alkaline phosphatase	-0.003	(-0.004, -0.002)	1.5×10^{-18}*	11.5%
Calcium	0.000	(0.000, 0.0001)	0.45	0.2%
Phosphate	-0.001	(-0.002, -0.001)	0.00002*	4.1%
Vitamin D	-0.001	(-0.002, -0.001)	1.2×10^{-9}*	4.8%
C Reactive Protein	-0.003	(-0.003, -0.002)	9.3×10^{-13}*	10.1%
Creatinine	-0.001	(-0.001, 0.000)	0.02	2.1%
IGF1	-0.001	(-0.002, -0.001)	0.00002*	4.0%
SHBG	0.005	(0.004, 0.006)	3.4×10^{-25}*	-17.2%
Testosterone	-0.002	(-0.002, -0.001)	1.1×10^{-11}*	6.7%
Oestradiol	0.000	(0.000, 0.001)	0.493	-0.6%
Cystatin C	-0.001	(-0.001, 0.000)	0.00008*	2.8%
Testosterone/SHBG	0.003	(0.002, 0.004)	10.0×10^{-10}*	-11.9%
Hypertension	-0.0004	(-0.001, -0.00008)	0.011	1.6%
Hypercholesterolaemia	0.000	(0.000, 0.00004)	0.839	0.0%
Diabetes	0.000	(0.000, 0.0002)	0.088	-0.4%

Table 5.8. *CI: confidence interval; IGF1: insulin like growth factor 1; SHBG: Sex hormone binding globulin. Significance level p<0.003. *indicates p-value<0.003.*

Table 5.9. Indirect effect (mediated effect) of speed of sound on arterial stiffness index through each mediator in women, tested individually

Mediator	Beta	95% CI	p-value	Percentage mediated
Alkaline phosphatase	-0.004	(-0.005, -0.004)	4.7×10^{-30}*	23.8%
Calcium	-0.0002	(-0.0004, -0.0001)	0.012	0.0%
Phosphate	-0.003	(-0.003, -0.002)	9.9×10^{-15}*	13.6%
Vitamin D	0.000	(0.000, 0.001)	0.303	0.0%
C Reactive Protein	0.003	(0.002, 0.004)	1.4×10^{-12}*	-14.3%
Creatinine	0.000	(0.000, 0.0002)	0.57	0.0%
IGF1	-0.0002	(0.000, 0.000)	0.028	0.0%
SHBG	0.006	(0.005, 0.007)	4.4×10^{-32}*	-27.3%
Testosterone	-0.0001	(0.000, 0.0004)	0.182	0.0%
Oestradiol	-0.0001	(0.000, 0.0002)	0.576	0.0%
Cystatin C	-0.001	(-0.001, -0.0002)	0.007	4.8%
Testosterone/SHBG	0.003	(0.002, 0.004)	1.9×10^{-10}*	-12.0%
Hypertension	0.002	(0.001, 0.002)	5.1×10^{-14}*	-5.0%
Hypercholesterolaemia	0.0004	(0.000, 0.0007)	0.001*	-2.0%
Diabetes	0.0008	(0.001, 0.0012)	9.9×10^{-6}*	-4.0%

Table 5.9. *CI: confidence interval; IGF1: insulin like growth factor 1; SHBG: Sex hormone binding globulin. Significance level p<0.003. *indicates p-value<0.003.*

Table 5.10. Independent indirect effect (mediated effect) of speed of sound on arterial stiffness index through each mediator in men

Mediator	Beta	95% CI	p-value	Percentage mediated
Alkaline phosphatase	-0.0021	(-0.0028, -0.0015)	6.6×10^{-11}	7.5%
Phosphate	-0.0013	(-0.0018, -0.0008)	1.8×10^{-7}	4.6%
Vitamin D	-0.0009	(-0.0012, -0.0005)	0.00001	3.2%
C Reactive Protein	-0.0017	(-0.0023, -0.0012)	1.4×10^{-9}	6.1%
IGF1	-0.0016	(-0.0022, -0.001)	7.0×10^{-8}	5.7%
SHBG	0.0048	(0.0032, 0.0064)	3.2×10^{-9}	-17.1%
Testosterone	0.001	(0.0005, 0.0014)	0.00009	-3.6%
Cystatin C	-0.0004	(-0.0006, -0.0001)	0.004	1.4%

Table 5.10. *CI: confidence interval; IGF1: insulin like growth factor 1; SHBG: Sex hormone binding globulin. Significance level p<0.006.*

Table 5.11. Independent indirect effect (mediated effect) of speed of sound on arterial stiffness index through each mediator in women

Mediator	Beta	95% CI	p-value	Percentage mediated
Alkaline phosphatase	-0.0021	(-0.0027, -0.016)	3.1×10^{-13}	9.6%
Phosphate	-0.0029	(-0.0036, -0.0022)	4.1×10^{-17}	13.2%
C Reactive Protein	0.0019	(0.0013, 0.0025)	2.1×10^{-9}	-8.6%
SHBG	0.0043	(0.0035, 0.0051)	1.6×10^{-27}	-19.6%
Hypertension	0.0007	(0.0004, 0.0011)	0.00003	-5.5%

Table 5.11. *CI: confidence interval; IGF1: insulin like growth factor 1; SHBG: Sex hormone binding globulin. Significance p<0.01.*

In summary, for men, the overall effect of the mediating variables was mediation, that is, the magnitude of the main exposure-outcome relationship was reduced by adjustment for the mediators. In women, the effect was one of suppression rather than mediation as the magnitude of the exposure-outcome relationship increased when we added the potential mediators. The association between ASI and SOS remained significant with all the mediators in the model.

5.4.7 Association of SOS with ischaemic cardiovascular outcomes

We estimated the association of bone quality as measured by SOS with IHD mortality and incident AMI. There were 477,683 participants with SOS recorded at baseline, including 263,273 women and 214,410 men. Baseline characteristics are presented in **Table 5.12**. For IHD mortality, follow-up time was 2,342,445 person years for women and 1,888,767 for men. During this period, there were 388 IHD deaths in women (incidence rate=0.17 per 1000 person years) and 1,722 (incidence rate=0.91 per 1000 person years) in men. Follow-up time for incident AMI was 2,123,170 person years for women and 1,659,850 person years for men. There were 2,415 AMI events in women (incidence rate=1.14 per 1000 person years) and 5,616 events (incidence rate=3.38 per 1000 person years) in men.

In crude models, with age adjustment only, SOS was associated with significantly reduced hazard of both incident AMI and IHD mortality in men; the associations in women were weaker and not statistically significant. The association with incident AMI was attenuated with adjustment for age, exercise, material deprivation, and alcohol. In a final model, with addition adjustment for hypertension, hypercholesterolaemia, and diabetes, SOS was associated with significantly lower risk of IHD mortality in men. In the fully adjusted model, one standard deviation increase of SOS was associated with 14% lower hazard of IHD mortality [SHR 0.86 (0.75-1.00), p-value 4.0×10^{-7}] in men (**Table 5.13**). We considered whether the relationship of SOS with IHD mortality may be explained

by previously observed associations of SOS with ASI. Thus, in a separate model, we added ASI as a covariate in the fully adjusted competing risk models. The magnitude of effect or statistical significance of the relationship were not altered in this model (**Table 5.14**). Thus, it appears that the association with IHD mortality may be occurring through alternative mechanisms to the ASI association.

Table 5.12. Baseline participant characteristics (ischaemic heart disease outcomes sample)

	Men		Women	
	No IHD death (n=212,688)	IHD death (n=1,722)	No IHD death (n=262,885)	IHD death (n=388)
Age	58 [50 to 64]	63 [58 to 66]	58 [50 to 63]	64 [60 to 67]
Ethnicity (White)	201,008 (95.0%)	1,631 (95.7%)	248,596 (94.9%)	371 (96.6%)
Townsend deprivation score	-2.2 [-3.7 to 0.6]	-1.0 [-3.0 to 2.3]	-2.2 [-3.7 to 0.4]	-0.9 [-3.0 to 2.0]
Body mass index kg/m^2	27.2 [24.9 to 29.9]	28.5 [25.9 to 32.0]	26.1 [23.5 to 29.7]	28.4 [25.0 to 32.7]
Current smoking	26,295 (12.4%)	456 (26.7%)	23,297 (8.9%)	83 (21.6%)
Regular alcohol use	109,932 (51.8%)	796 (46.4%)	96,430 (36.8%)	87 (22.7%)
Physical activity (metabolic equivalent minutes/week)	1,862 [824 to 3,822]	1,573 [582 to 3,506]	1,765 [820-3492]	1242 [506.5 to 3232.5]
Multimorbidity (number of non-cancer illnesses)	1 [0-3]	3 [2-5]	1 [0-3]	3 [2-5]
Hypertension	68,407 (32.2%)	1,053 (61.1%)	63,260 (24.1%)	232 (59.8%)
Diabetes	14,326 (6.7%)	419 (24.3%)	9,840 (3.7%)	91 (23.5%)
Hypercholesterolaemia	51,304 (24.1%)	934 (54.2%)	36,669 (13.9%)	178 (45.9%)
Post-menopausal	-	-	159766 (72.3%)	301 (93.7%)
Arterial stiffness index (m/s)	9.8 [7.7 to 11.8]	10.6 [8.5 to12.6]	8.3 [6.3 to 10.5]	9.6 [7.5 to 12.5]
Speed of sound (10^2m/s)	15.57 (0.30)	15.50 (0.32)	15.48 (0.29)	15.41 (0.32)

Table 5.12. *Data based on information collected at baseline assessment. Continuous variables presented as median [interquartile range] or mean (standard deviation). Discrete data presented as frequencies (percentages). IHD: ischaemic heart disease.*

Table 5.13. Competing risk models of the association of speed of sound with incident acute myocardial infarction and ischaemic heart disease mortality

n=477,683		Model 1: Age	Model 2: Age, exercise, smoking, deprivation, alcohol	Model 3: Model 2+ hypercholesterolaemia, diabetes, hypertension
	Incident AMI			
Men (n=214,410)	SHR (95% CI)	0.96 (0.93-0.99)	0.99 (0.96-1.02)	0.99 (0.96-1.02)
	p-value	0.002*	0.651	0.658
Women (n=263,273)	SHR (95% CI)	0.97 (0.93-1.01)	1.03 (0.97-1.08)	1.00 (0.95-1.05)
	p-value	0.159	0.352	0.987
	IHD mortality			
Men (n=214,410)	SHR (95% CI)	0.81 (0.77-0.85)	0.86 (0.81-0.91)	0.86 (0.81-0.91)
	p-value	7.8×10^{-15}*	9.9×10^{-7}*	4.0×10^{-7}*
Women (n=263,273)	SHR (95% CI)	0.92 (0.82-1.02)	0.91 (0.78-1.05)	0.86 (0.75-1.00)
	p-value	0.093	0.184	0.051

Table 5.13*. AMI: acute myocardial infarction; ASI: arterial stiffness index; CI: confidence interval; IHD: ischaemic heart disease; SHR: subdistribution hazard ratio; SOS: speed of sound. *indicates p-value <0.05.*

Table 5.14. Competing risk models of the association of speed of sound with incident acute myocardial infarction and ischaemic heart disease mortality

		Model 2: Age, exercise, smoking, deprivation, alcohol + ASI	Model 3: Model 2+ hypercholesterolaemia, diabetes, hypertension+ ASI
	IHD mortality		
Men	SHR (95% CI)	0.85 (0.76-0.95)	0.85 (0.76-0.95)
	p-value	5.6×10^{-3}*	3.5×10^{-3}*
Women	SHR (95% CI)	0.77 (0.54-1.09)	0.73 (0.51-1.03)
	p-value	0.134	0.076

Table 5.14. *AMI: acute myocardial infarction; ASI: arterial stiffness index; CI: confidence interval; IHD: ischaemic heart disease. SHR: subdistribution hazard ratio; SOS: speed of sound. *indicates p<0.05.*

5.5 Summary of findings

We demonstrate the association of better bone health with better vascular health. Specifically, our results indicate association of higher SOS measured by heel ultrasound with greater arterial compliance measured by AD (CMR) and ASI (finger plethysmography). The relationship was consistent in men and women and by menopause status. There was no clear differential relationship by smoking status, diabetes, or BMI. In the case of diabetes and BMI, results of stratified analysis are likely highly influenced by unbalanced sample sizes in the different strata. We considered the potential mediating effect of a range of blood biomarkers on the ASI and SOS relationship. Although there was some commonality, in general, the pattern of mediation varied for men and women, and in neither did these markers provide a complete explanation of the observed associations. Finally, we

estimated the association of SOS with incident ischaemic cardiovascular outcomes. In fully adjusted models, higher SOS was associated with significantly lower risk of IHD mortality in men (and less robustly in women). This relationship was not attenuated with addition of ASI to the model, indicating importance of alternative mechanisms.

5.6 Discussion

5.6.1 Comparison with existing literature

Previous studies have examined the association of bone quality with arterial stiffness, as measured by pulse wave velocity (PWV). There is little data on differential relationships by sex or menopause status. In a cohort of 7,685 individuals from Japan, Hirose et al.[174] report association of better bone quality (quantitative heel ultrasound) with lower arterial stiffness (PWV) in men and women; they report greater magnitude of effect in post-menopausal women. Avramovski et al.[175] and Zhang et al[176] also report similar associations between BMD and arterial stiffness, but are underpowered to test for any modifying effect of age or menopause. These associations have been replicated in smaller studies of Korean[177] and Turkish women[178]. For men, the relationship is less clear from existing studies. For example, in a cohort of 633 individuals, Giallauria et al.[179] report association of higher bone quality assessed by computed tomography and lower arterial stiffness by PWV for women, but not for men. Our analysis, in the largest sample studied to date, confirms the previously reported associations between bone and vascular health and demonstrates that these associations are consistent for men and women and in both pre- and post-menopausal women.

The association between better bone quality (higher SOS) with reduced risk of IHD mortality in men in our study, is consistent with previous findings, which, in common with our results, demonstrate a stronger relationship in men[180–182]. However, smaller studies in older women[183,184], and a larger study of 5,816 women[185] have demonstrated that these mortality associations are also applicable to women. In these reports, the study population was comprised of an older cohort of women, compared to our sample. Accordingly, we observed fewer events in the women in our sample compared to these cohorts, and compared to the men in our cohort. Therefore, it is possible that we were underpowered to detect specific associations with IHD outcomes for women.

5.6.2 Potential biological mechanisms

Limited studies have considered potential common biological processes linking bone mineralisation and atherosclerotic processes. To this end, several studies have considered the relationship between serum markers of bone metabolic and arterial stiffness. In a study of 1,003 diabetic patients, Sharif et al.[186] demonstrate association of higher levels of osteopontin (a plasma regulator of bone metabolism)

with higher arterial stiffness. In a study of 144 post-menopausal women, Albu et al.[187] document association of greater plasma osteoprotegerin levels with higher arterial stiffness, but not with osteopontin, suggesting possible differences in biological mechanisms for men and women. It is worth noting, that both osteoprotegin and osteopontin have been directly implicated in vascular pathology as well as bone mineralisation. Therefore, these observations do not necessarily indicate direct mechanisms between bone and vascular health[188]. We considered the potential mediating effect of a wide range of blood biomarkers (for the SOS-ASI relationship). Our results indicate likely sex-specific disease mechanisms, however the mediators studied did not provide an adequate explanation for men or women. Furthermore, whilst it seemed plausible that the association of SOS with IHD mortality may be mediated through its relationship with ASI, we did not find this to be the case. These observations demonstrate the complexity of the relationship between bone and cardiovascular health and the challenges in elucidating specific biological mechanism.

5.7 Critical appraisal of the results

Our findings adds strength to previous work suggesting independent links between bone and cardiovascular health. Additionally, we further existing knowledge by demonstrating the consistency of these relationships across the sexes and in pre- and post-menopause. The use of objectively defined standardised imaging and physical measures of bone and arterial health limits bias from misdiagnoses or subjectivity of clinical assessments. The clinical outcomes considered (incident AMI, and IHD death) are reliably and completely identified through data linkage with HES and death register data. The SOS measure was obtained at the baseline visit, whilst AD was measured several years later at imaging. Similarly, we considered incident clinical outcomes occurring after SOS measurement. Thus, there is temporal separation of SOS and arterial health indicators by a number of years. Overall, this makes a causal relationship between bone and vascular health likely. Of course, causal inference from observational data is highly challenging, particularly as, despite extensive consideration of confounders, residual confounding cannot be excluded. Dedicated causal inference methods, such as Mendelian Randomisation analysis would add strengths to our findings.

5.8 Conclusions

The results from this analysis support a positive link between bone and vascular health, which is consistent in men and women and with menopause. Analysis of underlying mediating mechanisms did not provide a complete explanation but indicated likely differences in mechanism for men and women. Higher SOS was associated with lower risk of IHD mortality in men (and less robustly in women), this relationship was not explained by association of SOS with ASI. Thus, although links between heart and musculoskeletal health appear robust, the underlying pathophysiology of the bone

heart axis is complex and likely varies by sex. Further research into biological mechanism is warranted.

6 Meat consumption and cardiovascular phenotypes

6.1 Abstract

Objectives: Higher intake of red and processed meat has been linked to poorer clinical cardiovascular outcomes. However, the association of these exposures with CMR phenotypes has not been studied. We evaluate associations of meat intake with CMR metrics and investigate underlying mechanisms through consideration of a range of covariates.

Methods and Results: The analysis sample includes 19,408 UK Biobank participants with CMR data available. We calculated a continuous measure of average daily red and processed meat intake from food frequency questionnaires. Oily fish was studied as a comparator, previously associated with healthier cardiovascular endpoints. We examined associations with conventional CMR metrics (ventricular volumes, ejection fraction, stroke volume, LV mass), novel CMR radiomics features (shape, first-order, texture), and arterial stiffness metrics (ASI, AD). We estimated the association of the dietary exposures with cardiovascular phenotypes using multivariable linear regression models, adjusting for confounders (age, sex, deprivation, educational level, smoking, alcohol intake, exercise) and potential mediators (hypertension, hypercholesterolaemia, diabetes, BMI). Greater red and processed meat consumption was associated with an adverse LV and RV remodelling, poorer ventricular function, and less compliant arteries. In comparison, higher oily fish intake was linked to healthier cardiac structure and function measures and more compliant arteries. There was partial attenuation of the red meat-CMR associations with addition of potential mediators, indicating a possible mechanistic role for these cardiometabolic factors. However, other associations were not altered with inclusion of these covariates, suggesting importance of alternative underlying biological mechanisms. CMR radiomics provided deeper phenotyping, demonstrating association of the different dietary habits with distinct ventricular geometry and LV myocardial texture patterns.

Conclusions: Greater red and processed meat consumption is associated with impaired cardiovascular health, both in terms of markers of arterial disease and of cardiac structure and function. Cardiometabolic morbidities appeared to have a mechanistic role in the associations of red meat with ventricular phenotypes, but less so for other associations suggesting importance of alternative mechanism for these relationships.

6.2 Background

The association between greater meat consumption and poorer cardiovascular endpoints has been repeatedly demonstrated in epidemiological studies[189–192]. Greater consumption of red and processed meat in particular has been linked to greater burden of atherosclerosis[193], higher risk of incident ischaemic cardiovascular events[194] and heart failure[195]. Animal studies have demonstrated association of higher red meat intake with adverse ventricular remodelling and heart failure phenotypes[196]. However, the impact of these exposures on cardiovascular phenotypes in humans has not been adequately studied.

Cardiometabolic morbidities have been proposed as possible mediators of these relationships[197,198]. Furthermore, recent studies suggest novel causal underlying mechanisms pertaining to cross-system interactions with the gut microbiome[199].

In this study, we examined novel associations between red and processed meat intake and cardiovascular structure and function quantifiers in the UK Biobank, considering a wide range of confounder and mediators. We included conventional CMR indices, novel CMR radiomics features, and measures of arterial compliance. We considered associations between oily fish intake as a comparator previously linked with favourable cardiovascular endpoints[194]. We hypothesised that greater red and processed meat intake would be linked to unhealthy cardiovascular phenotypes, whilst oily fish would be associated with healthy phenotypes.

6.3 Methods

6.3.1 Study population

We included UK Biobank participants with CMR or arterial stiffness index data. The cohort is described in detail in **Section 2.1.**

6.3.2 Ascertainment of meat intake variables

The UK Biobank baseline touchscreen questionnaire included a series of questions about dietary intake covering the main food groups. Participants were required to estimate their average weekly intake of a range of food products over the last 12 months. From the questionnaire, we extracted three main dietary exposure categories of interest: 1) Unprocessed red meat, 2) Processed meat, 3) Oily fish.

Unprocessed meat comprised a composite of average beef, lamb or mutton, and pork consumption; we also considered association with each of these categories individually. Processed meat comprised average consumption of any processed meat products (e.g., bacon, ham, sausages, meat pies, kebabs, burgers). Oily fish included consumption of any fresh oily fish (e.g., sardines, salmon, mackerel, herring). Please see **Table 6.1** for further details of the food frequency questionnaire items relating to these food products. We converted reported portion frequencies into probabilities of daily intake and multiplied by standard portion sizes[200] to derive average daily consumption in grams. As such, we were able to consider the meat exposures as continuous variables, as has been published previously using this dataset[201].

Table 6.1. Selected components of the UK Biobank food intake questionnaire

Meat type	Touchscreen question	Help message*
Lamb	How often do you eat lamb/mutton? (Do not count processed meats)	Please provide an average considering your intake over the last year. If you are unsure, please provide an estimate or select Do not know.
Beef	How often do you eat beef? (Do not count processed meats)	Please provide an average considering your intake over the last year. If you are unsure, please provide an estimate or select Do not know.
Pork	How often do you eat pork? (Do not count processed meats such as bacon or ham)	Please provide an average considering your intake over the last year. If you are unsure, please provide an estimate or select Do not know.
Processed meat	How often do you eat processed meats (such as bacon, ham, sausages, meat pies, kebabs, burgers, chicken nuggets)?	Please provide an average considering your intake over the last year. If you are unsure, please provide an estimate or select Do not know.
Oily fish	How often do you eat oily fish? (e.g., sardines, salmon, mackerel, herring)	Please provide an average considering your intake over the last year. If you are unsure, please provide an estimate or select Do not know. Oily fish include: Salmon, Anchovies, Trout, Swordfish, Mackerel, Bloater, Herring, Cacha, Sardines, Carp, Pilchards, Hilsa, Kipper, Jack fish, Ee,l Katla, Whitebait, Orange roughy, Tuna (fresh only), Pangas, Sprats

Table 6.1. **The help message was displayed if the participant activated the help button. For all questions the following answers were possible: never, less than once a week, once a week, 2-4 times a day, 5-6 times a week, once or more daily, do not know, prefer not to answer.*

6.3.3 Conventional CMR indices

CMR image acquisition and analysis was as described in **Section 2.1.6** and **Section 2.2.5.1.** For the present analysis, data was available from 19,408 CMR studies, including the following metrics: LV and RV volumes in end-diastole and end-systole, LV and RV ejection fraction, LV and RV stroke volume, and LV mass.

6.3.4 Novel CMR radiomics features

CMR radiomics is a novel image analysis technique which generates a large number of quantitative indices of shape and texture from a defined region of interest[71]. Radiomics features provide information that is complementary and potentially incremental to conventional CMR indices[71]. A detailed description of this methodology is presented in **Section 2.3.**

In the present study, we made use of existing segmentations from conventional CMR analysis, as described in **Section 2.2.5.1** to define three regions of interest in end-diastole and end-systole for radiomics analysis: 1) RV cavity, 2) LV cavity, 3) LV myocardium (**Figure 6.1**).

Figure 6.1. Three regions of interest were selected from short axis cine images

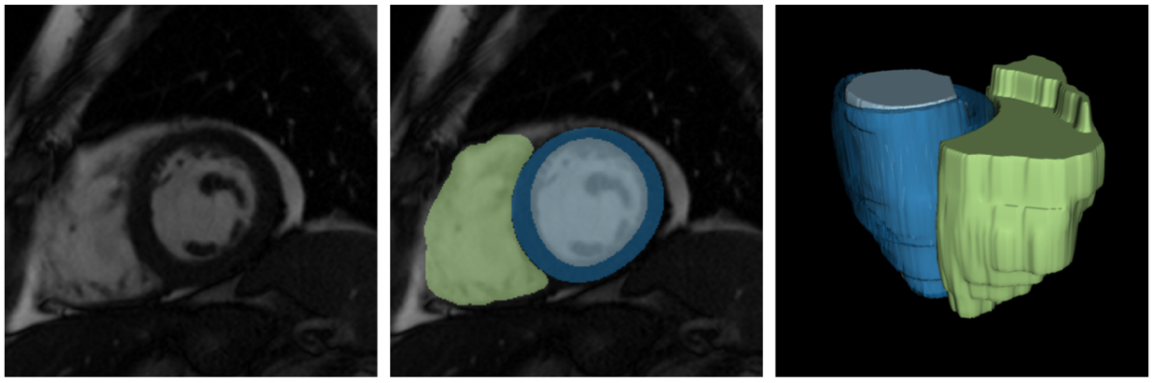

Figure 6.1. *From left to right: 2D short axis mid-ventricular slice; segmentation of the three regions of interest shown overlaid on the image: LV myocardium (blue), LV blood pool (light blue), and RV blood pool (green); 3D reconstructions of the segmented regions. For illustration, we present regions of interest in end-diastole, in the analysis, we considered also these three regions, derived in the same manner, in end-systole. Adapted from Raisi-Estabragh et al.*[99].

From the RV and LV cavity regions, we extracted radiomics shape features. From the LV myocardium region, we extracted signal intensity-based features, specifically, histogram derived first-order features and texture features. We used the PyRadiomics open-source platform for radiomics feature extraction[90]. The list of features extracted and used in this study is presented in **Table 6.2**.

To ensure that variation in signal intensity levels and patterns were due to biological differences rather than technical variations related to image acquisition, we performed intensity normalisation of CMR images through histogram matching, using as reference one of the studies from the dataset[202]. For grey level discretisation, we used a fixed bin width of 25 intensity values.

Table 6.2. List of cardiovascular magnetic resonance radiomics features extracted and included in the analysis grouped by feature category

Shape features	First-order features	Texture features
Volume	Energy	Autocorrelation (GLCM)
Surface Area	Total Energy	Joint Average (GLCM)
Surface Area To Volume Ratio	Entropy	Cluster Prominence (GLCM)
Sphericity	Minimum	Cluster Shade (GLCM)
Maximum 3D Diameter	10th Percentile	Cluster Tendency (GLCM)
Maximum 2D Diameter (Slice)	90th Percentile	Contrast (GLCM)
Maximum 2D Diameter (Column)	Maximum	Correlation (GLCM)
Maximum 2D Diameter (Row)	Mean	Difference Average (GLCM)
Major Axis Length	Median	Difference Entropy (GLCM)
Minor Axis Length	Interquartile Range	Difference Variance (GLCM)
Least Axis Length	Range	Joint Energy (GLCM)
Elongation	Mean Absolute Deviation	Joint Entropy (GLCM)
Flatness	Robust Mean Absolute Deviation	Informal Measure Of Correlation 1 (GLCM)
	Root Mean Squared	Informal Measure Of Correlation 2 (GLCM)
	Skewness	Inverse Difference Moment (GLCM)
	Kurtosis	Inverse Difference Moment Normalized (GLCM)
	Variance	Inverse Difference (GLCM)
	Uniformity	Inverse Difference Normalized (GLCM)
		Inverse Variance (GLCM)
		Maximum Probability (GLCM)
		Sum Average (GLCM)
		Sum Entropy (GLCM)
		Sum Of Squares (GLCM)
		Small Area Emphasis (GLSZM)
		Large Area Emphasis (GLSZM)
		Grey Level Non Uniformity (GLSZM)
		Size Zone Non Uniformity (GLSZM)
		Size Zone Non Uniformity Normalized (GLSZM)
		Zone Percentage (GLSZM)
		Grey Level Variance (GLSZM)
		Zone Variance (GLSZM)
		Zone Entropy (GLSZM)
		Low Grey Level Zone Emphasis (GLSZM)
		High Grey Level Zone Emphasis (GLSZM)

Shape features	First-order features	Texture features
		Small Area Low Grey Level Emphasis (GLSZM)
		Small Area High Grey Level Emphasis (GLSZM)
		Large Area Low Grey Level Emphasis (GLSZM)
		Large Area High Grey Level Emphasis (GLSZM)
		Short Run Emphasis (GLRLM)
		Long Run Emphasis (GLRLM)
		Grey Level Non Uniformity (GLRLM)
		Run Length Non Uniformity (GLRLM)
		Run Length Non Uniformity Normalized (GLRLM)
		Run Percentage (GLRLM)
		Grey Level Variance (GLRLM)
		Run Variance (GLRLM)
		Run Entropy (GLRLM)
		Low Grey Level Run Emphasis (GLRLM)
		High Grey Level Run Emphasis (GLRLM)
		Short Run Low Grey Level Emphasis (GLRLM)
		Short Run High Grey Level Emphasis (GLRLM)
		Long Run Low Grey Level Emphasis (GLRLM)
		Long Run High Grey Level Emphasis (GLRLM)
		Coarseness (NGTDM)
		Contrast (NGTDM)
		Busyness (NGTDM)
		Complexity (NGTDM)
		Strength (NGTDM)
		Small Dependence Emphasis (GLDM)
		Large Dependence Emphasis (GLDM)
		Grey Level Non Uniformity (GLDM)
		Dependence Non Uniformity (GLDM)
		Dependence Non Uniformity Normalized (GLDM)
		Grey Level Variance (GLDM)
		Dependence Variance (GLDM)
		Dependence Entropy (GLDM)
		Low Grey Level Emphasis (GLDM)
		High Grey Level Emphasis (GLDM)
		Small Dependence Low Grey Level Emphasis (GLDM)
		Small Dependence High Grey Level Emphasis (GLDM)
		Large Dependence Low Grey Level Emphasis (GLDM)
		Large Dependence High Grey Level Emphasis (GLDM)

Table 6.2. *CMR: cardiovascular magnetic resonance; GLCM: grey level co-occurrence matrix; GLDM: grey level dependence matrix; GLRLM: grey level run length matrix; GLSZM: grey level size zone matrix; NGTDM: neighboring grey tone difference matrix; LV: left ventricle.*

6.3.5 Aortic distensibility

AD is a measure of local aortic compliance. AD results were obtained from a fully automated image analysis pipeline as described in **Section 2.2.6.1.**

6.3.6 Arterial stiffness index

ASI was measured at both baseline and imaging visits using finger photoplethysmography according to a standardised protocol[70]. Further details on this measure are presented in **Section 2.2.6.2.** We used a 1.5 IQR rule to remove outliers from the ASI variable, consistent with previous publications[28].

6.3.7 Statistical analysis

For the statistical analysis, we used R Version 3.6.2[142] and RStudio Version 1.2.5019[143]. We used multivariable linear regression to estimate the association of each dietary exposure (unprocessed red meat, processed meat, oily fish) with each cardiovascular metric. For ease of interpretation, we report change in cardiovascular metric per 100g increase in daily meat consumption, alongside corresponding 95% confidence intervals (CIs) and p-values. As ASI was available at two time points (baseline, imaging), we estimated associations between the dietary intake exposures with measures taken at both baseline and imaging visits. In addition, in preliminary analyses, we identified significant interval change in ASI from baseline to imaging. Therefore, we also considered "change in ASI" as an additional outcome, expressed using standardised residuals derived from regression of ASI at imaging on ASI at baseline. The average time interval between baseline and imaging assessment was 7.5 years in the CMR set and 8.2 years in the ASI set.

We identified covariates on basis of association with both exposure and outcome in preliminary analyses and review of current evidence (**Figure 6.2**). In the main models, we control for potential confounders (age, sex, material deprivation, education, smoking, alcohol intake, exercise) to estimate the magnitude of the exposure-outcome associations. We selected hypertension, hypercholesterolaemia, diabetes, and body mass index (BMI) as potential mediators of the relationship, i.e., covariates potentially on the causal pathway (**Figure 6.2**). Covariates were ascertained as described in **Section 2.2.2** and **Section 2.2.3**.

In order to evaluate the impact of these variables, we tested associations with additional inclusion of these factors in the main models, with the expectation that covariates on the causal pathway would attenuate exposure-outcome associations. Thus, we present two sets of models: 1) Confounder adjusted models 2) Confounder and mediator adjusted models.

Figure 6.2. Covariates considered in the relationship between red and processed meat consumption and cardiovascular phenotypes

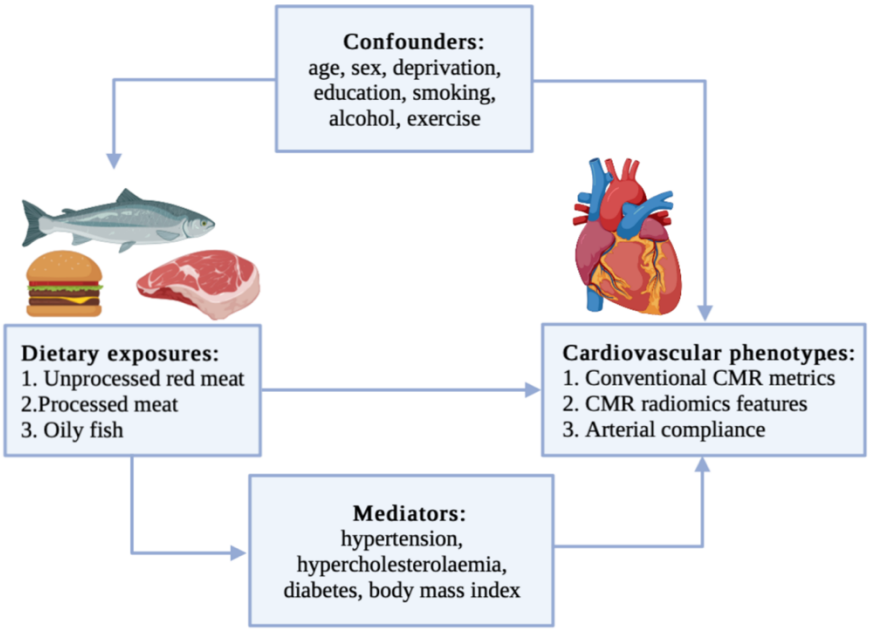

***Figure 6.2**. CMR: cardiovascular magnetic resonance. Reproduced from Raisi-Estabragh et al.*[203]

6.3.7.1 Additional steps for the radiomics analysis

To derive effect sizes that were comparable across different radiomics features, prior to regression analysis, we performed z-score normalisation of the features, this means that all the features were put on the same scale. The results for associations with radiomics features are thus reported as standardised beta coefficients per 100g daily increase in meat/fish intake. For the radiomics associations we present results from confounder adjusted models only.

Since the number of radiomics texture features was large (n=144), to improve interpretation, we performed cluster analysis to identify correlated feature groupings (**Figure 6.3**)[204]. We hierarchically clustered features using complete linkage on Pearson correlation distance between features. The optimal number of clusters was determined by computing the average silhouette using the cluster package in R[204]. The silhouette statistic is a measure of cluster consistency and represents the average distance between data points in the same cluster compared against average data points in other clusters and allows judgement of the optimal number of clusters within a sample. This approach ensures that clusters are constructed such that the distance between datapoints within clusters are minimised whilst the distance with datapoints outside the cluster (other clusters) is maximised. Higher silhouette statistics indicate better conformity with these criteria. We computed average silhouette statistic for 2 to 10 clusters. In our sample, the highest silhouette statistic was observed with 7 clusters, which we took as reflecting the optimal number of clusters (**Figure 6.3**).

We then examined the features within each cluster and assigned descriptive names to each cluster on the basis of the properties represented by its constituent features. Therefore, for the texture features, we present the mean beta-coefficient and 95% CIs for each cluster for the different dietary exposures. We compare effects between exposure categories through testing for the difference in mean beta coefficients using Kruskal-Wallis statistical testing followed by Dunn's correction for multiple comparisons.

Figure 6.3. Illustration of clustering method (hierarchical) and approach to defining the number of clusters (average silhouette approach) for the LV myocardium radiomics texture features

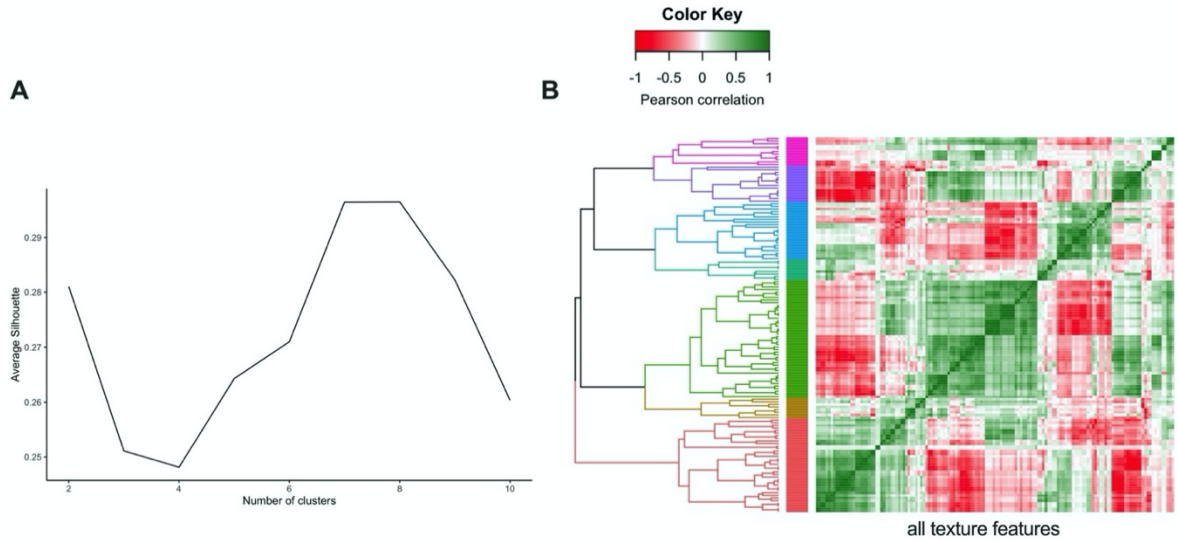

Figure 6.3. *(A) Average silhouette statistic for complete-linkage hierarchical clustering of texture feature correlations. The silhouette statistic reflects the average distance between data points in the same cluster compared against average data points in other clusters and allows judgement of the optimal number of clusters within a sample, such that distance between datapoints within clusters are minimised whilst maximising distance with datapoints from other clusters. We computed average silhouette statistic for 2 to 10 clusters. Maximum silhouette statistic was observed with 7 and 8 clusters. Hence, we take 7 clusters as representing the optimal number of clusters within our samples. (B) Correlation heatmap, rows and columns correspond to all texture features creating grid with all possible pairs of texture features, grid colour corresponds to Pearson Correlation between pair of features at that point. Grid rows re-ordered by hierarchical clustering of correlations with tree coloured for optimal seven cluster cut of the tree. Reproduced from Raisi-Estabragh et al.*[203]

6.4 Results

6.4.1 Baseline population characteristics

The analysis includes 10,105 women and 9,303 men, for whom CMR data were available. The average age was 55.0 (±7.5) years (**Table 6.3**). Most participants (97%, n= 18,810) were of White ethnic background; Black, Asian, and Other ethnicities made up 0.5%, 1.0%, and 1.5% of the study population respectively. The cohort was predominantly healthy, with only 5.5% (n=1,062) having a history of pre-existing cardiovascular disease. Hypertension, hypercholesterolaemia, diabetes, and smoking were present in 13.9%, 23.0%, 3.1%, and 6.4% respectively. Average consumption of unprocessed red meat was 22.3 (±15.2) grams/day. Average intake of processed meat and oily fish were 15.7 (±15.0) grams/day and 11.7 (±10.8) grams/day respectively.

Table 6.3. Baseline population characteristics (n=19,408)

Population characteristic	Frequency or. mean (SD)/median[IQR]
Male Female	9,303 (47.9%) 10,105 (52.1%)
Age (years)	55.0 (±7.5)
Townsend deprivation index	-2.0 (±2.6)
Body mass index (kg/m^2)	26.6 (±4.2)
Smoking (current smoker)	1,238 (6.4%)
Diabetes	606 (3.1%)
Hypertension	2,690 (13.9%)
Hypercholesterolaemia	4,464 (23.0%)
IPAQ score (METS/week)	1525.00 [2396.25]
Educational level: Left school age 14 or younger without qualifications Left school age 15 or older without qualifications High school diploma Sixth form qualification Professional qualification Higher education university degree	 53 (0.3%) 1,394 (7.2%) 2,679 (13.8%) 1,114 (5.7%) 5,506 (28.4%) 8,456 (43.6%)
Alcohol intake frequency: Never Special occasions only 1-3 times a month 1-2 times a week 3-4 times a week Daily or almost daily	 954 (4.9%) 1,587 (8.2%) 2,103 (10.8%) 4,997 (25.7%) 5,496 (28.3%) 4,260 (21.9%)
Unprocessed red meat intake (grams/day) Beef Lamb Pork	22.3 (± 15.2) 9.5 (± 9.0) 6.3 (± 5.4) 6.5 (± 5.9)
Processed meat intake (grams/day)	15.7 (± 15.0)
Oily fish intake (grams/day)	11.7 (± 10.8)

Table 6.3. *Results are frequencies and percentages for categorical variables; mean (standard deviation) or median [interquartile range] for continuous variable. IPAQ: international physical activity questionnaire; METS: metabolic equivalents.*

6.4.1.1 Association of meat and fish intake with conventional CMR indices

In the main confounder adjusted models, greater consumption of unprocessed red meat was associated with smaller LV volumes in end-diastole and end-systole, higher LV mass, and lower LV stroke volume (**Table 6.4**). Greater red meat consumption was also associated with smaller RV volumes in end-diastole and end-systole and smaller RV stroke volumes. These relationships were consistent across the different red meat types. Greater consumption of processed meat was associated with smaller RV and LV volumes in end-diastole and end-systole and with lower RV and LV stroke volumes (**Table 6.4**). Association with LV mass trended towards higher mass but did not reach statistical significance. Greater oily fish consumption was associated with larger RV and LV volumes in end-diastole and end-systole, greater LV mass, and higher RV and LV stroke volumes (**Table 6.4**).

In the models with additional adjustment for potential mediators (confounder and mediator adjusted models), the associations between unprocessed red meat consumption and RV and LV end-systolic and end-diastolic volumes and strokes volumes were attenuated, whilst associations with LV mass remained robust (**Table 6.5**). Associations between processed meat intake or oily fish intake and LV and RV CMR metrics remained largely unchanged with addition of these potential mediators (**Table 6.5**).

6.4.2 Association of meat and fish intake with arterial compliance measures

There was documentation of ASI for 167,432, 30,474, and 10,436 participants at baseline, imaging, and both time points respectively. We estimated associations between the dietary intake exposures and ASI recorded at baseline (n=167,432) and imaging (n=30,474). Additionally, for the participants with ASI recorded at both time points (n=10,436), we calculated standardised residuals to indicate "interval change in ASI" and considered this as another cardiovascular outcome. The baseline characteristics of the imaging set were largely similar to the CMR cohort (as reported in **Table 6.3**). However, the baseline set had slightly poorer cardiometabolic profile than the imaging cohort (**Table 6.6**). For aortic distensibility, the sample was as for the CMR subset.

In the confounder adjusted models, higher intake of red or processed meat was associated with higher ASI, indicating greater vascular resistance, at both the baseline and imaging visits (**Table 6.7**, **Figure 6.4**). Associations were consistent across red meat subgroups. In addition, higher unprocessed red meat intake was associated with significantly greater interval increase in ASI than would be expected from the baseline ASI (**Table 6.7**).

Table 6.4. Multivariable linear regression models showing change in cardiovascular magnetic resonance indices per 100g increase in daily meat/fish consumption (confounder adjusted model)

	LVEDVi (ml/m^2)	LVESVi (ml/m^2)	LVEF (%)	LVSVi (ml/m^2)	LVMi (g/m^2)	RVEDVi (ml/m^2)	RVESVi (ml/m^2)	RVSVi (ml/m^2)	RVEF (%)
Unprocessed red meat	-2.18*	-0.96*	0.04	-1.22*	1.57*	-1.77*	-0.61	-1.16*	-0.30
	[-3.36, -1.00]	[-1.70, -0.23]	[-0.504, 0.587]	[-1.97, -0.47]	[0.91, 2.23]	[-3.30, -0.24]	[-1.54, 0.33]	[-2.11, -0.21]	[-0.97, 0.37]
	2.91×10^{-4}	0.010	0.8817	0.002	3.19×10^{-6}	0.02	0.20	0.02	0.37
Beef	-3.05*	-1.25*	-0.011	-1.80*	2.13*	-3.77*	-2.14*	-1.63*	0.50
	[-5.04, -1.06]	[-2.48, -0.007]	[-0.933, 0.911]	[-3.07, -0.54]	[1.01, 3.24]	[-6.33, -1.22]	[-3.70, -0.58]	[-3.22, -0.05]	[-0.62, 1.62]
	0.003	0.049	0.9811	0.005	1.85×10^{-4}	0.004	0.007	0.04	0.38
Lamb	-5.59*	-2.67*	0.149	-2.92*	2.27*	-1.42	1.37	-2.79*	-2.53*
	[-8.96, -2.22]	[-4.76, -0.58]	[-1.403, 1.701]	[-5.06, -0.78]	[0.39, 4.15]	[-5.86, 3.04]	[-1.34, 4.09]	[-5.55, -0.02]	[-4.48, -0.59]
	1.10×10^{-3}	0.012	0.8509	0.008	0.018	0.53	0.322	0.048	0.01
Pork	-2.81	-1.29	0.129	-1.53	3.52*	-2.07	-0.19	-1.89	-1.25
	[-5.84, 0.21]	[-3.16, 0.59]	[-1.271, 1.529]	[-3.45, 0.40]	[1.83, 5.21]	[-6.12, 1.98]	[-2.66, 2.29]	[-4.41, 0.64]	[-3.02, 0.52]
	0.068	0.179	0.857	0.12	4.43×10^{-5}	0.32	0.88	0.14	0.17
Processed meat	-2.88*	-1.12*	-0.121	-1.77*	0.57	-2.88*	-0.84	-2.05*	-0.57
	[-4.12, -1.65]	[-1.89, -0.35]	[-0.693, 0.451]	[-2.55, -0.98]	[-0.12, 1.26]	[-4.46, -1.31]	[-1.80, 0.13]	[-3.03, -1.07]	[-1.26, 0.13]
	4.70×10^{-6}	0.0042	0.6785	1.06×10^{-5}	0.11	3.46×10^{-4}	0.09	4.30×10^{-5}	0.11
Oily fish	4.13*	1.75*	0.103	2.38*	2.38*	3.67*	1.97*	1.70*	-0.39
	[2.46, 5.80]	[0.71, 2.79]	[-0.671, 0.878]	[1.32, 3.45]	[1.44, 3.31]	[1.51, 5.82]	[0.66, 3.29]	[0.36, 3.03]	[-1.33, 0.55]
	1.28×10^{-6}	9.68×10^{-4}	0.7938	1.13×10^{-5}	6.40×10^{-7}	8.47×10^{-4}	0.003	0.01	0.42

Table 6.4. *Each cell represents a separate model, adjusted for: age, sex, social deprivation, educational level, smoking, alcohol intake, exercise level. First, second, and third row for every CMR measures corresponds to beta coefficient, 95% confidence interval and p-value, respectively. CMR: cardiovascular magnetic resonance; LVEDV: left ventricular end-diastolic volume; LVESV: left ventricular end-systolic volume; LVEF: left ventricular ejection fraction; LVM: left ventricular mass; LVSV: left ventricular stroke volume; RVEDV: right ventricular end-diastolic volume; RVEF: right ventricular ejection fraction; RVESV: right ventricular end-systolic volume; RVSV: right ventricular stroke volume i denotes indexation to body surface area calculated according to the Du Bois formula. *denotes p-value <0.05.*

Table 6.5. Multivariable linear regression models showing change in conventional cardiovascular magnetic resonance indices per 100g increase in daily meat/fish consumption (confounders and mediator adjusted models)

	LVEDVi (ml/m^2)	LVESVi (ml/m^2)	LVEF (%)	LVSVi (ml/m^2)	LVMi (g/m^2)	RVEDVi (ml/m^2)	RVESVi (ml/m^2)	RVSVi (ml/m^2)	RVEF (%)
Unprocessed red meat	-1.11	-0.57	0.09	-0.54	1.02*	-0.54	-0.14	-0.393	-0.190
	[-2.28, 0.07]	[-1.31, 0.17]	[-0.46, 0.64]	[-1.29, 0.22]	[0.36, 1.68]	[-2.06, 0.99]	[-1.08, 0.79]	[-1.342, 0.556]	[-0.863, 0.484]
	0.066	0.13	0.75	0.16	0.003	0.49	0.77	0.4169	0.5811
Beef	-1.41	-0.64	0.05	-0.78	1.19*	-1.85	-1.40	-0.448	0.664
	[-3.40, 0.58]	[-1.88, 0.60]	[-0.88, 0.98]	[-2.04, 0.49]	[0.08, 2.30]	[-4.39, 0.70]	[-2.96, 0.16]	[-2.030, 1.135]	[-0.459, 1.787]
	0.16	0.31	0.92	0.23	0.04	0.15	0.08	0.5793	0.2463
Lamb	-3.63*	-1.97	0.27	-1.66	1.51	0.74	2.11	-1.375	-2.236*
	[-6.98, -0.29]	[-4.06, 0.12]	[-1.29, 1.83]	[-3.79, 0.46]	[-0.36, 3.38]	[-3.68, 5.15]	[-0.60, 4.82]	[-4.123, 1.372]	[-4.186, -0.287]
	0.03	0.06	0.73	0.13	0.11	0.74	0.13	0.3264	0.0245
Pork	-1.06	-0.65	0.21	-0.41	2.62*	-0.05	0.59	-0.640	-1.081
	[-4.07, 1.95]	[-2.53, 1.23]	[-1.20, 1.61]	[-2.32, 1.50]	[0.94, 4.30]	[-4.07, 3.97]	[-1.88, 3.06]	[-3.143, 1.863]	[-2.858, 0.696]
	0.49	0.50	0.77	0.68	0.002	0.98	0.64	0.6163	0.2330
Processed meat	-2.08*	-0.82*	-0.09	-1.26*	0.05	-1.96*	-0.473	-1.487*	-0.500
	[-3.31, -0.85]	[-1.59, -0.05]	[-0.67, 0.48]	[-2.04, -0.48]	[-0.64, 0.74]	[-3.53, -0.39]	[-1.436, 0.489]	[-2.464, -0.511]	[-1.193, 0.193]
	9.23×10^{-4}	0.04	0.75	0.002	0.88	0.01	0.3351	0.0028	0.1571
Oily fish	4.34*	1.83*	0.10	2.51*	2.32*	4.06*	2.168*	1.894*	-0.402
	[2.68, 6.00]	[0.79, 2.86]	[-0.67, 0.88]	[1.46, 3.57]	[1.39, 3.24]	[1.93, 6.19]	[0.861, 3.476]	[0.567, 3.220]	[-1.343, 0.539]
	2.94×10^{-7}	5.42×10^{-4}	0.80	3.07×10^{-6}	9.73×10^{-7}	1.89×10^{-4}	0.0012	0.0051	0.4028

Table 6.5. *Each cell represents a separate model, adjusted for: age, sex, social deprivation, educational level, smoking, alcohol intake, exercise level, body mass index, hypertension, hypercholesterolaemia, diabetes. First, second, and third row for every CMR measures corresponds to beta coefficient, 95% confidence interval and p-value, respectively. CMR: cardiovascular magnetic resonance; LVEDV: left ventricular end-diastolic volume; LVESV: left ventricular end-systolic volume; LVEF: left ventricular ejection fraction; LVM: left ventricular mass; LVSV: left ventricular stroke volume; RVEDV: right ventricular end-diastolic volume; RVEF: right ventricular ejection fraction; RVESV: right ventricular end-systolic volume; RVSV: right ventricular stroke volume. i denotes indexation to body surface area calculated according to the Du Bois formula.*

Table 6.6. Baseline population characteristics (arterial stiffness index at baseline)

Population characteristic	Frequency or. mean (SD)/median[IQR]
Male	76,989 (45.9%)
Female	90,525 (54.1%)
Age (years)	56.7 (±8.2)
Townsend deprivation index**	-1.10 (±3.0)
Body mass index (kg/m^2)	27.5 (±4.8)
Smoking (current smoker)	16,682 (10.0%)
Diabetes	10,795 (6.4%)
Hypertension	35,514 (21.2%)
Hypercholesterolaemia	49,476 (29.6%)
IPAQ score (METS/week)	1593.00 [2644.50]
Educational level*:	
Left school age 14 or younger without qualifications	1,323 (0.8%)
Left school age 15 or older without qualifications	24,545 (14.7%)
High school diploma	28,249 (16.9%)
Sixth form qualification	9,506 (5.7%)
Professional qualification	45,817 (27.4%)
Higher education university degree	56,158 (33.5%)
Alcohol intake frequency:	
Never	14,745 (8.8%)
Special occasions only	20,461 (12.2%)
1-3 times a month	18,933 (11.3%)
1-2 times a week	41,901 (25.0%)
3-4 times a week	37,095 (22.2%)
Daily or almost daily	33,743 (20.2%)
Unprocessed red meat intake (grams/day):	22.4 (±16.32)
Beef	9.1 (±9.0)
Lamb	6.6 (±6.3)
Pork	6.8 (±6.8)
Processed meat intake (grams/day)	16.4 (±15.9)
Oily fish intake (grams/day)	12.1 (±11.6)

Table 6.6. *Results are frequencies and percentages for categorical variables and mean standard deviation for continuous variable. *High school diploma includes: O levels, GCSE, CSE, or equivalent; Sixth form qualification includes: A levels/AS levels, or equivalent; professional qualifications refer to nursing, teaching, or equivalent. I IPAQ: international physical activity questionnaire; METS: metabolic equivalents.** **Townsend index: zero, positive, and negative scores indicate average, higher, and lower levels of material deprivation respectively relative to UK national averages.*

Table 6.7. Multivariable linear regression models showing change of arterial compliance measures per 100g increase in daily meat/fish consumption (confounder adjusted model)

	AD (mm $\times 10^{-3}$)	ASI (baseline, m/s)	ASI (imaging, m/s)	Interval change in ASI (baseline-imaging, m/s)
Unprocessed red meat	-0.06	0.49*	0.35*	0.15*
	[-0.13, 0.02]	[0.41, 0.57]	[0.15, 0.55]	[0.03, 0.27]
	0.12	2.26×10^{-31}	5.46×10^{-4}	0.02
Beef	-0.12*	0.68*	0.53*	0.24*
	[-0.25, -0.001]	[0.53, 0.83]	[0.19, 0.86]	[0.02, 0.46]
	0.05	1.19×10^{-19}	0.002	0.03
Lamb	-0.02	0.89*	0.42	0.22
	[-0.23, 0.19]	[0.68, 1.10]	[-0.14, 0.97]	[-0.13, 0.58]
	0.85	1.86×10^{-16}	0.14	0.22
Pork	-0.08	0.83*	0.72*	0.26
	[-0.27, 0.10]	[0.64, 1.03]	[0.22, 1.22]	[-0.05, 0.57]
	0.38	1.32×10^{-16}	0.005	0.10
Processed meat	-0.00	0.45*	0.22*	0.05
	[-0.08, 0.08]	[0.36, 0.53]	[0.02, 0.43]	[-0.07, 0.17]
	1.00	4.47×10^{-24}	0.03	0.43
Oily fish	0.01	-0.22*	-0.43*	-0.17
	[-0.09, 0.12]	[-0.34, -0.11]	[-0.71, -0.16]	[-0.34, 0.01]
	0.81	1.70×10^{-4}	0.002	0.06

Table 6.7. *Each cell represents a separate model, adjusted for: age, sex, social deprivation, educational level, smoking, alcohol intake, and exercise level (confounder adjusted model). For 'interval change in ASI', results are average standard deviation change from that expected from baseline. First, second, and third row for every CMR measures corresponds to beta coefficient, 95% confidence interval and p-value, respectively. AD: aortic distensibility; ASI: arterial stiffness index. *indicates p-value <0.05.*

Oily fish intake demonstrated a reverse pattern of associations compared to the meat exposures, with greater consumption linked to lower ASI at both time points and with a smaller interval increase in ASI (not statistically significant) than would be expected from the baseline ASI (**Table 6.7**).

These pattern of associations with arterial compliance with aortic distensibility were consistent with those observed with ASI. Specifically, greater red and processed meat consumption was associated with lower aortic distensibility (lower compliance) and greater oily fish consumption was associated with higher aortic distensibility (higher compliance), however these associations did not reach statistical significance, likely due to smaller sample size and more noise associated with this metric (**Table 6.7**, **Figure 6.4**). In models additionally adjusted for mediators, the observed associations were broadly unchanged (**Table 6.8**).

Figure 6.4. Multivariable linear regression results for arterial compliance measures displaying beta coefficients and 95% confidence intervals per 100g increase in daily intake of meat/fish

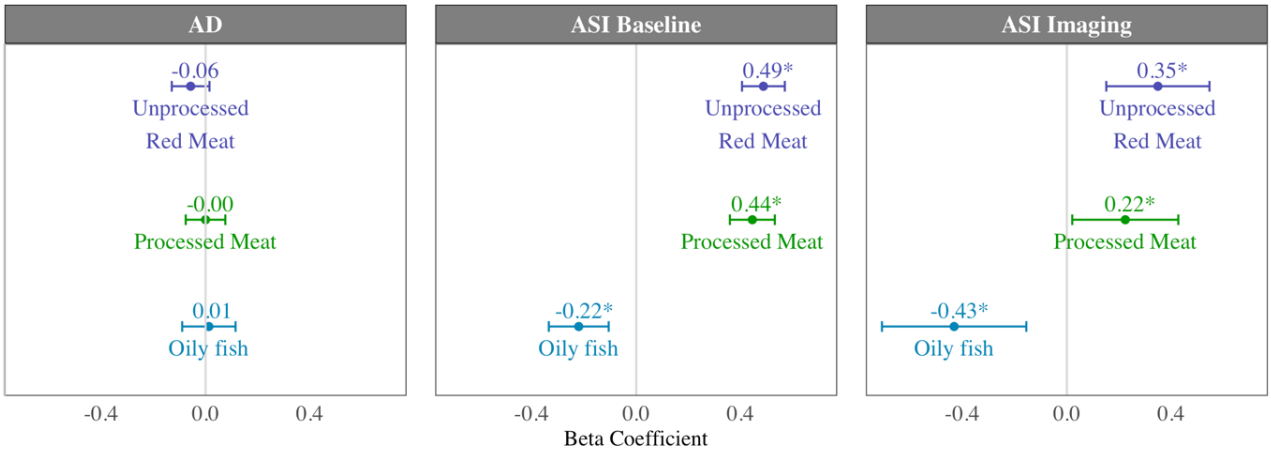

Figure 6.4. *Each bar is from a separate model adjusted for age, sex, social deprivation, educational level, smoking, alcohol intake, exercise level (confounder adjusted model). AD: aortic distensibility; ASI: arterial stiffness index.*

Table 6.8. Multivariable linear regression models for change of arterial compliance measures per 100g increase in daily meat/fish intake (confounder and mediator adjusted models)

	AD (mm $\times 10^{-3}$)	ASI (baseline, m/s)	ASI (imaging, m/s)	Interval change ASI (baseline-imaging, m/s)
Unprocessed red meat	-0.048	0.274*	0.203*	0.102
	[-0.121, 0.024]	[0.191, 0.356]	[0.004, 0.402]	[-0.022, 0.226]
	0.1919	7.15×10^{-11}	0.0457	0.1075
Beef	-0.108	0.374*	0.311	0.173
	[-0.230, 0.014]	[0.227, 0.521]	[-0.023, 0.646]	[-0.044, 0.389]
	0.0834	6.43×10^{-7}	0.0683	0.1173
Lamb	-0.018	0.551*	0.159	0.123
	[-0.224, 0.188]	[0.339, 0.763]	[-0.399, 0.716]	[-0.232, 0.479]
	0.8658	3.53×10^{-7}	0.5774	0.4966
Pork	-0.060	0.429*	0.472	0.180
	[-0.245, 0.125]	[0.231, 0.626]	[-0.029, 0.972]	[-0.127, 0.487]
	0.5258	2.11×10^{-5}	0.0649	0.2516
Processed meat	0.011	0.249*	0.108	0.020
	[-0.065, 0.087]	[0.163, 0.335]	[-0.096, 0.312]	[-0.100, 0.140]
	0.7685	1.56×10^{-8}	0.3005	0.7449
Oily fish	0.014	-0.254*	-0.434*	-0.181*
	[-0.088, 0.116]	[-0.368, -0.140]	[-0.710, -0.158]	[-0.355, -0.007]
	0.7850	1.31×10^{-5}	0.0021	0.0418

Table 6.8. *Each cell represents a separate model, adjusted for: age, sex, social deprivation, educational level, smoking, alcohol intake, exercise level, body mass index, hypertension, hypercholesterolaemia, diabetes (mediator adjusted models). For 'interval change in ASI', results are average standard deviation change from that expected from baseline. First, second, and third row for every CMR measures corresponds to beta coefficient, 95% confidence interval and p-value, respectively. AD: aortic distensibility; ASI: arterial stiffness index.*

6.4.3 Association of meat and fish intake with LV and RV radiomics shape features

We extracted 13 radiomics shape features from each ventricle (LV and RV) in end-diastole and end-systole (i.e., 26 shape features in total for each ventricle). Higher oily fish intake was associated with significantly larger LV volumes, larger short and long axis cavity dimensions, and larger LV cavity surface area (**Figure 6.5, Figure 6.7**).

Greater consumption of red and processed meat was associated with lower "flatness" [range: 0 (a flat object) to 1 (sphere-like)], lower "elongation" [range: 0 (a maximally elongated object, i.e., a one-dimensional line) to 1 (non-elongated)], and lower "sphericity" (range: 0 to 1, "sphericity" is a dimensionless measure of the roundness of the region of interest relative to a sphere where a value of 1 indicates a perfect sphere). Thus, greater red and processed meat intake is associated with a more elongated, less spherical, LV shape (**Figure 6.5, Figure 6.7**). In contrast, greater oily fish consumption showed trends toward greater elongation and flatness (not statistically significant) indicating a more spherical overall shape of the chamber.

Considering these relationships as well as association with lower LV stroke volume, the overall picture suggests that greater red and processed meat intake is associated with of an unhealthy LV phenotype with impaired myocardial contractility. The pattern of associations of cardiac structure and function metrics with greater oily fish intake is distinctly different to that of the meat exposures and, considered alongside previously observed associations of higher stroke volume, overall suggestive of a healthy phenotype.

The same pattern of associations was observed across the different red meat types in end-diastole and end-systole (**Figure 6.5**) and consistent associations were observed with RV shape radiomics (**Figure 6.6, Figure 6.7**). Results from individual associations between meat and fish exposures and LV and RV radiomics features in end-diastole and end-systole are presented in **Table 6.9, Table 6.10, Table 6.11,** and **Table 6.12**.

Figure 6.5. Multivariable linear regression models showing change in left ventricular radiomics shape features per 100g increase in daily meat consumption

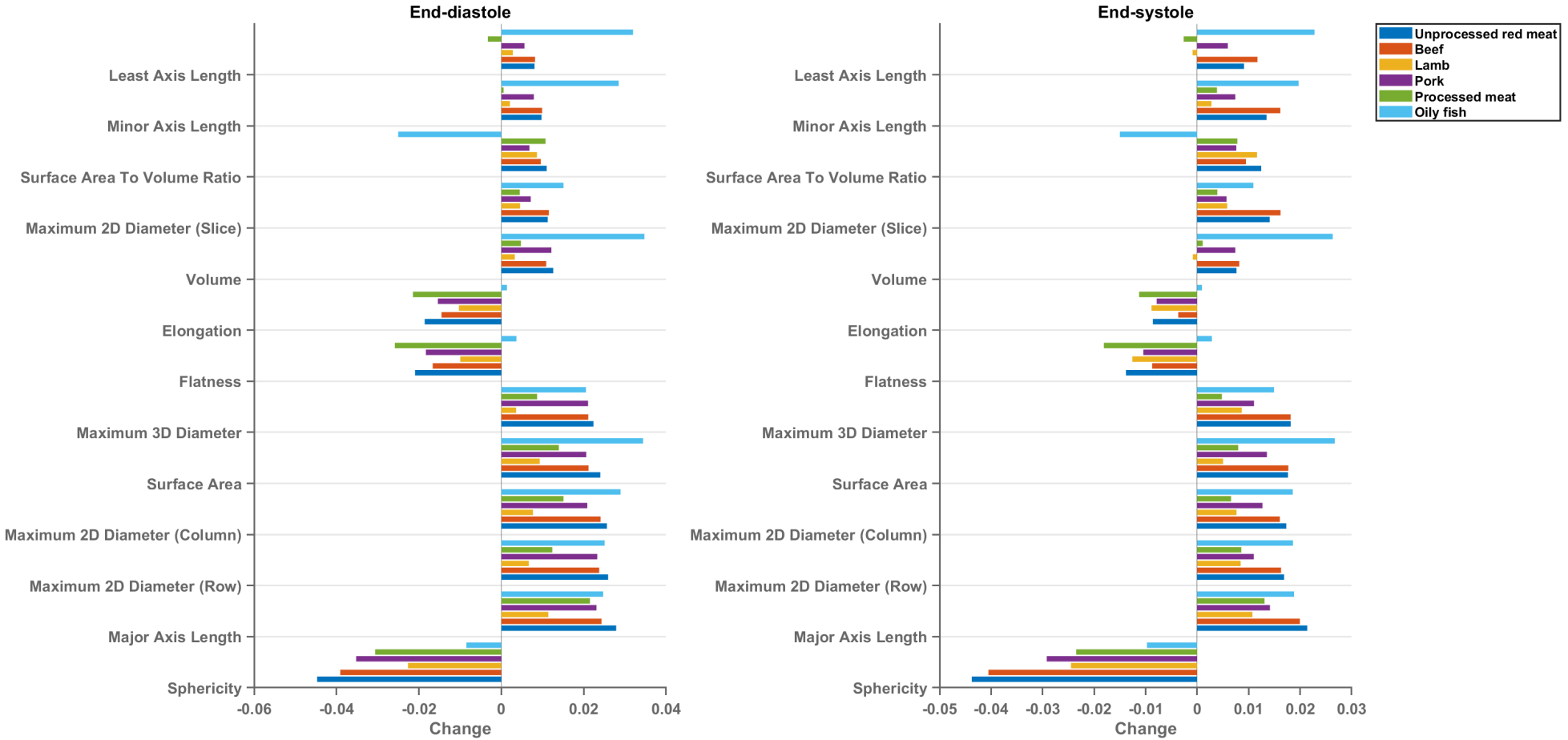

Figure 6.5. *Each bar represents standardised beta coefficients corresponding to the indicated radiomics shape feature. Each bar is from a separate model adjusted for age, sex, social deprivation, educational level, smoking, alcohol intake, exercise level (confounder adjusted model). Reproduced from Raisi-Estabragh et al.*[203]

Figure 6.6. Multivariable linear regression models showing change in right ventricular radiomics shape features per 100g increase in daily meat consumption

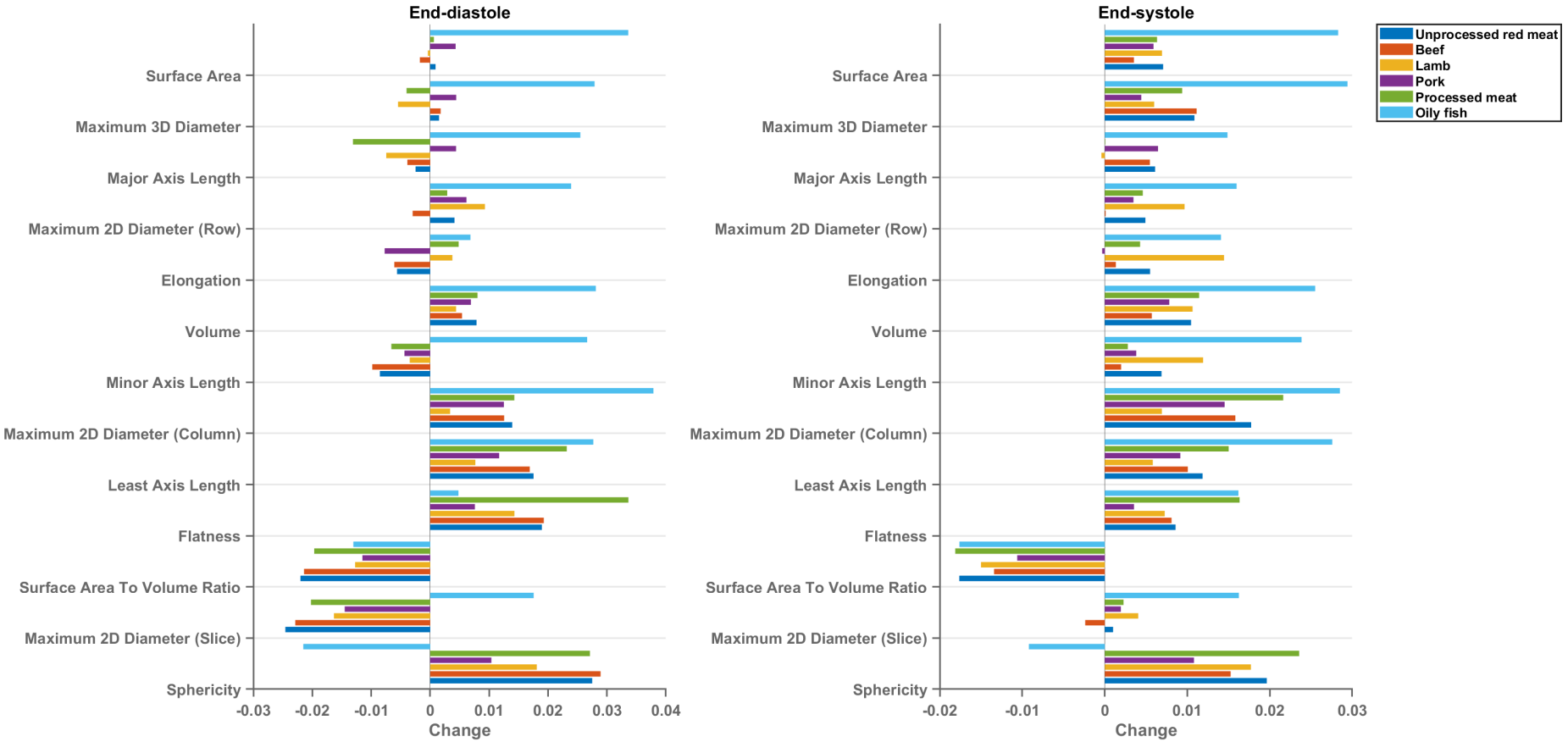

Figure 6.6. *Each bar represents standardised beta coefficients corresponding to the indicated radiomics shape feature. Each bar is from a separate model adjusted for age, sex, social deprivation, educational level, smoking, alcohol intake, exercise level (confounder adjusted model). Black lines represent half-length of confidence interval for the corresponding bar. Reproduced from Raisi-Estabragh et al.*[203].

Figure 6.7. Summary of the association of the oily fish, processed meat, and unprocessed red meat intake with the radiomics shape and signal intensity-based features

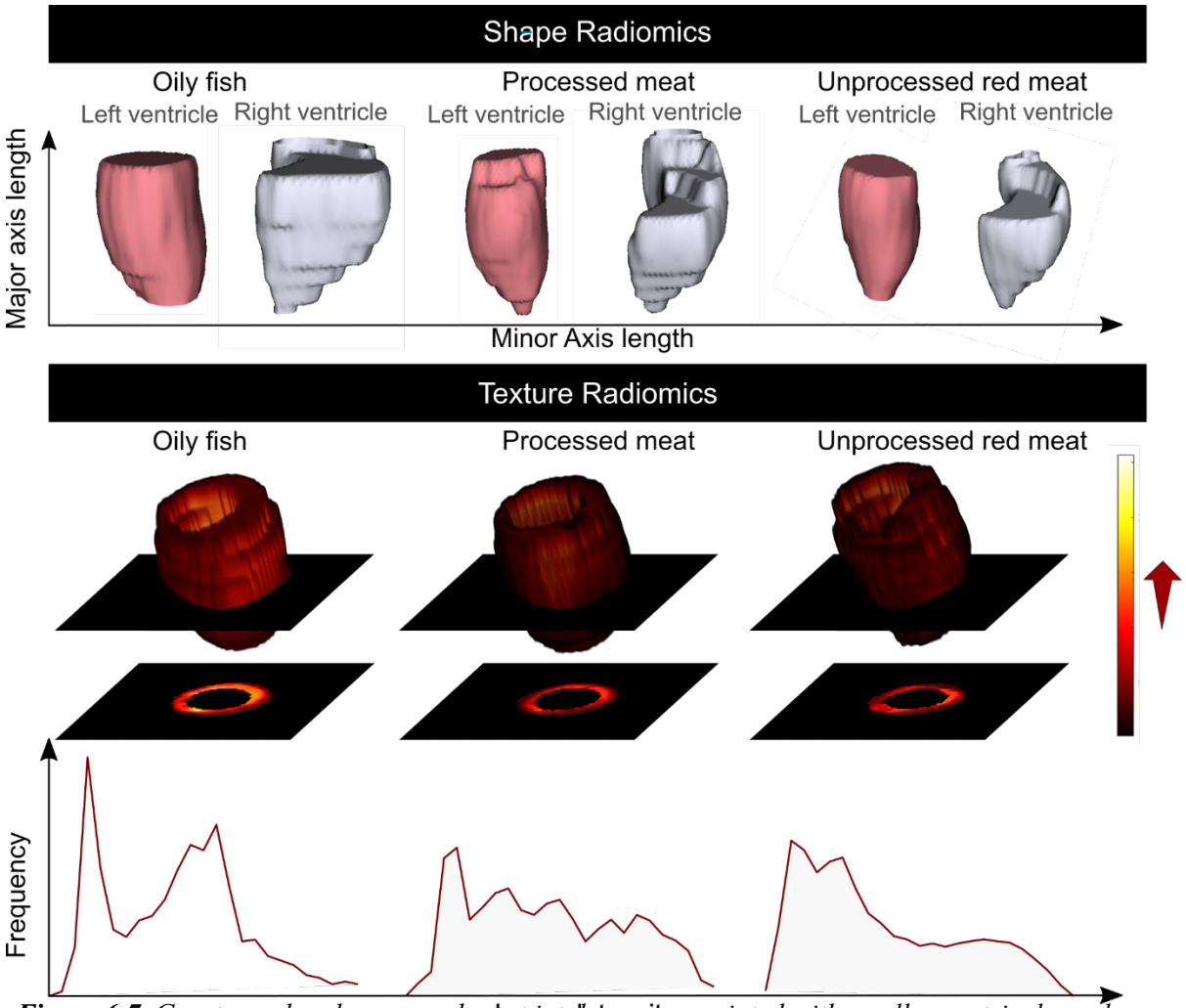

Figure 6.7. *Greater red and processed meat intake was associated with smaller ventricular volumes, reduced short axis dimension, and a more elongated shape; lower global signal intensity levels, and less variation in SI levels within the LV myocardium. Greater oily fish consumption was associated with larger ventricles with overall less elongated (more spherical) shape, higher global myocardial intensity levels and more variation of myocardial intensities. *Histograms are from a selection of most illustrative cases and do not represent findings from the whole dataset. Reproduced from Raisi-Estabragh et al.*[203].

Table 6.9. Multivariate linear regression models showing change in left ventricular radiomics shape features in end-diastole per 100g increase in daily meat/fish consumption

	Unprocessed red meat	Beef	Lamb	Pork	Processed meat	Oily fish
Volume	0.0126	0.0109	0.0033	0.0121	0.0048	0.0347*
	[0.0013, 0.0239]	[-0.0003, 0.0221]	[-0.008, 0.0145]	[0.001, 0.0234]	[-0.0069, 0.0164]	[0.0234, 0.046]
	0.0285	0.0575	0.5692	0.0335	0.4236	$1.9x10^{-9}$
Surface Area	0.024*	0.0212*	0.0093	0.0206*	0.014	0.0344*
	[0.013, 0.0351]	[0.0102, 0.0322]	[-0.0017, 0.0204]	[0.0096, 0.0316]	[0.0025, 0.0254]	[0.0233, 0.0455]
	2.09×10^{-5}	0.0002	0.0983	0.0002	0.0167	$1.33x10^{-9}$
Surface Area To Volume Ratio	0.011	0.0096	0.0086	0.0068	0.0107	-0.025*
	[-0.0018, 0.0238]	[-0.0032, 0.0223]	[-0.0042, 0.0214]	[-0.0059, 0.0196]	[-0.0025, 0.024]	[-0.0379, -0.0122]
	0.0924	0.142	0.1855	0.2944	0.1125	0.0001
Sphericity	-0.0447*	-0.0391*	-0.0227	-0.0352*	-0.0306*	-0.0085
	[-0.0585, -0.0309]	[-0.0528, -0.0253]	[-0.0364, -0.0089]	[-0.049, -0.0215]	[-0.0449, -0.0164]	[-0.0224, 0.0054]
	2.21×10^{-10}	2.53×10^{-8}	0.0013	4.8×10^{-7}	2.54×10^{-5}	0.2305
Maximum 3D Diameter	0.0224*	0.0211*	0.0036	0.021*	0.0087	0.0205
	[0.0104, 0.0343]	[0.0092, 0.033]	[-0.0083, 0.0155]	[0.0092, 0.0329]	[-0.0037, 0.021]	[0.0086, 0.0325]
	0.0002	0.0005	0.5544	0.0005	0.1678	0.0008
Maximum 2D Diameter (Slice)	0.0113	0.0115	0.0045	0.0071	0.0045	0.0151
	[-0.0019, 0.0245]	[-0.0016, 0.0247]	[-0.0086, 0.0177]	[-0.006, 0.0203]	[-0.0092, 0.0181]	[0.0018, 0.0283]
	0.0945	0.0853	0.4985	0.2855	0.5198	0.0259
Maximum 2D Diameter (Column)	0.0256*	0.0241*	0.0077	0.0209*	0.0151	0.0289*
	[0.0143, 0.037]	[0.0128, 0.0354]	[-0.0037, 0.019]	[0.0096, 0.0321]	[0.0034, 0.0268]	[0.0175, 0.0403]
	9.77×10^{-6}	3.00×10^{-5}	0.1852	0.0003	0.0117	$6.76x10^{-7}$
Maximum 2D Diameter (Row)	0.0259*	0.0237*	0.0067	0.0233*	0.0124	0.0251*
	[0.0141, 0.0377]	[0.012, 0.0355]	[-0.0051, 0.0184]	[0.0116, 0.035]	[0.0002, 0.0246]	[0.0132, 0.0369]
	1.66×10^{-5}	7.41×10^{-5}	0.2667	9.87×10^{-5}	0.0465	$3.39x10^{-5}$
Major Axis Length	0.0279*	0.0243*	0.0114	0.0231*	0.0215*	0.0247*
	[0.0166, 0.0392]	[0.013, 0.0356]	[0.0001, 0.0227]	[0.0118, 0.0343]	[0.0098, 0.0332]	[0.0133, 0.0361]
	1.39×10^{-6}	2.37×10^{-5}	0.048	5.77×10^{-5}	0.0003	$2.06x10^{-5}$
Minor Axis Length	0.0098	0.0099	0.0021	0.0079	0.0005	0.0285*

	Unprocessed red meat	Beef	Lamb	Pork	Processed meat	Oily fish
	[-0.0026, 0.0221]	[-0.0024, 0.0222]	[-0.0103, 0.0144]	[-0.0044, 0.0202]	[-0.0122, 0.0133]	[0.0161, 0.0409]
	0.1216	0.1149	0.7411	0.2074	0.933	$6.94x10^{-6}$
Least Axis Length	0.0081	0.0082	0.0028	0.0056	-0.0033	0.032*
	[-0.0042, 0.0203]	[-0.004, 0.0204]	[-0.0094, 0.015]	[-0.0065, 0.0178]	[-0.0159, 0.0094]	[0.0197, 0.0443]
	0.1967	0.188	0.6539	0.3655	0.612	$3.46x10^{-7}$
Elongation	-0.0186	-0.0145	-0.0103	-0.0154	-0.0215	0.0014
	[-0.0327, -0.0045]	[-0.0286, -0.0005]	[-0.0244, 0.0038]	[-0.0294, -0.0014]	[-0.036, -0.0069]	[-0.0128, 0.0155]
	0.0098	0.0429	0.1518	0.0312	0.0039	0.8509
Flatness	-0.0209	-0.0167	-0.01	-0.0183	-0.0259*	0.0036
	[-0.0351, -0.0068]	[-0.0307, -0.0026]	[-0.0241, 0.0041]	[-0.0323, -0.0043]	[-0.0404, -0.0113]	[-0.0105, 0.0178]
	0.0036	0.0202	0.1656	0.0105	0.0005	0.6143

Table 6.9. Each cell represents a separate model, adjusted for: age, sex, social deprivation, educational level, smoking, alcohol intake, exercise level. Results are degree of change in radiomics shape feature per 100g increase in daily meat/fish consumption with corresponding 95% confidence intervals and p-values. First, second, and third row for every CMR measures corresponds to beta coefficient, 95% confidence interval and p-value, respectively. Bonferroni adjusted significance threshold p-value =0.0006 (corrected for 78 comparisons).

Table 6.10. Multivariate linear regression models showing change in left ventricular radiomics shape features in end-systole per 100g increase in daily meat/fish consumption

	Unprocessed red meat	Beef	Lamb	Pork	Processed meat	Oily fish
Volume	0.0076	0.0082	-0.0008	0.0074	0.0011	0.0263*
	[-0.0041, 0.0194]	[-0.0035, 0.0199]	[-0.0126, 0.0109]	[-0.0043, 0.0191]	[-0.011, 0.0132]	[0.0145, 0.0381]
	0.2015	0.1704	0.8879	0.2131	0.8611	$1.2x10^{-5}$
Surface Area	0.0176*	0.0177*	0.005	0.0135*	0.008	0.0267*
	[0.0063, 0.029]	[0.0064, 0.029]	[-0.0063, 0.0163]	[0.0023, 0.0248]	[-0.0037, 0.0197]	[0.0153, 0.0381]
	0.0023	0.0021	0.3824	0.0182	0.1813	$4.16x10^{-6}$
Surface Area To Volume Ratio	0.0124	0.0095	0.0116	0.0076	0.0078	-0.015*
	[-0.0003, 0.0252]	[-0.0032, 0.0222]	[-0.0011, 0.0244]	[-0.0051, 0.0203]	[-0.0054, 0.021]	[-0.0278, -0.0022]
	0.0562	0.144	0.0736	0.2405	0.2457	0.0218
Sphericity	-0.0438*	-0.0405*	-0.0245*	-0.0292*	-0.0235*	-0.0097
	[-0.0574, -0.0301]	[-0.0542, -0.0269]	[-0.0382, -0.0108]	[-0.0428, -0.0156]	[-0.0376, -0.0094]	[-0.0235, 0.004]
	3.69×10^{-10}	5.67×10^{-9}	0.0004	2.59×10^{-5}	0.0011	0.1654
Maximum 3D Diameter	0.0182*	0.0182*	0.0087	0.011	0.0048	0.0149*
	[0.0062, 0.0302]	[0.0062, 0.0301]	[-0.0033, 0.0206]	[-0.0009, 0.023]	[-0.0076, 0.0172]	[0.0029, 0.027]
	0.003	0.0029	0.156	0.0697	0.4477	0.0153
Maximum 2D Diameter (Slice)	0.0141*	0.0162*	0.0058	0.0057	0.0039	0.0109
	[0.0014, 0.0268]	[0.0035, 0.0289]	[-0.0069, 0.0185]	[-0.0069, 0.0184]	[-0.0092, 0.0171]	[-0.0019, 0.0237]
	0.0301	0.0123	0.3676	0.3755	0.5598	0.0945
Maximum 2D Diameter (Column)	0.0173*	0.0161*	0.0076	0.0127*	0.0066	0.0186*
	[0.0055, 0.0291]	[0.0043, 0.0278]	[-0.0041, 0.0194]	[0.001, 0.0244]	[-0.0056, 0.0187]	[0.0067, 0.0304]
	0.0039	0.0072	0.2024	0.0335	0.2886	0.0021
Maximum 2D Diameter (Row)	0.0169*	0.0163*	0.0085	0.011	0.0086	0.0186*
	[0.005, 0.0287]	[0.0045, 0.0281]	[-0.0034, 0.0203]	[-0.0008, 0.0228]	[-0.0037, 0.0208]	[0.0067, 0.0305]
	0.0052	0.0068	0.1608	0.067	0.1693	0.0022
Major Axis Length	0.0214*	0.02*	0.0107	0.0141*	0.0131*	0.0188*
	[0.0099, 0.0329]	[0.0085, 0.0314]	[-0.0007, 0.0222]	[0.0027, 0.0255]	[0.0012, 0.025]	[0.0073, 0.0304]
	0.0003	0.0006	0.0665	0.0153	0.0307	0.0014
Minor Axis Length	0.0135*	0.0161*	0.0028	0.0074	0.0038	0.0197*

	Unprocessed red meat	Beef	Lamb	Pork	Processed meat	Oily fish
	[0.0013, 0.0257]	[0.004, 0.0283]	[-0.0094, 0.0149]	[-0.0047, 0.0195]	[-0.0087, 0.0164]	[0.0075, 0.0319]
	0.0299	0.009	0.654	0.2298	0.5486	0.0016
Least Axis Length	0.0091	0.0117	-0.0009	0.006	-0.0026	0.0228*
	[-0.003, 0.0212]	[-0.0004, 0.0238]	[-0.013, 0.0112]	[-0.0061, 0.018]	[-0.0152, 0.0099]	[0.0106, 0.035]
	0.1418	0.0579	0.8867	0.3332	0.6825	0.0003
Elongation	-0.0086	-0.0037	-0.0089	-0.0079	-0.0113	0.0009
	[-0.0229, 0.0057]	[-0.0179, 0.0105]	[-0.0231, 0.0054]	[-0.022, 0.0063]	[-0.026, 0.0035]	[-0.0134, 0.0153]
	0.2373	0.6126	0.2218	0.2769	0.1338	0.8975
Flatness	-0.0138	-0.0087	-0.0126	-0.0105	-0.0181*	0.0029
	[-0.028, 0.0004]	[-0.0229, 0.0054]	[-0.0268, 0.0016]	[-0.0246, 0.0037]	[-0.0328, -0.0034]	[-0.0114, 0.0172]
	0.0569	0.2266	0.0823	0.1471	0.0157	0.6946

Table 6.10. *Each cell represents a separate model, adjusted for: age, sex, social deprivation, educational level, smoking, alcohol intake, exercise level. Results are degree of change in radiomics shape feature per 100g increase in daily meat/fish consumption with corresponding 95% confidence intervals and p-values. First, second, and third row for every CMR measures corresponds to beta coefficient, 95% confidence interval and p-value, respectively. Bonferroni adjusted significance threshold p-value =0.0006 (corrected for 78 comparisons).*

Table 6.11. Multivariate linear regression models showing change in right ventricular radiomics shape features shape radiomics in end-diastole per 100g increase in daily meat/fish consumption

	Unprocessed red meat	Beef	Lamb	Pork	Processed meat	Oily fish
Volume	0.0079	0.0054	0.0044	0.0069	0.008	0.0281*
	[-0.0028, 0.0185]	[-0.0052, 0.016]	[-0.0062, 0.015]	[-0.0037, 0.0175]	[-0.003, 0.019]	[0.0174, 0.0388]
	0.1479	0.3177	0.4173	0.2006	0.152	$2.61x10^{-7}$
Surface Area	0.0009	-0.0017	-0.0004	0.0043	0.0006	0.0336*
	[-0.0099, 0.0117]	[-0.0125, 0.009]	[-0.0111, 0.0104]	[-0.0064, 0.015]	[-0.0105, 0.0118]	[0.0228, 0.0444]
	0.8687	0.7495	0.9424	0.4286	0.912	$1.13x10^{-9}$
Surface Area To Volume Ratio	-0.022*	-0.0214*	-0.0127	-0.0115	-0.0197	-0.013
	[-0.0338, -0.0102]	[-0.0332, -0.0096]	[-0.0245, -0.0009]	[-0.0233, 0.0003]	[-0.0319, -0.0075]	[-0.0249, -0.0012]
	0.0003	0.0004	0.0344	0.0552	0.0016	0.0316
Sphericity	0.0275*	0.0289*	0.0181	0.0104	0.0271*	-0.0215
	[0.0132, 0.0418]	[0.0147, 0.0431]	[0.0038, 0.0323]	[-0.0038, 0.0246]	[0.0124, 0.0419]	[-0.0359, -0.0072]
	0.0002	6.79×10^{-5}	0.0129	0.1519	0.0003	0.0033
Maximum 3D Diameter	0.0015	0.0018	-0.0055	0.0044	-0.004	0.0279*
	[-0.0101, 0.0131]	[-0.0098, 0.0133]	[-0.017, 0.0061]	[-0.0071, 0.0159]	[-0.016, 0.008]	[0.0163, 0.0395]
	0.7979	0.7626	0.3541	0.4512	0.5112	$2.59x10^{-6}$
Maximum 2D Diameter (Slice)	-0.0246*	-0.0229*	-0.0163	-0.0145	-0.0202	0.0176
	[-0.0375, -0.0117]	[-0.0358, -0.01]	[-0.0292, -0.0034]	[-0.0273, -0.0017]	[-0.0336, -0.0069]	[0.0046, 0.0305]
	0.0002	0.0005	0.013	0.0269	0.003	0.008
Maximum 2D Diameter (Column)	0.0139	0.0125	0.0034	0.0125	0.0143	0.0379*
	[0.0019, 0.026]	[0.0005, 0.0246]	[-0.0087, 0.0154]	[0.0005, 0.0245]	[0.0018, 0.0268]	[0.0258, 0.05]
	0.0238	0.0409	0.582	0.041	0.0248	$9.36x10^{-10}$
Maximum 2D Diameter (Row)	0.0041	-0.003	0.0093	0.0062	0.0029	0.0239*
	[-0.0081, 0.0164]	[-0.0152, 0.0092]	[-0.0029, 0.0215]	[-0.006, 0.0183]	[-0.0097, 0.0155]	[0.0116, 0.0362]
	0.5086	0.6321	0.1355	0.3205	0.6543	0.0001
Major Axis Length	-0.0025	-0.0039	-0.0075	0.0044	-0.0131	0.0255*
	[-0.0142, 0.0093]	[-0.0156, 0.0078]	[-0.0192, 0.0043]	[-0.0073, 0.0161]	[-0.0252, -0.001]	[0.0137, 0.0373]
	0.6785	0.5165	0.2117	0.4596	0.0341	$2.29x10^{-5}$
Minor Axis Length	-0.0085	-0.0098	-0.0035	-0.0044	-0.0066	0.0266*

	Unprocessed red meat	Beef	Lamb	Pork	Processed meat	Oily fish
	[-0.0208, 0.0038]	[-0.0221, 0.0024]	[-0.0158, 0.0088]	[-0.0166, 0.0079]	[-0.0193, 0.0061]	[0.0143, 0.039]
	0.1741	0.1158	0.5794	0.484	0.3095	2.41×10^{-5}
Least Axis Length	0.0175	0.0169	0.0077	0.0117	0.0232*	0.0277*
	[0.0056, 0.0295]	[0.005, 0.0288]	[-0.0043, 0.0196]	[-0.0001, 0.0236]	[0.0109, 0.0355]	[0.0157, 0.0397]
	0.004	0.0053	0.2074	0.0529	0.0002	6.02×10^{-6}
Elongation	-0.0056	-0.0061	0.0038	-0.0077	0.0048	0.0068
	[-0.0199, 0.0087]	[-0.0203, 0.0081]	[-0.0105, 0.018]	[-0.0219, 0.0065]	[-0.0099, 0.0196]	[-0.0075, 0.0212]
	0.4403	0.4018	0.6042	0.2861	0.5206	0.3511
Flatness	0.019	0.0193	0.0143	0.0076	0.0336*	0.0048
	[0.0049, 0.033]	[0.0053, 0.0333]	[0.0003, 0.0283]	[-0.0064, 0.0216]	[0.0191, 0.0482]	[-0.0093, 0.0189]
	0.0082	0.007	0.046	0.2872	5.64×10^{-6}	0.5056

Table 6.11. *Each cell represents a separate model, adjusted for: age, sex, social deprivation, educational level, smoking, alcohol intake, exercise level. Results are degree of change in radiomics shape feature per 100g increase in daily meat/fish consumption with corresponding 95% confidence intervals and p-values. First, second, and third row for every CMR measures corresponds to beta coefficient, 95% confidence interval and p-value, respectively. Bonferroni adjusted significance threshold p-value =0.0006 (corrected for 78 comparisons).*

Table 6.12. Multivariate linear regression models showing change in right ventricular radiomics shape features shape radiomics in end-systole per 100g increase in daily meat/fish consumption

	Unprocessed red meat	Beef	Lamb	Pork	Processed meat	Oily fish
Volume	0.0105	0.0057	0.0106	0.0078	0.0114	0.0255*
	[-0.0003, 0.0212]	[-0.0051, 0.0164]	[-0.0001, 0.0214]	[-0.0029, 0.0185]	[0.0003, 0.0226]	[0.0147, 0.0363]
	0.0576	0.2989	0.0527	0.1529	0.0443	4.03×10^{-6}
Surface Area	0.0071	0.0035	0.0069	0.0059	0.0063	0.0283*
	[-0.0036, 0.0177]	[-0.0071, 0.0142]	[-0.0037, 0.0176]	[-0.0047, 0.0165]	[-0.0047, 0.0173]	[0.0176, 0.039]
	0.1938	0.5145	0.2014	0.2742	0.2597	2.29×10^{-7}
Surface Area To Volume Ratio	-0.0176	-0.0134	-0.015	-0.0106	-0.0181	-0.0176*
	[-0.0293, -0.0059]	[-0.0251, -0.0018]	[-0.0267, -0.0033]	[-0.0222, 0.001]	[-0.0302, -0.006]	[-0.0294, -0.0059]
	0.0031	0.024	0.0118	0.0736	0.0033	0.0033
Sphericity	0.0196	0.0153	0.0177	0.0108	0.0236	-0.0092
	[0.0053, 0.0339]	[0.001, 0.0295]	[0.0034, 0.032]	[-0.0034, 0.025]	[0.0088, 0.0383]	[-0.0236, 0.0052]
	0.0071	0.0359	0.0151	0.1361	0.0018	0.2096
Maximum 3D Diameter	0.0109	0.0111	0.006	0.0044	0.0094	0.0294*
	[-0.0009, 0.0226]	[-0.0005, 0.0228]	[-0.0057, 0.0177]	[-0.0072, 0.0161]	[-0.0027, 0.0215]	[0.0176, 0.0412]
	0.0694	0.0617	0.3159	0.4572	0.129	9.88×10^{-7}
Maximum 2D Diameter (Slice)	0.001	-0.0024	0.0041	0.0019	0.0023	0.0162
	[-0.0119, 0.014]	[-0.0153, 0.0105]	[-0.0089, 0.017]	[-0.0109, 0.0148]	[-0.0111, 0.0156]	[0.0032, 0.0293]
	0.8794	0.7178	0.5383	0.7666	0.7394	0.0144
Maximum 2D Diameter (Column)	0.0177	0.0158	0.0069	0.0145	0.0216	0.0285*
	[0.0054, 0.0301]	[0.0036, 0.0281]	[-0.0054, 0.0192]	[0.0023, 0.0268]	[0.0089, 0.0343]	[0.0161, 0.0409]
	0.0048	0.0114	0.2696	0.02	0.0009	6.38×10^{-6}
Maximum 2D Diameter (Row)	0.0049	0.0001	0.0097	0.0035	0.0046	0.016
	[-0.0079, 0.0177]	[-0.0127, 0.0129]	[-0.0031, 0.0225]	[-0.0093, 0.0162]	[-0.0086, 0.0178]	[0.0031, 0.0289]
	0.452	0.9873	0.1384	0.5928	0.4951	0.015
Major Axis Length	0.0061	0.0055	-0.0004	0.0065	0.0001	0.0149
	[-0.0061, 0.0183]	[-0.0067, 0.0176]	[-0.0126, 0.0117]	[-0.0056, 0.0186]	[-0.0125, 0.0126]	[0.0026, 0.0271]
	0.3259	0.377	0.9472	0.2958	0.9926	0.0172
Minor Axis Length	0.0069	0.002	0.0119	0.0038	0.0028	0.0238*

	Unprocessed red meat	Beef	Lamb	Pork	Processed meat	Oily fish
	[-0.0053, 0.019]	[-0.0101, 0.0141]	[-0.0002, 0.024]	[-0.0083, 0.0159]	[-0.0098, 0.0154]	[0.0116, 0.0361]
	0.2673	0.7484	0.0542	0.5358	0.6623	0.0001
Least Axis Length	0.0119	0.0101	0.0058	0.0092	0.015	0.0276*
	[0.0005, 0.0232]	[-0.0013, 0.0214]	[-0.0055, 0.0172]	[-0.0021, 0.0205]	[0.0033, 0.0268]	[0.0161, 0.039]
	0.0411	0.0818	0.3151	0.1123	0.0123	$2.27x10^{-6}$
Elongation	0.0055	0.0013	0.0145	-0.0003	0.0043	0.0141
	[-0.0085, 0.0195]	[-0.0126, 0.0153]	[0.0005, 0.0284]	[-0.0142, 0.0136]	[-0.0102, 0.0187]	[0, 0.0282]
	0.4419	0.8503	0.0424	0.9643	0.5615	0.0496
Flatness	0.0086	0.0081	0.0073	0.0035	0.0163	0.0162
	[-0.0055, 0.0227]	[-0.006, 0.0222]	[-0.0068, 0.0214]	[-0.0105, 0.0176]	[0.0018, 0.0309]	[0.002, 0.0304]
	0.2336	0.2595	0.312	0.6207	0.0281	0.0252

Table 6.12. *Each cell represents a separate model, adjusted for: age, sex, social deprivation, educational level, smoking, alcohol intake, exercise level. Results are degree of change in radiomics shape feature per 100g increase in daily meat/fish consumption with corresponding 95% confidence intervals and p-values. First, second, and third row for every CMR measures corresponds to beta coefficient, 95% confidence interval and p-value, respectively. Bonferroni adjusted significance threshold p-value =0.0006 (corrected for 78 comparisons).*

6.4.4 Association of meat and fish intake with LV myocardium radiomics first-order features

We extracted 18 radiomics first-order features from the LV myocardium in end-diastole and end-systole (in total 36 features). These features summarise the global distribution of signal intensities in the defined region of interest, in this case, the LV myocardium.

Our results demonstrate that the associations of the red/processed meat and oily fish exposures with first-order features were markedly different, often with opposite directions of effect (**Figure 6.8**).

Higher intake of red and processed meat consumption was associated with lower average signal intensity levels (e.g., mean, median) and less variation in signal intensity levels (e.g., range, variance, entropy). These relationships were consistent for individual red meat subtypes (**Figure 6.8**). In contrast, higher oily fish intake was associated with higher average signal intensity levels, greater variation in signal intensity levels, larger number of pixels with extreme signal intensity values (kurtosis), and higher randomness (entropy) of signal intensity levels within the LV myocardium (**Figure 6.8**). Associations were consistent in end-diastole and end-systole.

Thus, associations with the global pattern of signal intensities in the LV myocardium are substantially different between the meat and fish exposures. Our results indicate that the different dietary exposures may be associated with differing patterns of global myocardial alterations.

These findings suggest that these exposures may be associated with different global pattern of alterations at the myocardial level. Results from individual associations between meat and fish exposures and LV myocardium first-order features in end-diastole and end-systole are presented in **Table 6.13** and **Table 6.14.**

Figure 6.8. Multivariable linear regression models showing change in myocardium cardiovascular magnetic resonance first-order radiomics per 100g increase in daily meat consumption

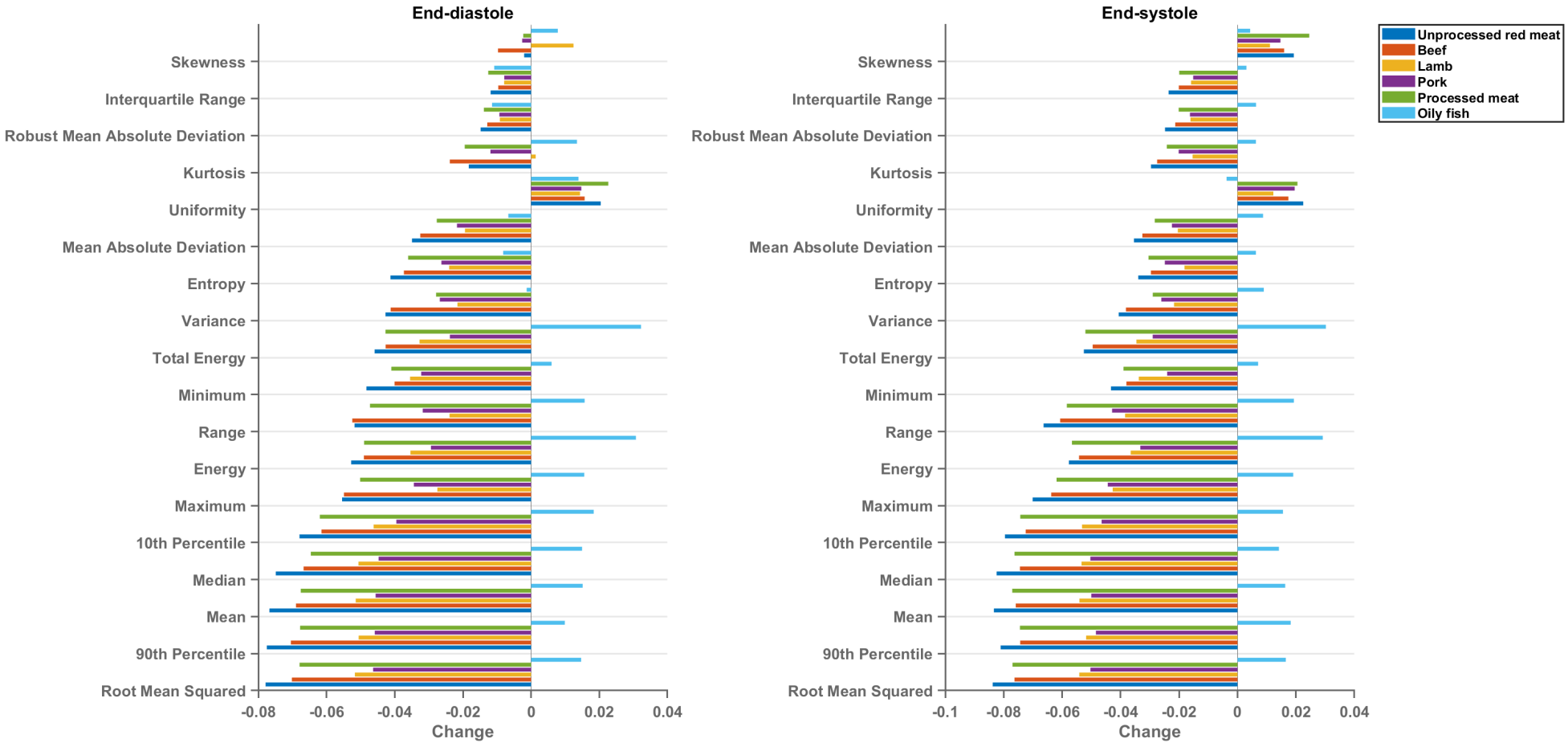

Figure 6.8. *Features are in descending order of change in unprocessed red meat in end-diastole. Each bar is from a separate model adjusted for age, sex, social deprivation, educational level, smoking, alcohol intake, exercise level (confounder adjusted model). Reproduced from Raisi-Estabragh et al.*[203].

Table 6.13. Multivariate linear regression models showing change in left ventricular myocardium first-order radiomics features in end-diastole per 100g increase in daily meat/fish consumption

	Unprocessed red meat	Beef	Lamb	Pork	Processed meat	Oily fish
Energy	-0.0528*	-0.049*	-0.0354*	-0.0294*	-0.049*	0.0307*
	[-0.0656, -0.04]	[-0.0618, -0.0363]	[-0.0482, -0.0226]	[-0.0421, -0.0167]	[-0.0622, -0.0358]	[0.0178, 0.0436]
	6.86×10^{-16}	5.03×10^{-14}	5.86×10^{-8}	6.17×10^{-6}	4.02×10^{-13}	$2.95\text{x}10\times10^{-6}$
Total Energy	-0.0459*	-0.0427*	-0.0327*	-0.0238*	-0.0427*	0.0322*
	[-0.0586, -0.0333]	[-0.0553, -0.0301]	[-0.0453, -0.0201]	[-0.0364, -0.0113]	[-0.0558, -0.0296]	[0.0195, 0.045]
	1.16×10^{-12}	3.19×10^{-11}	3.82×10^{-7}	0.0002	1.51×10^{-10}	$6.81\text{x}10\times10^{-7}$
Entropy	-0.0413*	-0.0373*	-0.024*	-0.0263*	-0.0361*	-0.0082
	[-0.0544, -0.0281]	[-0.0504, -0.0243]	[-0.0371, -0.0109]	[-0.0394, -0.0133]	[-0.0496, -0.0225]	[-0.0214, 0.005]
	7.33×10^{-10}	2.22×10^{-8}	0.0003	7.67×10^{-5}	1.87×10^{-7}	0.2228
Minimum	-0.0483*	-0.0401*	-0.0355*	-0.0322*	-0.041*	0.006
	[-0.0625, -0.0341]	[-0.0542, -0.0259]	[-0.0497, -0.0213]	[-0.0464, -0.0181]	[-0.0557, -0.0263]	[-0.0083, 0.0203]
	2.83×10^{-11}	3.05×10^{-8}	9.64×10^{-7}	7.9×10^{-6}	4.6×10^{-8}	0.4109
10th Percentile	-0.0679*	-0.0615*	-0.0462*	-0.0395*	-0.062*	0.0184
	[-0.0817, -0.0541]	[-0.0752, -0.0477]	[-0.06, -0.0324]	[-0.0533, -0.0258]	[-0.0762, -0.0477]	[0.0045, 0.0323]
	5.32×10^{-22}	1.93×10^{-18}	5.12×10^{-11}	1.68×10^{-8}	1.69×10^{-17}	0.0096
90th Percentile	-0.0775*	-0.0705*	-0.0506*	-0.0459*	-0.0678*	0.0099
	[-0.0916, -0.0635]	[-0.0845, -0.0565]	[-0.0646, -0.0365]	[-0.0599, -0.0319]	[-0.0823, -0.0532]	[-0.0043, 0.0241]
	4.04×10^{-27}	7.42×10^{-23}	1.81×10^{-12}	1.39×10^{-10}	7.16×10^{-20}	0.1721
Maximum	-0.0554*	-0.0549*	-0.0275*	-0.0344*	-0.0502*	0.0156
	[-0.0696, -0.0413]	[-0.069, -0.0408]	[-0.0416, -0.0134]	[-0.0484, -0.0204]	[-0.0648, -0.0356]	[0.0014, 0.0298]
	1.46×10^{-14}	2.07×10^{-14}	0.0001	1.57×10^{-6}	1.63×10^{-11}	0.0317
Mean	-0.0768*	-0.069*	-0.0514*	-0.0456*	-0.0676*	0.0151
	[-0.0908, -0.0628]	[-0.0829, -0.055]	[-0.0655, -0.0374]	[-0.0596, -0.0317]	[-0.082, -0.0531]	[0.001, 0.0292]
	7.91×10^{-27}	4.04×10^{-22}	6.15×10^{-13}	1.48×10^{-10}	6.59×10^{-20}	0.036
Median	-0.0749*	-0.0667*	-0.0506*	-0.0447*	-0.0646*	0.0149
	[-0.0889, -0.0609]	[-0.0806, -0.0528]	[-0.0646, -0.0367]	[-0.0586, -0.0309]	[-0.0791, -0.0502]	[0.0009, 0.029]
	8.6×10^{-26}	5.83×10^{-21}	1.14×10^{-12}	2.82×10^{-10}	1.8×10^{-18}	0.0373
Interquartile Range	-0.0119	-0.0096	-0.0079	-0.0079	-0.0126	-0.0108
	[-0.0253, 0.0015]	[-0.023, 0.0037]	[-0.0213, 0.0054]	[-0.0212, 0.0054]	[-0.0264, 0.0013]	[-0.0243, 0.0026]

	Unprocessed red meat	Beef	Lamb	Pork	Processed meat	Oily fish
	0.082	0.156	0.2452	0.2457	0.0746	0.1147
Range	-0.0518*	-0.0525*	-0.0239	-0.0318*	-0.0473*	0.0157
	[-0.0659, -0.0377]	[-0.0665, -0.0384]	[-0.038, -0.0098]	[-0.0458, -0.0178]	[-0.0619, -0.0327]	[0.0015, 0.0299]
	6.73×10^{-13}	2.72×10^{-13}	0.0009	9.05×10^{-6}	2.18×10^{-10}	0.0304
Mean Absolute Deviation	-0.0349*	-0.0325*	-0.0194	-0.0217	-0.0277*	-0.0067
	[-0.048, -0.0219]	[-0.0455, -0.0195]	[-0.0324, -0.0064]	[-0.0347, -0.0088]	[-0.0412, -0.0142]	[-0.0198, 0.0064]
	1.52×10^{-7}	9.37×10^{-7}	0.0035	0.001	5.69×10^{-5}	0.318
Robust Mean Absolute Deviation	-0.0148*	-0.0129	-0.0092	-0.0093	-0.0139	-0.0115
	[-0.0281, -0.0016]	[-0.0261, 0.0003]	[-0.0224, 0.004]	[-0.0225, 0.0038]	[-0.0275, -0.0002]	[-0.0248, 0.0018]
	0.0285	0.0559	0.1731	0.165	0.0472	0.0913
Root Mean Squared	-0.0779*	-0.0702*	-0.0517*	-0.0463*	-0.0679*	0.0147
	[-0.0919, -0.0638]	[-0.0842, -0.0562]	[-0.0657, -0.0377]	[-0.0603, -0.0324]	[-0.0824, -0.0534]	[0.0005, 0.0288]
	2.02×10^{-27}	9.86×10^{-23}	5.53×10^{-13}	8.49×10^{-11}	5.35×10^{-20}	0.0425
Skewness	-0.0021	-0.0097	0.0124	-0.0026	-0.0023	0.0078
	[-0.0162, 0.012]	[-0.0238, 0.0043]	[-0.0017, 0.0265]	[-0.0166, 0.0114]	[-0.0169, 0.0123]	[-0.0063, 0.022]
	0.7751	0.1746	0.0835	0.7131	0.7553	0.2789
Kurtosis	-0.0183	-0.0238	0.0013	-0.0119	-0.0195*	0.0134
	[-0.0325, -0.0041]	[-0.038, -0.0097]	[-0.0128, 0.0155]	[-0.026, 0.0022]	[-0.0341, -0.0048]	[-0.0008, 0.0277]
	0.0115	0.0009	0.8542	0.0971	0.0092	0.065
Variance	-0.0427*	-0.0412*	-0.0216	-0.0268*	-0.0279*	-0.0013
	[-0.0565, -0.029]	[-0.0549, -0.0275]	[-0.0353, -0.0079]	[-0.0405, -0.0131]	[-0.0421, -0.0137]	[-0.0152, 0.0125]
	1.18×10^{-9}	3.85×10^{-9}	0.0021	0.0001	0.0001	0.8523
Uniformity	0.0204	0.0157	0.0143	0.0147	0.0226	0.0139
	[0.007, 0.0339]	[0.0023, 0.0291]	[0.0009, 0.0278]	[0.0014, 0.0281]	[0.0087, 0.0365]	[0.0004, 0.0274]
	0.0029	0.0217	0.0363	0.0308	0.0014	0.0442

Table 6.13. *Each cell represents a separate model, adjusted for: age, sex, social deprivation, educational level, smoking, alcohol intake, exercise level. Results are degree of change in radiomics first-order feature per 100g increase in daily meat/fish consumption with corresponding 95% confidence intervals and p-values. First, second, and third row for every CMR measures corresponds to beta coefficient, 95% confidence interval and p-value, respectively. Bonferroni adjusted significance threshold p-value =0.0004 (corrected for 108 comparisons). Cardiovascular magnetic resonance: CMR.*

Table 6.14. Multivariate linear regression models showing change in left ventricular myocardium first-order radiomics features in end-systole per 100g increase in daily meat/fish consumption

	Unprocessed red meat	Beef	Lamb	Pork	Processed meat	Oily fish
Energy	-0.0577*	-0.0542*	-0.0365*	-0.0333*	-0.0567*	0.0292*
	[-0.0703, -0.0451]	[-0.0668, -0.0416]	[-0.0492, -0.0239]	[-0.0458, -0.0207]	[-0.0697, -0.0436]	[0.0164, 0.0419]
	3.9×10^{-19}	3.27×10^{-17}	1.41×10^{-8}	2.19×10^{-7}	1.9×10^{-17}	$7.03\text{x}10^{-6}$
Total Energy	-0.0526*	-0.0496*	-0.0346*	-0.029*	-0.0521*	0.0302*
	[-0.0651, -0.0401]	[-0.062, -0.0371]	[-0.0471, -0.0221]	[-0.0415, -0.0166]	[-0.065, -0.0392]	[0.0177, 0.0428]
	1.69×10^{-16}	6.21×10^{-15}	5.54×10^{-8}	4.75×10^{-6}	2.8×10^{-15}	$2.45\text{x}10^{-6}$
Entropy	-0.034*	-0.0296*	-0.0182*	-0.0249*	-0.0305*	0.0063
	[-0.048, -0.0199]	[-0.0436, -0.0157]	[-0.0322, -0.0041]	[-0.0388, -0.0109]	[-0.045, -0.016]	[-0.0078, 0.0204]
	2.15×10^{-6}	3.3×10^{-5}	0.0111	0.0005	3.88×10^{-5}	0.3831
Minimum	-0.0433*	-0.038*	-0.0338*	-0.0241*	-0.039*	0.007
	[-0.0575, -0.0291]	[-0.0522, -0.0239]	[-0.048, -0.0196]	[-0.0382, -0.01]	[-0.0537, -0.0243]	[-0.0073, 0.0214]
	2.44×10^{-9}	1.46×10^{-7}	3.14×10^{-6}	0.0008	1.96×10^{-7}	0.3344
10th Percentile	-0.0796*	-0.0725*	-0.0532*	-0.0465*	-0.0743*	0.0155*
	[-0.0934, -0.0657]	[-0.0863, -0.0587]	[-0.0671, -0.0394]	[-0.0603, -0.0327]	[-0.0887, -0.06]	[0.0016, 0.0295]
	2.82×10^{-29}	9.37×10^{-25}	5.4×10^{-14}	4.12×10^{-11}	3.05×10^{-24}	0.0292
90th Percentile	-0.0811*	-0.0744*	-0.0518*	-0.0484*	-0.0745*	0.0182*
	[-0.0949, -0.0673]	[-0.0881, -0.0606]	[-0.0656, -0.038]	[-0.0622, -0.0347]	[-0.0887, -0.0602]	[0.0043, 0.0321]
	1.31×10^{-30}	3.24×10^{-26}	1.85×10^{-13}	4.8×10^{-12}	1.53×10^{-24}	0.0103
Maximum	-0.0701*	-0.0638*	-0.0427*	-0.0444*	-0.0619*	0.019*
	[-0.0842, -0.056]	[-0.0778, -0.0497]	[-0.0568, -0.0287]	[-0.0584, -0.0304]	[-0.0765, -0.0474]	[0.0049, 0.0332]
	1.7×10^{-22}	5.16×10^{-19}	2.62×10^{-9}	5.07×10^{-10}	7.24×10^{-17}	0.0084
Mean	-0.0834*	-0.0759*	-0.0541*	-0.05*	-0.0771*	0.0163*
	[-0.0971, -0.0696]	[-0.0896, -0.0621]	[-0.0679, -0.0403]	[-0.0638, -0.0363]	[-0.0913, -0.0629]	[0.0024, 0.0302]
	2.47×10^{-32}	2.88×10^{-27}	1.44×10^{-14}	9.12×10^{-13}	3.1×10^{-26}	0.0213
Median	-0.0824*	-0.0744*	-0.0534*	-0.0504*	-0.0763*	0.0142*
	[-0.0962, -0.0687]	[-0.0882, -0.0607]	[-0.0671, -0.0396]	[-0.0641, -0.0367]	[-0.0905, -0.0621]	[0.0003, 0.028]
	9.84×10^{-32}	2.23×10^{-26}	3.02×10^{-14}	6.08×10^{-13}	8.34×10^{-26}	0.0455
Interquartile Range	-0.0236*	-0.0201*	-0.0159*	-0.0152*	-0.0199*	0.003
	[-0.0376, -0.0096]	[-0.0341, -0.0061]	[-0.0299, -0.0019]	[-0.0291, -0.0012]	[-0.0344, -0.0055]	[-0.0111, 0.0172]
	0.001	0.0049	0.026	0.033	0.007	0.6725
Range	-0.0664*	-0.0607*	-0.0385*	-0.0429*	-0.0584*	0.0193*
	[-0.0804, -0.0523]	[-0.0747, -0.0467]	[-0.0525, -0.0244]	[-0.0569, -0.0289]	[-0.073, -0.0439]	[0.0051, 0.0335]
	2.63×10^{-20}	2.26×10^{-17}	8.29×10^{-8}	1.9×10^{-9}	3.62×10^{-15}	0.0076

	Unprocessed red meat	Beef	Lamb	Pork	Processed meat	Oily fish
Mean Absolute Deviation	-0.0354*	-0.0326*	-0.0204*	-0.0224*	-0.0283*	0.0087
	[-0.0495, -0.0214]	[-0.0465, -0.0186]	[-0.0344, -0.0064]	[-0.0364, -0.0085]	[-0.0428, -0.0138]	[-0.0054, 0.0228]
	7.38×10^{-7}	4.99×10^{-6}	0.0043	0.0016	0.0001	0.2251
Robust Mean Absolute Deviation	-0.0248*	-0.0213*	-0.0161*	-0.0163*	-0.0201*	0.0063
	[-0.0388, -0.0108]	[-0.0353, -0.0073]	[-0.0301, -0.0021]	[-0.0302, -0.0023]	[-0.0346, -0.0056]	[-0.0078, 0.0205]
	0.0005	0.0028	0.0242	0.0221	0.0065	0.3784
Root Mean Squared	-0.0838*	-0.0763*	-0.0541*	-0.0503*	-0.077*	0.0165*
	[-0.0975, -0.07]	[-0.09, -0.0626]	[-0.0679, -0.0404]	[-0.0641, -0.0366]	[-0.0912, -0.0628]	[0.0026, 0.0304]
	1.22×10^{-32}	1.42×10^{-27}	1.38×10^{-14}	6.62×10^{-13}	3.51×10^{-26}	0.0198
Skewness	0.0193*	0.0159*	0.0111	0.0147*	0.0245*	0.0043
	[0.0052, 0.0334]	[0.0019, 0.03]	[-0.003, 0.0252]	[0.0007, 0.0287]	[0.01, 0.0391]	[-0.0099, 0.0185]
	0.0075	0.0263	0.1225	0.0402	0.001	0.5503
Kurtosis	-0.0296*	-0.0275*	-0.0154*	-0.0201*	-0.0242*	0.0063
	[-0.0439, -0.0153]	[-0.0417, -0.0133]	[-0.0296, -0.0011]	[-0.0343, -0.0059]	[-0.0389, -0.0094]	[-0.0081, 0.0206]
	4.85×10^{-5}	0.0002	0.0344	0.0054	0.0013	0.3911
Variance	-0.0406*	-0.0382*	-0.0217*	-0.0261*	-0.029*	0.009
	[-0.0548, -0.0265]	[-0.0523, -0.0241]	[-0.0359, -0.0076]	[-0.0402, -0.012]	[-0.0437, -0.0144]	[-0.0053, 0.0233]
	1.92×10^{-8}	1.17×10^{-7}	0.0026	0.0003	0.0001	0.216
Uniformity	0.0225*	0.0174*	0.0123	0.0196*	0.0205*	-0.0037
	[0.0084, 0.0366]	[0.0034, 0.0315]	[-0.0018, 0.0264]	[0.0055, 0.0336]	[0.0059, 0.0351]	[-0.0179, 0.0105]
	0.0018	0.0153	0.0883	0.0063	0.0059	0.6057

Table 6.14. *Each cell represents a separate model, adjusted for: age, sex, social deprivation, educational level, smoking, alcohol intake, exercise level. Results are degree of change in radiomics first-order feature per 100g increase in daily meat/fish consumption with corresponding 95% confidence intervals and p-values. First, second, and third row for every CMR measures corresponds to beta coefficient, 95% confidence interval and p-value, respectively. Bonferroni adjusted significance threshold p-value =0.0004 (corrected for 108 comparisons). Cardiovascular magnetic resonance: CMR.*

6.4.4.1 Association of meat and fish intake with LV myocardium radiomics texture features

Radiomics texture features represent patterns of signal intensity levels within the region of interest. When applied to the LV myocardium, radiomics texture features may reflect tissue level alterations and provide insight into myocardial disease processes. In this study, we extracted 72 texture features from the LV myocardium in end-diastole and end-systole (total 144 texture features extracted from the LV myocardium per study). As detailed previously, we performed hierarchical cluster analysis to identify seven groupings of inter-correlated texture features (**Figure 6.3**). We assigned descriptive terms to each cluster based on the properties of its constituent features (**Table 6.15**).

Table 6.15. Description of clusters identified from the radiomics texture features

Assigned cluster name	Exemplar feature from the cluster	Properties represented by cluster
Low Grey Level Emphasis	Low Grey Level Emphasis	Local distribution and clustering of low SI values
Spatial Non-Uniformity	Size Zone Non-Uniformity	Non-uniformity in the size of pixel groupings
Grey Level Variance	Grey Level Variance	Distribution of SI values
Coarseness	Run Percentage	Tendency to small groupings of pixels with similar SI values
Local Heterogeneity	Dependence Entropy	Randomness of neighbouring pixel SI values
Large Scale Emphasis	Large Area Emphasis	Larger areas of similar pixel SI values
Grey Level Skewness	Cluster Prominence	Skewness of the SI distribution

Table 6.15. The table summarises the seven distinct groups of radiomics texture features identified through cluster analysis of these features (n=144, **Figure 6.3**). Each cluster incorporates a number of inter-correlated features. For each cluster, we provide an assigned name, an exemplar feature, and a general description of the properties represented. SI: signal intensity

There were different magnitude and direction of association between the different dietary exposures and mean effects in the texture clusters (**Figure 6.9**). Higher intakes of red and processed meat were associated with lower intensity levels, less variation in intensity levels, less local heterogeneity, and less skewness in the local distribution of signal intensity values (**Figure 6.7**, **Figure 6.9**). Greater intake of oily fish was associated with more local heterogeneity in signal intensity levels and greater skewness in intensity level distributions (**Figure 6.7**, **Figure 6.9**).

Results from individual associations between meat and fish exposures and individual LV myocardium texture features in end-diastole and end-systole are presented in **Table 6.16** and **Table 6.17.**

Figure 6.9. Mean change in left ventricular myocardium radiomics texture feature clusters per 100g increase in daily meat consumption

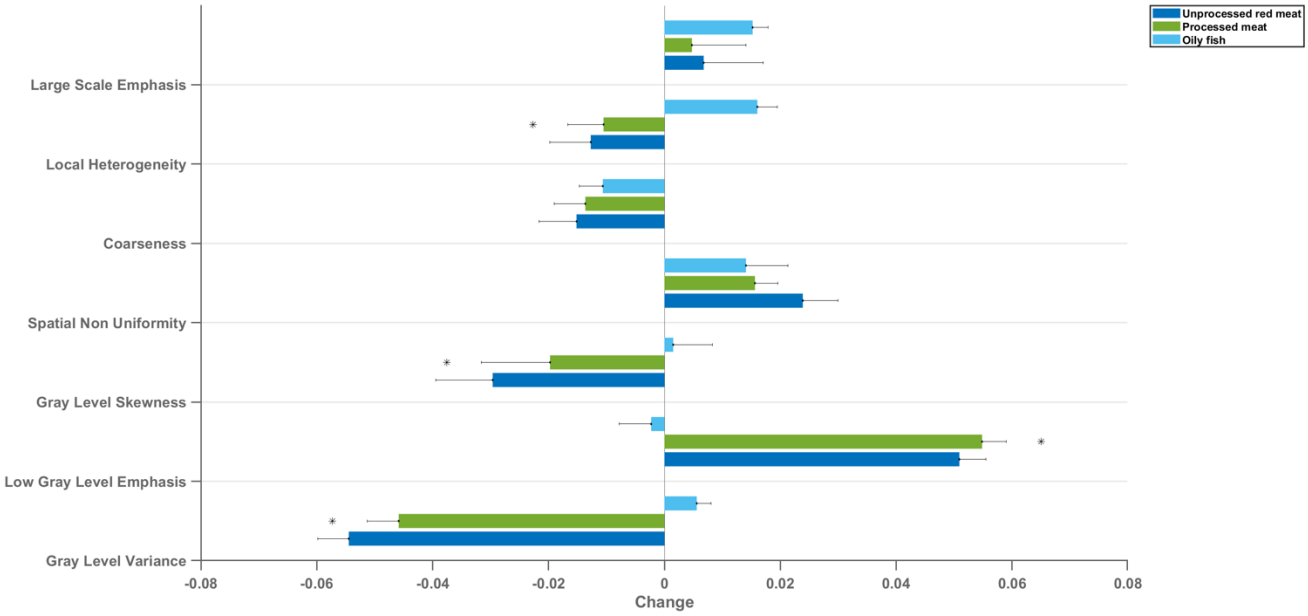

Figure 6.9. *Each bar represents mean standardised beta coefficients corresponding to the indicated texture feature cluster. Models are adjusted for age, sex, social deprivation, educational level, smoking, alcohol intake, exercise level (confounder adjusted model). Black lines represent half-length of confidence interval for the corresponding bar. CMR: cardiovascular magnetic resonance; LV: left ventricle *denotes p < 0.05 in using Kruskal-Wallis statistical testing followed by Dunn's correction test for multiple comparisons, between oily fish and unprocessed red meat and between oily fish and processed red meat. Reproduced from Raisi-Estabragh et al.*[203].

Table 6.16. Multivariable linear regression models showing change in left ventricular myocardium texture radiomics in end-diastole per 100g increase in daily meat/fish consumption

Feature (sub-category)	Unprocessed red meat	Beef	Lamb	Pork	Processed meat	Oily fish
Autocorrelation (GLCM)	-0.0765	-0.069	-0.0518	-0.0443	-0.0652	0.0178
	[-0.0905, -0.0625]	[-0.083, -0.055]	[-0.0659, -0.0378]	[-0.0582, -0.0303]	[-0.0797, -0.0507]	[0.0037, 0.032]
	1.49×10^{-26}	4.41×10^{-22}	4.56×10^{-13}	5.41×10^{-10}	1.37×10^{-18}	0.0135
Joint Average (GLCM)	-0.0754	-0.0677	-0.0512	-0.044	-0.0675	0.0151
	[-0.0894, -0.0614]	[-0.0817, -0.0538]	[-0.0652, -0.0372]	[-0.0579, -0.03]	[-0.082, -0.0531]	[0.001, 0.0293]
	5.85×10^{-26}	1.97×10^{-21}	7.84×10^{-13}	6.42×10^{-10}	6.32×10^{-20}	0.0354
Cluster Prominence (GLCM)	-0.0165	-0.0173	-0.004	-0.0124	-0.0012	-0.0032
	[-0.0309, -0.0021]	[-0.0316, -0.0029]	[-0.0184, 0.0104]	[-0.0267, 0.0019]	[-0.0161, 0.0137]	[-0.0177, 0.0113]
	0.025	0.0183	0.587	0.0903	0.8733	0.6676
Cluster Shade (GLCM)	-0.015	-0.0168	-0.0013	-0.0118	-0.0035	-0.001
	[-0.0293, -0.0007]	[-0.0311, -0.0026]	[-0.0156, 0.013]	[-0.026, 0.0024]	[-0.0183, 0.0113]	[-0.0154, 0.0134]
	0.0405	0.0205	0.8574	0.1046	0.6447	0.8933
Cluster Tendency (GLCM)	-0.0348	-0.0332	-0.0184	-0.0217	-0.0191	-0.0004
	[-0.0488, -0.0208]	[-0.0471, -0.0192]	[-0.0324, -0.0044]	[-0.0356, -0.0078]	[-0.0336, -0.0046]	[-0.0145, 0.0137]
	1.14×10^{-6}	3.23×10^{-6}	0.0099	0.0023	0.0097	0.9596
Contrast (GLCM)	-0.0438	-0.0404	-0.024	-0.0284	-0.0335	-0.0042
	[-0.057, -0.0307]	[-0.0535, -0.0273]	[-0.0371, -0.0109]	[-0.0415, -0.0154]	[-0.0471, -0.0199]	[-0.0174, 0.009]
	6.09×10^{-11}	1.45×10^{-9}	0.0003	1.99×10^{-5}	1.3×10^{-6}	0.5321
Correlation (GLCM)	0.0017	0.0028	-0.0043	0.0037	0.0064	0.0176
	[-0.012, 0.0155]	[-0.0109, 0.0165]	[-0.018, 0.0095]	[-0.01, 0.0173]	[-0.0078, 0.0206]	[0.0038, 0.0315]
	0.8053	0.6909	0.5418	0.6001	0.3792	0.0124
Difference Average (GLCM)	-0.0369	-0.0322	-0.0221	-0.0245	-0.0321	-0.012
	[-0.0495, -0.0242]	[-0.0448, -0.0196]	[-0.0348, -0.0095]	[-0.0371, -0.0119]	[-0.0452, -0.019]	[-0.0247, 0.0007]

Feature (sub-category)	Unprocessed red meat	Beef	Lamb	Pork	Processed meat	Oily fish
	1.14×10^{-8}	5.75×10^{-7}	0.0006	0.0001	1.52×10^{-6}	0.0649
Difference Entropy (GLCM)	-0.0441	-0.04	-0.0251	-0.0285	-0.0361	-0.01
	[-0.0566, -0.0317]	[-0.0524, -0.0276]	[-0.0375, -0.0127]	[-0.0408, -0.0161]	[-0.049, -0.0233]	[-0.0225, 0.0025]
	3.52×10^{-12}	2.42×10^{-10}	7.27×10^{-5}	6.3×10^{-6}	3.48×10^{-8}	0.1164
Difference Variance (GLCM)	-0.0487	-0.0463	-0.0255	-0.0307	-0.0352	0.0012
	[-0.0621, -0.0353]	[-0.0596, -0.0329]	[-0.0389, -0.0121]	[-0.0441, -0.0174]	[-0.0491, -0.0213]	[-0.0123, 0.0148]
	1.2×10^{-12}	1.2×10^{-11}	0.0002	6.34×10^{-6}	6.74×10^{-7}	0.8562
Joint Energy (GLCM)	0.0183	0.0122	0.015	0.014	0.0206	0.0143
	[0.0046, 0.032]	[-0.0014, 0.0259]	[0.0014, 0.0287]	[0.0004, 0.0277]	[0.0064, 0.0347]	[0.0005, 0.0281]
	0.0087	0.0789	0.0309	0.0432	0.0043	0.0416
Joint Entropy (GLCM)	-0.0377	-0.0325	-0.024	-0.0243	-0.0318	-0.0103
	[-0.0509, -0.0245]	[-0.0457, -0.0194]	[-0.0371, -0.0108]	[-0.0375, -0.0112]	[-0.0455, -0.0182]	[-0.0236, 0.003]
	2.25×10^{-8}	1.25×10^{-6}	0.0004	0.0003	4.75×10^{-6}	0.1276
Informal Measure Of Correlation 1 (GLCM)	-0.0051	-0.0024	-0.0003	-0.0082	-0.0075	-0.0251
	[-0.0186, 0.0084]	[-0.0159, 0.011]	[-0.0138, 0.0132]	[-0.0216, 0.0052]	[-0.0215, 0.0065]	[-0.0387, -0.0115]
	0.4611	0.7234	0.9651	0.2317	0.2924	0.0003
Informal Measure Of Correlation 2 (GLCM)	-0.0199	-0.0196	-0.016	-0.0072	-0.0103	0.0193
	[-0.0341, -0.0058]	[-0.0337, -0.0055]	[-0.0301, -0.0018]	[-0.0212, 0.0069]	[-0.0249, 0.0044]	[0.0051, 0.0335]
	0.0058	0.0063	0.0267	0.3178	0.1692	0.0079
Inverse Difference Moment (GLCM)	0.0303	0.0253	0.0192	0.0207	0.0285	0.0155
	[0.0177, 0.043]	[0.0127, 0.0379]	[0.0066, 0.0319]	[0.0081, 0.0332]	[0.0154, 0.0416]	[0.0028, 0.0283]
	2.63×10^{-6}	8.17×10^{-5}	0.0029	0.0013	1.94×10^{-5}	0.0167
Inverse Difference Moment Normalized (GLCM)	-0.0359	-0.0344	-0.0214	-0.0221	-0.0405	0.0226
	[-0.0499, -0.022]	[-0.0483, -0.0205]	[-0.0354, -0.0074]	[-0.036, -0.0082]	[-0.0549, -0.026]	[0.0085, 0.0366]
	4.83×10-7	1.34×10^{-6}	0.0027	0.0019	4.16×10^{-8}	0.0017
Inverse Difference (GLCM)	0.029	0.0237	0.0187	0.0201	0.0277	0.0162
	[0.0162, 0.0417]	[0.011, 0.0364]	[0.0059, 0.0314]	[0.0074, 0.0328]	[0.0145, 0.0409]	[0.0033, 0.029]

Feature (sub-category)	Unprocessed red meat	Beef	Lamb	Pork	Processed meat	Oily fish
	8.53×10^{-6}	0.0002	0.0041	0.0019	3.74×10^{-5}	0.0135
Inverse Difference Normalized (GLCM)	-0.0268	-0.0286	-0.0129	-0.0152	-0.0284	0.0266
	[-0.0406, -0.0131]	[-0.0423, -0.0149]	[-0.0266, 0.0008]	[-0.0289, -0.0016]	[-0.0427, -0.0142]	[0.0127, 0.0404]
	0.0001	4.4×10^{-5}	0.0657	0.0291	8.8×10^{-5}	0.0002
Inverse Variance (GLCM)	-0.0099	-0.0039	-0.0093	-0.0101	-0.0147	-0.0194
	[-0.0237, 0.0038]	[-0.0176, 0.0098]	[-0.0231, 0.0044]	[-0.0238, 0.0035]	[-0.0289, -0.0005]	[-0.0332, -0.0056]
	0.1577	0.5777	0.1831	0.146	0.0432	0.006
Maximum Probability (GLCM)	0.0162	0.0107	0.014	0.012	0.0201	0.0116
	[0.0023, 0.0301]	[-0.0031, 0.0246]	[0.0001, 0.0279]	[-0.0018, 0.0258]	[0.0057, 0.0345]	[-0.0024, 0.0256]
	0.0225	0.1294	0.0479	0.0886	0.0061	0.1044
Sum Average (GLCM)	-0.0754	-0.0677	-0.0512	-0.044	-0.0675	0.0151
	[-0.0894, -0.0614]	[-0.0817, -0.0538]	[-0.0652, -0.0372]	[-0.0579, -0.03]	[-0.082, -0.0531]	[0.001, 0.0293]
	5.85×10^{-26}	1.97×10^{-21}	7.84×10^{-13}	6.42×10^{-10}	6.32×10^{-20}	0.0354
Sum Entropy (GLCM)	-0.0374	-0.0321	-0.0249	-0.0237	-0.0313	-0.0047
	[-0.051, -0.0239]	[-0.0456, -0.0186]	[-0.0384, -0.0114]	[-0.0372, -0.0102]	[-0.0453, -0.0174]	[-0.0183, 0.0089]
	6.12×10^{-8}	3.09×10^{-6}	0.0003	0.0006	1.14×10^{-5}	0.4998
Sum Of Squares (GLCM)	-0.039	-0.0367	-0.0209	-0.0246	-0.0244	-0.0016
	[-0.0528, -0.0252]	[-0.0504, -0.023]	[-0.0346, -0.0071]	[-0.0383, -0.011]	[-0.0386, -0.0102]	[-0.0154, 0.0122]
	2.8×10^{-8}	1.52×10^{-7}	0.0029	0.0004	0.0008	0.8212
Small Area Emphasis (GLSZM)	-0.0343	-0.0309	-0.0196	-0.0237	-0.0337	0.0149
	[-0.0486, -0.02]	[-0.0451, -0.0167]	[-0.0338, -0.0053]	[-0.0379, -0.0095]	[-0.0484, -0.0189]	[0.0006, 0.0293]
	2.53×10^{-6}	2.05×10^{-5}	0.0071	0.0011	7.62×10^{-6}	0.0417
Large Area Emphasis (GLSZM)	0.0412	0.0378	0.0248	0.0242	0.0332	0.0181
	[0.0299, 0.0524]	[0.0266, 0.049]	[0.0135, 0.036]	[0.0131, 0.0354]	[0.0216, 0.0449]	[0.0068, 0.0294]
	7.63×10^{-13}	3.77×10^{-11}	1.56×10^{-5}	2.17×10^{-5}	2.13×10^{-8}	0.0018
Grey Level Non Uniformity (GLSZM)	0.0164	0.0078	0.0132	0.0175	0.0188	0.0125

Feature (sub-category)	Unprocessed red meat	Beef	Lamb	Pork	Processed meat	Oily fish
	[0.0024, 0.0303]	[-0.0061, 0.0217]	[-0.0008, 0.0271]	[0.0037, 0.0314]	[0.0043, 0.0332]	[-0.0015, 0.0266]
	0.0216	0.2712	0.064	0.0132	0.0108	0.0802
Size Zone Non Uniformity (GLSZM)	0.0164	0.0078	0.0132	0.0175	0.0188	0.0125
	[0.0024, 0.0303]	[-0.0061, 0.0217]	[-0.0008, 0.0271]	[0.0037, 0.0314]	[0.0043, 0.0332]	[-0.0015, 0.0266]
	0.0216	0.2712	0.064	0.0132	0.0108	0.0802
Size Zone Non Uniformity Normalized (GLSZM)	-0.036	-0.0316	-0.0216	-0.0252	-0.0348	0.0143
	[-0.0502, -0.0217]	[-0.0458, -0.0174]	[-0.0359, -0.0074]	[-0.0394, -0.011]	[-0.0495, -0.02]	[0, 0.0287]
	8.09×10^{-7}	1.34×10^{-5}	0.0029	0.0005	3.83×10^{-6}	0.0507
Zone Percentage (GLSZM)	-0.0574	-0.0537	-0.0347	-0.0333	-0.0417	0.0009
	[-0.0702, -0.0447]	[-0.0665, -0.041]	[-0.0474, -0.022]	[-0.046, -0.0206]	[-0.0549, -0.0285]	[-0.0119, 0.0138]
	1.23×10^{-18}	1.23×10^{-16}	9.69×10^{-8}	2.82×10^{-7}	6.22×10^{-10}	0.8865
Grey Level Variance (GLSZM)	-0.0627	-0.0613	-0.0333	-0.0373	-0.0544	0.0074
	[-0.0768, -0.0485]	[-0.0754, -0.0472]	[-0.0475, -0.0192]	[-0.0514, -0.0232]	[-0.0691, -0.0398]	[-0.0069, 0.0217]
	4.56×10^{-18}	1.75×10^{-17}	3.96×10^{-6}	2.16×10^{-7}	3.19×10^{-13}	0.3085
Zone Variance (GLSZM)	0.041	0.0375	0.0248	0.0242	0.033	0.0183
	[0.0298, 0.0522]	[0.0264, 0.0487]	[0.0135, 0.036]	[0.0131, 0.0354]	[0.0214, 0.0446]	[0.007, 0.0296]
	8.87×10^{-13}	4.97×10^{-11}	1.54×10^{-5}	2.13×10^{-5}	2.57×10^{-8}	0.0015
Zone Entropy (GLSZM)	-0.037	-0.0414	-0.0174	-0.0149	-0.0388	0.0073
	[-0.0512, -0.0229]	[-0.0555, -0.0273]	[-0.0315, -0.0033]	[-0.0289, -0.0008]	[-0.0534, -0.0242]	[-0.007, 0.0215]
	3×10^{-7}	8.83×10^{-9}	0.0158	0.0385	1.99×10^{-7}	0.3162
Low Grey Level Zone Emphasis (GLSZM)	0.0645	0.0559	0.0458	0.0396	0.0575	-0.0245
	[0.0504, 0.0786]	[0.0418, 0.0699]	[0.0317, 0.0599]	[0.0255, 0.0536]	[0.0429, 0.0721]	[-0.0388, -0.0103]
	4.04×10^{-19}	7.9×10^{-15}	2.14×10^{-10}	3.53×10^{-8}	1.26×10^{-14}	0.0007
High Grey Level Zone Emphasis (GLSZM)	-0.0733	-0.0684	-0.0447	-0.044	-0.0652	0.0148
	[-0.0873, -0.0592]	[-0.0824, -0.0543]	[-0.0588, -0.0306]	[-0.058, -0.03]	[-0.0798, -0.0507]	[0.0006, 0.029]
	2.14×10^{-24}	1.33×10^{-21}	4.8×10^{-10}	7.59×10^{-10}	1.64×10^{-18}	0.0405
	0.0581	0.05	0.0423	0.0352	0.0518	-0.0224

Feature (sub-category)	Unprocessed red meat	Beef	Lamb	Pork	Processed meat	Oily fish
Small Area Low Grey Level Emphasis (GLSZM)	[0.044, 0.0723]	[0.0359, 0.064]	[0.0282, 0.0565]	[0.0212, 0.0493]	[0.0372, 0.0664]	[-0.0366, -0.0082]
	8.08×10^{-16}	3.64×10^{-12}	4.13×10^{-9}	9.11×10-7	3.82×10^{-12}	0.002
Small Area High Grey Level Emphasis (GLSZM)	-0.0738	-0.0689	-0.0449	-0.0443	-0.0673	0.0152
	[-0.0879, -0.0597]	[-0.083, -0.0549]	[-0.0589, -0.0308]	[-0.0583, -0.0303]	[-0.0818, -0.0528]	[0.001, 0.0294]
	9.86×10^{-25}	6.07×10^{-22}	4.11×10^{-10}	5.75×10^{-10}	1.28×10^{-19}	0.0358
Large Area Low Grey Level Emphasis (GLSZM)	0.0455	0.0407	0.0303	0.0266	0.0549	0.0182
	[0.0318, 0.0592]	[0.027, 0.0544]	[0.0166, 0.044]	[0.013, 0.0403]	[0.0407, 0.069]	[0.0044, 0.0321]
	8.54×10^{-11}	5.52×10^{-9}	1.5×10^{-5}	0.0001	3.35×10^{-14}	0.0096
Large Area High Grey Level Emphasis (GLSZM)	0.0013	0.0034	-0.0051	0.0014	-0.0046	0.024
	[-0.0104, 0.0129]	[-0.0082, 0.015]	[-0.0167, 0.0065]	[-0.0101, 0.013]	[-0.0166, 0.0075]	[0.0123, 0.0357]
	0.8328	0.5628	0.3892	0.8068	0.4584	5.98×10^{-5}
Short Run Emphasis (GLRLM)	-0.0299	-0.0236	-0.0226	-0.0189	-0.0266	-0.0152
	[-0.0419, -0.0178]	[-0.0356, -0.0116]	[-0.0347, -0.0106]	[-0.0309, -0.007]	[-0.0391, -0.0142]	[-0.0273, -0.0031]
	1.2×10^{-6}	0.0001	0.0002	0.0019	2.76×10^{-5}	0.0141
Long Run Emphasis (GLRLM)	0.0311	0.0238	0.0222	0.0221	0.0278	0.0185
	[0.0188, 0.0434]	[0.0116, 0.036]	[0.0099, 0.0345]	[0.0099, 0.0343]	[0.0151, 0.0405]	[0.0061, 0.0308]
	7.18×10^{-7}	0.0001	0.0004	0.0004	1.83×10^{-5}	0.0034
Grey Level Non Uniformity (GLRLM)	0.035	0.0278	0.0213	0.0273	0.0249	0.0279
	[0.0248, 0.0453]	[0.0176, 0.038]	[0.011, 0.0315]	[0.0171, 0.0375]	[0.0143, 0.0355]	[0.0176, 0.0383]
	2.23×10^{-11}	1.03×10^{-7}	4.8×10^{-5}	1.58×10^{-7}	4.28×10^{-6}	1.12×10^{-7}
Run Length Non Uniformity (GLRLM)	0.0173	0.0106	0.0112	0.0182	0.0067	0.0201
	[0.0046, 0.0301]	[-0.0021, 0.0234]	[-0.0016, 0.0239]	[0.0055, 0.0309]	[-0.0065, 0.0199]	[0.0073, 0.033]
	0.0077	0.1008	0.086	0.0049	0.3219	0.0021
Run Length Non Uniformity Normalized (GLRLM)	-0.0279	-0.0222	-0.0216	-0.0168	-0.0246	-0.0138
	[-0.04, -0.0157]	[-0.0343, -0.0101]	[-0.0338, -0.0095]	[-0.0289, -0.0048]	[-0.0372, -0.0121]	[-0.0261, -0.0016]
	7.13×10^{-6}	0.0003	0.0005	0.0063	0.0001	0.0268
Run Percentage (GLRLM)	-0.0267	-0.0205	-0.0207	-0.0172	-0.0236	-0.0143

Feature (sub-category)	Unprocessed red meat	Beef	Lamb	Pork	Processed meat	Oily fish
	[-0.0389, -0.0144]	[-0.0326, -0.0083]	[-0.0329, -0.0085]	[-0.0293, -0.005]	[-0.0362, -0.011]	[-0.0266, -0.002]
	1.91×10^{-5}	0.001	0.0009	0.0056	0.0002	0.0223
Grey Level Variance (GLRLM)	-0.0453	-0.0442	-0.0221	-0.0285	-0.0301	0.0005
	[-0.0591, -0.0315]	[-0.0579, -0.0304]	[-0.0359, -0.0083]	[-0.0423, -0.0148]	[-0.0444, -0.0158]	[-0.0135, 0.0144]
	1.43×10^{-10}	3.5×10^{-10}	0.0017	4.89×10^{-5}	3.8×10^{-5}	0.948
Run Variance (GLRLM)	0.0298	0.0227	0.0211	0.0214	0.0261	0.0191
	[0.0173, 0.0422]	[0.0103, 0.0351]	[0.0087, 0.0335]	[0.0091, 0.0338]	[0.0133, 0.039]	[0.0066, 0.0317]
	2.75×10^{-6}	0.0003	0.0009	0.0007	6.71×10^{-5}	0.0027
Run Entropy (GLRLM)	-0.025	-0.0286	-0.0065	-0.0154	-0.0206	0.014
	[-0.0388, -0.0111]	[-0.0424, -0.0148]	[-0.0204, 0.0073]	[-0.0292, -0.0017]	[-0.0349, -0.0063]	[0.0001, 0.028]
	0.0004	4.93×10^{-5}	0.3557	0.0282	0.0048	0.0485
Low Grey Level Run Emphasis (GLRLM)	0.0573	0.0523	0.0387	0.0327	0.0628	-0.0016
	[0.0434, 0.0713]	[0.0385, 0.0662]	[0.0248, 0.0526]	[0.0188, 0.0465]	[0.0484, 0.0772]	[-0.0157, 0.0124]
	7.92×10^{-16}	1.5×10^{-13}	5.01×10^{-8}	3.85×10^{-6}	1.26×10^{-17}	0.8202
High Grey Level Run Emphasis (GLRLM)	-0.0768	-0.0702	-0.0506	-0.0444	-0.066	0.0164
	[-0.0909, -0.0627]	[-0.0842, -0.0562]	[-0.0647, -0.0366]	[-0.0585, -0.0304]	[-0.0805, -0.0514]	[0.0022, 0.0306]
	1.38×10^{-26}	1.22×10^{-22}	1.85×10^{-12}	5.28×10^{-10}	7.22×10^{-19}	0.0236
Short Run Low Grey Level Emphasis (GLRLM)	0.0558	0.0515	0.037	0.0317	0.0604	-0.0047
	[0.0419, 0.0696]	[0.0377, 0.0653]	[0.0232, 0.0509]	[0.0179, 0.0454]	[0.0461, 0.0747]	[-0.0186, 0.0093]
	2.95×10^{-15}	2.6×10^{-13}	1.51×10-7	6.54×10^{-6}	1.29×10^{-16}	0.511
Short Run High Grey Level Emphasis (GLRLM)	-0.0779	-0.071	-0.0509	-0.0457	-0.0666	0.013
	[-0.092, -0.0638]	[-0.085, -0.057]	[-0.065, -0.0368]	[-0.0597, -0.0317]	[-0.0811, -0.052]	[-0.0011, 0.0272]
	2.39×10^{-27}	3.81×10^{-23}	1.37×10^{-12}	1.68×10^{-10}	3.22×10^{-19}	0.0714
Long Run Low Grey Level Emphasis (GLRLM)	0.0542	0.0473	0.0379	0.0328	0.0629	0.0088
	[0.0401, 0.0683]	[0.0332, 0.0613]	[0.0238, 0.0519]	[0.0188, 0.0468]	[0.0483, 0.0775]	[-0.0054, 0.023]
	5.1×10^{-14}	4.27×10^{-11}	1.37×10^{-7}	4.49×10^{-6}	2.64×10^{-17}	0.2234
	-0.0497	-0.047	-0.0341	-0.0257	-0.0437	0.027

Feature (sub-category)	Unprocessed red meat	Beef	Lamb	Pork	Processed meat	Oily fish
Long Run High Grey Level Emphasis (GLRLM)	[-0.0629, -0.0365]	[-0.0601, -0.0339]	[-0.0473, -0.021]	[-0.0388, -0.0126]	[-0.0573, -0.0301]	[0.0137, 0.0402]
	1.62×10^{-13}	2.36×10^{-12}	3.8×10^{-7}	0.0001	3.3×10^{-10}	6.8×10^{-5}
Coarseness (NGTDM)	-0.0288	-0.0259	-0.0181	-0.0166	-0.0096	-0.0183
	[-0.0401, -0.0174]	[-0.0373, -0.0146]	[-0.0295, -0.0068]	[-0.0279, -0.0053]	[-0.0214, 0.0021]	[-0.0298, -0.0069]
	7.04×10^{-7}	7.02×10^{-6}	0.0017	0.004	0.108	0.0017
Contrast (NGTDM)	0.0242	0.0216	0.0167	0.0157	0.0303	-0.0216
	[0.0104, 0.038]	[0.0079, 0.0353]	[0.0029, 0.0304]	[0.002, 0.0294]	[0.0161, 0.0446]	[-0.0354, -0.0077]
	0.0006	0.002	0.0174	0.0247	2.97×10^{-5}	0.0022
Busyness (NGTDM)	0.0573	0.0495	0.0386	0.0369	0.064	0.001
	[0.0433, 0.0713]	[0.0356, 0.0635]	[0.0246, 0.0526]	[0.023, 0.0508]	[0.0496, 0.0785]	[-0.0131, 0.0152]
	1.16×10^{-15}	3.69×10^{-12}	6.47×10^{-8}	2.09×10^{-7}	4.46×10^{-18}	0.884
Complexity (NGTDM)	-0.0468	-0.0458	-0.0229	-0.0297	-0.0431	0.0109
	[-0.0608, -0.0328]	[-0.0597, -0.0319]	[-0.0369, -0.009]	[-0.0436, -0.0159]	[-0.0576, -0.0287]	[-0.0031, 0.025]
	5.32×10^{-11}	1.1×10^{-10}	0.0013	2.7×10^{-5}	4.71×10^{-9}	0.1279
Strength (NGTDM)	-0.0373	-0.0387	-0.0148	-0.0239	-0.0267	0.0089
	[-0.0512, -0.0235]	[-0.0525, -0.0249]	[-0.0287, -0.0009]	[-0.0377, -0.0101]	[-0.041, -0.0123]	[-0.0051, 0.0228]
	1.38×10^{-7}	4.3×10^{-8}	0.0364	0.0007	0.0003	0.2136
Small Dependence Emphasis (GLDM)	-0.0554	-0.0509	-0.0344	-0.0325	-0.0432	-0.0025
	[-0.0678, -0.0431]	[-0.0632, -0.0386]	[-0.0468, -0.0221]	[-0.0448, -0.0203]	[-0.056, -0.0305]	[-0.0149, 0.01]
	1.42×10^{-18}	4.87×10^{-16}	4.36×10^{-8}	2.06×10^{-7}	3.19×10^{-11}	0.699
Large Dependence Emphasis (GLDM)	0.0241	0.0175	0.0194	0.0164	0.0216	0.0146
	[0.0117, 0.0366]	[0.0051, 0.0299]	[0.007, 0.0318]	[0.004, 0.0287]	[0.0087, 0.0344]	[0.0021, 0.0271]
	0.0001	0.0057	0.0022	0.0094	0.001	0.0222
Grey Level Non Uniformity (GLDM)	0.0335	0.0253	0.023	0.0252	0.0251	0.028
	[0.0229, 0.0441]	[0.0148, 0.0359]	[0.0124, 0.0336]	[0.0147, 0.0358]	[0.0142, 0.0361]	[0.0173, 0.0387]
	6.42×10^{-10}	2.7×10^{-6}	2.05×10^{-5}	2.83×10^{-6}	6.99×10^{-6}	2.69×10^{-7}
Dependence Non Uniformity (GLDM)	0.0215	0.0158	0.013	0.0195	0.0114	0.0197

Feature (sub-category)	Unprocessed red meat	Beef	Lamb	Pork	Processed meat	Oily fish
	[0.0088, 0.0342]	[0.0032, 0.0285]	[0.0003, 0.0257]	[0.0068, 0.0321]	[-0.0017, 0.0245]	[0.007, 0.0325]
	0.0009	0.0142	0.0445	0.0025	0.089	0.0024
Dependence Non Uniformity Normalized (GLDM)	-0.019	-0.013	-0.0165	-0.0126	-0.016	-0.0127
	[-0.0318, -0.0062]	[-0.0258, -0.0003]	[-0.0292, -0.0037]	[-0.0253, 0.0001]	[-0.0292, -0.0028]	[-0.0256, 0.0002]
	0.0036	0.0446	0.0114	0.0524	0.0176	0.0529
Grey Level Variance (GLDM)	-0.0397	-0.0383	-0.02	-0.025	-0.0258	-0.0028
	[-0.0535, -0.026]	[-0.052, -0.0246]	[-0.0337, -0.0063]	[-0.0387, -0.0114]	[-0.04, -0.0116]	[-0.0166, 0.0111]
	1.44×10^{-8}	4.06×10^{-8}	0.0043	0.0003	0.0004	0.6961
Dependence Variance (GLDM)	0.0166	0.0092	0.0153	0.0136	0.0138	0.0117
	[0.0035, 0.0297]	[-0.0039, 0.0222]	[0.0022, 0.0284]	[0.0006, 0.0266]	[0.0003, 0.0273]	[-0.0014, 0.0249]
	0.0128	0.1684	0.0216	0.0401	0.0458	0.0804
Dependence Entropy (GLDM)	2.99×10^{-6}	-0.004	0.0023	0.003	-0.006	0.0077
	[-0.0136, 0.0136]	[-0.0175, 0.0095]	[-0.0113, 0.0158]	[-0.0105, 0.0165]	[-0.0201, 0.008]	[-0.006, 0.0213]
	0.9997	0.5607	0.7444	0.6672	0.3994	0.2693
Low Grey Level Emphasis (GLDM)	0.0558	0.0509	0.0377	0.032	0.0621	-0.0001
	[0.0419, 0.0697]	[0.037, 0.0647]	[0.0238, 0.0515]	[0.0182, 0.0458]	[0.0477, 0.0764]	[-0.0141, 0.0139]
	3.77×10^{-15}	6.06×10^{-13}	1.06×10^{-7}	5.72×10^{-6}	2.49×10^{-17}	0.9882
High Grey Level Emphasis (GLDM)	-0.0766	-0.0696	-0.0512	-0.0443	-0.0656	0.0163
	[-0.0907, -0.0625]	[-0.0836, -0.0555]	[-0.0653, -0.0371]	[-0.0583, -0.0303]	[-0.0801, -0.051]	[0.0021, 0.0304]
	1.82×10^{-26}	2.73×10^{-22}	1.04×10^{-12}	6.11×10^{-10}	1.13×10^{-18}	0.0247
Small Dependence Low Grey Level Emphasis (GLDM)	0.0332	0.0288	0.0244	0.0203	0.0349	-0.0187
	[0.0199, 0.0465]	[0.0155, 0.0421]	[0.0111, 0.0377]	[0.007, 0.0335]	[0.0212, 0.0487]	[-0.0321, -0.0053]
	1.07×10^{-6}	2.18×10^{-5}	0.0003	0.0027	6.65×10^{-7}	0.0064
Small Dependence High Grey Level Emphasis (GLDM)	-0.0725	-0.0669	-0.0446	-0.0437	-0.0586	0.0091
	[-0.0863, -0.0588]	[-0.0806, -0.0532]	[-0.0584, -0.0309]	[-0.0574, -0.03]	[-0.0728, -0.0444]	[-0.0047, 0.023]
	5.18×10^{-25}	1.18×10^{-21}	1.96×10^{-10}	3.98×10^{-10}	6.79×10^{-16}	0.1958
	0.0523	0.0452	0.0379	0.031	0.0591	0.009

Feature (sub-category)	Unprocessed red meat	Beef	Lamb	Pork	Processed meat	Oily fish
Large Dependence Low Grey Level Emphasis (GLDM)	[0.0382, 0.0664]	[0.0312, 0.0592]	[0.0239, 0.052]	[0.017, 0.045]	[0.0446, 0.0737]	[-0.0052, 0.0232]
	3.54×10^{-13}	2.84×10^{-10}	1.24×10^{-7}	1.44×10^{-5}	1.73×10^{-15}	0.2127
Large Dependence High Grey Level Emphasis (GLDM)	-0.0439	-0.0421	-0.03	-0.0223	-0.0379	0.0253
	[-0.0569, -0.031]	[-0.055, -0.0292]	[-0.0429, -0.0171]	[-0.0351, -0.0094]	[-0.0512, -0.0245]	[0.0123, 0.0383]
	2.78×10^{-11}	1.46×10^{-10}	5.25×10^{-6}	0.0007	2.76×10^{-8}	0.0001

Table 6.16. *Each cell represents a separate model, adjusted for: age, sex, social deprivation, educational level, smoking, alcohol intake, exercise level. Results are degree of change in radiomics shape feature per 100g increase in daily meat/fish consumption with corresponding 95% confidence intervals and p-values. First, second, and third row for every CMR measures corresponds to beta coefficient, 95% confidence interval and p-value, respectively. Bonferroni adjusted significance threshold p-value =0.0001 (corrected for 432 comparisons). GLCM: grey level co-occurrence matrix; GLDM: grey level dependence matrix; GLRLM: grey level run length matrix; GLSZM: grey level size zone matrix; NGTDM: neighboring grey tone difference matrix; CMR: Cardiovascular magnetic resonance.*

Table 6.17. Multivariable linear regression models showing change in left ventricular myocardium texture radiomics in end-systole per 100g increase in daily meat/fish consumption

	Unprocessed red meat	Beef	Lamb	Pork	Processed meat	Oily fish
Autocorrelation (GLCM)	-0.0763	-0.0729	-0.045	-0.0442	-0.0703	0.0103
	[-0.0901, -0.0624]	[-0.0867, -0.0591]	[-0.0588, -0.0311]	[-0.058, -0.0305]	[-0.0846, -0.0559]	[-0.0037, 0.0242]
	4.23×10^{-27}	4.67×10^{-25}	1.95×10^{-10}	3.22×10^{-10}	7.23×10^{-22}	0.1487
Joint Average (GLCM)	-0.0755	-0.0721	-0.0445	-0.0438	-0.0709	0.0074
	[-0.0894, -0.0617]	[-0.0859, -0.0583]	[-0.0584, -0.0307]	[-0.0576, -0.03]	[-0.0852, -0.0566]	[-0.0065, 0.0214]
	1.41×10^{-26}	1.37×10^{-24}	2.99×10^{-10}	4.81×10^{-10}	2.93×10^{-22}	0.2973
Cluster Prominence (GLCM)	-0.0112	-0.0123	-0.0013	-0.009	0.0012	-0.001
	[-0.0257, 0.0032]	[-0.0267, 0.0021]	[-0.0157, 0.0131]	[-0.0233, 0.0054]	[-0.0137, 0.0161]	[-0.0155, 0.0135]
	0.1272	0.0934	0.8603	0.2198	0.876	0.8934
Cluster Shade (GLCM)	-0.0066	-0.0089	0.0008	-0.0044	0.0055	0.0013
	[-0.021, 0.0078]	[-0.0233, 0.0054]	[-0.0135, 0.0152]	[-0.0187, 0.0099]	[-0.0094, 0.0203]	[-0.0132, 0.0158]
	0.3696	0.223	0.9084	0.5456	0.4725	0.8612
Cluster Tendency (GLCM)	-0.0274	-0.026	-0.0142	-0.0176	-0.0175	0.0117
	[-0.0416, -0.0132]	[-0.0402, -0.0119]	[-0.0283, 0]	[-0.0317, -0.0035]	[-0.0322, -0.0029]	[-0.0026, 0.026]
	0.0002	0.0003	0.0503	0.0147	0.0192	0.109
Contrast (GLCM)	-0.031	-0.0285	-0.0156	-0.021	-0.0213	-0.0032
	[-0.045, -0.017]	[-0.0424, -0.0145]	[-0.0296, -0.0017]	[-0.0349, -0.0071]	[-0.0358, -0.0069]	[-0.0172, 0.0109]
	1.38×10^{-5}	6.16×10^{-5}	0.028	0.003	0.0038	0.6572
Correlation (GLCM)	-0.0052	-0.0024	-0.0079	-0.0035	-0.0043	0.0232
	[-0.0185, 0.0081]	[-0.0156, 0.0109]	[-0.0212, 0.0054]	[-0.0167, 0.0097]	[-0.0181, 0.0094]	[0.0099, 0.0366]
	0.444	0.7267	0.2427	0.6022	0.5356	0.0007
Difference Average (GLCM)	-0.0213	-0.0199	-0.0098	-0.0143	-0.0164	-0.0036
	[-0.0351, -0.0075]	[-0.0336, -0.0062]	[-0.0235, 0.004]	[-0.028, -0.0006]	[-0.0306, -0.0021]	[-0.0174, 0.0103]
	0.0025	0.0045	0.164	0.041	0.0244	0.6155
Difference Entropy (GLCM)	-0.0297	-0.0279	-0.0143	-0.0195	-0.0247	-0.0033
	[-0.0434, -0.016]	[-0.0415, -0.0142]	[-0.028, -0.0006]	[-0.0331, -0.0059]	[-0.0388, -0.0105]	[-0.017, 0.0105]
	2.23×10^{-5}	6.3×10^{-5}	0.0406	0.0051	0.0006	0.6437
Difference Variance (GLCM)	-0.0376	-0.0346	-0.0192	-0.0254	-0.0255	-0.002
	[-0.0516, -0.0235]	[-0.0486, -0.0207]	[-0.0333, -0.0052]	[-0.0393, -0.0114]	[-0.04, -0.011]	[-0.0161, 0.0121]
	1.6×10^{-7}	1.22×10^{-6}	0.0072	0.0004	0.0006	0.7819

	Unprocessed red meat	Beef	Lamb	Pork	Processed meat	Oily fish
Joint Energy (GLCM)	0.0136	0.0098	0.0073	0.0129	0.0126	-0.0011
	[-0.0006, 0.0278]	[-0.0044, 0.0239]	[-0.0068, 0.0215]	[-0.0012, 0.0269]	[-0.0021, 0.0272]	[-0.0154, 0.0131]
	0.0598	0.1752	0.3097	0.0732	0.0923	0.8748
Joint Entropy (GLCM)	-0.0247	-0.0218	-0.0131	-0.0176	-0.0217	0.0032
	[-0.0388, -0.0107]	[-0.0358, -0.0078]	[-0.0271, 0.001]	[-0.0316, -0.0036]	[-0.0363, -0.0072]	[-0.0109, 0.0174]
	0.0006	0.0023	0.0681	0.0136	0.0035	0.656
Informal Measure Of Correlation 1 (GLCM)	0.0142	0.0117	0.011	0.0098	0.0108	-0.0216
	[0.0011, 0.0273]	[-0.0014, 0.0248]	[-0.0021, 0.0241]	[-0.0032, 0.0229]	[-0.0027, 0.0244]	[-0.0348, -0.0085]
	0.0338	0.0794	0.1005	0.1385	0.1172	0.0013
Informal Measure Of Correlation 2 (GLCM)	-0.0196	-0.0149	-0.016	-0.0138	-0.0151	0.0195
	[-0.033, -0.0061]	[-0.0283, -0.0016]	[-0.0294, -0.0026]	[-0.0272, -0.0005]	[-0.0289, -0.0012]	[0.006, 0.033]
	0.0043	0.0285	0.0191	0.0421	0.0333	0.0047
Inverse Difference Moment (GLCM)	0.0164	0.0154	0.0069	0.011	0.0133	0.0037
	[0.0026, 0.0301]	[0.0017, 0.0292]	[-0.0069, 0.0206]	[-0.0027, 0.0247]	[-0.0009, 0.0275]	[-0.0101, 0.0176]
	0.0198	0.0272	0.3254	0.1141	0.0669	0.5976
Inverse Difference Moment Normalized (GLCM)	-0.0414	-0.0371	-0.0266	-0.0268	-0.0497	0.0174
	[-0.0553, -0.0275]	[-0.051, -0.0233]	[-0.0404, -0.0127]	[-0.0406, -0.013]	[-0.0641, -0.0354]	[0.0034, 0.0314]
	5.17×10^{-9}	1.44×10^{-7}	0.0002	0.0001	1.11×10^{-11}	0.0146
Inverse Difference (GLCM)	0.0144	0.0135	0.0058	0.0098	0.0119	0.0038
	[0.0006, 0.0282]	[-0.0002, 0.0273]	[-0.008, 0.0195]	[-0.0039, 0.0235]	[-0.0024, 0.0261]	[-0.01, 0.0177]
	0.0408	0.053	0.4092	0.159	0.1017	0.5876
Inverse Difference Normalized (GLCM)	-0.0313	-0.0285	-0.0208	-0.0194	-0.0358	0.0151
	[-0.0451, -0.0176]	[-0.0423, -0.0148]	[-0.0345, -0.007]	[-0.0332, -0.0057]	[-0.0501, -0.0216]	[0.0012, 0.0289]
	8.48×10^{-6}	4.68×10^{-5}	0.0031	0.0054	8.25×10^{-7}	0.033
Inverse Variance (GLCM)	-0.0013	-0.0011	0.0014	-0.0018	-0.0026	-0.0042
	[-0.0152, 0.0126]	[-0.0149, 0.0127]	[-0.0124, 0.0152]	[-0.0156, 0.012]	[-0.017, 0.0117]	[-0.0182, 0.0097]
	0.8549	0.8724	0.8435	0.7951	0.7193	0.5522
Maximum Probability (GLCM)	0.0125	0.0069	0.008	0.0137	0.0089	0.0003
	[-0.0017, 0.0267]	[-0.0072, 0.0211]	[-0.0061, 0.0222]	[-0.0004, 0.0278]	[-0.0058, 0.0236]	[-0.0139, 0.0146]
	0.0842	0.3386	0.2663	0.0567	0.2341	0.9634
Sum Average (GLCM)	-0.0755	-0.0721	-0.0445	-0.0438	-0.0709	0.0074
	[-0.0894, -0.0617]	[-0.0859, -0.0583]	[-0.0584, -0.0307]	[-0.0576, -0.03]	[-0.0852, -0.0566]	[-0.0065, 0.0214]
	1.41×10^{-26}	1.37×10^{-24}	2.99×10^{-10}	4.81×10^{-10}	2.93×10^{-22}	0.2973

	Unprocessed red meat	Beef	Lamb	Pork	Processed meat	Oily fish
Sum Entropy (GLCM)	-0.0237	-0.0202	-0.0134	-0.0174	-0.0211	0.008
	[-0.0378, -0.0096]	[-0.0343, -0.0062]	[-0.0275, 0.0007]	[-0.0314, -0.0033]	[-0.0357, -0.0065]	[-0.0062, 0.0223]
	0.001	0.0048	0.062	0.0153	0.0046	0.2666
Sum Of Squares (GLCM)	-0.0298	-0.028	-0.0153	-0.0194	-0.0194	0.0087
	[-0.044, -0.0155]	[-0.0422, -0.0139]	[-0.0295, -0.0011]	[-0.0335, -0.0052]	[-0.0341, -0.0047]	[-0.0056, 0.023]
	4.15×10^{-5}	0.0001	0.0349	0.0073	0.0097	0.2333
Small Area Emphasis (GLSZM)	-0.0212	-0.022	-0.0151	-0.0075	-0.0016	0.0076
	[-0.0354, -0.0069]	[-0.0362, -0.0078]	[-0.0293, -0.0008]	[-0.0216, 0.0067]	[-0.0164, 0.0131]	[-0.0068, 0.0219]
	0.0037	0.0024	0.038	0.3022	0.8284	0.2999
Large Area Emphasis (GLSZM)	0.0412	0.0331	0.0265	0.0295	0.0387	0.0201
	[0.0289, 0.0534]	[0.0209, 0.0453]	[0.0143, 0.0388]	[0.0173, 0.0416]	[0.026, 0.0514]	[0.0078, 0.0324]
	4.5×10^{-11}	1.06×10^{-7}	2.15×10^{-5}	2.12×10^{-6}	2.09×10^{-9}	0.0014
Grey Level Non Uniformity (GLSZM)	0.0356	0.0263	0.0255	0.0291	0.019	-0.0009
	[0.0217, 0.0495]	[0.0124, 0.0401]	[0.0117, 0.0394]	[0.0152, 0.0429]	[0.0047, 0.0334]	[-0.0149, 0.013]
	5.38×10^{-7}	0.0002	0.0003	3.74×10^{-5}	0.0094	0.8948
Size Zone Non Uniformity (GLSZM)	0.0356	0.0263	0.0255	0.0291	0.019	-0.0009
	[0.0217, 0.0495]	[0.0124, 0.0401]	[0.0117, 0.0394]	[0.0152, 0.0429]	[0.0047, 0.0334]	[-0.0149, 0.013]
	5.38×10^{-7}	0.0002	0.0003	3.74×10^{-5}	0.0094	0.8948
Size Zone Non Uniformity Normalized (GLSZM)	-0.0199	-0.0209	-0.0146	-0.0066	0.0001	0.008
	[-0.0342, -0.0057]	[-0.0351, -0.0067]	[-0.0289, -0.0004]	[-0.0208, 0.0076]	[-0.0147, 0.0148]	[-0.0064, 0.0223]
	0.0062	0.004	0.0443	0.3611	0.9933	0.2776
Zone Percentage (GLSZM)	-0.0443	-0.0364	-0.0311	-0.0285	-0.0398	-0.01
	[-0.0579, -0.0306]	[-0.05, -0.0228]	[-0.0448, -0.0175]	[-0.0421, -0.0149]	[-0.0539, -0.0257]	[-0.0237, 0.0038]
	2.26×10-10	1.6×10^{-7}	7.76×10^{-6}	4.02×10^{-5}	3.36×10^{-8}	0.1557
Grey Level Variance (GLSZM)	-0.0671	-0.0599	-0.0408	-0.0439	-0.0529	0.0094
	[-0.0812, -0.053]	[-0.074, -0.0459]	[-0.0549, -0.0267]	[-0.058, -0.0299]	[-0.0674, -0.0383]	[-0.0048, 0.0236]
	1.06×10^{-20}	5.84×10^{-17}	1.35×10^{-8}	7.85×10^{-10}	1.1×10^{-12}	0.1926
Zone Variance (GLSZM)	0.0414	0.0332	0.0266	0.0297	0.0383	0.0203
	[0.0292, 0.0536]	[0.0211, 0.0454]	[0.0145, 0.0388]	[0.0176, 0.0418]	[0.0257, 0.0509]	[0.0081, 0.0326]
	3.09×10^{-11}	8.66×10^{-8}	1.83×10^{-5}	1.61×10^{-6}	2.68×10^{-9}	0.0012
Zone Entropy (GLSZM)	-0.0421	-0.0375	-0.0232	-0.0294	-0.0517	0.0092
	[-0.0562, -0.028]	[-0.0516, -0.0234]	[-0.0373, -0.0091]	[-0.0434, -0.0153]	[-0.0663, -0.0372]	[-0.0051, 0.0234]
	5.22×10^{-9}	1.78×10^{-7}	0.0013	4.17×10^{-5}	3.72×10^{-12}	0.2067

	Unprocessed red meat	Beef	Lamb	Pork	Processed meat	Oily fish
Low Grey Level Zone Emphasis (GLSZM)	0.059	0.0558	0.0361	0.0341	0.0615	-0.0129
	[0.0448, 0.0731]	[0.0418, 0.0699]	[0.022, 0.0502]	[0.02, 0.0481]	[0.0469, 0.0761]	[-0.0272, 0.0013]
	2.85×10^{-16}	7.46×10^{-15}	5.3×10^{-7}	1.98×10^{-6}	1.48×10^{-16}	0.0741
High Grey Level Zone Emphasis (GLSZM)	-0.0713	-0.0673	-0.0412	-0.0436	-0.0633	0.0168
	[-0.0854, -0.0573]	[-0.0813, -0.0533]	[-0.0553, -0.0272]	[-0.0576, -0.0296]	[-0.0778, -0.0488]	[0.0026, 0.0309]
	3.13×10^{-23}	5.2×10^{-21}	9.05×10^{-9}	1.05×10^{-9}	1.48×10^{-17}	0.0204
Small Area Low Grey Level Emphasis (GLSZM)	0.0516	0.0477	0.0304	0.0327	0.0573	-0.0135
	[0.0374, 0.0658]	[0.0335, 0.0618]	[0.0162, 0.0445]	[0.0187, 0.0469]	[0.0426, 0.0719]	[-0.0278, 0.0007]
	1.03×10^{-12}	3.93×10^{-11}	2.66×10^{-5}	5.36×10^{-6}	1.91×10-14	0.0629
Small Area High Grey Level Emphasis (GLSZM)	-0.0702	-0.0653	-0.0414	-0.0434	-0.0598	0.0164
	[-0.0842, -0.0561]	[-0.0793, -0.0513]	[-0.0554, -0.0273]	[-0.0574, -0.0294]	[-0.0743, -0.0453]	[0.0022, 0.0305]
	1.51×10^{-22}	7.09×10^{-20}	7.9×10^{-9}	1.2×10^{-9}	7.61×10^{-16}	0.0234
Large Area Low Grey Level Emphasis (GLSZM)	0.0462	0.0399	0.0264	0.0331	0.0522	0.0217
	[0.0322, 0.0601]	[0.026, 0.0538]	[0.0125, 0.0403]	[0.0192, 0.047]	[0.0378, 0.0666]	[0.0077, 0.0358]
	8.64×10^{-11}	1.83×10^{-8}	0.0002	2.85×10^{-6}	1.23×10^{-12}	0.0024
Large Area High Grey Level Emphasis (GLSZM)	-0.0118	-0.0158	-0.0048	-0.0035	-0.0143	0.0171
	[-0.0243, 0.0006]	[-0.0282, -0.0034]	[-0.0173, 0.0077]	[-0.0159, 0.0089]	[-0.0272, -0.0015]	[0.0046, 0.0296]
	0.0626	0.0126	0.4495	0.5841	0.0291	0.0076
Short Run Emphasis (GLRLM)	-0.0139	-0.0117	-0.0086	-0.0084	-0.0136	-0.0036
	[-0.0274, -0.0005]	[-0.0251, 0.0017]	[-0.022, 0.0048]	[-0.0218, 0.005]	[-0.0275, 0.0004]	[-0.0171, 0.0099]
	0.0428	0.0875	0.2097	0.2178	0.056	0.603
Long Run Emphasis (GLRLM)	0.0177	0.0134	0.0113	0.0133	0.0142	0.0086
	[0.0045, 0.0309]	[0.0002, 0.0265]	[-0.0019, 0.0245]	[0.0002, 0.0264]	[0.0006, 0.0279]	[-0.0047, 0.0219]
	0.0086	0.0462	0.0931	0.047	0.0408	0.2041
Grey Level Non Uniformity (GLRLM)	0.0485	0.0373	0.0317	0.0382	0.0346	0.0265
	[0.0374, 0.0596]	[0.0262, 0.0484]	[0.0205, 0.0428]	[0.0271, 0.0492]	[0.0231, 0.0461]	[0.0153, 0.0377]
	1.38×10^{-17}	4.23×10^{-11}	2.39×10^{-8}	1.39×10^{-11}	3.7×10^{-9}	3.67×10^{-6}
Run Length Non Uniformity (GLRLM)	0.017	0.0096	0.0153	0.0159	0.0093	0.0229
	[0.0036, 0.0304]	[-0.0038, 0.0229]	[0.0019, 0.0286]	[0.0026, 0.0292]	[-0.0045, 0.0231]	[0.0095, 0.0364]
	0.0128	0.1594	0.0249	0.0191	0.1874	0.0008
Run Length Non Uniformity Normalized (GLRLM)	-0.0151	-0.0129	-0.0092	-0.0089	-0.0134	-0.0029
	[-0.0286, -0.0015]	[-0.0264, 0.0006]	[-0.0227, 0.0043]	[-0.0223, 0.0046]	[-0.0274, 0.0005]	[-0.0165, 0.0107]
	0.0291	0.0602	0.1802	0.1953	0.0594	0.6732

	Unprocessed red meat	Beef	Lamb	Pork	Processed meat	Oily fish
Run Percentage (GLRLM)	-0.0172	-0.0141	-0.0108	-0.0112	-0.0148	-0.0044
	[-0.0306, -0.0038]	[-0.0275, -0.0008]	[-0.0241, 0.0026]	[-0.0244, 0.0021]	[-0.0286, -0.001]	[-0.0178, 0.0091]
	0.0116	0.0371	0.1133	0.0996	0.036	0.5238
Grey Level Variance (GLRLM)	-0.0416	-0.0388	-0.021	-0.0281	-0.0309	0.0089
	[-0.0558, -0.0274]	[-0.053, -0.0247]	[-0.0352, -0.0069]	[-0.0422, -0.014]	[-0.0456, -0.0163]	[-0.0054, 0.0231]
	9.29×10^{-9}	7.09×10^{-8}	0.0036	9.53×10^{-5}	3.49×10^{-5}	0.2232
Run Variance (GLRLM)	0.0195	0.0149	0.0127	0.0142	0.0133	0.009
	[0.0064, 0.0326]	[0.0019, 0.028]	[-0.0004, 0.0258]	[0.0012, 0.0272]	[-0.0003, 0.0268]	[-0.0042, 0.0222]
	0.0036	0.025	0.0565	0.0323	0.0546	0.1793
Run Entropy (GLRLM)	-0.0195	-0.0187	-0.0085	-0.0152	-0.0191	0.0154
	[-0.0326, -0.0065]	[-0.0317, -0.0057]	[-0.0215, 0.0045]	[-0.0281, -0.0022]	[-0.0325, -0.0056]	[0.0023, 0.0285]
	0.0034	0.0048	0.2012	0.0217	0.0055	0.0211
Low Grey Level Run Emphasis (GLRLM)	0.0567	0.0553	0.0339	0.0311	0.0601	0.0042
	[0.0427, 0.0707]	[0.0414, 0.0693]	[0.02, 0.0479]	[0.0172, 0.0451]	[0.0457, 0.0746]	[-0.0099, 0.0183]
	1.98×10^{-15}	7.16×10^{-15}	1.92×10^{-6}	1.16×10^{-5}	3.66×10^{-16}	0.5603
High Grey Level Run Emphasis (GLRLM)	-0.0756	-0.0729	-0.0444	-0.043	-0.0692	0.0113
	[-0.0895, -0.0618]	[-0.0868, -0.0591]	[-0.0583, -0.0305]	[-0.0569, -0.0292]	[-0.0836, -0.0549]	[-0.0027, 0.0253]
	1.48×10^{-26}	5.35×10^{-25}	3.67×10^{-10}	1.05×10^{-9}	3.51×10^{-21}	0.1134
Short Run Low Grey Level Emphasis (GLRLM)	0.0543	0.0536	0.033	0.0285	0.0583	0.0019
	[0.0404, 0.0682]	[0.0397, 0.0675]	[0.0191, 0.047]	[0.0147, 0.0424]	[0.0439, 0.0727]	[-0.0121, 0.0159]
	2.34×10^{-14}	3.86×10^{-14}	3.32×10^{-6}	5.51×10^{-5}	2.11×10^{-15}	0.7914
Short Run High Grey Level Emphasis (GLRLM)	-0.0733	-0.0703	-0.0433	-0.0418	-0.0666	0.0104
	[-0.0873, -0.0594]	[-0.0842, -0.0564]	[-0.0573, -0.0293]	[-0.0558, -0.0279]	[-0.0811, -0.0522]	[-0.0037, 0.0245]
	9.99×10^{-25}	5.18×10^{-23}	1.28×10^{-9}	3.9×10^{-9}	1.73×10^{-19}	0.1492
Long Run Low Grey Level Emphasis (GLRLM)	0.0523	0.0474	0.0307	0.034	0.053	0.0099
	[0.0383, 0.0664]	[0.0335, 0.0614]	[0.0167, 0.0447]	[0.0201, 0.048]	[0.0385, 0.0675]	[-0.0042, 0.024]
	2.78×10^{-13}	2.97×10^{-11}	1.74×10^{-5}	1.77×10^{-6}	8.25×10^{-13}	0.1695
Long Run High Grey Level Emphasis (GLRLM)	-0.0526	-0.0521	-0.0298	-0.0295	-0.0503	0.0129
	[-0.066, -0.0391]	[-0.0655, -0.0388]	[-0.0432, -0.0164]	[-0.0429, -0.0162]	[-0.0642, -0.0364]	[-0.0006, 0.0264]
	1.7×10^{-14}	2.11×10^{-14}	1.35×10^{-5}	1.44×10^{-5}	1.18×10^{-12}	0.0613
Coarseness (NGTDM)	-0.031	-0.0261	-0.0241	-0.0172	-0.0168	-0.0175
	[-0.0432, -0.0188]	[-0.0383, -0.014]	[-0.0362, -0.0119]	[-0.0293, -0.0051]	[-0.0294, -0.0042]	[-0.0298, -0.0053]
	6.34×10^{-7}	2.48×10^{-5}	0.0001	0.0054	0.0089	0.0051

	Unprocessed red meat	Beef	Lamb	Pork	Processed meat	Oily fish
Contrast (NGTDM)	0.0256	0.0231	0.0181	0.0153	0.0372	-0.0124
	[0.0115, 0.0398]	[0.009, 0.0372]	[0.004, 0.0322]	[0.0013, 0.0294]	[0.0226, 0.0518]	[-0.0266, 0.0018]
	0.0004	0.0013	0.0119	0.0324	5.9×10^{-7}	0.0868
Busyness (NGTDM)	0.0629	0.0537	0.0422	0.0414	0.069	0.0064
	[0.0489, 0.0768]	[0.0399, 0.0676]	[0.0283, 0.0561]	[0.0275, 0.0552]	[0.0547, 0.0834]	[-0.0076, 0.0204]
	9.47×10^{-19}	3.25×10^{-14}	2.73×10^{-9}	4.88×10^{-9}	5.45×10^{-21}	0.3726
Complexity (NGTDM)	-0.054	-0.0472	-0.0317	-0.0381	-0.0465	0.0093
	[-0.0683, -0.0398]	[-0.0613, -0.033]	[-0.0459, -0.0175]	[-0.0522, -0.0239]	[-0.0612, -0.0318]	[-0.005, 0.0236]
	9.63×10^{-14}	6.84×10^{-11}	1.23×10^{-5}	1.31×10^{-7}	5.72×10^{-10}	0.2029
Strength (NGTDM)	-0.0549	-0.0482	-0.0311	-0.0394	-0.045	0.0074
	[-0.0691, -0.0407]	[-0.0623, -0.0341]	[-0.0453, -0.017]	[-0.0535, -0.0253]	[-0.0596, -0.0303]	[-0.0069, 0.0217]
	3.26×10^{-14}	2.28×10^{-11}	1.63×10^{-5}	4.39×10^{-8}	1.81×10^{-9}	0.3089
Small Dependence Emphasis (GLDM)	-0.0422	-0.0342	-0.0296	-0.0276	-0.0353	-0.0082
	[-0.0557, -0.0287]	[-0.0477, -0.0208]	[-0.043, -0.0161]	[-0.041, -0.0142]	[-0.0492, -0.0214]	[-0.0218, 0.0053]
	9.06×10^{-10}	5.92×10^{-7}	1.68×10^{-5}	5.46×10^{-5}	7×10^{-7}	0.2349
Large Dependence Emphasis (GLDM)	0.0152	0.0127	0.0093	0.0097	0.013	0.0043
	[0.0019, 0.0286]	[-0.0006, 0.0261]	[-0.004, 0.0227]	[-0.0036, 0.0229]	[-0.0008, 0.0268]	[-0.0092, 0.0177]
	0.0255	0.0606	0.1711	0.1545	0.0645	0.532
Grey Level Non Uniformity (GLDM)	0.0423	0.0324	0.0269	0.0337	0.0284	0.0214
	[0.0308, 0.0538]	[0.0209, 0.0439]	[0.0155, 0.0384]	[0.0222, 0.0451]	[0.0165, 0.0403]	[0.0098, 0.033]
	6.03×10^{-13}	3.11×10^{-8}	4.34×10^{-6}	8.11×10^{-9}	2.85×10^{-6}	0.0003
Dependence Non Uniformity (GLDM)	0.0313	0.0213	0.0248	0.0251	0.0221	0.0267
	[0.02, 0.0427]	[0.01, 0.0326]	[0.0135, 0.0361]	[0.0138, 0.0363]	[0.0104, 0.0338]	[0.0153, 0.0381]
	5.65×10^{-8}	0.0002	1.63×10^{-5}	1.24×10^{-5}	0.0002	4.32×10^{-6}
Dependence Non Uniformity Normalized (GLDM)	-0.0098	-0.0082	-0.0053	-0.0067	-0.0036	-0.0048
	[-0.0237, 0.004]	[-0.022, 0.0056]	[-0.0191, 0.0085]	[-0.0205, 0.007]	[-0.0179, 0.0108]	[-0.0187, 0.0091]
	0.165	0.2424	0.4514	0.3387	0.6262	0.4968
Grey Level Variance (GLDM)	-0.0346	-0.0321	-0.0178	-0.0233	-0.0244	0.0079
	[-0.0488, -0.0204]	[-0.0463, -0.018]	[-0.032, -0.0037]	[-0.0374, -0.0092]	[-0.0391, -0.0097]	[-0.0064, 0.0222]
	1.75×10^{-6}	8.45×10^{-6}	0.0137	0.0012	0.0011	0.2776
Dependence Variance (GLDM)	0.0074	0.0064	0.0047	0.0041	0.0025	0.0039
	[-0.0064, 0.0212]	[-0.0074, 0.0201]	[-0.0091, 0.0184]	[-0.0096, 0.0178]	[-0.0118, 0.0167]	[-0.01, 0.0177]
	0.2908	0.3647	0.5062	0.5573	0.7314	0.5831

	Unprocessed red meat	Beef	Lamb	Pork	Processed meat	Oily fish
Dependence Entropy (GLDM)	-0.0143	-0.0102	-0.008	-0.0142	-0.0151	0.0115
	[-0.0281, -0.0005]	[-0.024, 0.0036]	[-0.0218, 0.0057]	[-0.028, -0.0005]	[-0.0293, -0.0008]	[-0.0024, 0.0254]
	0.0427	0.1459	0.2526	0.0419	0.0385	0.1037
Low Grey Level Emphasis (GLDM)	0.0565	0.0546	0.0335	0.0323	0.0591	0.0059
	[0.0426, 0.0705]	[0.0407, 0.0685]	[0.0195, 0.0474]	[0.0184, 0.0462]	[0.0447, 0.0735]	[-0.0082, 0.0199]
	2.27×10^{-15}	1.49×10^{-14}	2.61×10^{-6}	5.31×10^{-6}	1.02×10^{-15}	0.4136
High Grey Level Emphasis (GLDM)	-0.0763	-0.0731	-0.045	-0.0439	-0.0701	0.0104
	[-0.0901, -0.0624]	[-0.0869, -0.0593]	[-0.0588, -0.0311]	[-0.0577, -0.0301]	[-0.0844, -0.0558]	[-0.0035, 0.0244]
	4.86×10^{-27}	3.84×10^{-25}	2.08×10^{-10}	4.54×10^{-10}	9.82×10^{-22}	0.1429
Small Dependence Low Grey Level Emphasis (GLDM)	0.0412	0.0417	0.0234	0.0223	0.0432	-0.013
	[0.0274, 0.0549]	[0.0281, 0.0554]	[0.0097, 0.0371]	[0.0087, 0.036]	[0.029, 0.0574]	[-0.0268, 0.0008]
	4.27×10^{-9}	2.2×10^{-9}	0.0008	0.0014	2.44×10^{-9}	0.0652
Small Dependence High Grey Level Emphasis (GLDM)	-0.0673	-0.0604	-0.041	-0.043	-0.0572	0.0058
	[-0.0814, -0.0532]	[-0.0745, -0.0464]	[-0.0551, -0.027]	[-0.057, -0.029]	[-0.0717, -0.0427]	[-0.0084, 0.02]
	7.74×10^{-21}	3.08×10^{-17}	1.1×10^{-8}	1.69×10^{-9}	1.31×10^{-14}	0.4222
Large Dependence Low Grey Level Emphasis (GLDM)	0.0555	0.0514	0.0319	0.0355	0.0547	0.008
	[0.0415, 0.0695]	[0.0374, 0.0653]	[0.0179, 0.0459]	[0.0216, 0.0494]	[0.0402, 0.0691]	[-0.0061, 0.0221]
	8.06×10^{-15}	5.36×10^{-13}	7.73×10-6	5.93×10^{-7}	1.31×10^{-13}	0.2651
Large Dependence High Grey Level Emphasis (GLDM)	-0.0587	-0.0569	-0.034	-0.0343	-0.0545	0.0102
	[-0.0724, -0.0451]	[-0.0705, -0.0434]	[-0.0476, -0.0204]	[-0.0478, -0.0207]	[-0.0686, -0.0405]	[-0.0035, 0.0239]
	2.92×10^{-17}	1.99×10^{-16}	9.87×10^{-7}	7.1×10^{-7}	3.14×10^{-14}	0.1433

Table 6.17. *Each cell represents a separate model, adjusted for: age, sex, social deprivation, educational level, smoking, alcohol intake, exercise level. Results are degree of change in radiomics shape feature per 100g increase in daily meat/fish consumption with corresponding 95% confidence intervals and p-values. First, second, and third row for every CMR measures corresponds to beta coefficient, 95% confidence interval and p-value, respectively. Bonferroni adjusted significance threshold p-value =0.0001 (corrected for 432 comparisons). Cardiovascular magnetic resonance: CMR; GLCM: grey level co-occurrence matrix; GLDM: grey level dependence matrix; GLRLM: grey level run length matrix; GLSZM: grey level size zone matrix; NGTDM: neighboring grey tone difference matrix; LV: left ventricle.*

6.5 Summary of findings

In this study of 19,408 UK Biobank participants, higher intake or red and processed meat consumption was associated with poorer cardiovascular health, regarding both measures of arterial health and ventricular structure and function. In contrast, greater consumption of oily fish was associated with a healthier cardiovascular phenotype.

Specifically, higher red and processed meat consumption was associated with smaller ventricular cavity volumes with poorer myocardial function (lower stroke volume) and lower arterial compliance (higher ASI, greater interval change in ASI, lower aortic distensibility). Conversely, higher consumption of oily fish was associated with larger ventricular volumes with better function (higher stroke volumes) and better arterial health (lower ASI, smaller interval increase in ASI, higher aortic compliance). There was evidence that adverse cardiometabolic alterations may be a mediator of the associations between unprocessed red meat and adverse ventricular phenotypes. However, these factors did not appear important for any other associations.

The radiomics analysis demonstrated distinct ventricular geometry and LV myocardial signal intensity patterns associated with the different dietary exposures. Higher red and processed meat consumption were associated with smaller and more elongated ventricles, whereas greater oily fish consumption was associated with larger and more spherical ventricles. Greater red and processed meat intake were also associated with lower average signal intensity levels in the LV myocardium, less variation in signal intensity levels, and all together a darker more homogeneous signal intensity pattern. Higher oily fish consumption was associated with a brighter LV myocardium, with higher average signal intensity levels, more variation and randomness in signal intensity levels, and greater heterogeneity in pattern of signal intensity levels. It thus appears that the fish and meat exposures are not only associated with differences in gross ventricular anatomy, but also differences at the myocardial level, which is detectable by radiomics analysis.

6.6 Discussion

6.6.1 Comparison with existing literature

Our findings of the association of greater red and processed meat consumption with adverse cardiovascular phenotypes is consistent with epidemiologic studies linking these dietary habits to poorer clinical cardiovascular outcomes. The specific association of red and processed meat intake with CMR phenotypes has not been previously studied. Two studies, both from the MESA cohort, have previously considered the association of certain diets on CMR phenotypes. These studies report association of CMR ventricular with a Mediterranean diet[205] and the Dietary Approaches to Stop

Hypertension (DASH) diet[206]. Both dietary habits are reported to associate with healthier CMR phenotypes. In common with our findings, this comprised of larger ventricular volumes, higher LV mass, and higher stroke volume. We also document association of greater red and processed meat consumption with poorer arterial health. Our findings are consistent with those of Haring et al.[193], who also report association of greater red and processed meat intake with greater intima medial thickness and atherosclerosis burden on carotid ultrasound. Our analysis with CMR radiomics demonstrates the feasibility of this technique and, for the first time, its potential utility as a research tool for deeper cardiovascular phenotyping. Our findings provide corroborating evidence for existing research and provide new and more detailed information on associations with cardiovascular phenotypes.

6.6.2 Potential biological mechanisms

Higher intake of red and processed meat has been linked to a poorer cardiometabolic profile, specifically adverse lipid profiles[198], higher blood pressure[197], poorer glycaemic control[207], and adverse body composition[208]. As such, it has been suggested that the association of these dietary habits with poorer cardiovascular health is mediated by these factors. In our analysis, we found that the associations of red meat with ventricular metrics were significantly attenuated with inclusion of these exposures. However, associations of red meat with arterial stiffness remained robust, as did all phenotypic associations for processed meat and oily fish. This suggests the influence of multiple disease mechanisms, which likely vary by the aspect of cardiovascular health impacted (ventricles vs arteries) and the meat type (red meat vs unprocessed meat). Indeed, recent evidence has emerged in support of a role for the gut microbiome dependent trimethylamine N-oxide (TMAO) pathway. Red meat, which has high levels of carnitine, has been demonstrated to increase blood and urine levels of TMAO, through provision of the precursors, L-carnitine, and reduced renal excretion of TMAO[209]. TMAO has, in turn, been mechanistically associated with atherosclerotic disease[199]. Our findings support exploration of novel disease pathways that may link dietary habits and cardiovascular health.

The healthy pattern of associations observed between greater oily fish consumption and CMR metrics is consistent with previous studies of this dietary exposure. There is evidence to support the role of eicosapentaenoic acid (EPA) and docosahexaenoic acid (DHA), found in oily fish, as beneficial compounds for cardiac and vascular function[210]. The cardioprotective effect of EPA and DHA is most likely due to beneficial modification of multiple known vascular risk factors, such as serum lipids, blood pressure, heart rate, platelet aggregation, endothelial function, and inflammatory pathways[211].

6.7 Critical appraisal of the results

In this study we demonstrate novel associations of higher meat and fish intake with adverse CMR phenotypes. Our findings are complementary and additive to previous work linking these dietary exposures to poorer clinical outcomes. The use of CMR metrics for assessment of cardiovascular health removes subjectivity of clinical assessments and potential misdiagnoses. CMR in the UK Biobank is performed in a highly standardised manner; as such, biases related to image acquisition and analysis are minimised. Capturing dietary information is challenging and may be hampered by recall bias. The UK Biobank dietary health questionnaire has demonstrable validity with evidence of good longitudinal tracking in previous work. However, the dietary information collected is not particularly extensive and, importantly, does not permit calculation of estimated total energy intake, which would ordinarily be included as a covariate in modelling to extract more specific nutritional effects.[212] Furthermore, there is potential confounding of the meat/fish associations by other dietary factors, as intakes of foods and nutrients are highly correlated. For example, individuals who eat a lot of oily fish are likely to have intakes of antioxidant-rich fruit and vegetables, which are associated with cardiovascular risk[213]; furthermore, macronutrient intake has previously been shown to associated with cardiovascular disease in the UK Biobank[214]. Additionally, habitual diet is closely linked to deprivation and other key lifestyle behaviours, although we attempt to account for these factors in our analyses, such variables are extremely challenging to capture and express completely in a quantitative manner, so an element of residual confounding likely remains. We took dietary variables as reported at baseline and CMR measures from the imaging visit (several years later), so there is temporal separation of our exposure and outcome. However, it was not possible, with the data available, to examine in detail the effect of change in diet during this time. It is possible that the observed associations are causal (this would indeed be consistent with prior work and biologically plausible). However, we should also consider potential confounding from unmeasured and imperfectly measured confounders (other dietary habits, energy intake, deprivation). These considerations reflect the challenging nature of nutritional epidemiology and limitations of evaluating such relationships using observational data from a secondary source.

6.8 Conclusions

Higher consumption of red and processed meat is associated with unhealthy cardiovascular phenotypes as characterised by CMR measures of ventricular structure and function, novel radiomics features, and arterial compliance metrics. Cardiometabolic morbidities appeared to have a mechanistic role in the associations of red meat with ventricular phenotypes, but less so for other associations suggesting importance of alternative mechanism for these relationships. Our findings support previous clinical associations and provide greater insight into potential mechanisms of dietary impact on cardiovascular health.

7 Cardiovascular phenotypes and incident coronavirus disease 2019

7.1 Abstract

Objectives: Existing work indicates persistent cardiovascular involvement after recovery from SARS-CoV-2 infection. However, causal inference is severely limited by the absence of baseline data. This is because we cannot know for certain whether CMR abnormalities identified after infection are a result of COVID-19 or were present prior to the occurrence of infection. To investigate this possibility, we evaluated the association of CMR metrics from pre-infection imaging with incident COVID-19 in the UK Biobank.

Methods and Results: The study sample comprised participants with CMR and SARS-CoV-2 testing (n=310). Median age was 63.8 [57.5, 72.1] years; 51.0% (n = 158) were male. The following CMR metrics were included: LV and RV volumes, LV and RV ejection fractions, and LV and RV stroke volumes, LV mass, global longitudinal strain (GLS), global circumferential strain (GCS), global radial strain (GRS), myocardial native T1, AD, ASI. COVID-19 status was ascertained from linkages with Public Health England testing data. Co-morbidities were ascertained from self-report and HES. Critical care requirement and mortality were from HES and death register records. 70 participants had a positive test result, 78.7% (n = 244) were tested in hospital, 3.5% (n = 11) required critical care admission, and 6.1% (n = 19) died. In fully adjusted multivariable logistic regression models (covariates: age, sex, ethnicity, deprivation, body mass index, smoking, diabetes, hypertension, high cholesterol, prior AMI), we observed association of smaller LV/RV end-diastolic volumes, smaller LV stroke volume, and poorer GLS with significantly higher odds of COVID-19 (positive test result).

Conclusions: Our findings demonstrate association of adverse pre-infection CMR phenotypes with greater odds of incident COVID-19. These relationships appeared significant after adjustment for demographic and clinical confounders. Thus, demonstrating the high risk of residual confounding and reverse causation in studies drawing conclusions from imaging performed after infection. It is likely that existing reports of cardiovascular involvement after COVID-19 may, at least partly, reflect pre-existing cardiac status rather than COVID-19 induced alterations.

7.2 Background

The SARS-CoV-2 infection, which causes COVID-19, is increasingly recognised as a multi-system disease[215]. Cardiovascular involvement in association with COVID-19 has been reported both in the acute and post-acute phases of the illness.

The profound systemic inflammatory activation in acute COVID-19 has been hypothesized to lead to endothelial inflammation, myocarditis, and cardiac arrhythmias[216–219]. In addition, the associated hypercoagulable state increases the risk of both venous and arterial thrombi and related presentations such as pulmonary emboli, as well as thromboembolic myocardial and cerebral infarctions[220]. Whilst cardiovascular involvement in acute COVID-19 often reflects the severity of systemic and pulmonary disease, it is also an independent risk factor for poorer clinical endpoints. Indeed, patients with myocardial injury during acute COVID-19 have been shown to have higher risk of death independent of factors such as acute respiratory distress syndrome[221,222]. Furthermore, there are selected case reports of primary cardiac presentations of COVID-19 without pulmonary involvement [223–225]. These observations have led to speculations of potential cardio-specific actions of SARS-CoV-2. Limited in vitro studies are supportive of these suppositions, demonstrating the ability of SARS-CoV-2 to enter and induce cytotoxicity in human cardiomyocytes[226]. Similarly, autopsy studies demonstrate evidence of direct cardiotoxicity in patients with COVID-19[227].

Growing reports indicate that a subset of patients experience a more prolonged illness after apparent recovery from the acute phase of SARS-CoV-2 infection, including persistence of potentially cardiac symptoms[228–230]. In addition, CMR studies of individuals recovered from COVID-19 indicate possible sustained cardiovascular involvement[231–234]. However, the lack of baseline (pre-COVID-19) data severely limits any causal inference from these studies. Given the high burden of cardiovascular disease and vascular risk factors in patients with COVID-19, it is possible that the differences observed in the CMR metrics of these cohorts after recovery from COVID-19 is, at least partly, a reflection of their baseline cardiac status, rather than new changes occurring as a result of COVID-19. This distinction is clearly highly important for clinical decision making and public health planning.

In this study, we investigated whether baseline CMR phenotypes were associated with subsequent COVID-19 in the subset of UK Biobank participants tested for SARS-CoV-2 infection. We hypothesised that poorer baseline CMR phenotypes would be associated with higher likelihood of SARS-CoV-2 infection.

7.3 Methods

7.3.1 Study population

In light of the COVID-19 pandemic, the UK Biobank established linkages with Public Health England enabling tracking of SARS-CoV-2 test results for all UK Biobank participants[235]. Thus, SARS-CoV-2 test results for participants could be linked to all the other demographic, clinical, and imaging available in the UK Biobank (as detailed in **Section 2.1)**. In this study, we included all UK Biobank participants who were tested for SARS-CoV-2 (between 16th March 2020 to 22nd August 2020) and who had CMR imaging.

7.3.2 SARS-CoV-2 testing

Real-time polymerase chain reaction (RT-PCR) assay antigen tests were used to detect SARS-CoV-2 infection. In the majority of cases, the test sample was obtained from combined nose and throat swabs. Lower respiratory samples may have been used for patients in critical care. We considered samples labelled as "inpatient" to be from a hospital setting. Critical care admissions and deaths were defined based on HES and death register data.

7.3.3 CMR imaging and analysis

CMR was performed at the first UK Biobank imaging visit, an average of 3.0 years prior to SARS-CoV-2 testing. Details of the UK Biobank CMR acquisition protocol is discussed in **Section 2.1.6**. LV/RV volumes, LV mass, and LV strain (by tissue tracking) were derived from analysis of short axis and long axis images using the automated segmentation tool from Circle Cardiovascular Imaging (Version 5.11, Circle Cardiovascular Imaging Inc., Calgary, Canada). Image analysis was performed blind to all participant details and all study contours were examined for accuracy by a single reader with manual correction of segmentation where necessary. In the UK Biobank, native T1 maps are acquired at a single mid-ventricular short axis level using Shortened Modified Look-Locker Inversion recovery technique (ShMOLLI, WIP780B) acquisitions. After excluding cases with poor quality maps or excess septal motion, T1 was measured from a manual septal contour extending to half of the anterior-septal wall and half of the inferior-septal wall. AD was derived using an automated quality-controlled image analysis tool as detailed in **Section 2.2.6.1.** We limited analysis to AD measurements with detection probability >0.75. Thus, the following CMR metrics available were included in the analysis: LV and RV volumes in end-diastole and end-systole, LV and RV stroke volume, LV and RV ejection fraction, LV mass, mid-ventricular radial strain, mid-ventricular circumferential strain, global longitudinal strain (GLS), torsion, septal native T1, AD at the ascending and descending aorta.

7.3.4 Arterial stiffness index

We included ASI as a measure of larger artery stiffness measured at the baseline visit[58]. ASI was derived from finger plethysmography measured with the PulseTrace PCA2 (CareFusion, USA) device according to a pre-defined protocol and is described in more detail in **Section 2.2.6.2**[70]. We used a 1·5× IQR rule to remove outliers from this variable, as previously published using this dataset[59].

7.3.5 Statistical analysis

We used R Version 3.6.2 and RStudio Version 1.2.5019 for statistical analysis[142,143]. We used multivariable logistic regression models to estimate the association of each cardiovascular phenotype (exposure) with SARS-CoV-2 test result (binary outcome- positive/negative) whilst adjusting for age, sex, ethnicity, deprivation, BMI, smoking, diabetes, hypertension, high cholesterol, and prior AMI. Results are presented as odds ratios (ORs) with 95% CIs and p-values for positive SARS-CoV-2 test result per one unit increase in cardiovascular measure. In a sensitivity analysis, we restricted the analysis sample to individuals tested in a hospital setting. As the ASI was available in a larger sample, for this variable we were able to estimate the association of ASI with death and critical care admission separately within SARS-CoV-2 positive and negative cohorts.

7.3.6 Ascertainment of covariates

Age was taken as recorded at time of SARS-CoV-2 testing. Sex was taken as recorded at baseline recruitment. Ethnicity was classified into a binary variable of White and BAME (Black, Asian and minority ethnic) ethnicity based on self-report at baseline. Deprivation, smoking status, hypertension, diabetes, and high cholesterol were ascertained as detailed in **Section 2.2.2** and **Section 2.2.3.** Previous AMI was ascertained from UK Biobank algorithmically defined health outcome data.

7.4 Results

7.4.1 Population characteristics

There were 18,162 UK Biobank participants who had been tested for SARS-CoV-2 within the defined study period. From these, 315 participants also had prior CMR imaging and 310 had at least one analysable CMR metric. Thus, the analysis sample comprised 310 participants tested for SARS-CoV-2 and with at least one analysable CMR measure (**Figure 7.1**, **Table 7.1**). Within the analysis sample, 70 participants had a positive SARS-CoV-2 test result. The majority were tested in a hospital setting (78.7%, n=244), 3.5% (n=11) had requirement for critical care, and 6.1% (n=19) died. There were 158 men (51.0%) and the median age was 63.8 [57·5, 72·1] years. On average, CMR imaging was

performed 3.0 years prior to SARS-CoV-2 testing. The rates of smoking, diabetes, hypertension, high cholesterol, and previous AMI were 45.2%, 9.4%, 40.6%, 29.4%, and 3.5% respectively (**Table 7.1**).

There were greater proportions of men (58.6%) and individuals from BAME backgrounds (10.0% vs 3.3%) in the test positive compared to the test negative group (**Table 7.1**). There were greater rates of adverse outcomes in the SARS-CoV-2 positive group compared to those testing negative, with greater proportion of people requiring critical care admission (5·7% vs 2·9%) and higher proportion of deaths (11·4% vs 4·6%), but this was not statistically significant.

Figure 7.1. Approach to selection of participants for inclusion in the analysis

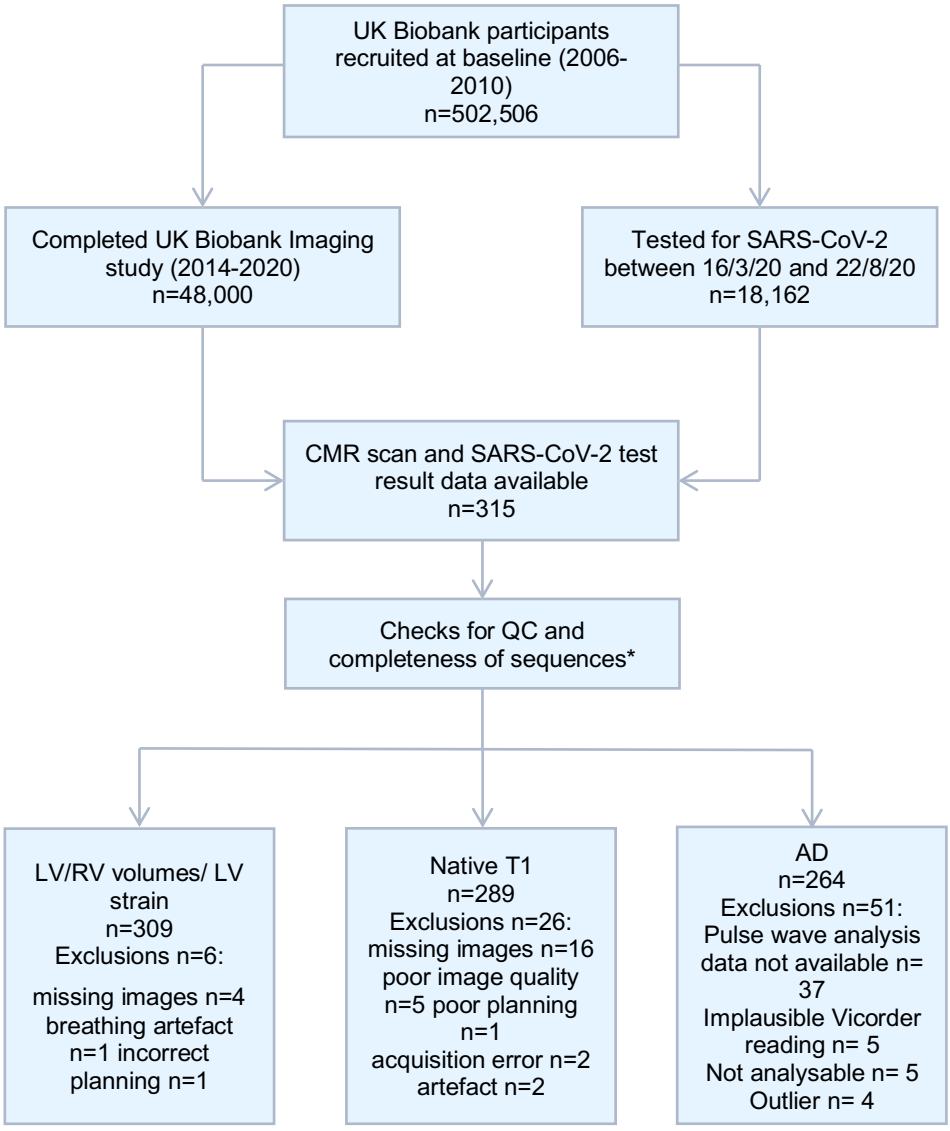

Figure 7.1. *There were 310 participants with at least one analysable CMR measure, this included one participant with analysable native T1, but not volumetric images. AD: aortic distensibility; CMR: cardiovascular magnetic resonance; LV: left ventricle; RV: right ventricle; SARS-CoV-2: severe acute respiratory syndrome coronavirus 2. Reproduced from Raisi-Estabragh et al.*[236]

Table 7.1. Baseline participant characteristics

	Whole sample n=310	SARS-CoV-2 negatives n=240	SARS-CoV-2 positives n=70	p-value [test]
Age	63.8 [57.5, 72.1]	65.1 [58.2, 72.1]	61.4 [55.5, 72.4]	0.154 [2]
Sex (Male)	158 (51.0%)	117 (48.8%)	41 (58.6%)	0.190[3]
White	295 (95.2%)	232 (96.7%)	63 (90.0%)	0.049 [3]
BAME	15 (4.8%)	8 (3.3%)	7 (10.0%)	
Asian	8 (2.6%)	5 (2.1%)	3 (4.3%)	0.046 [4]
Black	2 (0.6%)		2 (2.9%)	
Mixed	3 (1.0%)	2 (0.8%)	1 (1.4%)	
Other	2 (0.6%)	1 (0.4%)	1 (1.4%)	
Townsend deprivation score	-2.5 [-3.8, 0.2]	-2.5 [-3.8, 0.0]	-2.4 [-4.1, 0.4]	0.960 [2]
Smoking (current/previous)	140 (45.2%)	108 (45.0%)	32 (45.7%)	1.000 [3]
BMI	27.4 (± 4.9)	27.3 (± 4.7)	27.6 (± 5.6)	0.629 [1]
Diabetes	29 (9.4%)	24 (10.0%)	5 (7.1%)	0.641 [4]
Hypertension	126 (40.6%)	101 (42.1%)	25 (35.7%)	0.414 [3]
High cholesterol	91 (29.4%)	70 (29.2%)	21 (30.0%)	1.000 [3]
Prior myocardial infarction	11 (3.5%)	10 (4.2%)	1 (1.4%)	0.466 [4]
Tested in hospital	244 (78.7%)	194 (80.8%)	50 (71.4%)	0.127 [3]
Critical care admission	11 (3.5%)	7 (2.9%)	4 (5.7%)	0.276 [4]
Death	19 (6.1%)	11 (4.6%)	8 (11.4%)	0.069 [3]

Table 7.1. *[1] Welch Two Sample t-test (numeric data with unequal variances); [2] Wilcoxon rank sum test with continuity correction (numeric skewed); [3] Two-sample test for equality of proportions with continuity correction (where minimum count > 5); [4] Fisher's Exact Test for Count Data (where minimum count ≤ 5). Abbreviations: BAME: Black, Asian, and minority ethnic; BMI: body mass index; SARS-CoV-2: severe acute respiratory syndrome coronavirus 2.*

Amongst those testing positive for SARS-CoV-2, those who required critical care admission had poorer overall cardiometabolic profile, greater levels of deprivation, and included a higher proportion of men and individuals from BAME backgrounds, compared to those who did not (**Table 7.2**). Those who died had poorer cardiometabolic profile and were older than those who survived (**Table 7.2**). Amongst individuals testing negative for SARS-CoV-2, we observed similar but less marked differences (**Table 7.2**).

Table 7.2. Baseline characteristics by mortality and critical care outcomes in SARS-CoV-2 positives and negatives

	SARS-CoV-2 positive (n= 70)				SARS-CoV-2 negative (n= 240)			
	Alive n=62	**Dead n=8**	**No critical care n=66**	**Critical care n=4**	**Alive n=229**	**Dead n=11**	**No critical care n=233**	**Critical care n=7**
Age	60.4 [55.0, 67. 1]	78.0 [75.7, 81.0]	62.1 [55.5, 72.4]	59.6 [57.6, 64.0]	64.0 [58.0, 72.0]	71.2 [66.2, 75.1]	65.1 [58.1, 72.1]	66.5 [61.0, 71.8]
Sex (Male)	35 (56.5%)	6 (75.0%)	37 (56.1%)	4 (100.0%)	111 (48.5%)	6 (54.5%)	111 (47.6%)	6 (85.7%)
White	55 (88.7%)	8 (100.0%)	59 (89.4%)	4 (100.0%)	221 (96.5%)	11 (100.0%)	225 (96.6%)	7 (100.0%)
BAME	7 (11.3%)		7 (10.6%)		8 (3.5%)		8 (3.4%)	
Asian	3 (4.8%)		3 (4.5%)		5 (2.2%)		5 (2.1%)	
Black	2 (3.2%)		2 (3.0%)					
Mixed	1 (1.6%)		1 (1.5%)		2 (0.9%)		2 (0.9%)	
Other	1 (1.6%)		1 (1.5%)		1 (0.4%)		1 (0.4%)	
Townsend score	-2.2 [-4.0, 0.4]	-3.6 [-4.2, -0.8]	-2.4 [-4.2, 0.3]	0.2 [-3.3, 3. 8]	-2.6 [-3.9, 0.2]	-2.4 [-3. 7, -1.2]	-2.5 [-3.8, 0.0]	-2.6 [-3.1, 0.7]
Smoking*	27 (43.5%)	5 (62.5%)	30 (45.5%)	2 (50.0%)	102 (44.5%)	6 (54.5%)	105 (45.1%)	3 (42.9%)
BMI	27.4 (± 5.9)	29.3 (± 1. 9)	27.3 (± 5. 6)	32.9 (± 4.9)	27.3 (± 4.5)	27.5 (± 7.4)	27.2 (± 4.7)	28.5 (± 5. 0)
Diabetes	4 (6.5%)	1 (12.5%)	4 (6.1%)	1 (25.0%)	23 (10.0%)	1 (9.1%)	23 (9.9%)	1 (14.3%)
Hypertension	20 (32.3%)	5 (62.5%)	23 (34.8%)	2 (50.0%)	93 (40.6%)	8 (72.7%)	96 (41.2%)	5 (71.4%)
High cholesterol	17 (27.4%)	4 (50.0%)	18 (27.3%)	3 (75.0%)	64 (27.9%)	6 (54.5%)	69 (29.6%)	1 (14.3%)
Prior AMI	1 (1.6%)		1 (1.5%)		7 (3.1%)	3 (27.3%)	10 (4.3%)	
Tested in hospital	43 (69.4%)	7 (87.5%)	47 (71.2%)	3 (75.0%)	185 (80.8%)	9 (81.8%)	189 (81.1%)	5 (71.4%)

Table 7.2. *Green shading indicates p-value of difference between 0.1–0.05. Yellow shading indicated p-value of difference <0.05. *smoking indicated previous/current smoking. AMI: acute myocardial infarction; BAME: Black, Asian, and minority ethnic; BMI: body mass index; SARS-CoV-2: severe acute respiratory syndrome coronavirus 2.*

ASI was recorded for 167,423 participants at baseline. From these, 6,160 had SARS-CoV-2 testing within our defined study period, after outlier removal (n=94), 6,066 participants had analysable ASI and SARS-CoV-2 testing and are included in the analysis. Within this cohort, 667 participants tested positive, and 5,399 participants tested negative. The baseline characteristics are summarised in **Table 7.3**.

Table 7.3. Baseline population characteristics (arterial stiffness index set)

	Whole sample n=6,066	**SARS-CoV-2 negatives n=5,399**	**SARS-CoV-2 positives n=667**	**p-value [test]**
Age	70.9 [62.2, 75.7]	71.0 [62.8, 75.8]	68.1 [59.0, 75.1]	$4.4x10^{-7}$ [2]
Sex (Male)	2,947 (48.6%)	2,586 (47.9%)	361 (54.1%)	$2.8x10^{-3}$ [3]
White	5,357 (88.3%)	4,810 (89.1%)	547 (82.0%)	$1.5x10^{-7}$ [4]
BAME	660 (10.9%)	545 (10.1%)	115 (17.2%)	
Asian	288 (4.7%)	243 (4.5%)	45 (6.7%)	$5.0x10^{-4}$ [4]
Black	208 (3.4%)	162 (3.0%)	46 (6.9%)	
Chinese	15 (0.2%)	12 (0.2%)	3 (0.4%)	
Mixed	42 (0.7%)	38 (0.7%)	4 (0.6%)	
Other	156 (2.6%)	134 (2.5%)	22 (3.3%)	
Townsend deprivation score	-1.4 [-3.2, 1.4]	-1.5 [-3.2, 1.4]	-0.8 [-3.0, 2.1]	$1.0x10^{-3}$ [2]
Smoking (current/previous)	2,946 (48.6%)	2,609 (48.3%)	337 (50.5%)	0.302 [3]
BMI	28.3 (± 5.1)	28.2 (± 5.1)	28.7 (± 5.12)	0.023 [1]
Diabetes	954 (15.7%)	817 (15.1%)	137 (20.5%)	$3.7x10^{-4}$ [3]
Hypertension	3,073 (50.7%)	2,731 (50.6%)	342 (51.3%)	0.767 [3]
High cholesterol	2,253 (37.1%)	2,017 (37.4%)	236 (35.4%)	0.340 [3]
Prior myocardial infarction	397 (6.5%)	348 (6.4%)	49 (7.3%)	0.421 [3]
ASI (m/s)	9.3 (± 2.9)	9.3 (± 2.9)	9.2 (± 2.7)	0.348 [1]
Testing in hospital	4,546 (74.9%)	4,128 (76.5%)	418 (62.7%)	$1.3x10^{-14}$ [3]
Critical care admission	149 (2.5%)	97 (1.8%)	52 (7.8%)	$1.3x10^{-20}$ [3]
Death	347 (5.7%)	217 (4.0%)	130 (19.5%)	$1.3x10^{-58}$ [3]

Table 7.3. *[1] Welch Two Sample t-test (numeric data with unequal variances); [2] Wilcoxon rank sum test with continuity correction (numeric skewed); [3] Two-sample test for equality of proportions with continuity correction (where minimum count > 5); [4] Fisher's Exact Test for Count Data (where minimum count ≤5). BAME: Black, Asian, and minority ethnic; BMI: body mass index; SARS-CoV-2: severe acute respiratory syndrome coronavirus 2*

7.4.2 Baseline cardiovascular phenotypes

Participants with a positive SARS-CoV-2 test had, on average, smaller LV end-diastolic volumes, lower stroke volume, lower ejection fraction, and lower LV mass, compared to those testing negative (**Table 7.4, Figure 7.2**). A similar pattern was observed in RV metrics of test positives and test negatives (**Figure 7.2**). Compared to test negatives, test positives also had, on average, poorer LV function by strain metrics, higher average native T1, and greater arterial compliance (higher aortic distensibility, lower ASI), however, there was significant overlap of distributions for these variables (**Figure 7.2**, **Table 7.3**, **Table 7.4**). Amongst participants with a positive SARS-CoV-2 test result, those who died had significantly lower LV stroke volume, worse global longitudinal strain, and poorer arterial compliance (lower AD, higher ASI), compared to those who survived (**Table 7.5**). Within the test negative group, there were no significant differences in the LV metrics of those who died and those who survived, however those who died had higher ASI.

Table 7.4. Cardiovascular magnetic resonance metrics stratified by SARS-CoV-2 test result

	Whole sample n=310	COVID-19 negatives n=240	COVID-19 positives n=70	p-value [test]
LVEDVi (ml/m^2)	80.0 (± 14.2)	80.8 (± 14.3)	77.1 (± 13.2)	0.046 [1]
LVESVi (ml/m^2)	31.5 (± 8.3)	31.6 (± 8.4)	31.4 (± 8.1)	0.863 [1]
LVSVi (ml/m^2)	48.5 (± 9.3)	49.2 (± 9.4)	45.7 (± 8.4)	0.004 [1]
LVEF (%)	60.8 (± 6.5)	61.1 (± 6.4)	59.6 (± 6.5)	0.083 [1]
LVMi (g/m^2)	46.7 (± 8.8)	46.9 (± 8.8)	45.7 (± 8.4)	0.318 [1]
RVEDVi (ml/m^2)	79.2 (± 15.5)	79.9 (± 15.6)	76.9 (± 15.0)	0.148 [1]
RVESVi (ml/m^2)	30.8 (± 8.4)	31.0 (± 8.5)	30.0 (± 8.1)	0.393 [1]
RVSVi (ml/m^2)	48.4 (± 10.4)	48.9 (± 10.5)	46.8 (± 9.8)	0.133 [1]
RVEF (%)	61.3 (± 6.6)	61.3 (± 6.8)	61.1 (± 6.2)	0.808 [1]
Native T1 (ms)	923.2 (± 39.1)	922.9 (± 40.1)	924.2 (± 35.9)	0.808 [1]
MRS (%)	35.5 (± 9.1)	35.6 (± 9.3)	34.9 (± 8.5)	0.558 [1]
MCS (%)	-20.0 (± 3.2)	-20.1 (± 3.2)	-19.8 (± 3.1)	0.562 [1]
GLS (%)	-15.4 (± 2.6)	-15.5 (± 2.5)	-15.0 (± 2.6)	0.206 [1]
Torsion (degrees)	0.9 (± 0.8)	0.9 (± 0.7)	0.8 (± 1.0)	0.437 [1]
AA AoD (× 10^{-3} mmHg^{-1})	1.4 [0.8, 2.3]	1.3 [0.8, 2.3]	1.4 [0.9, 2.3]	0.665 [2]
PDA AoD (× 10^{-3} mmHg^{-1})	2.2 [1.7, 3.1]	2.2 [1.7, 3.1]	2.4 [1.6, 3.2]	0.511 [2]

Table 7.4. *[1] Welch Two Sample t-test (numeric data with unequal variances); [2] Wilcoxon rank sum test with continuity correction (numeric skewed). Abbreviations: AA: ascending aorta; AoD: aortic distensibility; LVEDV: left ventricular endo-diastolic volume; LVEF: left ventricular ejection fraction; LVESV: left ventricular endo-systolic volume; LVSV: left ventricular stroke volume; GLS: global longitudinal strain; MCS: circumferential strain at the mid short axis level; MRS: radial strain at the mid short axis level; PDA: proximal descending aorta; RVEDV: right ventricular endo-diastolic volume; RVEF: right ventricular ejection fraction; RVESV: right ventricular end-systolic volume; RVSV: right ventricular stroke volume; SARS-CoV-2: severe acute respiratory syndrome coronavirus 2.*

Figure 7.2. Summary of Cardiovascular measures stratified by SARS-CoV-2 test result

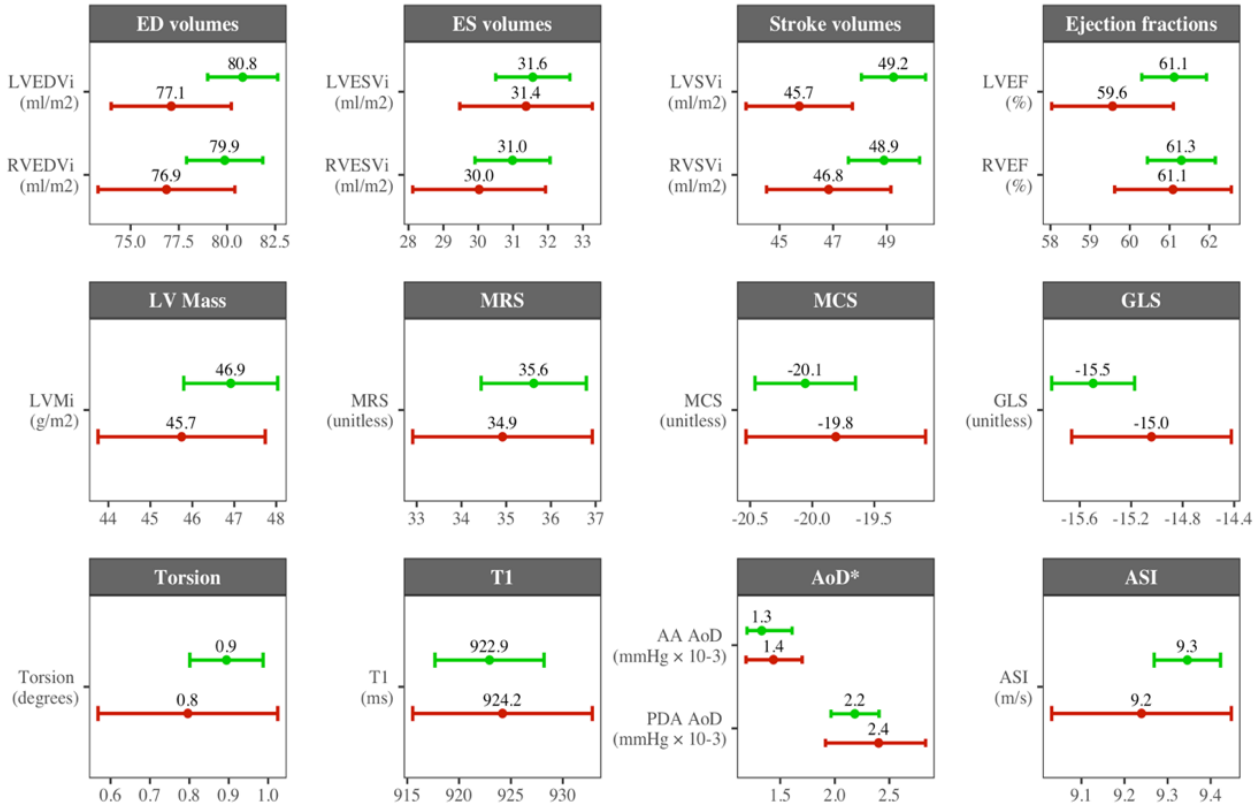

Figure 7.2. *Green and red bars indicate SARS-CoV-2 test negative and positive, respectively. AA AoD: aortic distensibility at the ascending aorta; ASI: arterial stiffness index; CMR: cardiovascular magnetic resonance;; ED: end-diastole; ES: end-systole; GLS: global longitudinal strain; MCS: circumferential strain at the mid short axis level; MRS: radial strain at the mid short axis level; LV: left ventricle; PDA AoD: aortic distensibility at the proximal descending aorta; SARS-CoV-2 : severe acute respiratory syndrome coronavirus 2. Intervals for AoD show the 95% confidence interval for the median, all others are 95% confidence interval for the mean.*

Table 7.5. Cardiovascular phenotypes by mortality and critical care outcome in SARS-CoV-2 positives and negatives

	COVID-19 positive (n= 70)				COVID-19 negative (n= 240)			
	Alive n=62	Dead n=8	No critical care n=66	Critical care n=4	Alive n=229	Dead n=11	No critical care n=233	Critical care n=7
LVEDVi (ml/m^2)	77.5 (± 13.2)	73.2 (± 13.3)	76.8 (± 13.4)	81.5 (± 8.1)	81.0 (± 14.4)	76.2 (± 14.1)	80.6 (± 13.8)	89.4 (± 26.4)
LVESVi (ml/m^2)	31.1 (± 7.8)	33.9 (± 10.4)	31.3 (± 8.2)	32.3 (± 6.0)	31.6 (± 8.2)	31.0 (± 12.4)	31.5 (± 8.2)	33.3 (± 14.0)
LVSVi (ml/m^2)	46.5 (± 8.3)	39.3 (± 6.5)	45.5 (± 8.4)	49.3 (± 9.3)	49.4 (± 9.5)	45.2 (± 7.7)	49.0 (± 9.2)	56.1 (± 15.9)
LVEF (%)	60.2 (± 6.2)	54.3 (± 7.1)	59.5 (± 6.5)	60.2 (± 7.7)	61.2 (± 6.2)	60.4 (± 10.1)	61.1 (± 6.4)	63.0 (± 9.1)
LVMi (g/m^2)	45.9 (± 8.4)	44.5 (± 9.2)	45.3 (± 8.4)	53.3 (± 5.9)	46.8 (± 8.6)	50.2 (± 13.3)	46.6 (± 8.7)	55.9 (± 10.3)
RVEDVi (ml/m^2)	77.5 (± 15.0)	71.5 (± 15.2)	76.9 (± 15.2)	76.7 (± 13.4)	80.1 (± 15.7)	74.3 (± 12.2)	79.8 (± 15.3)	83.2 (± 24.8)
RVESVi (ml/m^2)	30.1 (± 8.0)	29.3 (± 9.3)	29.9 (± 8.2)	32.5 (± 6.0)	31.1 (± 8.5)	28.5 (± 8.9)	30.8 (± 8.2)	36.0 (± 15.8)
RVSVi (ml/m^2)	47.4 (± 10.0)	42.2 (± 7.1)	47.0 (± 10.0)	44.1 (± 7.4)	49.0 (± 10.6)	45.7 (± 8.6)	48.9 (± 10.5)	47.2 (± 11.5)
RVEF (%)	61.3 (± 6.3)	59.5 (± 5.1)	61.3 (± 6.4)	57.6 (± 0.6)	61.3 (± 6.7)	61.9 (± 9.0)	61.4 (± 6.7)	57.5 (± 6.5)
T1 (ms)	924.8 (± 37.0)	919.0 (± 26.4)	924.3 (± 36.7)	921.0 (± 10.7)	922.7 (± 39.3)	928.3 (± 54.4)	923.5 (± 40.2)	904.8 (± 31.7)
MRS (%)	35.4 (± 8.4)	30.2 (± 7.7)	34.9 (± 8.7)	34.6 (± 4.3)	35.6 (± 9.0)	36.6 (± 14.6)	35.8 (± 9.4)	31.0 (± 4.7)
MCS (%)	-20.0 (± 2.9)	-17.8 (± 3.9)	-19.8 (± 3.1)	-20.0 (± 1.5)	-20.1 (± 3.1)	-20.0 (± 4.3)	-20.1 (± 3.2)	-18.6 (± 1.8)
GLS (%)	-15.4 (± 2.4)	-11.8 (± 1.8)	-15.0 (± 2.7)	-15.0 (± 2.1)	-15.6 (± 2.5)	-14.2 (± 2.2)	-15.5 (± 2.6)	-15.4 (± 1.5)
Torsion (degrees)	0.8 (± 0.9)	0.5 (± 1.7)	0.8 (± 1.0)	0.7 (± 1.0)	0.9 (± 0.8)	1.0 (± 0.3)	0.9 (± 0.7)	1.1 (± 0.5)
AA AoD (× 10^{-3} mmHg^{-1})	1.5 [1.0, 2.6]	0.7 [0.4, 1.3]	1.4 [0.9, 2.3]	1.6 [1.1, 2.6]	1.4 [0.8, 2.4]	1.0 [0.6, 1.3]	1.3 [0.8, 2.3]	2.5 [1.3, 3.7]
PDA AoD (× 10^{-3} mmHg^{-1})	2.4 [1.8, 3.5]	1.6 [0.8, 2.1]	2.4 [1.6, 3.3]	1.8 [1.8, 2.3]	2.2 [1.7, 3.1]	2.1 [1.4, 2.4]	2.2 [1.7, 3.1]	2.2 [1.8, 4.3]
ASI (m/s)	9.1 (± 2.7)	9.7 (± 2.7)	9.2 (± 2.8)	9.6 (± 2.2)	9.3 (± 2.9)	9.8 (± 2.8)	9.3 (± 2.9)	10.0 (± 2.8)

Table 7.5. *Green shading indicates p-value of difference between 0.1–0.05. Yellow shading indicated p-value of difference <0.05 AA: ascending aorta; AoD: aortic distensibility; LVEDV: left ventricular endo-diastolic volume; LVEF: left ventricular ejection fraction; LVESV: left ventricular endo-systolic volume; LVSV: left ventricular stroke volume; GLS: global longitudinal strain; MCS: circumferential strain at the mid short axis level; MRS: radial strain at the mid short axis level; PDA: proximal descending aorta; RVEDV: right ventricular endo-diastolic volume; RVEF: right ventricular ejection fraction; RVESV: right ventricular end-systolic volume; RVSV: right ventricular stroke volume; SARS-CoV-2: severe acute respiratory syndrome coronavirus 2. shading indicates comparison between dead vs alive and critical care vs no critical care within the test positive and test negative cohorts.*

7.4.3 Association of cardiovascular phenotypes with incident SARS-CoV-2 infection

In multivariable logistic regression models with full covariate adjustment (age, sex, ethnicity, deprivation, body mass index, smoking, diabetes, hypertension, high cholesterol, prior myocardial infarction), smaller LV and RV volumes in end-diastole, lower LV stroke volume, and poorer global longitudinal strain (higher value) were associated with significantly higher odds of a positive SARS-CoV-2 test result (**Figure 7.3**, **Table 7.6**). Associations with other cardiac metrics were not statistically significant. We additionally performed sensitivity analysis limiting to the subset of participants tested in a hospital setting (positive n=50, negative n=194). The previously observed associations remained unchanged in this subset, and additionally, we observed a significant association between smaller RV end-systolic volume and greater odds of a positive test result (**Table 7.7**).

Figure 7.3. Odds ratios from fully adjusted multivariable logistic regression models demonstrating association of cardiovascular phenotype measures with positive SARS-CoV-2 status

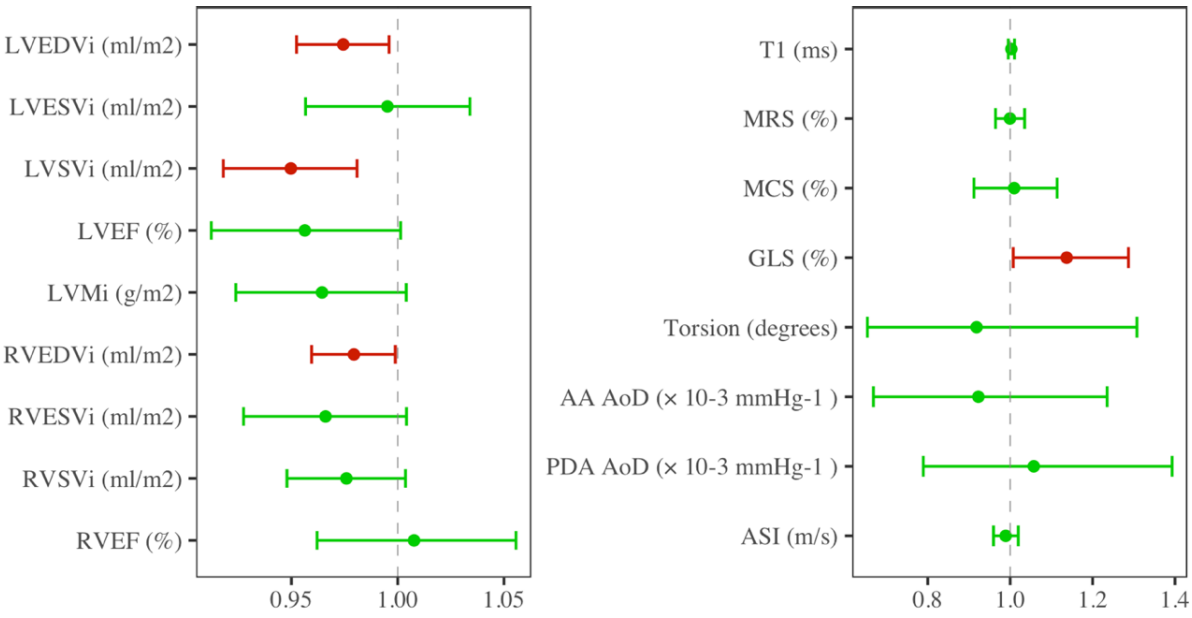

Figure 7.3. *Association of each cardiovascular measure with SARS-CoV-2 result (positive vs negative) in multivariable logistic regression models adjusting for age, sex, ethnicity, deprivation, body mass index, smoking, diabetes, hypertension, high cholesterol, and prior myocardial infarction. Results are from individual models and expressed as odds ratio and 95% confidence interval (CI) corresponding to each cardiovascular measure. Green: 95% CI includes 1. Red: 95% CI does not include 1. SARS-CoV-2: severe acute respiratory syndrome coronavirus 2.*

Table 7.6. Odds ratios from logistic regression models demonstrating association of cardiovascular phenotype measures with positive SARS-CoV-2 status

	Univariate	Age and Sex Adjusted	Fully Adjusted
LVEDVi (ml/m2)	0.98 [0.96, 1.00]	0.97* [0.95, 0.99]	0.97* [0.95, 1.00]
	0.057	8.50×10^{-3}	0.022
LVESVi (ml/m2)	1.00 [0.96, 1.03]	0.99 [0.95, 1.02]	1.00 [0.96, 1.03]
	0.865	0.416	0.806
LVSVi (ml/m2)	0.96* [0.93, 0.99]	0.95* [0.92, 0.98]	0.95* [0.92, 0.98]
	6.4×10^{-3}	1.4×10^{-3}	2.2×10^{-3}
LVEF (%)	0.96 [0.93, 1.00]	0.97 [0.93, 1.01]	0.96 [0.91, 1.00]
	0.081	0.127	0.059
LVMi (g/m2)	0.98 [0.95, 1.02]	0.96* [0.92, 1.00]	0.96 [0.92, 1.00]
	0.328	0.036	0.087
RVEDVi (ml/m2)	0.99 [0.97, 1.00]	0.98* [0.96, 1.00]	0.98* [0.96, 1.00]
	0.155	0.023	0.042
RVESVi (ml/m2)	0.99 [0.95, 1.02]	0.96* [0.92, 1.00]	0.97 [0.93, 1.00]
	0.404	0.050	0.087
RVSVi (ml/m2)	0.98 [0.95, 1.01]	0.97 [0.95, 1.00]	0.98 [0.95, 1.00]
	0.146	0.065	0.093
RVEF (%)	1.00 [0.96, 1.04]	1.01 [0.97, 1.06]	1.01 [0.96, 1.06]
	0.816	0.682	0.746
Native T1 (ms)	1.00 [0.99, 1.01]	1.00 [1.00, 1.01]	1.00 [1.00, 1.01]
	0.818	0.536	0.483
MRS (%)	0.99 [0.96, 1.02]	1.00 [0.97, 1.04]	1.00 [0.96, 1.03]
	0.575	0.828	0.972
MCS (%)	1.02 [0.94, 1.11]	0.99 [0.90, 1.09]	1.01 [0.91, 1.11]
	0.569	0.914	0.851
GLS (%)	1.07 [0.96, 1.19]	1.10 [0.98, 1.24]	1.14* [1.01, 1.29]
	0.197	0.113	0.039
Torsion (degrees)	0.86 [0.62, 1.20]	0.88 [0.63, 1.24]	0.92 [0.65, 1.31]
	0.366	0.443	0.628
AA AoD ($\times 10^{-3}$ mmHg^{-1})	1.06 [0.84, 1.33]	0.93 [0.68, 1.23]	0.92 [0.67, 1.24]
	0.602	0.625	0.606
PDA AoD ($\times 10^{-3}$ mmHg^{-1})	1.12 [0.89, 1.41]	1.04 [0.79, 1.35]	1.06 [0.79, 1.39]
	0.372	0.863	0.812
ASI (m/s)	0.99 [0.96, 1.02]	0.99 [0.96, 1.02]	0.99 [0.96, 1.02]
	0.367	0.549	0.481

Table 7.6. *Covariates in fully adjusted models include: age, sex, ethnicity, deprivation, body mass index, smoking, diabetes, hypertension, high cholesterol, and prior myocardial infarction. Results are odds ratio [95% confidence interval] and p-value, each belonging to a separate logistic regression model with covariate adjustment as indicated in columns. Abbreviations: AA: ascending aorta; AoD: aortic distensibility; ASI: arterial stiffness index; LVEDV: left ventricular endo-diastolic volume; LVEF: left ventricular ejection fraction; LVESV: left ventricular endo-systolic volume; LVSV: left ventricular stroke volume; GLS: global longitudinal strain; MCS: circumferential strain at the mid short axis level; MRS: radial strain at the mid short axis level; PDA: proximal descending aorta; RVEDV: right ventricular endo-diastolic volume; RVEF: right ventricular ejection fraction; RVESV: right ventricular end-systolic volume; RVSV: right ventricular stroke volume. SARS-CoV-2: severe acute respiratory syndrome coronavirus 2.*

Table 7.7. Odds ratios from logistic regression models demonstrating association of cardiovascular phenotype measures with SARS-CoV-2 status in the subset tested in hospital

	Univariate	Age and Sex Adjusted	Fully Adjusted
LVEDVi (ml/m^2)	0.98 [0.96, 1.00]	0.97* [0.94, 0.99]	0.97* [0.94, 1.00]
	0.064	0.010	0.028
LVESVi (ml/m^2)	1.00 [0.96, 1.04]	0.98 [0.94, 1.02]	0.99 [0.95, 1.04]
	0.899	0.338	0.755
LVSVi (ml/m^2)	0.95* [0.92, 0.99]	0.94* [0.91, 0.98]	0.94* [0.90, 0.98]
	7.2×10^{-3}	2.5×10^{-3}	3.9×10^{-3}
LVEF (%)	0.96 [0.91, 1.01]	0.97 [0.92, 1.02]	0.95 [0.90, 1.01]
	0.078	0.194	0.089
LVMi (g/m^2)	0.99 [0.95, 1.02]	0.95* [0.91, 1.00]	0.96 [0.92, 1.01]
	0.459	0.047	0.137
RVEDVi (ml/m^2)	0.98 [0.96, 1.00]	0.97* [0.95, 0.99]	0.97* [0.95, 1.00]
	0.098	0.014	0.022
RVESVi (ml/m^2)	0.98 [0.94, 1.01]	0.95* [0.90, 0.99]	0.95* [0.91, 1.00]
	0.244	0.018	0.049
RVSVi (ml/m^2)	0.98 [0.95, 1.01]	0.97 [0.94, 1.00]	0.97 [0.93, 1.00]
	0.125	0.070	0.065
RVEF (%)	1.00 [0.96, 1.05]	1.03 [0.97, 1.08]	1.02 [0.96, 1.07]
	0.911	0.341	0.581
T1 (ms)	1.00 [0.99, 1.01]	1.01 [1.00, 1.01]	1.00 [1.00, 1.01]
	0.645	0.258	0.287
MRS (%)	0.98 [0.95, 1.02]	1.00 [0.96, 1.04]	0.99 [0.94, 1.03]
	0.303	0.882	0.567
MCS (%)	1.05 [0.95, 1.16]	1.01 [0.91, 1.13]	1.04 [0.93, 1.17]
	0.294	0.802	0.478
GLS (%)	1.12 [0.99, 1.26]	1.14 [1.00, 1.31]	1.18* [1.02, 1.37]
	0.072	0.053	0.026
Torsion (degrees)	0.86 [0.60, 1.25]	0.88 [0.60, 1.31]	0.88 [0.60, 1.31]
	0.418	0.509	0.527
AA AoD ($\times 10^{-3}$ mmHg^{-1})	1.12 [0.84, 1.48]	0.99 [0.67, 1.38]	1.00 [0.67, 1.42]
	0.425	0.938	0.983
PDA AoD ($\times 10^{-3}$ mmHg^{-1})	1.12 [0.85, 1.47]	1.04 [0.74, 1.42]	1.09 [0.76, 1.52]
	0.409	0.832	0.637
ASI (m/s)	0.99 [0.96, 1.02]	0.98 [0.95, 1.01]	0.98 [0.95, 1.02]
	0.528	0.348	0.391

Table 7.7. *Analysis sample n=244 (n=50 positive); Fully adjusted model includes adjustment for age, sex, ethnicity, deprivation, body mass index, smoking, diabetes, hypertension, high cholesterol, and prior myocardial infarction. Results are odds ratio [95% confidence interval] and p-value, each belonging to a separate logistic regression model with covariate adjustment as indicated in columns. Abbreviations: AA: ascending aorta; AoD: aortic distensibility; ASI: arterial stiffness index; LVEDV: left ventricular endo-diastolic volume; LVEF: left ventricular ejection fraction; LVESV: left ventricular endo-systolic volume; LVSV: left ventricular stroke volume; GLS: global longitudinal strain; MCS: circumferential strain at the mid short axis level; MRS: radial strain at the mid short axis level; PDA: proximal descending aorta; RVEDV: right ventricular endo-diastolic volume; RVEF: right ventricular ejection fraction; RVESV: right ventricular end-systolic volume; RVSV: right ventricular stroke volume. SARS-CoV-2: severe acute respiratory syndrome coronavirus 2.*

As a larger sample was available in the ASI subset (n=6,066), we had adequate power to test association of ASI with COVID-19 outcomes. Amongst those testing positive for SARS-CoV-2, we found no statistically significant associations between ASI and death or need for critical care admission (**Table 7.8**).

Table 7.8. Logistic regression models demonstrating association of arterial stiffness index with SARS-CoV-2 status, death, and critical care admission in different sample subsets

Sample	Outcome	Univariate	Age and Sex Adjusted	Fully Adjusted
Whole sample	SARS-CoV-2 test result	0.99 [0.96, 1.02]	0.99 [0.96, 1.02]	0.99 [0.96, 1.02]
		0.367	0.549	0.481
Tested in hospital	SARS-CoV-2 test result	0.99 [0.95, 1.02]	0.98 [0.95, 1.02]	0.98 [0.95, 1.02]
		0.528	0.348	0.391
SARS-CoV-2 negatives	Death	1.06* [1.01, 1.11]	1.02 [0.97, 1.07]	1.01 [0.97, 1.07]
		0.017	0.486	0.553
SARS-CoV-2 positives	Death	1.08* [1.01, 1.16]	1.00 [0.92, 1.07]	0.98 [0.91, 1.06]
		0.032	0.899	0.699
SARS-CoV-2 negatives	Critical care admission	1.08* [1.01, 1.16]	1.07 [1.00, 1.15]	1.07 [0.99, 1.15]
		0.021	0.064	0.072
SARS-CoV-2 positives	Critical care admission	1.06 [0.96, 1.17]	1.03 [0.92, 1.15]	1.02 [0.91, 1.14]
		0.268	0.601	0.758

Table 7.8. *Fully adjusted model includes adjustment for age, sex, ethnicity, deprivation, body mass index, smoking, diabetes, hypertension, high cholesterol, and prior myocardial infarction. Results are odds ratio [95% confidence interval] and p-value, each belonging to a separate logistic regression model with covariate adjustment as indicated in columns. SARS-CoV-2: severe acute respiratory syndrome coronavirus 2.*

7.5 Summary of findings

In this analysis of 310 UK Biobank participants tested for SARS-CoV-2 and prior CMR scanning, we observed association of adverse CMR measures of cardiovascular structure and function with greater odds of subsequent positive SARS-CoV-2 test. In particular, in fully adjusted models, smaller LV and RV end-diastolic volumes, lower stroke volume, and poorer global longitudinal strain were associated with significantly higher odds of SARS-CoV-2 infection. We found no significant associations with measures of arterial compliance (aortic distensibility, ASI) or native T1 and SARS-CoV-2 test result.

7.6 Discussion

7.6.1 Comparison with existing literature

Our study is the first to assess association of pre-existing cardiovascular phenotypes with incident COVID-19. Observational studies of CMR scans performed after recovery from COVID-19 suggest possible indolent cardiovascular involvement. In a study of 100 patients recovered from SARS-CoV-2 infection, Puntmann et al.[232] report larger LV end-diastolic volumes, lower LV and RV ejection fraction, higher native T1, higher T1, and greater proportion of late gadolinium enhancement (LGE) abnormalities (ischaemic: 32% vs 17%, non-ischaemic 20% vs 7%) in the cases compared to controls. Overall, these findings suggest possible persistent myocardial involvement after recovery from COVID-19. However, the frequency of abnormalities reported is higher than would be expected from the cardiac blood biomarkers (5% abnormal troponin at the time of CMR). This suggests that some of the observed differences in CMR metrics may reflect pre-existing cardiac status, rather than ongoing cardiac involvement. Indeed, in our analysis of CMR scans performed on average 3.0 years prior to SARS-CoV-2 testing, we found similar significant associations between measures of poorer LV function (lower LV stroke volume, poorer GLS) and incident COVID-19, after adjustment for demographic and vascular risk factors, demonstrating the potential for residual confounding from other exposures.

Subsequent reports have not confirmed the same degree of post-infection abnormalities as outlined by Puntmann et al.[232]. For example, in a cohort of 40 patients recovered from COVID-19, Li et al.[237] report LGE in only 3% and no difference in volumetric LV or RV metrics compared to controls. They report significantly higher mean global native T1 and ECV, and, in common with our results, poorer LV function by GLS in cases compared to healthy controls. In a study of 26 recovered COVID-19 patients, Huang et al.[234] report no significant difference in LV function or volume metrics between cases and controls. Consistent with Puntmann et al.[232] and Li et al.[237], they report higher native T1 and T2 in cases compared to controls. In our study, we did not document significant association between native T1 and COVID-19 status. It is possible, that we were underpowered to detect a small effect associated with this metric, or that abnormalities in T1 are caused by SARS-CoV-2 infection and thus would not be detected on baseline scans.

In the largest study reported to date, Kotecha et al.[238] compare CMR findings from 148 patients recovered from severe COVID-19 with match controls. They report no significant differences in LV metrics, native T1, or T2 between cases and controls. Although the proportion of participants with LGE was high, this was not significantly different between cases and controls (49% vs 45%). The matching in this study was the most extensive of the studies reported, which may account for the absence of significant difference between the disease and comparator cohorts, which would also

suggest that a substantial proportion of CMR findings reported by other studies reflects residual confounding and reverse causation.

7.6.2 Potential biological mechanisms

COVID-19 in increasingly recognised as a multi-system disease, with high inflammatory burden during the acute illness, which has been proposed as the driver of cardiovascular manifestations during acute COVID-19[216–219]. Acute myocardial injury is frequently observed during acute illness and is linked to poorer outcomes[221,222]. Furthermore, in vitro evidence has suggested that SARS-CoV-2 may directly enter cardiomyocytes leading to toxicity in these cells[226]. Limited autopsy studies have confirmed potential of direct SARS-CoV-2 cardiotoxicity[227].

The evidence for ongoing cardiovascular involvement after recovery from the acute phase of the illness is more contentious. Current evidence is limited to cross-sectional comparisons of CMR from infected and non-infected individuals, without clear corroboration with serum cardiac biomarkers. Given the high burden of cardiovascular disease and vascular risk factors in patients with COVID-19, it is possible that the differences observed in the CMR metrics of these cohorts after recovery from COVID-19 is, at least partly, a reflection of their baseline cardiac status. The absence of baseline imaging data prior to COVID-19 severely limits any causal inference from existing data. Further research, in diverse settings, with longitudinal follow up and repeat imaging are needed to better understand the cardiovascular consequences of COVID-19.

7.7 Critical appraisal of the results

Our findings demonstrate that individuals with unhealthy baseline CMR measures are at higher risk of incident COVID-19. Of course, CMR abnormalities do not appear spontaneously, rather occur as a result of exposure to a risk factor. Thus, the persistence of associations in our study despite adjustment for demographic and classical vascular risk factors indicates that the observed relationships are due to confounding, likely due to a combination of imperfections in measured confounders and the presence of unmeasured confounders (e.g. non-classical vascular risk factors). These observations highlight the high risk of residual confounding and reverse causation in studies using post-infection CMR measures to make inferences about the long-term cardiovascular impact of COVID-19. CMR in our study typically occurred several years prior to COVID-19, obviating the possibility of reverse causation.

Another issue that merits discussion is that of selection bias. Between March to May 2020, SARS-CoV-2 testing in the UK was limited to individuals in a hospital setting. As such, infections identified

in the early months of the pandemic would have been (mostly) in individuals with moderate-severe symptoms requiring hospitalisation. Beyond May 2020, there was extension of testing to community settings; thus, allowing identification of individuals with milder symptoms. Our study includes participants tested between March to August 2020. It is likely that our study sample includes a disproportionate number of individuals with more severe manifestations of COVID-19 identified in the first three months of the study. We cannot be certain that our observations would be generalisable to individuals with mild or asymptomatic infection. With wider availability of testing, the sampling bias from selection into testing will become less problematic. However, it is essential to remain vigilant to such potential sources of bias in epidemiologic and in particular COVID-19 research, whilst also bearing in mind that our methods are limited by the national approach to testing, and additionally in our case, the data available in UK Biobank.

7.8 Conclusions

Our findings, in a predominantly hospitalised cohort, indicate that several pre-existing adverse cardiac phenotypes are linked to higher risk of incident SARS-CoV-2 infection. This suggests that these phenotypes may be risk factors for, rather than a consequence of, SARS-CoV-2 infection. Existing observational studies suggesting cardiovascular involvement after COVID-19 may, in part, reflect residual confounding or reverse causation from baseline cardiac status rather than COVID-19 induced alterations.

Volumetric and ventricular function measures appeared dominant in our analysis, differences in tissue characteristics were more marked in CMR studies after recovery from COVID-19 infection. Therefore, whilst certain unhealthy cardiac phenotypes may pre-dispose to more severe COVID-19 and need for hospitalisation, SARS-CoV-2 infection itself might also lead to distinct phenotypic alterations. Further research in larger populations, with appropriate control groups and ideally imaging before and after COVID-19, together with prospective follow-up, are required for definitive conclusions.

8 Discussion

8.1 Summary of results

We demonstrate, in this series of observational studies from the UK Biobank, the association of several novel cardiovascular risk factors with clinical cardiovascular endpoints and/or CMR phenotypes. We demonstrate that these non-classical risk factors may be of both clinical and biological importance, with evidence of exposure effects extending across organ systems. The observed associations were independent of classical cardiovascular risk factors suggesting that they provide additive information on population cardiovascular risk. In summary, our key findings are as follows:

- Higher resting heart rate is associated with greater all-cause mortality, cardiovascular disease mortality, and cancer mortality for men and women. In men, ischaemic cardiovascular outcomes were a major driver of the excess mortality, whilst in women this was not the case. There was also a modifying effect from age, with greater magnitude of effect in younger ages for the associations with all-cause mortality, cancer mortality, and incident AMI.

- Better cognitive performance (FI, RT) is associated with healthier CMR phenotypes in both men and women. In particular, higher cognition scores were associated with larger ventricular volumes, higher LVM, greater LV stroke volumes, and greater aortic distensibility (AD). These associations remained robust with adjustment for a range of lifestyle, demographic, and cardiometabolic morbidities, suggesting mediation by alternative mechanisms.

- Better bone health (higher SOS) is associated with better vascular health (higher AD, lower ASI). This relationship is consistent for men and women and with menopause status, but with evidence of sex differential disease mechanisms. There was no convincing evidence to suggest differential associations relating to BMI, diabetes, or smoking. Better bone health was also associated with significantly lower risk of IHD mortality in men (and less robustly for women), this relationship was not mediated by the associations between SOS and ASI.

- Greater consumption of red and processed meat is associated with poorer CMR measures of cardiovascular health. In particular, smaller ventricular volumes, lower stroke volume, and lower arterial compliance (AD, ASI), and greater interval increase in large artery stiffness (interval change in ASI). In contrast, greater oily fish intake is associated with larger ventricular volumes, greater stroke volumes, higher LVM, greater arterial compliance (AD,

ASI), and less interval increase in arterial stiffness. The radiomics analysis demonstrated association of the different dietary habits with distinct patterns of ventricular geometry (shape features) and myocardial texture (first-order and texture features), suggesting different patterns of remodelling related to the different dietary exposures.

- Adverse baseline CMR measures are associated with higher risk of incident COVID-19, as per analysis of UK Biobank participants tested for SARS-CoV-2 (mostly in hospital). Smaller ventricular volumes, lower LV stroke volume, and poorer LV GLS were associated with significantly higher risk of positive SARS-CoV-2 test result. This indicates that studies reporting cardiovascular involvement based on imaging after recovery from COVID-19, may in part reflect pre-existing cardiac status, which has predisposed to rather than occurred as a result of COVID-19.

8.2 Strengths and limitations

The large sample size available in the UK Biobank permitted adequately powered analyses for the relationships studied and for stratified analysis by sex and other important factors. The standardised data collection procedures in the UK Biobank permitted reliable ascertainment of exposures and outcomes. Similarly, there was reliable tracking of prospective clinical outcomes recorded in accordance with ICD codes through linkages with HES and death register data for all UK Biobank participants. Imaging in the UK Biobank is also performed using standardised equipment and protocols and presents a very large and uniform image bank, which is ideally suited to epidemiologic research. Furthermore, the detailed characterisation of participants in the UK Biobank allowed investigation of a wide range of exposure-outcome associations, comprehensive confounder adjustment, and consideration of possible mediating variables. The standardised protocols in UK Biobank were extremely helpful in providing a uniform dataset for analysis. However, it also meant that we had no influence into these protocols and research questions had to be designed around the data available with no option to modify or extend protocols.

The observational nature of the studies presented means that we cannot exclude residual confounding due to unmeasured confounders or measurement error. It is particularly challenging to quantify and fully account for the social determinants of health. In our analyses we incorporate the Townsend deprivation score, educational level, and multiple lifestyle factors. However, it is likely that these variables do not fully encompass the socio-economic aspects of health experienced by individuals throughout the life course. Such factors are important across all exposures, but particularly with regards dietary exposures, where certain dietary habits have strong links to social and lifestyle factors (**Section 6**). Furthermore, we express smoking status smoking as a categorical variable. A continuous

measure of this variable, e.g., in smoking pack-years, would have provided more detailed information and likely provided better adjustment. At the time of writing, such more quantitative measures of smoking were not readily available in the UK Biobank. Since writing, derived data from an external group of researchers has been returned to the UK Biobank resource, which includes a cigarette pack year estimate for participants. This continuous measure may provide better quantification of smoking exposure. The usefulness of this estimate merits investigation in future work. There is also likely measurement error with regards other important covariates which may also increase confounding of observed relationships. For example, the cardiometabolic variables are defined according to self-report, ICD classification, and a single biochemistry measure. There is risk of misclassification of disease status with this approach. For example, this approach would overlook individuals who were diagnosed with a chronic health condition after baseline assessment but did not require hospital admission (or the condition was not coded on hospitalisation). In 2019, linked primary care data was released by UK Biobank, which will go some way in addressing these shortcomings. At the time of writing the linked primary care data is in a raw format, and not readily usable for research. Clinical endpoints may be reliably ascertained in UK Biobank, particularly as we selected unambiguous outcomes relating to mortality and AMI. There would be limitations for consideration of clinical outcomes where there is greater uncertainty or subjectivity around the diagnosis (e.g., heart failure) or for conditions that do not always require hospitalisation (e.g. atrial fibrillation).

Consideration of association of exposures with CMR phenotypes provided added insight in delineating the impact of the exposure on different aspects of heart health (e.g. ventricular structure and function, arterial health). Interpretation of associations with CMR phenotypes in the UK Biobank requires special consideration. The significant healthy participant effect in the UK Biobank and the dominance of healthy participants within the CMR subset means that associations of exposures with CMR phenotypes are, almost exclusively, within the spectrum of normality (health). The pattern of associations observed within these limits is different to that seen in clinical cohorts and interpretations should be made with consideration of phenotypic traits in healthy aging (**Table 8.1**).

In general, healthy exposures in UK Biobank are associated with a pattern of CMR phenotypes reflecting decelerated healthy aging. That is, healthy exposures are associated with larger ventricular volumes, higher LV mass, higher stroke volumes, greater AD, and lower ASI (as illustrated in the associations with oily fish intake and cognitive performance). The reverse pattern is seen with unhealthy exposures (smaller ventricular volumes, lower LV mass, lower stroke volume, less compliant arteries). These relationships may be a source of confusion, as for some metrics they are the reverse of what would be considered in a clinical cohort (where most studies of CMR associations originate). A careful approach to selection of CMR metrics is advisable, with preferential selection of measures that have an unambiguous, and preferably linear, trend with aging e.g., stroke volume, ASI,

AD - **Table 8.1**). In addition, these observations present a case for deeper CMR phenotyping, availability of measures such as strain and atrial metrics would be helpful in distinguishing more definitively between health and disease.

The UK Biobank CMR protocol was designed with purpose of providing a detailed, but rapid assessment of cardiac status, whilst minimising health risk to participants. As such, the protocol does not include extensive mapping, administration of contrast, or stress perfusion imaging. These metrics have been particularly implicated in reports of cardiovascular involvement related to COVID-19. Thus, although we can make assertions regarding the association of CMR phenotypes with COVID-19, we cannot directly address questions regarding these tissue characterisation metrics with the UK Biobank dataset.

The UK Biobank imaging visit also includes carotid ultrasonography, which can detect the presence of carotid atheroma. The work presented uses two measures of arterial health, AD derived from CMR and ASI derived from finger plethysmography. These measures of arterial compliance are established validated indicators of cardiovascular (particularly ischaemic) risk. An important strength of the AD and ASI measures is that they provide a continuous measure of arterial health for the whole UK Biobank cohort, regardless of the presence of clinical disease. As such, these measures provide a quantitative indicator of level of risk in individuals with and without disease, which is particularly relevant for population cohorts such as the UK Biobank where the majority of participants do not have clinical disease. The additive value of carotid atheroma as an indicator of clinical cardiovascular outcomes over other measures of arterial health (e.g., AD and ASI) requires formal study. We were unable to conduct such analyses as part of the current work, as results from analysis of the carotid ultrasound in UK Biobank have not yet been made available to researchers.

Table 8.1. Age and sex stratified cardiovascular magnetic resonance indices in the UK Biobank cohort without cardiovascular disease (n=29,801)

	Men			
CMR indices	**≤55 years**	**56-65 years**	**66-75 years**	**≥76 years**
n	**2,633**	**5,143**	**5,624**	**620**
LVEDVi (ml/m^2)	87.7 (±14.0)	84.5 (±13.9)	81.1 (±14.2)	77.8 (±14.4)
LVESVi (ml/m^2)	36.9 [31.8, 42.6]	34.9 [30.0, 40.2]	33.0 [28.3, 38.6]	31.6 [26.60 37.3]
LVSVi (ml/m^2)	50.3 (±8.9)	48.9 (±8.8)	47.0 (±8.8)	45.0 (±8.9)
LVMi (g/m^2)	52.7 (±8.0)	51.5 (±7.7)	50.0 (±7.6)	48.6 (±7.5)
LVEF (%)	57.5 (±5.4)	58.0 (±5.8)	58.1 (±6.3)	58.1 (±6.7)
AA AoD (10^{-3} mmHg^{-1})	2.44 [1.79, 3.22]	1.56 [1.04, 2.17]	0.95 [0.63, 1.38]	0.69 [0.48, 1.05]
PDA AoD (10^{-3} mmHg^{-1})	3.28 [2.62, 4.14]	2.54 [1.95, 3.20]	1.89 [1.43, 2.44]	1.46 [1.13, 1.91]
ASI (unitless)	8.6 (±2.2)	9.8 (±2.7)	10.2 (±2.8)	10.5 (±2.8)
	Women			
CMR indices	**≤55 years**	**56-65 years**	**66-75 years**	**≥76 years**
n	**3,271**	**6,542**	**5,525**	**443**
LVEDVi (ml/m^2)	78.2 (±10.9)	74.4 (±10.6)	71.2 (±10.8)	67.3 (±10.1)
LVESVi (ml/m^2)	30.6 [26.8, 34.8]	28.4 [24.7, 32.6]	26.9 [23.1, 31.1]	25.3 [22.0, 29.3]
LVSVi (ml/m^2)	47.1 (±7.4)	45.4 (±7.3)	43.6 (±7.0)	41.5 (±6.9)
LVMi (g/m^2)	41.0 (±5.7)	40.6 (±5.7)	40.3 (±6.0)	39.3 (±5.8)
LVEF (%)	60.3 (±5.2)	61.2 (±5.4)	61.4 (±5.9)	61.7 (±5.7)
AA AoD (10^{-3} mmHg^{-1})	2.40 [1.67, 3.39]	1.26 [0.79, 1.95]	0.70 [0.48, 1.06]	0.55 [0.38, 0.80]
PDA AoD (10^{-3} mmHg^{-1})	3.28 [2.57, 4.15]	2.31 [1.75, 3.01]	1.58 [1.20, 2.11]	1.20 [0.94, 1.54]
ASI (unitless)	7.5 (±2.3)	8.3 (±2.6)	8.9 (±2.9)	9.2 (±3.0)

Table 8.1. *Results are mean (standard deviation) or median [interquartile range] depending on distribution. For ASI, outliers have been removed as per 1.5 IQR rule. Age is at recorded at time of imaging. Cardiovascular disease reflect status at time of imaging based on criteria outlined in* ***Table 2.3****.*

8.3 Grand discussion

8.4 Implications for clinical practice and research

Current approaches to risk assessment and disease prevention are mostly limited to targeting of classical cardiovascular risk factors. However, the trends in improvements in cardiovascular outcomes are starting to plateau, indicating that alternative approaches are necessary to achieve continued outcome improvements. There is strong support for identification of novel cardiovascular risk factors, often with moderate effect sizes, on which intervention would be worthwhile. Growing evidence indicates complex interconnected relationships between health status in key organ systems. In the present work we describe associations of several novel exposures with cardiovascular health in the UK Biobank. The scale and deep phenotyping in UK Biobank, permitted adequately powered analyses and investigation of several aspects of cardiovascular health.

We investigated, firstly, the sex- age- and disease- specific associations of resting heart rate with incident cardiovascular outcomes, demonstrating its utility as an indicator of all-cause and cardiovascular mortality in both men and women. Associations of resting heart rate with ischaemic cardiovascular outcomes appeared more robust for men than women. Overall, resting heart rate seems to have potential as a low cost and readily accessible indicator of cardiovascular risk. The integration of this resting heart rate as an additional risk measure within current risk stratification tools warrants explorations to determine whether it can truly increment the predictive performance of existing tools.

In the second study, we demonstrated association of better cognitive performance with healthier CMR phenotypes for men and women independent of classical cardiovascular risk factors. This is an important observation. Although there is growing evidence for association of brain and heart health, many previous studies have attributed these links entirely to shared vascular risk factors. Our findings demonstrate that these links are robust to adjustment for a wide range of demographic, lifestyle, and cardiometabolic factors. Therefore, our results indicate the importance of alternative potential mechanism linking heart and brain health, which merit investigation. Better understanding of the connectivity of the heart-brain axis is of huge importance in alleviating the global burden of disease related to both organ systems.

Thirdly, we demonstrated the association between better vascular health (greater arterial compliance) and better bone quality (heel ultrasound), beyond classical cardiovascular risk factors. The observed relationships were consistent across the sexes and in pre- and post- menopause. Findings from previous studies regarding the potential modifying effect of these factors were mixed, and so our findings in the largest sample to address this question to date, provide more definitive conclusions to the existing evidence base. Interestingly, although we observed consistent associations for men and

women, examination of mediating factors suggested that underlying biological mechanisms varied by sex. Understanding these potential common biological mechanisms is key to improvement of health across both cardiovascular and musculoskeletal systems.

In the fourth presented study, we considered association of red and processed meat intake with cardiovascular phenotypes, taking oily fish as a comparator with expected reverse associations. Our findings demonstrate association of higher red and processed meat intake with poorer cardiovascular phenotypes across all metrics considered, whilst greater oily fish consumption was associated with healthier phenotypes. These associations were robust to confounder adjustment. However, additional adjustment for cardiometabolic factors resulted in broad attenuation of the associations between red meat consumption and ventricular phenotypes, whilst associations between red meat and arterial stiffness measures remained robust, as did all associations for processed meat and oily fish intake. It therefore appears, that although both red meat and processed meat are "adverse" dietary exposures, in terms of cardiovascular health, their mechanism of action may be distinct. Similarly, whilst the associations between red meat and ventricular phenotypes may be largely explained by cardiometabolic morbidities, this is not the case for its relationships with arterial health. Indeed, previous studies have indicated distinct mechanism between red meat and ischaemic vascular outcomes (of which arterial stiffness is a reliable indicator) [209]. Our results suggest that exploration of such alternative mechanism is worthwhile. Furthermore, in general, public health advice to limit red and processed meat intake for reasons of cardiovascular health seem sensible. Of course, these findings should be interpreted in the context of other evidence.

Finally, we studied the association of baseline CMR phenotypes with incident SARS-CoV-2 infection in the UK Biobank. We demonstrate, as expected, that individuals with adverse pre-existing cardiovascular phenotypes are at greater risk of subsequent SARS-CoV-2 infection. Our findings are not surprising, given that COVID-19 patients have high burden of cardiovascular disease and risk factors. The observed associations were robust to adjustment for demographic and cardiovascular risk factors, demonstrating the potential for residual confounding from measurement error and other unmeasured exposures. This work was motivated by studies reporting cardiovascular involvement after recovery from COVID-19 based on comparison of CMR studies of infected cases with uninfected controls. Our findings demonstrate the high potential for residual confounding and reverse causation with such approaches and the need for caution in the interpretation of such results.

The results presented here make a meaningful contribution to the scientific literature and may be used in conjunction with other evidence to inform risk stratification and disease prevention approaches and to prioritise research efforts into understanding underlying biology of the demonstrated relationships.

8.5 Future work

In the presented work, we examine the relationships between a range of novel exposures and measures of cardiovascular healthy considering sex-specific associations and potential underlying mechanisms. The observational nature of the presented studies means that we cannot infer causation from the results. Although an experimental approach would not be appropriate for any of our study questions, alternative methods, such as Mendelian Randomisation, may provide added insight into potential causal nature (or otherwise) of the observed associations.

The large sample in the UK Biobank permitted examination of sex-specific associations. However, there was marked variation in the distribution of incident events in men and women. For example, as would be expected in a cohort of predominantly healthy middle-aged women, there were markedly fewer incident ischaemic outcomes for women than men. As such, we may have been underpowered to detect female specific associations for outcomes relating to IHD, particularly where effect sizes were small. For these endpoints, examination of associations in cohorts of older women with higher risk profile would be advisable. The UK Biobank itself may be a useful resource for such analyses as the participants age and incident outcomes accrue. Furthermore, the relationships reported in this project, for both men and women, represent, associations within the range of healthy populations. Thus, the reported patten of associations may not be directly applicable to clinical cohorts. Examination of these associations in disease cohorts may provide novel insights into the observed relationships and how they may be altered with the onset of disease.

Finally, and importantly, despite consideration of a wide range of potential mediators, it was highly challenging to delineate underlying biological mechanisms for the observed associations. This reflects the complexity of elucidating such mechanistic pathways and making specific links to disease processes. Our findings provide useful hypothesis for biological (and perhaps genetic) studies into underlying mechanisms of observed associations. For instance, there is potential to elucidate mechanistic links between resting heart rate and incident cardiovascular events, through incorporation of brain MRI phenotypes in future work. Such work is highly important for understanding the underlying biology and identification of novel therapeutic targets for disease prevention or treatment.

8.6 Conclusions

In this doctoral thesis, we characterise the relationships between cardiovascular health and several novel disease exposures acting across different organ systems (heart, brain, gut, bone). We demonstrate the value of a multi-system approach to understanding cardiovascular health and the importance of cross-system interactions in disease occurrence and progression. We further illustrate the utility of population level CMR data to gain added insights into such relationships and describe

and illustrate the use of deeper cardiovascular phenotyping using CMR radiomics. Our findings suggests that the search for such novel disease determinants is worthwhile and may be key in alleviating the global burden of cardiovascular disease.

9 References

1. Ten Great Public Health Achievements - United States, 1900-1999. *MMWR Morb Mortal Wkly Rep* 1999;**48**:241–243.
2. Fenner F, Henderson D, Arita I, Jezek Z, Ladnyi I. Smallpox and its eradication. Geneva; 1988.
3. The History of the NHS. https://wellcomecollection.org/series/WyjG4ycAACrGnmBX?utm_source=Google&utm_medium=adgrant&utm_campaign=history_nhs&gclid=EAIaIQobChMI5e7z1oDc6gIVh6ztCh0xmwmqEAAYAyAAEgIhYPD_BwE (20 July 2020)
4. Fielding JE. Public Health in the twentieth Century: Advances and Challenges. *Annu Rev Public Health* 1999;**20**:xiii–xxx.
5. Achievements in Public Health, 1900-1999: Changes in the Public Health. *J Am Med Assoc* 2000;**283**:735–738.
6. Mahmood SS, Levy D, Vasan RS, Wang TJ. The Framingham Heart Study and the epidemiology of cardiovascular disease: A historical perspective. *Lancet* 2014;**383**:999–1008.
7. United States Department of Health and Human Services. The Health Consequences of Smoking—50 Years of Progress A Report of the Surgeon General. *A Rep Surg Gen* 2014;1081.
8. Roth GA, Abate D, Hassen Abate K, Abay SM, Abbafati C, Abbasi N, Abbastabar H, Abd-Allah F, Abdela J, Abdelalim A, Abdollahpour I, Suliankatchi Abdulkader R, Temesgen Abebe H, Abebe M, Abebe Z, Negesse Abejie A, Abera SF, Zewdie Abil O, Niguse Abraha H, Roba Abrham A, Jamal Abu-Raddad L, Mario Kokou Accrombessi M, Acharya D, Adamu AA, Adebayo OM, Adesoji Adedoyin R, Adekanmbi V, Adetokunboh OO, Meressa Adhena B, Adib MG, et al. Global, regional, and national age-sex-specific mortality for 282 causes of death in 195 countries and territories, 1980-2017: a systematic analysis for the Global Burden of Disease Study 2017 GBD 2017 Causes of Death Collaborators*. *Lancet* 2018;**392**:1736–1788.
9. Townsend N, Wilson L, Bhatnagar P, Wickramasinghe K, Rayner M, Nichols M. Cardiovascular disease in Europe: Epidemiological update 2016. *Eur Heart J* 2016;**37**:3232–3245.
10. Heart statistics - Heart and Circulatory Diseases in the UK | BHF. https://www.bhf.org.uk/what-we-do/our-research/heart-statistics (18 April 2021)
11. Wilmot KA, O'Flaherty M, Capewell S, Ford ES, Vaccarino V. Coronary heart disease mortality declines in the United States from 1979 through 2011: Evidence for stagnation in young adults, especially women. *Circulation* 2015;**132**:997–1002.
12. Garcia M, Mulvagh SL, Merz CNB, Buring JE, Manson JAE. Cardiovascular disease in

women: Clinical perspectives. *Circ Res* 2016;**118**:1273–1293.

13. Kannel WB. The Framingham Study: Its 50-year legacy and future promise. *J Atheroscler Thromb* 2000;**6**:60–66.
14. Banegas JR, López-García E, Dallongeville J, Guallar E, Halcox JP, Borghi C, Massó-González EL, Jiménez FJ, Perk J, Steg PG, Backer G De, Rodríguez-Artalejo F. Achievement of treatment goals for primary prevention of cardiovascular disease in clinical practice across Europe: The EURIKA study. *Eur Heart J* 2011;**32**:2143–2152.
15. Barabási AL. Network Medicine — From Obesity to the " Diseasome ". *N Engl J Med* 2007;**357**:404–407.
16. Lefkowitz RJ, Willerson JT. Prospects for cardiovascular research. *J Am Med Assoc* 2001;**285**:581–587.
17. Rothman KJ, Greenland S, Lash TL. Modern Epidemiology. 3rd ed. Lippincott Williams & Wilkins; 2008.
18. Javier Nieto F. Cardiovascular disease and risk factor epidemiology: A look back at the epidemic of the 20th century. *Am J Public Health* 1999;**89**:292–294.
19. Coggon D, Rose G, Barker D. Epidemiology for the uninitiated. 5th ed. BMJ Books; 2003.
20. Davey Smith G, Phillips AN. Confounding in epidemiological studies: Why 'independent' effects may not be all they seem. *Br Med J* 1992;**305**:757–759.
21. Deaton A, Cartwright N. Understanding and misunderstanding randomized controlled trials. *Soc Sci Med* 2018;**210**:2–21.
22. Morgan S, Winship C. Counterfactuals and Causal Inference: Methods And Principles For Social Research. 2nd ed. Cambridge University Press; 2014.
23. Pearl J. Structural counterfactuals: A brief introduction. *Cogn Sci* 2013;**37**:977–985.
24. Greenland S, Pearl J, Robins JM. Causal diagrams for epidemiologic research. *Epidemiology* 1999;**10**:37–48.
25. Tennant PW, Harrison W, Murray E, Arnold K, Berrie L, Fox M, Gadd S, Keeble C, Ranker L, Textor J, Tomova G, Gilthorpe M, Ellison GT. Use of directed acyclic graphs (DAGs) in applied health research: review and recommendations. 2020;50:620-632.
26. Krieger N, Smith GD. The tale wagged by the DAG: Broadening the scope of causal inference and explanation for epidemiology. *Int J Epidemiol* 2016;**45**:1787–1808.
27. Lawlor DA, Tilling K, Smith GD. Triangulation in aetiological epidemiology. *Int J Epidemiol* 2016;**45**:1866–1886.
28. Smith GD, Ebrahim S. Epidemiology - Is it time to call it a day? *Int J Epidemiol* 2001;**30**:1–11.
29. Lombardi M, Plein S, Petersen S, Bucciarelli-Ducci C, Buechel EV, Basso C, Ferrari V, eds. The EACVI Textbook of Cardiovascular Magnetic Resonance. EACVI Textb. Cardiovasc. Magn. Reson. Oxford University Press; 2018.

30. Kramer CM, Barkhausen J, Flamm SD, Kim RJ, Nagel E. Standardized cardiovascular magnetic resonance (CMR) protocols 2013 update. *J Cardiovasc Magn Reson* 2013;15:91.
31. Knobelsdorff-Brenkenhoff F Von, Schulz-Menger J. Role of cardiovascular magnetic resonance in the guidelines of the European Society of Cardiology. *J Cardiovasc Magn Reson* 2016;**18**:1–18.
32. Knobelsdorff-Brenkenhoff F Von, Pilz G, Schulz-Menger J. Representation of cardiovascular magnetic resonance in the AHA / ACC guidelines. *J Cardiovasc Magn Reson* 2017;**19**:1–21.
33. Beyer SE, Petersen SE. Advances in population-based imaging using cardiac magnetic resonance. *Prog Biomed Eng* 2019;**1**:012003.
34. Bild DE, Bluemke DA, Burke GL, Detrano R, Diez Roux A V., Folsom AR, Greenland P, Jacobs DR, Kronmal R, Liu K, Nelson JC, O'Leary D, Saad MF, Shea S, Szklo M, Tracy RP. Multi-Ethnic Study of Atherosclerosis: Objectives and design. *Am J Epidemiol* 2002;**156**:871–881.
35. Salton CJ, Chuang ML, O'Donnell CJ, Kupka MJ, Larson MG, Kissinger K V., Edelman RR, Levy D, Manning WJ. Gender differences and normal left ventricular anatomy in an adult population free of hypertension: A cardiovascular magnetic resonance study of the Framingham Heart Study Offspring cohort. *J Am Coll Cardiol* 2002;**39**:1055–1060.
36. Petersen SE, Matthews PM, Francis JM, Robson MD, Zemrak F, Boubertakh R, Young AA, Hudson S, Weale P, Garratt S, Collins R, Piechnik S, Neubauer S. UK Biobank's cardiovascular magnetic resonance protocol. *J Cardiovasc Magn Reson* 2015;**18**:8.
37. Baumgartner H, Falk V, Bax JJ, Bonis M De, Hamm C, Holm PJ, Iung B, Lancellotti P, Lansac E, Muñoz DR, Rosenhek R, Sjögren J, Tornos Mas P, Vahanian A, Walther T, Wendler O, Windecker S, Zamorano JL, Roffi M, Alfieri O, Agewall S, Ahlsson A, Barbato E, Bueno H, Collet JP, Coman IM, Czerny M, Delgado V, Fitzsimons D, Folliguet T, et al. 2017 ESC/EACTS Guidelines for the management of valvular heart disease. *Eur Heart J* 2017;**38**:2739–2786.
38. Nishimura RA, Otto CM, Bonow RO, Carabello BA, Erwin JP, Fleisher LA, Jneid H, Mack MJ, McLeod CJ, O'Gara PT, Rigolin VH, Sundt TM, Thompson A. 2017 AHA/ACC Focused Update of the 2014 AHA/ACC Guideline for the Management of Patients With Valvular Heart Disease: A Report of the American College of Cardiology/American Heart Association Task Force on Clinical Practice Guidelines. *J Am Coll Cardiol* 2017;**70**:252–289.
39. Moss AJ, Zareba W, Jackson Hall W, Klein H, Wilber DJ, Cannom DS, Daubert JP, Higgins SL, Brown MW, Andrews ML. Prophylactic implantation of a defibrillator in patients with myocardial infarction and reduced ejection fraction. *N Engl J Med* 2002;**346**:877–883.
40. Stecker EC, Vickers C, Waltz J, Socoteanu C, John BT, Mariani R, McAnulty JH, Gunson K, Jui J, Chugh SS. Population-based analysis of sudden cardiac death with and without left ventricular systolic dysfunction: Two-year findings from the Oregon sudden unexpected death

study. *J Am Coll Cardiol* 2006;**47**:1161–1166.

41. Littlejohns TJ, Sudlow C, Allen NE, Collins R. UK Biobank: Opportunities for cardiovascular research. *Eur Heart J* 2019;**40**:1158–1166.
42. UK Biobank Coordinating Centre. UK Biobank: Protocol for a large-scale prospective epidemiological resource. UKBB-PROT-09-06 (Main Phase). 2007.
43. UK Biobank. https://www.ukbiobank.ac.uk/ (15 November 2019)
44. UK Biobank Imaging Study. https://imaging.ukbiobank.ac.uk/ (15 November 2019)
45. Schnier C, Sudlow Biobank CU. Algorithmically-defined health outcomes (Chief Scientist), with input from members of the UK Biobank Follow-up and Outcomes Adjudication Group. 2017. https://biobank.ctsu.ox.ac.uk/crystal/crystal/docs/alg_outcome_main.pdf (27 March 2020)
46. Manolio TA, Collins R. Enhancing the feasibility of large cohort studies. *JAMA* 2010;**304**:2290–2291.
47. Batty GD, Gale CR, Kivimäki M, Deary IJ, Bell S. Comparison of risk factor associations in UK Biobank against representative, general population based studies with conventional response rates: prospective cohort study and individual participant meta-analysis. *BMJ* 2020;**368**:1–8.
48. Fry A, Littlejohns TJ, Sudlow C, Doherty N, Adamska L, Sprosen T, Collins R, Allen NE. Comparison of Sociodemographic and Health-Related Characteristics of UK Biobank Participants With Those of the General Population. *Am J Epidemiol* 2017;**186**:1026–1034.
49. Raisi-Estabragh Z, Harvey NC, Neubauer S, Petersen SE. Cardiovascular magnetic resonance imaging in the UK Biobank: a major international health research resource. *Eur Hear J - Cardiovasc Imaging* 2021;**22**:251–258.
50. Gjesdal O, Bluemke DA, Lima JA. Cardiac remodeling at the population level—risk factors, screening, and outcomes. *Nat Rev Cardiol* 2011;**8**:673–685.
51. Bluemke DA, Kronmal RA, Lima JAC, Liu K, Olson J, Burke GL, Folsom AR. The Relationship of Left Ventricular Mass and Geometry to Incident Cardiovascular Events. *J Am Coll Cardiol* 2008;**52**:2148–2155.
52. Curtis JP, Sokol SI, Wang Y, Rathore SS, Ko DT, Jadbabaie F, Portnay EL, Marshalko SJ, Radford MJ, Krumholz HM. The association of left ventricular ejection fraction, mortality, and cause of death in stable outpatients with heart failure. *J Am Coll Cardiol* 2003;**42**:736–742.
53. Buss SJ, Breuninger K, Lehrke S, Voss A, Galuschky C, Lossnitzer D, Andre F, Ehlermann P, Franke J, Taeger T, Frankenstein L, Steen H, Meder B, Giannitsis E, Katus HA, Korosoglou G. Assessment of myocardial deformation with cardiac magnetic resonance strain imaging improves risk stratification in patients with dilated cardiomyopathy. *Eur Hear J – Cardiovasc Imaging* 2015;**16**:307–315.

54. Delgado V, Tops LF, Bommel RJ van, Kley F van der, Marsan NA, Klautz RJ, Versteegh MIM, Holman ER, Schalij MJ, Bax JJ. Strain analysis in patients with severe aortic stenosis and preserved left ventricular ejection fraction undergoing surgical valve replacement. *Eur Heart J* 2009;**30**:3037–3047.
55. Claus P, Omar AMS, Pedrizzetti G, Sengupta PP, Nagel E. Tissue Tracking Technology for Assessing Cardiac Mechanics: Principles, Normal Values, and Clinical Applications. *JACC Cardiovasc Imaging* 2015;**8**:1444–1460.
56. Haaf P, Garg P, Messroghli DR, Broadbent DA, Greenwood JP, Plein S. Cardiac T1 Mapping and Extracellular Volume (ECV) in clinical practice: A comprehensive review. *J Cardiovasc Magn Reson* 2016;**18**:89.
57. Resnick LM, Militianu D, Cunnings AJ, Pipe JG, Evelhoch JL, Soulen RL. Direct Magnetic Resonance Determination of Aortic Distensibility in Essential Hypertension. *Hypertension* 1997;**30**:654–659.
58. Laurent S, Cockcroft J, Bortel L Van, Boutouyrie P, Giannattasio C, Hayoz D, Pannier B, Vlachopoulos C, Wilkinson I, Struijker-Boudier H. Expert consensus document on arterial stiffness: Methodological issues and clinical applications. *Eur Heart J* 2006;**27**:2588–2605.
59. Abdullah Said M, Eppinga RN, Lipsic E, Verweij N, Harst P van der. Relationship of arterial stiffness index and pulse pressure with cardiovascular disease and mortality. *J Am Heart Assoc* 2018;**7**:e007621.
60. Petersen SE, Aung N, Sanghvi MM, Zemrak F, Fung K, Paiva JM, Francis JM, Khanji MY, Lukaschuk E, Lee AM, Carapella V, Kim YJ, Leeson P, Piechnik SK, Neubauer S. Reference ranges for cardiac structure and function using cardiovascular magnetic resonance (CMR) in Caucasians from the UK Biobank population cohort. *J Cardiovasc Magn Reson* 2017;**19**:18.
61. Bai W, Sinclair M, Tarroni G, Oktay O, Rajchl M, Vaillant G, Lee AM, Aung N, Lukaschuk E, Sanghvi MM, Zemrak F, Fung K, Paiva JM, Carapella V, Kim YJ, Suzuki H, Kainz B, Matthews PM, Petersen SE, Piechnik SK, Neubauer S, Glocker B, Rueckert D. Automated cardiovascular magnetic resonance image analysis with fully convolutional networks. *J Cardiovasc Magn Reson* 2018;**20**:65.
62. Attar R, Pereañez M, Gooya A, Albà X, Zhang L, Vila MH de, Lee AM, Aung N, Lukaschuk E, Sanghvi MM, Fung K, Paiva JM, Piechnik SK, Neubauer S, Petersen SE, Frangi AF. Quantitative CMR population imaging on 20,000 subjects of the UK Biobank imaging study: LV/RV quantification pipeline and its evaluation. *Med Image Anal* 2019;**56**:26–42.
63. Biasiolli L, Hann E, Lukaschuk E, Carapella V, Paiva JM, Aung N, Rayner JJ, Werys K, Fung K, Puchta H, Sanghvi MM, Moon NO, Thomson RJ, Thomas KE, Robson MD, Grau V, Petersen SE, Neubauer S, Piechnik SK. Automated localization and quality control of the aorta in cine CMR can significantly accelerate processing of the UK Biobank population data. *PLoS One* 2019;**14**:e0212272.

64. Townsend P, Phillimore P, Beattie A. Health and Deprivation: Inequality and the North. *Nurs Stand* 1988;**2**:34–34.
65. Craig CL, Marshall AL, Sjöström M, Bauman AE, Booth ML, Ainsworth BE, Pratt M, Ekelund U, Yngve A, Sallis JF, Oja P. International physical activity questionnaire: 12-country reliability and validity. *Med Sci Sports Exerc* 2003;**35**:1381–1395.
66. Schnier C, Bush K, Nolan J, Sudlow C. Definitions of Acute Myocardial Infarction and Main Myocardial Infarction Pathological Types UK Biobank Phase 1 Outcomes Adjudication Documentation on behalf of UK Biobank Outcome Adjudication Group Definitions of Acute Myocardial Infarction. 2017. http://biobank.ndph.ox.ac.uk/showcase/showcase/docs/alg_outcome_mi.pdf
67. Fine JP, Gray RJ. A Proportional Hazards Model for the Subdistribution of a Competing Risk. *J Am Stat Assoc* 1999;**94**:496–509.
68. Pannier BM, Avolio AP, Hoeks A, Mancia G, Takazawa K. Methods and devices for measuring arterial compliance in humans. *Am J Hypertens* 2002;**15**:743–753.
69. Raisi-Estabragh Z, Biasiolli L, Cooper J, Aung N, Fung K, Paiva JM, Sanghvi MM, Thomson RJ, Curtis E, Paccou J, Rayner JJ, Werys K, Puchta H, Thomas KE, Lee AM, Piechnik SK, Neubauer S, Munroe PB, Cooper C, Petersen SE, Harvey NC, Raisi-Estabragh Z, Biasiolli L, Cooper J, Aung N, Fung K, Paiva JM, Sanghvi MM, Thomson RJ, Curtis E, et al. Poor Bone Quality is Associated With Greater Arterial Stiffness: Insights From the UK Biobank. *J Bone Miner Res* 2020;**36**:90–99.
70. UK Biobank Arterial Pulse-Wave Velocity. 2011.
71. Raisi-Estabragh Z, Izquierdo C, Campello VM, Martin-Isla C, Jaggi A, Harvey NC, Lekadir K, Petersen SE. Cardiac magnetic resonance radiomics: basic principles and clinical perspectives. *Eur Hear J - Cardiovasc Imaging* 2020;**21**:349–356.
72. Wibmer A, Hricak H, Gondo T, Matsumoto K, Veeraraghavan H, Fehr D, Zheng J, Goldman D, Moskowitz C, Fine SW, Reuter VE, Eastham J, Sala E, Vargas HA. Haralick texture analysis of prostate MRI: utility for differentiating non-cancerous prostate from prostate cancer and differentiating prostate cancers with different Gleason scores. *Eur Radiol* 2015;**25**:2840–2850.
73. Ahmed A, Gibbs P, Pickles M, Turnbull L. Texture analysis in assessment and prediction of chemotherapy response in breast cancer. *J Magn Reson Imaging* 2013;**38**:89–101.
74. Coroller TP, Agrawal V, Huynh E, Narayan V, Lee SW, Mak RH, Aerts HJWL. Radiomic-Based Pathological Response Prediction from Primary Tumors and Lymph Nodes in NSCLC. *J Thorac Oncol* 2017;**12**:467–476.
75. Coroller TP, Grossmann P, Hou Y, Rios Velazquez E, Leijenaar RTH, Hermann G, Lambin P, Haibe-Kains B, Mak RH, Aerts HJWL. CT-based radiomic signature predicts distant metastasis in lung adenocarcinoma. *Radiother Oncol* 2015;**114**:345–350.

76. Pinamonti B, Picano E, Ferdeghini EM, Lattanzi F, Slavich G, Landini L, Camerini F, Benassi A, Distante A, L'Abbate A. Quantitative texture analysis in two-dimensional echocardiography: Application to the diagnosis of myocardial amyloidosis. *J Am Coll Cardiol* 1989;**14**:666–671.
77. Lattanzi F, Bellotti P, Picano E, Chiarella F, Paterni M, Forni G, Landini L, Distante A, Vecchio C. Quantitative texture analysis in two-dimensional echocardiography: Application to the diagnosis of myocardial hemochromatosis. *Echocardiography* 1996;**13**:9–20.
78. Kolossváry M, Kellermayer M, Merkely B, Maurovich-Horvat P. Cardiac Computed Tomography Radiomics. *J Thorac Imaging* 2018;**33**:26–34.
79. Oikonomou EK, Williams MC, Kotanidis CP, Desai MY, Marwan M, Antonopoulos AS, Thomas KE, Thomas S, Akoumianakis I, Fan LM, Kesavan S, Herdman L, Alashi A, Centeno EH, Lyasheva M, Griffin BP, Flamm SD, Shirodaria C, Sabharwal N, Kelion A, Dweck MR, Beek EJR Van, Deanfield J, Hopewell JC, Neubauer S, Channon KM, Achenbach S, Newby DE, Antoniades C. A novel machine learning-derived radiotranscriptomic signature of perivascular fat improves cardiac risk prediction using coronary CT angiography. *Eur Heart J* 2019;**40**:3529–3543.
80. Baeßler B, Mannil M, Maintz D, Alkadhi H, Manka R. Texture analysis and machine learning of non-contrast T1-weighted MR images in patients with hypertrophic cardiomyopathy—Preliminary results. *Eur J Radiol* 2018;**102**:61–67.
81. Cetin I, Petersen SE, Napel S. A radiomics approach to analyze cardiac alterations in hypertension. *IEEE International Symposium on Biomedical Imaging (ISBI)* 2019.
82. Cetin I, Raisi-Estabragh Z, Petersen SE, Napel S, Piechnik SK, Neubauer S, Gonzalez Ballester MA, Camara O, Lekadir K. Radiomics Signatures of Cardiovascular Risk Factors in Cardiac MRI: Results From the UK Biobank. *Front Cardiovasc Med* 2020;**7**:591368.
83. Neisius U, El-Rewaidy H, Nakamori S, Rodriguez J, Manning WJ, Nezafat R. Radiomic Analysis of Myocardial Native T1 Imaging Discriminates Between Hypertensive Heart Disease and Hypertrophic Cardiomyopathy. *JACC Cardiovasc Imaging* 2019;1–9.
84. Baessler B, Luecke C, Lurz J, Klingel K, Roeder M von, Waha S de, Besler C, Maintz D, Gutberlet M, Thiele H, Lurz P. Cardiac MRI Texture Analysis of T1 and T2 Maps in Patients with Infarctlike Acute Myocarditis. *Radiology* 2018;**289**:357–365.
85. Baessler B, Mannil M, Oebel S, Maintz D, Alkadhi H, Manka R. Subacute and Chronic Left Ventricular Myocardial Scar: Accuracy of Texture Analysis on Nonenhanced Cine MR Images. *Radiology* 2018;**286**:103–112.
86. Larroza A, Materka A, López-Lereu MP, Monmeneu J V., Bodí V, Moratal D. Texture analysis of cardiac cine magnetic resonance imaging to detect non-viable segments in patients with chronic myocardial infarction. *Med Phys* 2018;**45**:1471–1480.
87. Larroza A, Materka A, López-Lereu MP, Monmeneu J V., Bodí V, Moratal D. Differentiation

between acute and chronic myocardial infarction by means of texture analysis of late gadolinium enhancement and cine cardiac magnetic resonance imaging. *Eur J Radiol* 2017;**92**:78–83.

88. Kotu LP, Engan K, Borhani R, Katsaggelos AK, Ørn S, Woie L, Eftestøl T. Cardiac magnetic resonance image-based classification of the risk of arrhythmias in post-myocardial infarction patients. *Artif Intell Med* 2015;**64**:205–215.
89. Cheng S, Fang M, Cui C, Chen X, Yin G, Prasad SK, Dong D, Tian J, Zhao S. LGE-CMR-derived texture features reflect poor prognosis in hypertrophic cardiomyopathy patients with systolic dysfunction: preliminary results. *Eur Radiol* 2018;**28**:4615–4624.
90. Griethuysen JJM Van, Fedorov A, Parmar C, Hosny A, Aucoin N, Narayan V, Beets-Tan RGH, Fillion-Robin JC, Pieper S, Aerts HJWL. Computational radiomics system to decode the radiographic phenotype. *Cancer Res* 2017;**77**:e104–e107.
91. Freeman J. The modelling of spatial relations. *Comput Graph Image Process* 1975;**4**:156–171.
92. Chu A, Sehgal CM, Greenleaf JF. Use of gray value distribution of run lengths for texture analysis. *Pattern Recognit Lett* 1990;**11**:415–419.
93. Haralick RM, Shanmugam K, Dinstein I, Shanmugam K. Textural Features for Image Classification. *IEEE Trans Syst Man Cybern* 1973;**SMC-3**:610–621.
94. Galloway MM. Texture analysis using gray level run lengths. *Comput Graph Image Process* 1975;**4**:172–179.
95. Tustison N, Gee JC. Run-Length Matrices For Texture Analysis. *Insight J* 2008;
96. Tang X. Texture information in run-length matrices. *IEEE Trans Image Process* 1998;**7**:1602–1609.
97. Xu D, Xu D, Kurani AS, Furst JD, Raicu DS. Run-length Encoding for Volumetric Texture. *4TH IASTED Int Conf Vis IMAGING, IMAGE Process* 2004;
98. Jang J, Ngo LH, Mancio J, Kucukseymen S, Rodriguez J, Pierce P, Goddu B, Nezafat R. Reproducibility of Segmentation-based Myocardial Radiomic Features with Cardiac MRI. *Radiol Cardiothorac Imaging* Radiological Society of North America (RSNA); 2020;**2**:e190216.
99. Raisi-Estabragh Z, Gkontra P, Jaggi A, Cooper J, Augusto J, Bhuva AN, Davies RH, Manisty CH, Moon JC, Munroe PB, Harvey NC, Lekadir K, Petersen SE. Repeatability of Cardiac Magnetic Resonance Radiomics: A Multi-Centre Multi-Vendor Test-Retest Study. *Front Cardiovasc Med* 2020;**7**:1–16.
100. Cetin I, Petersen SE, Napel S, Camara O, Ballester MAG, Lekadir K. A radiomics approach to analyse cardiac alterations in hypertension. *Int Symp Biomed Imaging* 2019;640–643.
101. Gulani V, Calamante F, Shellock FG, Kanal E, Reeder SB. Gadolinium deposition in the brain: summary of evidence and recommendations. *Lancet Neurol* 2017;16:564–570.
102. Amano Y, Suzuki Y, Yanagisawa F, Omori Y, Matsumoto N. Relationship between Extension

or Texture Features of Late Gadolinium Enhancement and Ventricular Tachyarrhythmias in Hypertrophic Cardiomyopathy. *Biomed Res Int* 2018;**2018**:4092469.

103. Aerts HJWL, Velazquez ER, Leijenaar RTH, Parmar C, Grossmann P, Carvalho S, Bussink J, Monshouwer R, Haibe-Kains B, Rietveld D, Hoebers F, Rietbergen MM, Leemans CR, Dekker A, Quackenbush J, Gillies RJ, Lambin P. Decoding tumour phenotype by noninvasive imaging using a quantitative radiomics approach. *Nat Commun* 2014;**5**:4006.
104. Diaz A, Bourassa MG, Guertin M-C, Tardif J-C. Long-term prognostic value of resting heart rate in patients with suspected or proven coronary artery disease. *Eur Heart J* 2005;**26**:967–974.
105. Custodis F, Roggenbuck U, Lehmann N, Moebus S, Laufs U, Mahabadi A-A, Heusch G, Mann K, Jöckel K-H, Erbel R, Böhm M, Möhlenkamp S, Möhlenkamp stefanmoehlenkamp S. Resting heart rate is an independent predictor of all-cause mortality in the middle aged general population. *Clin Res Cardiol* 2016;**105**:601–612.
106. Sharashova E, Wilsgaard T, Mathiesen EB, Løchen M-L, Njølstad I, Brenn T. Resting heart rate predicts incident myocardial infarction, atrial fibrillation, ischaemic stroke and death in the general population: the Tromsø Study. *J Epidemiol Community Health* 2016;**70**:902–909.
107. Zhang D, Shen X, Qi X. Resting heart rate and all-cause and cardiovascular mortality in the general population: a meta-analysis. *CMAJ* 2016;**188**:E53–E63.
108. Aune D, Sen A, ó'Hartaigh B, Janszky I, Romundstad PR, Tonstad S, Vatten LJ. Resting heart rate and the risk of cardiovascular disease, total cancer, and all-cause mortality – A systematic review and dose–response meta-analysis of prospective studies. *Nutr Metab Cardiovasc Dis* 2017;**27**:504–517.
109. Gillum RF, Makuc DM, Feldman JJ. Pulse rate, coronary heart disease, and death: the NHANES I Epidemiologic Follow-up Study. *Am Heart J* 1991;**121**:172–177.
110. Goldberg RJ, Larson M, Levy D. Factors Associated With Survival to 75 Years of Age in Middle-aged Men and Women. *Arch Intern Med* 1996;**156**:505.
111. Greenland P, Daviglus ML, Dyer AR, Liu K, Huang C-F, Goldberger JJ, Stamler J. Resting Heart Rate is a Risk Factor for Cardiovascular and Noncardiovascular Mortality. *Am J Epidemiol* 1999;**149**:853–862.
112. Benetos A, Rudnichi A, Thomas F, Safar M, Guize L. Influence of heart rate on mortality in a French population: role of age, gender, and blood pressure. *Hypertens* 1999;**33**:44–52.
113. Tverdal A, Hjellvik V, Selmer R. Heart rate and mortality from cardiovascular causes: a 12 year follow-up study of 379 843 men and women aged 40-45 years. *Eur Heart J* 2008;**29**:2772–2781.
114. Chen X, Barywani SB, Hansson P-O, Östgärd Thunström E, Rosengren A, Ergatoudes C, Mandalenakis Z, Caidahl K, Fu ML. Impact of changes in heart rate with age on all-cause death and cardiovascular events in 50-year-old men from the general population. *Open Hear*

2019;**6**:e000856.

115. Jensen MT, Suadicani P, Hein HO, Gyntelberg F. Elevated resting heart rate, physical fitness and all-cause mortality: a 16-year follow-up in the Copenhagen Male Study. *Heart* 2013;**99**:882–887.
116. Kristal-Boneh E, Silber H, Harari G, Froom P. The association of resting heart rate with cardiovascular, cancer and all-cause mortality. Eight year follow-up of 3527 male Israeli employees (the CORDIS Study). *Eur Heart J* 2000;**21**:116–124.
117. Li K, Yao C, Yang X, Dong L. Effect of Resting Heart Rate on All-Cause Mortality and Cardiovascular Events According to Age. *J Am Geriatr Soc* 2017;**65**:989–994.
118. Woodward M, Webster R, Murakami Y, Barzi F, Lam T-HH, Fang X, Suh I, Batty GD, Huxley R, Rodgers A, from the Asia Pacific Cohort Studies Collaboration. The association between resting heart rate, cardiovascular disease and mortality: Evidence from 112,680 men and women in 12 cohorts. *Eur J Prev Cardiol* 2014;**21**:719–726.
119. Kannel WB, Kannel C, Paffenbarger Jr RS. Heart rate and cardiovascular mortality: The Framingham study. *Am Heart J* 1987;**113**:1489–1494.
120. UK Biobank Blood Pressure. 2011.
121. Hsia J, Larson JC, Ockene JK, Sarto GE, Allison MA, Hendrix SL, Robinson JG, LaCroix AZ, Manson JE. Resting heart rate as a low tech predictor of coronary events in women: Prospective cohort study. *BMJ* 2009;**338**:577–579.
122. Cooney MT, Vartiainen E, Laakitainen T, Juolevi A, Dudina A, Graham IM. Elevated resting heart rate is an independent risk factor for cardiovascular disease in healthy men and women. *Am Heart J* 2010;**159**:612-619.e3.
123. Palatini P. Elevated Heart Rate in Cardiovascular Diseases: A Target for Treatment? *Prog Cardiovasc Dis* 2009;**52**:46–60.
124. Fox K, Borer JS, Camm AJ, Danchin N, Ferrari R, Lopez Sendon JL, Steg PG, Tardif J-C, Tavazzi L, Tendera M. Resting Heart Rate in Cardiovascular Disease. *J Am Coll Cardiol* 2007;**50**:823–830.
125. Palatini P. Heart rate and the cardiometabolic risk. *Curr Hypertens Rep* 2013;**15**:253–259.
126. He W, Goodkind D, Kowal P. International Federation on Aging, An Aging World: 2015. 2016. https://ifa.ngo/publication/demographics/aging-world-2015/ (28 January 2020)
127. Dementia a public health priority. World Health Organisation. 2012. ISBN 978 92 4 156445 8
128. Martin Prince A, Wimo A, Guerchet M, Gemma-Claire Ali M, Wu Y-T, Prina M, Yee Chan K, Xia Z. World Alzheimer Report 2015 The Global Impact of Dementia an Analysis of prevalence, Incidence, cost and Trends. 2015.
129. Fineberg NA, Haddad PM, Carpenter L, Gannon B, Sharpe R, Young AH, Joyce E, Rowe J, Wellsted D, Nutt DJ, Sahakian BJ. The size, burden and cost of disorders of the brain in the UK. *J Psychopharmacol* 2013;**27**:761–770.

130. Brookmeyer R, Johnson E, Ziegler-Graham K, Arrighi HM. Forecasting the global burden of Alzheimer's disease. *Alzheimer's Dement* 2007;**3**:186–191.
131. Qiu C, Fratiglioni L. A major role for cardiovascular burden in age-related cognitive decline. *Nat Rev Cardiol* 2015;**12**:267–277.
132. Knopman D, Boland LL, Mosley T, Howard G, Liao D, Szklo M, McGovern P, Folsom AR. Cardiovascular risk factors and cognitive decline in middle-aged adults. *Neurology* 2001;**56**:42–48.
133. Mielke MM, Rosenberg PB, Tschanz J, Cook L, Corcoran C, Hayden KM, Norton M, Rabins P V., Green RC, Welsh-Bohmer KA, Breitner JCS, Munger R, Lyketsos CG. Vascular factors predict rate of progression in Alzheimer disease. *Neurology* 2007;**69**:1850–1858.
134. Deschaintre Y, Richard F, Leys D, Pasquier F. Treatment of vascular risk factors is associated with slower decline in Alzheimer disease. *Neurology* 2009;**73**:674–680.
135. Rusanen M, Kivipelto M, Levälahti E, Laatikainen T, Tuomilehto J, Soininen H, Ngandu T. Heart Diseases and Long-Term Risk of Dementia and Alzheimer's Disease: A Population-Based CAIDE Study. *J Alzheimer's Dis* 2014;**42**:183–191.
136. Lyall DM, Celis-Morales CA, Anderson J, Gill JMR, Mackay DF, McIntosh AM, Smith DJ, Deary IJ, Sattar N, Pell JP, La Torre JC De, Lyall DM, Celis-Morales CA, Anderson J, Gill JMR, Mackay DF, McIntosh AM, Smith DJ, Deary IJ, Sattar N, Pell JP. Associations between single andmultiple cardiometabolic diseases and cognitive abilities in 474 129 UK Biobank participants. *Eur Heart J* 2017;**38**:584–585.
137. Cox SR, Lyall DM, Ritchie SJ, Bastin ME, Harris MA, Buchanan CR, Fawns-Ritchie C, Barbu MC, Nooij L De, Reus LM, Alloza C, Shen X, Neilson E, Alderson HL, Hunter S, Liewald DC, Whalley HC, McIntosh AM, Lawrie SM, Pell JP, Tucker-Drob EM, Wardlaw JM, Gale CR, Deary IJ. Associations between vascular risk factors and brain MRI indices in UK Biobank. *Eur Heart J* 2019;**40**:2290–2299.
138. Hagenaars SP, Harris SE, Davies G, Hill WD, Liewald DCM, Ritchie SJ, Marioni RE, Fawns-Ritchie C, Cullen B, Malik R, Worrall BB, Sudlow CLM, Wardlaw JM, Gallacher J, Pell J, McIntosh AM, Smith DJ, Gale CR, Deary IJ. Shared genetic aetiology between cognitive functions and physical and mental health in UK Biobank (N=112 151) and 24 GWAS consortia. *Mol Psychiatry* 2016;**21**:1624–1632.
139. Fawns-Ritchie C, Deary IJ. Reliability and validity of the UK Biobank cognitive tests. Blanch A, ed. *PLoS One* 2020;**15**:e0231627.
140. UK Biobank Fluid intelligence test UK Biobank Touch-screen Fluid intelligence test. 2012.
141. Gaddis ML, Gaddis GM. Introduction to biostatistics: Part 1, basic concepts. *Ann Emerg Med* 1990;**19**:86–89.
142. R Core Team (2019). R: A language and environment for statistical computing. R Foundation for Statistical Computing, Vienna, Austria.

143. RStudio: Integrated Development for R. RStudio, Inc., Boston, MA. https://rstudio.com/ (18 October 2020)
144. Benjamini Y, Hochberg Y. Controlling the False Discovery Rate: A Practical and Powerful Approach to Multiple Testing. *Source J R Stat Soc Ser B* 1995;**57**:289–300.
145. Zuccalà G, Cattel C, Manes-Gravina E, Niro MG Di, Cocchi A, Bernabei R. Left ventricular dysfunction: A clue to cognitive impairment in older patients with heart failure. *J Neurol Neurosurg Psychiatry* 1997;**63**:509–512.
146. Vogels RLC, Flier WM van der, Harten B van, Gouw AA, Scheltens P, Schroeder-Tanka JM, Weinstein HC. Brain magnetic resonance imaging abnormalities in patients with heart failure. *Eur J Heart Fail* 2007;**9**:1003–1009.
147. Oh JE, Shin JW, Sohn EH, Jung JO, Jeong SH, Song HJ, Kim JM, Lee AY. Effect of cardiac function on cognition and brain structural changes in dementia. *J Clin Neurol* 2012;**8**:123–129.
148. Sanna GD, Nusdeo G, Piras MR, Forteleoni A, Murru MR, Saba PS, Dore S, Sotgiu G, Parodi G, Ganau A. Cardiac Abnormalities in Alzheimer Disease: Clinical Relevance Beyond Pathophysiological Rationale and Instrumental Findings? *JACC Hear Fail* 2019;**7**:121–128.
149. Troncone L, Luciani M, Coggins M, Wilker EH, Ho CY, Codispoti KE, Frosch MP, Kayed R, Monte F del. Aβ Amyloid Pathology Affects the Hearts of Patients With Alzheimer's Disease: Mind the Heart. *J Am Coll Cardiol* 2016;**68**:2395–2407.
150. Manolio TA, Kronmal RA, Burke GL, Poirier V, O'Leary DH, Gardin JM, Fried LP, Steinberg EP, Bryan RN. Magnetic resonance abnormalities and cardiovascular disease in older adults the cardiovascular health study. *Stroke* 1994;**25**:318–327.
151. Lu FP, Lin KP, Kuo HK. Diabetes and the risk of multi-system aging phenotypes: A systematic review and meta-analysis. *PLoS One* 2009;**4**.
152. Peters R, Poulter R, Warner J, Beckett N, Burch L, Bulpitt C. Smoking, dementia and cognitive decline in the elderly, a systematic review. *BMC Geriatr* 2008;**8**:36.
153. Anstey KJ, Lipnicki DM, Low L-F. Cholesterol as a Risk Factor for Dementia and Cognitive Decline: A Systematic Review of Prospective Studies With Meta-Analysis. *Am J Geriatr Psychiatry* 2008;**16**:343–354.
154. Novak V, Hajjar I. The relationship between blood pressure and cognitive function. *Nat Rev Cardiol* 2010;**7**:686–698.
155. Anstey KJ, Cherbuin N, Budge M, Young J. Body mass index in midlife and late-life as a risk factor for dementia: A meta-analysis of prospective studies. *Obes Rev* 2011;**12**:e426–e437.
156. Gelber RP, Launer LJ, White LR. The Honolulu-Asia Aging Study: epidemiologic and neuropathologic research on cognitive impairment. *Curr Alzheimer Res* 2012;**9**:664–672.
157. Fratiglioni L, Winblad B, Strauss E von. Prevention of Alzheimer's disease and dementia. Major findings from the Kungsholmen Project. *Physiol Behav* 2007;**92**:98–104.
158. Soysal P, Arik F, Smith L, Jackson SE, Isik AT. Inflammation, Frailty and Cardiovascular

Disease. *Adv Exp Med Biol*; 2020;**1216**:55–64.
159. Irwin MR, Vitiello M V. Implications of sleep disturbance and inflammation for Alzheimer's disease dementia. *Lancet Neurol* 2019;**18**:296–306.
160. Staa TP Van, Dennison EM, Leufkens HGM, Cooper C. Epidemiology of fractures in England and Wales. *Bone* 2001;**29**:517–522.
161. Annual mid-year population estimates, UK - Office for National Statistics. https://www.ons.gov.uk/peoplepopulationandcommunity/populationandmigration/populationestimates/bulletins/annualmidyearpopulationestimates/2014-06-26 (18 January 2021)
162. Kiel DP, Kauppila LI, Cupples LA, Hannan MT, O'Donnell CJ, Wilson PW. Bone loss and the progression of abdominal aortic calcification over a 25 year period: the Framingham Heart Study.[Erratum appears in Calcif Tissue Int. 2004 Feb;74(2):208]. *Calcif Tissue Int* 2001;**68**:271–276.
163. Hak AE, Pols HAP, Hemert AM Van, Hofman A, Witteman JCM. Progression of aortic calcification is associated with metacarpal bone loss during menopause: A population-based longitudinal study. *Arterioscler Thromb Vasc Biol* 2000;**20**:1926–1931.
164. Barengolts EI, Herman M, Kukreja SC, Kouznetsova T, Lin C, Chomka E V. Osteoporosis and coronary atherosclerosis in asymptomatic postmenopausal women. *Calcif Tissue Int* 1998;**62**:209–213.
165. Lee SN, Cho JY, Eun YM, Song SW, Moon KW. Associations between osteoporosis and coronary artery disease in postmenopausal women. *Climacteric* 2016;**19**:458–462.
166. Luo G, Ducy P, McKee MD, Pinero GJ, Loyer E, Behringer RR, Karsenty G. Spontaneous calcification of arteries and cartilage in mice lacking matrix GLA protein. *Nature* 1997;**386**:78–81.
167. Bucay N, Sarosi I, Dunstan CR, Morony S, Tarpley J, Capparelli C, Scully S, Tan HL, Xu W, Lacey DL, Boyle WJ, Simonet WS. Osteoprotegerin-deficient mice develop early onset osteoporosis and arterial calcification. *Genes Dev* 1998;**12**:1260–1268.
168. Papanicolaou DA, Wilder RL, Manolagas SC, Chrousos GP. The Pathophysiologic Roles of Interleukin-6 in Human Disease. *Ann Intern Med* 1998;**128**:127.
169. Krieg MA, Barkmann R, Gonnelli S, Stewart A, Bauer DC, Rio Barquero L Del, Kaufman JJ, Lorenc R, Miller PD, Olszynski WP, Poiana C, Schott AM, Lewiecki EM, Hans D. Quantitative Ultrasound in the Management of Osteoporosis: The 2007 ISCD Official Positions. *J Clin Densitom* 2008;**11**:163–187.
170. Chin KY, Ima-Nirwana S. Calcaneal quantitative ultrasound as a determinant of bone health status: What properties of bone does it reflect? *Int J Med Sci* 2013;**10**:1778–1783.
171. UK Biobank Ultrasound Bone Densitometry. 2011.
172. Senthamarai Kannan K, Manoj K, Arumugam S. Labeling Methods for Identifying Outliers. *Int J Stat Syst* 2015;**10**:231–238.

173. Weele T Van Der, Vansteelandt S. Mediation analysis with multiple mediators. *Epidemiol Method* 2014;**2**:95–115.
174. Hirose KI, Tomiyama H, Okazaki R, Arai T, Koji Y, Zaydun G, Hori S, Yamashina A. Increased pulse wave velocity associated with reduced calcaneal quantitative osteo-sono index: Possible relationship between atherosclerosis and osteopenia. *J Clin Endocrinol Metab* 2003;**88**:2573–2578.
175. Avramovski P, Avramovska M, Sikole A. Bone Strength and Arterial Stiffness Impact on Cardiovascular Mortality in a General Population. *J Osteoporos* 2016;7030272.
176. Zhang M, Bai L, Kang J, Ge J, Peng W. Links between arterial stiffness and bone mineral density in middle-aged and elderly Chinese individuals: A cross-sectional study. *BMJ Open* 2019;**9**:e029946.
177. Kim NL, Suh HS. Correlation of arterial stiffness and bone mineral density by measuring brachial-ankle pulse wave velocity in healthy Korean women. *Korean J Fam Med* 2015;**36**:323–327.
178. Baykara M, Öztürk C, Elbüken F. The relationship between bone mineral density and arterial stiffness in women. *Diagnostic Interv Radiol* 2012;**18**:441–445.
179. Giallauria F, Ling SM, Schreiber C, Maggio M, Shetty V, Muller D, Vigorito C, Ferrucci L, Najjar SS. Arterial stiffness and bone demineralization: The Baltimore longitudinal study of aging. *Am J Hypertens* 2011;**24**:970–975.
180. Klift M Van der, Pols HAP, Geleijnse JM, Kuip DAM Van der, Hofman A, Laet CEDH De. Bone mineral density and mortality in elderly men and women: The Rotterdam study. *Bone* 2002;**30**:643–648.
181. Trivedi DP, Khaw KT. Bone mineral density at the hip predicts mortality in elderly men. *Osteoporos Int* 2001;**12**:259–265.
182. Mussolino ME, Madans JH, Gillum RF. Bone mineral density and mortality in women and men: The NHANES I epidemiologic follow-up study. *Ann Epidemiol* 2003;**13**:692–697.
183. González-Macías J, Marín F, Vila J, Carrasco E, Benavides P, Castell M V., Magaña JE, Chavida F, Díez-Pérez A. Relationship between bone quantitative ultrasound and mortality: A prospective study. *Osteoporos Int* 2009;**20**:257–264.
184. Pinheiro MM, Castro CM, Szejnfeld VL. Low Femoral Bone Mineral Density and Quantitative Ultrasound Are Risk Factors for New Osteoporotic Fracture and Total and Cardiovascular Mortality: A 5-Year Population-Based Study of Brazilian Elderly Women. *J Gerontol* 2006;**16A**:196–203.
185. Bauer DC, Palermo L, Black D, Cauley JA. Quantitative ultrasound and mortality: A prospective study. *Osteoporos Int* 2002;**13**:606–612.
186. Sharif S, Bots ML, Schalkwijk C, Stehouwer CDA, Visseren FLJ, Westerink J. Association between bone metabolism regulators and arterial stiffness in type 2 diabetes patients. *Nutr*

Metab Cardiovasc Dis 2018;**28**:1245–1252.

187. Albu A, Fodor D, Bondor C, Crâciun AM. Bone metabolism regulators and arterial stiffness in postmenopausal women. *Maturitas* 2013;**76**:146–150.
188. Roumeliotis S, Roumeliotis A, Dounousi E, Eleftheriadis T, Liakopoulos V. Biomarkers of vascular calcification in serum. *Adv Clin Chem* 2020;**98**:91–147.
189. Bovalino S, Charleson G, Szoeke C. The impact of red and processed meat consumption on cardiovascular disease risk in women. *Nutrition* 2016;**32**:349–354.
190. Sinha R, Cross AJ, Graubard BI, Leitzmann MF, Schatzkin A. Meat Intake and Mortality A Prospective Study of Over Half a Million People. *Arch Intern Med* 2009;**169**:562–571.
191. Kontogianni MD, Panagiotakos DB, Pitsavos C, Chrysohoou C, Stefanadis C. Relationship between meat intake and the development of acute coronary syndromes: The CARDIO2000 case - Control study. *Eur J Clin Nutr* 2008;**62**:171–177.
192. Bernstein AM, Sun Q, Hu FB, Stampfer MJ, Manson JE, Willett WC. Major dietary protein sources and risk of coronary heart disease in women. *Circulation* 2010;**122**:876–883.
193. Haring B, Wang W, Fretts A, Shimbo D, Lee ET, Howard B V., Roman MJ, Devereux RB. Red meat consumption and cardiovascular target organ damage (from the Strong Heart Study). *J Hypertens* 2017;**35**:1794–1800.
194. Zhong VW, Horn L Van, Greenland P, Carnethon MR, Ning H, Wilkins JT, Lloyd-Jones DM, Allen NB. Associations of Processed Meat, Unprocessed Red Meat, Poultry, or Fish Intake with Incident Cardiovascular Disease and All-Cause Mortality. *JAMA Intern Med* 2020;**180**:503–512.
195. Wolk A. Potential health hazards of eating red meat. *J Intern Med* 2017;**281**:106–122.
196. Organ CL, Otsuka H, Bhushan S, Wang Z, Bradley J, Trivedi R, Polhemus DJ, Tang WHW, Wu Y, Hazen SL, Lefer DJ. Choline Diet and Its Gut Microbe-Derived Metabolite, Trimethylamine N-Oxide, Exacerbate Pressure Overload-Induced Heart Failure. *Circ Hear Fail* 2016;**9**:e002314.
197. Steffen LM, Kroenke CH, Yu X, Pereira MA, Slattery ML, Horn L Van, Gross MD, Jacobs DR. Associations of plant food, dairy product, and meat intakes with 15-y incidence of elevated blood pressure in young black and white adults: The Coronary Artery Risk Development in Young Adults (CARDIA) Study. *Am J Clin Nutr* 2005;**82**:1169–1177.
198. Wolmarans P, Benadé AJ, Kotze TJ, Daubitzer AK, Marais MP, Laubscher R. Plasma lipoprotein response to substituting fish for red meat in the diet. *Am J Clin Nutr* 1991;**53**:1171–1176.
199. Koeth RA, Wang Z, Levison BS, Buffa JA, Org E, Sheehy BT, Britt EB, Fu X, Wu Y, Li L, Smith JD, Didonato JA, Chen J, Li H, Wu GD, Lewis JD, Warrier M, Brown JM, Krauss RM, Tang WHW, Bushman FD, Lusis AJ, Hazen SL. Intestinal microbiota metabolism of l-carnitine, a nutrient in red meat, promotes atherosclerosis. *Nat Med* 2013;**19**:576–585.

200. Schenker S. Portion sizes Food Fact Sheet. 2016. www.bda.uk.com/foodfacts (25 April 2020)
201. Anderson JJ, Darwis NDM, Mackay DF, Celis-Morales CA, Lyall DM, Sattar N, Gill JMR, Pell JP. Red and processed meat consumption and breast cancer: UK Biobank cohort study and meta-analysis. *Eur J Cancer* 2018;**90**:73–82.
202. Gonzalez R, Fittes B. 2nd Conference on Remotely Manned Systems: Technology and Applications. *Gray-level transformations for interactive image enhancement* Los Angeles, California; 1975. p. 17–19.
203. Raisi-Estabragh Z, McCracken C, Gkontra P, Jaggi A, Ardissino M, Cooper J, Biasiolli L, Aung N, Piechnik SK, Neubauer S, Munroe PB, Lekadir K, Harvey NC, Petersen SE. Associations of Meat and Fish Consumption With Conventional and Radiomics Cardiovascular Magnetic Resonance Phenotypes in the UK Biobank. *Front Cardiovasc Med* 2021;**8**.
204. Maechler M. 'Finding Groups in Data': Cluster Analysis Extended Rousseeuw et al. R Packag. version 2.0. 2019. https://www.rdocumentation.org/packages/cluster/versions/2.1.0 (3 May 2020)
205. Levitan EB, Ahmed A, Arnett DK, Polak JF, Hundley WG, Bluemke DA, Heckbert SR, Jacobs DR, Nettleton JA. Mediterranean diet score and left ventricular structure and function: The multi-ethnic study of atherosclerosis. *Am J Clin Nutr* 2016;**104**:595–602.
206. Nguyen HT, Bertoni AG, Nettleton JA, Bluemke DA, Levitan EB, Burke GL. Dash eating pattern is associated with favorable left ventricular function in the multi-ethnic study of atherosclerosis. *J Am Coll Nutr* 2012;**31**:401–407.
207. Shang X, Scott D, Hodge AM, English DR, Giles GG, Ebeling PR, Sanders KM. Dietary protein intake and risk of type 2 diabetes: Results from the Melbourne Collaborative Cohort Study and a meta-analysis of prospective studies. *Am J Clin Nutr* 2016;**104**:1352–1365.
208. Baak MA van, Larsen TM, Jebb SA, Martinez A, Saris WHM, Handjieva-Darlenska T, Kafatos A, Pfeiffer AFH, Kunešová M, Astrup A. Dietary intake of protein from different sources and weight regain, changes in body composition and cardiometabolic risk factors afterweight loss: The DIOgenes study. *Nutrients* 2017;**9**:1326.
209. Wang Z, Bergeron N, Levison BS, Li XS, Chiu S, Jia X, Koeth RA, Li L, Wu Y, Tang WHW, Krauss RM, Hazen SL. Impact of chronic dietary red meat, white meat, or non-meat protein on trimethylamine N-oxide metabolism and renal excretion in healthy men and women. *Eur Heart J* 2019;**40**:583–594.
210. Ghasemi Fard S, Wang F, Sinclair AJ, Elliott G, Turchini GM. How does high DHA fish oil affect health? A systematic review of evidence. *Crit Rev Food Sci Nutr* 2019;**59**:1684–1727.
211. Innes JK, Calder PC. Marine omega-3 (N-3) fatty acids for cardiovascular health: An update for 2020. *Int J Mol Sci* 2020;**21**:1–21.
212. WILLETT W, STAMPFER MJ. Total energy intake: Implications for epidemiologic analyses.

Am J Epidemiol 1986;**124**:17–27.

213. Aune D, Giovannucci E, Boffetta P, Fadnes LT, Keum NN, Norat T, Greenwood DC, Riboli E, Vatten LJ, Tonstad S. Fruit and vegetable intake and the risk of cardiovascular disease, total cancer and all-cause mortality-A systematic review and dose-response meta-analysis of prospective studies. *Int J Epidemiol* 2017;**46**:1029–1056.
214. Ho FK, Gray SR, Welsh P, Petermann-Rocha F, Foster H, Waddell H, Anderson J, Lyall D, Sattar N, Gill JMR, Mathers JC, Pell JP, Celis-Morales C. Associations of fat and carbohydrate intake with cardiovascular disease and mortality: Prospective cohort study of UK Biobank participants. *BMJ* 2020;**368**:1–11.
215. Gupta A, Madhavan M V., Sehgal K, Nair N, Mahajan S, Sehrawat TS, Bikdeli B, Ahluwalia N, Ausiello JC, Wan EY, Freedberg DE, Kirtane AJ, Parikh SA, Maurer MS, Nordvig AS, Accili D, Bathon JM, Mohan S, Bauer KA, Leon MB, Krumholz HM, Uriel N, Mehra MR, Elkind MSV, Stone GW, Schwartz A, Ho DD, Bilezikian JP, Landry DW. Extrapulmonary manifestations of COVID-19. *Nat Med* 2020;**26**:1017–1032.
216. Madjid M, Safavi-Naeini P, Solomon SD, Vardeny O. Potential Effects of Coronaviruses on the Cardiovascular System: A Review. *JAMA Cardiol* 2020;**10**:1–10.
217. Libby P, Lüscher T. COVID-19 is, in the end, an endothelial disease. *Eur Heart J* 2020;**41**:3038–3044.
218. Böhm M, Frey N, Giannitsis · Evangelos, Sliwa K, Zeiher AM. Coronavirus Disease 2019 (COVID-19) and its implications for cardiovascular care: expert document from the German Cardiac Society and the World Heart Federation. *Clin Res Cardiol* 2020;**27**:1–14.
219. Siripanthong B, Nazarian S, Muser D, Deo R, Santangeli P, Khanji MY, Cooper LT, Anwar # C, Chahal A. Recognizing COVID-19-related myocarditis: The possible pathophysiology and proposed guideline for diagnosis and management. *Hear Rhythm* 2020;**17**:1463–1470.
220. Lodigiani C, Iapichino G, Carenzo L, Cecconi M, Ferrazzi P, Sebastian T, Kucher N, Studt JD, Sacco C, Alexia B, Sandri MT, Barco S. Venous and arterial thromboembolic complications in COVID-19 patients admitted to an academic hospital in Milan, Italy. *Thromb Res* 2020;**191**:9–14.
221. Guo T, Fan Y, Chen M, Wu X, Zhang L, He T, Wang H, Wan J, Wang X, Lu Z. Cardiovascular Implications of Fatal Outcomes of Patients with Coronavirus Disease 2019 (COVID-19). *JAMA Cardiol* 2020;**5**:811–818.
222. Shi S, Qin M, Shen B, Cai Y, Liu T, Yang F, Gong W, Liu X, Liang J, Zhao Q, Huang H, Yang B, Huang C. Association of Cardiac Injury with Mortality in Hospitalized Patients with COVID-19 in Wuhan, China. *JAMA Cardiol* 2020;**5**:802–810.
223. Caballeros Lam M, la Fuente Villena A de, Hernández Hernández A, García de Yébenes M, Bastarrika Alemañ G. Cardiac magnetic resonance characterization of COVID-19 myocarditis. *Rev Española Cardiol* 2020;**73**:863–864.

224. Hu H, Ma F, Wei X, Fang Y. Coronavirus fulminant myocarditis saved with glucocorticoid and human immunoglobulin. *Eur Heart J* 2020;**42**:206.
225. Inciardi RM, Lupi L, Zaccone G, Italia L, Raffo M, Tomasoni D, Cani DS, Cerini M, Farina D, Gavazzi E, Maroldi R, Adamo M, Ammirati E, Sinagra G, Lombardi CM, Metra M. Cardiac Involvement in a Patient with Coronavirus Disease 2019 (COVID-19). *JAMA Cardiol* 2020;**5**:819–824.
226. Bojkova D, Wagner JUG, Shumliakivska M, Aslan GS, Saleem U, Hansen A, Luxán G, Günther S, Pham MD, Krishnan J, Harter PN, Ermel UH, Frangakis AS, Milting H, Zeiher AM, Klingel K, Cinatl J, Dendorfer A, Eschenhagen T, Tschöpe C, Ciesek S, Dimmeler S. SARS-CoV-2 infects and induces cytotoxic effects in human cardiomyocytes. *Cardiovasc Res* 2020;**116**:2207–2215.
227. Buja LM, Wolf D, Zhao B, Akkanti B, McDonald M, Lelenwa L, Reilly N, Ottaviani G, Elghetany MT, Trujillo DO, Aisenberg GM, Madjid M, Kar B. The emerging spectrum of cardiopulmonary pathology of the coronavirus disease 2019 (COVID-19): Report of 3 autopsies from Houston, Texas, and review of autopsy findings from other United States cities. *Cardiovasc Pathol* 2020;**48**:107233.
228. Greenhalgh T, Knight M, A'Court C, Buxton M, Husain L. Management of post-acute covid-19 in primary care. *BMJ* 2020;**370**:m3026.
229. Carfì A, Bernabei R, Landi F. Persistent Symptoms in Patients after Acute COVID-19. *JAMA - J Am Med Assoc* 2020;**324**:603–605.
230. Tenforde MW, Kim SS, Lindsell CJ, Billig Rose E, Shapiro NI, Files DC, Gibbs KW, Erickson HL, Steingrub JS, Smithline HA, Gong MN, Aboodi MS, Exline MC, Henning DJ, Wilson JG, Khan A, Qadir N, Brown SM, Peltan ID, Rice TW, Hager DN, Ginde AA, Stubblefield WB, Patel MM, Self WH, Feldstein LR, Hart KW, McClellan R, Dorough L, Dzuris N, et al. Symptom Duration and Risk Factors for Delayed Return to Usual Health Among Outpatients with COVID-19 in a Multistate Health Care Systems Network — United States, March–June 2020. *MMWR Morb Mortal Wkly Rep* 2020;**69**:993–998.
231. Clark DE, Diamond AB, Fish FA. COVID-19 Myocardial Pathology Evaluated Through scrEening Cardiac Magnetic Resonance (COMPETE CMR). *medRxiv Prepr* 2020;1–25.
232. Puntmann VO, Carerj ML, Wieters I, Fahim M, Arendt C, Hoffmann J, Shchendrygina A, Escher F, Vasa-Nicotera M, Zeiher AM, Vehreschild M, Nagel E. Outcomes of Cardiovascular Magnetic Resonance Imaging in Patients Recently Recovered From Coronavirus Disease 2019 (COVID-19). *JAMA Cardiol* 2020;**5**:1265.
233. Rajpal S, Tong MS, Borchers J, Zareba KM, Obarski TP, Simonetti OP, Daniels CJ. Cardiovascular Magnetic Resonance Findings in Competitive Athletes Recovering from COVID-19 Infection. *JAMA Cardiol* 2021;6:116–118.
234. Huang L, Zhao P, Tang D, Zhu T, Han R, Zhan C, Liu W, Zeng H, Tao Q, Xia L. Cardiac

Involvement in Patients Recovered From COVID-2019 Identified Using Magnetic Resonance Imaging. *JACC Cardiovasc Imaging* 2020;**13**:2330–2339.

235. Armstrong J, Rudkin JK, Allen N, Crook DW, Wilson DJ, Wyllie DH, O'Connell AM. Dynamic linkage of COVID-19 test results between Public Health England's Second Generation Surveillance System and UK Biobank. *Microb Genomics* 2020;**6**:mgen000397.
236. Raisi-Estabragh Z, McCracken C, Cooper J, Fung K, Paiva JM, Khanji MY, Rauseo E, Biasiolli L, Raman B, Piechnik SK, Neubauer S, Munroe PB, Harvey NC, Petersen SE. Adverse cardiovascular magnetic resonance phenotypes are associated with greater likelihood of incident coronavirus disease 2019: findings from the UK Biobank. *Aging Clin Exp Res* 2021;**33**:1133–1144.
237. Li X, Wang H, Zhao R, Wang T, Zhu Y, Qian Y, Liu B, Yu Y, Han Y. Elevated Extracellular Volume Fraction and Reduced Global Longitudinal Strains in Patients Recovered from COVID-19 without Clinical Cardiac Findings. *Radiology* 2021;203998.
238. Kotecha T, Knight DS, Razvi Y, Kumar K, Vimalesvaran K, Thornton G, Patel R, Chacko L, Brown JT, Coyle C, Leith D, Shetye A, Ariff B, Bell R, Captur G, Coleman M, Goldring J, Gopalan D, Heightman M, Hillman T, Howard L, Jacobs M, Jeetley PS, Kanagaratnam P, Kon OM, Lamb LE, Manisty CH, Mathurdas P, Mayet J, Negus R, et al. Patterns of myocardial injury in recovered troponin-positive COVID-19 patients assessed by cardiovascular magnetic resonance. *Eur Heart J* 2021;
239. Chadeau-Hyam M, Bodinier B, Elliott J, Whitaker MD, Tzoulaki I, Vermeulen R, Kelly-Irving M, Delpierre C, Elliott P. Risk factors for positive and negative COVID-19 tests: a cautious and in-depth analysis of UK biobank data. *Int J Epidemiol* 2020;**49**:1454–1467.